Function of energy-converting hydrogenases and transhydrogenase in the metabolism of the thermophilic acetogenic bacterium *Thermoanaerobacter kivui*

Dissertation

for

obtaining the academic degree

Doctur rerum naturalium (Dr. rer. Nat.)

submitted to the

Faculty of Mathematics and Natural Sciences

at the

University of Rostock

by

Christoph Ferdinand Baum

Born 17.08.1989 in Kassel, Germany

https://doi.org/10.18453/rosdok_id00005153

Supervisor: Prof. Dr. Mirko Basen
Microbiology
Institute of Biological Sciences
Faculty of Mathematics and Natural Sciences
University of Rostock

Reviewer: Prof. Dr. Uwe Deppenmeier
Institut für Mikrobiologie und Biotechnologie
Universität Bonn

Date of submission: 10.09.2024

Date of defense: 24.01.2025

Abstract

Electron transfer between electron carriers is crucial for maintaining all organism's redox balance and overall metabolic processes. In acetogenic bacteria, such as *Thermoanaerobacter kivui*, four primary electron carriers (H_2, ferredoxins (Fd), NADH, and NADPH) are fundamental to energy and redox metabolism. *T. kivui* is an anaerobic, thermophilic acetogenic bacterium known for its high temperature optimum (66°C) and ability to grow fast lithotrophically and organotrophically.

In *T. kivui*, two energy-converting hydrogenases (Ech) are annotated in its genome, Ech1 and Ech2. Both catalyze the oxidation of H_2, providing Fd_{red} or vice versa. Additionally, they enable the translocation of protons across the cell membrane, thereby conserving energy by an electrochemical membrane potential. Biochemical studies have confirmed Ech activity in *T. kivui*, indicating that Ech1, Ech2, or both are vital for its energy conservation, although, during growth on H_2/CO_2 or CO, their specific physiological roles remain unclear. In this work, the deletion of the entire *ech2* operon was successful, and the resulting Δ*ech2* strain grew as fast as the wild type on sugar substrates and H_2/CO_2, indicating that another enzyme might compensate for the loss of Ech2 in oxidizing H_2 to reduce Fd_{ox} during growth on these substrates. The hydrogen-dependent carbon dioxide reductase (HDCR) is the most likely candidate for this role. However, the utilization of ferredoxin-dependent substrates such as pyruvate and CO was impaired in the Δ*ech2* strain, although to varying degrees. While the mutant strain adapted to pyruvate after four passages, it was unsuccessful in adapting to CO. Moreover, resting cells of the Δ*ech2* strain could not convert CO to acetate, unlike the wild type strain DSM 2030. Genome analyses of CO-adapted strains indicated fragmentation of the HDCR filamentous structure, losing the ability to reduce or oxidize ferredoxins. This suggests that Ech2 is essential for CO metabolism. Moreover, it was not possible to delete the *ech1* operon, but changing its promoter with a fructose-inducible promoter (P_{frc}) allowed for the downregulation of *ech1* expression in the presence of glucose. Two mutant strains, P_{frc}*ech1* and P_{frc}*ech1*Δ*ech2*, were successfully generated. Both strains showed lower *ech1a* expression on glucose than on fructose, although their growth rate on glucose was only slightly reduced compared to the wild type. However, when grown on pyruvate, P_{frc}*ech1* showed impaired growth, reaching a lower final OD_{600} than the wild type, while P_{frc}*ech1*Δ*ech2* showed no significant growth. These findings indicate that both Ech's are involved in the re-oxidation of Fd_{red}.

Furthermore, the electron bifurcating transhydrogenase NfnAB is described to couple exergonic and endergonic reactions, allowing energy-efficient transfer of electrons between the involved electron carriers. It is, therefore, assumed to be essential for redox balance. The successful deletion of *nfnB* in *T. kivui* showed a clear phenotype. The mutant was able to grow on all tested organic substrates, yet the strain took significantly longer compared to the wild type. In addition, the resting cells of the mutant could not utilize glucose, while pyruvate was consumed. This suggests that NfnAB is required to re-oxidate NADH in resting cells, though growing cells might re-oxidize NADH in their anabolism.

In *Thermoanaerobacter kivui*, hydrogen (H_2) plays a crucial role in energy and redox metabolism, being oxidized by various complexes such as the Ech complexes, hydrogen-dependent carbon dioxide reductase (HDCR), and the electron-bifurcating hydrogenase (HydABC). However, its impact under mixotrophic growth conditions was not well understood. Experiments revealed that adding H_2 during exponential growth inhibited the growth of cells grown on glucose or mannitol but did not affect cells grown on pyruvate. Gene expression analyses revealed that the addition of H_2 during growth on glucose did not cause significant changes in the expression of genes encoding the Ech complexes (*ech1A*, *ech2D*), HDCR (*fhs*), HydABC (*hydB*) and glyceraldehyde 3-phosphate dehydrogenase (*gap*). In contrast, cells growing on pyruvate showed significant downregulation of *hydB* after the addition of H_2, with an even

stronger effect in the *nfnB* mutant, which showed growth inhibition upon addition of H_2. RNA sequencing of cells grown on glucose exposed to H_2 during the exponential growth phase showed a clear upregulation of genes involved in glycogen biosynthesis and a significant downregulation of genes involved in pyrimidine and arginine biosynthesis. These observations suggest that the addition of H_2 triggers a cellular stress response, likely due to an imbalance of the electron carriers H_2, NADH, and NADPH, leading to growth inhibition.

This study provides fundamental insights into the roles of enzymes and electron carriers like H_2, Fd_{red}, NADH and NADPH involved in the energy and redox metabolism of *Thermoanaerobacter kivui*, solidifying its status as a model organism for acetogens.

Zusammenfassung

Der Elektronentransfer zwischen Elektronenträgern ist von entscheidender Bedeutung für die Aufrechterhaltung des Redox-Gleichgewichts und aller Stoffwechselprozesse eines jeden Organismus. Bei acetogenen Bakterien, wie *Thermoanaerobacter kivui*, sind vier primäre Elektronenträger (H_2, Ferredoxine (Fd), NADH und NADPH) für den Energie- und Redoxstoffwechsel von fundamentaler Bedeutung. *T. kivui* ist ein anaerobes, thermophiles, acetogenes Bakterium, das für sein hohes Temperaturoptimum (66 °C) und seine Fähigkeit zu schnellem lithotrophen und organotrophen Wachstum bekannt ist.

In *T. kivui* sind zwei Energie-konvertierende Hydrogenasen (Ech) in seinem Genom annotiert, Ech1 und Ech2. Beide katalysieren die Oxidation von H_2 und liefern Fd_{red} oder umgekehrt. Darüber hinaus ermöglichen sie die Translokation von Protonen über die Zellmembran und konservieren so Energie durch ein elektrochemisches Membranpotenzial. Biochemische Studien haben enzymatische Aktivität von Energie konvertierende Hydrogenasen in *T. kivui* bestätigt und gezeigt, dass Ech1, Ech2 oder beide für die Energieerhaltung von entscheidender Bedeutung sind, obwohl die spezifischen physiologischen Rollen während des Wachstums auf H_2/CO_2 oder CO unklar blieben. In dieser Arbeit gelang die Deletion des gesamten ech2 Operons, und der resultierende Δ*ech2* Stamm wuchs auf Zuckersubstraten und H_2/CO_2 genauso schnell wie der Wildtyp. Dies deutet darauf hin, dass bei Verlust des Ech2 Komplexes ein anderes Enzym dessen Funktion der H_2 Oxidation und Fd_{ox} Reduktion übernimmt. Die Wasserstoff-abhängige CO_2-Reduktase (HDCR) ist der wahrscheinlichste Kandidat für diese Rolle. Dennoch war die Verwertung von Ferredoxin-abhängigen Substraten wie Pyruvat und CO im Δ*ech2* Stamm beeinträchtigt, wenn auch in unterschiedlichem Maße. Nach vier Passagen konnte sich die Mutante erfolgreich an Pyruvat anpassen, jedoch gelang die Anpassung an CO nicht. Zudem konnten ruhende Zellen des Δ*ech2* Stammes CO nicht in Acetat umwandeln, im Gegensatz zum Wildtyp Stamm DSM 2030. Genomanalysen von CO-adaptierten Stämmen weisen darauf hin, dass die filamentösen Struktur der HDCR fragmentiert wurde, wodurch Ferredoxine nicht mehr reduziert oder oxidiert werden können. Dies deutet darauf hin, dass Ech2 für den CO-Stoffwechsel unerlässlich ist. Die Deletion des *ech1* Operons war nicht erfolgreich, jedoch konnte dessen Promotor durch einen fruktoseinduzierbaren Promotor (P_{frc}) ersetzt werden. Dies ermöglichte die Herunterregulierung der *ech1* Expression in Gegenwart von Glukose. Zwei Mutantenstämme, P_{frc}*ech1* and P_{frc}*ech1*Δ*ech2*, wurden erfolgreich generiert. Beide Stämme zeigten auf Glukose eine geringere *ech1a* Expression im Vergleich zu Fruktose. Allerdings war ihre Wachstumsrate auf Glukose im Vergleich zum Wildtyp nur leicht reduziert. Jedoch zeigten die Mutanten ein unterschiedliches Wachstumsverhalten, wenn sie auf Pyruvate wuchsen. P_{frc}*ech1* wuchs langsamer und erreichte eine geringere Finale OD_{600} als der Wildtyp, während P_{frc}*ech1Δech2* nahezu kein Wachstum zeigte. Diese Ergebnisse deuten darauf hin, dass beide Ech-Komplexe eine wichtige Rolle bei der Re-oxidation von reduziertem Ferredoxin haben.

Darüber hinaus wird die Elektronen-bifurkierende Transhydrogenase NfnAB beschrieben, die exergonische und endergonische Reaktionen koppelt und so einen energieeffizienten Elektronentransfer zwischen den beteiligten Elektronenträgern ermöglicht. Daher wird angenommen, dass sie für das Redoxgleichgewicht unerlässlich ist. Die erfolgreiche Deletion von *nfnB* in *T. kivui* zeigte einen deutlichen Phänotyp. Die Mutante konnte auf allen getesteten organischen Substraten wachsen, benötigte jedoch deutlich länger als der Wildtyp. Zudem konnten ruhende Zellen der Mutante Glucose nicht verwerten, während Pyruvat konsumiert wurde. Dies deutet darauf hin, dass NfnAB erforderlich ist, um NADH in ruhenden Zellen zu re-oxidieren, während wachsende Zellen NADH möglicherweise in ihrem Anabolismus re-oxidieren können.

In *Thermoanaerobacter kivui* spielt Wasserstoff (H_2) eine zentrale Rolle im Energie- und Redoxstoffwechsel, indem er von verschiedenen Enzymkomplexen wie die Ech Komplexe, der Wasserstoff-abhängige CO_2-Reduktase (HDCR) und der Elektronen-bifurkierenden Hydrogenase (HydABC) oxidiert wird. Dennoch war sein Einfluss auf das Zellwachstum unter mixotrophen Bedingungen bisher nicht ausreichend erforscht. In Experimenten zeigte sich, dass die Zugabe von H_2 während der exponentiellen Wachstumsphase das Wachstum von Zellen, die auf Glukose oder Mannitol kultiviert worden waren, deutlich hemmte. Im Gegensatz dazu blieb das Wachstum von Zellen, die auf Pyruvat wuchsen, von der H_2-Zugabe unbeeinflusst. Genexpressionsanalysen ergaben, dass die Zugabe von H_2 während des Wachstums auf Glukose keine signifikanten Veränderungen in der Expression der Gene bewirkte, die die Ech-Komplexe (*ech1A*, *ech2D*), HDCR (*fhs*), HydABC (*hydB*) und Glycerinaldehyd-3-Phosphat-Dehydrogenase (*gap*) kodieren. Im Gegensatz dazu wiesen Zellen die auf Pyruvate wuchsen nach der Zugabe von H_2 signifikante Herunterregulation von *hydB*, mit einem noch stärkeren Effekt im *nfnB*-Mutanten, der beim Zusatz von H_2 eine Wachstumshemmung zeigte. Diese Beobachtungen legen nahe, dass zusätzliches H_2 das Gleichgewicht von NADPH/$NADP^+$ und NADH/NAD^+ stören könnte, was zu Wachstumshemmung führt. RNA-Sequenzierung von auf Glukose gewachsenen Zellen, die während der exponentiellen Wachstumsphase H_2 ausgesetzt waren, zeigte eine deutliche Hochregulation von Genen, die an der Glykogenbiosynthese beteiligt sind, sowie eine signifikante Herunterregulation von Genen, die in die Pyrimidin- und Arginin-Biosynthese involviert sind. Diese Beobachtungen weisen darauf hin, dass die Zugabe von H_2 eine zelluläre Stressreaktion hervorruft, vermutlich durch ein Ungleichgewicht der Elektronenträger H_2, NADH und NADPH, was letztlich in einer Wachstumshemmung resultiert.

Diese Studie liefert grundlegende Erkenntnisse über die Rolle von Enzymen und Elektronenträger wie H_2, Fd_{red}, NADH und NADPH, die am Energie- und Redox-Stoffwechsel von *Thermoanaerobacter kivui* beteiligt sind, und festigt seinen Status als Modellorganismus für Acetogene

.

List of Contents

List of Figures

List of tables

Abbreviations

$\Delta\mu_{H+}$	transmembrane electrochemical proton gradient	i.e	id est (that is to say)
$\Delta\mu_{Na+}$	transmembrane electrochemical sodium ion gradient	Kan	Kanamycin
5-FOA	5-Fluoroorotic acid/5-fluoroorotate	LB	Luria Bertani
ACK	Acetate kinase	LUCA	last universal common ancestor
ACS	acetyl-CoA synthase	MetFV	methylenetetrahydrofolate reductases
Amp	Ampicillin	mRNA	messenger RNA
ATP	Adenosine triphosphate	NAD(H)	Nicotinamide adenine dinucleotide
cDNA	Complementary DNA	NADP(H)	Nicotinamide adenine dinucleotide phosphate
CFeSP	corrinoid iron-sulfur protein	Nfn	electron bifurcating transhydrogenase
CoA	coenzyme A	OD_{600}	optical density at a wavelength of 600 nm
CODH	carbon monoxide dehydrogenase	ox	oxidized
DFR	downstream flanking region	PCR	Polymerase chain reaction
Dir.	direction	qPCR	Quantitative polymerase chain reaction
DNA	Deoxyribonucleic acid	red	reduced
E_0'	Standard redox potential	rev	reverse
Ech	Energy-converting hydrogenase	RNA	Ribonucleic acid
$Em_{,7}$	Redox midpoint potential at pH 7	Rnf	*Rhodobacter* nitrogen fixation
Fd	ferredoxin	THF	tetrahydrofolate
FDH	formate dehydrogenase	TKV	*Thermoanaerobacter kivui* DSM2030
fwd	forward	TRIS	Tris-(hydroxymethyl)-amino methane
HDCR	hydrogen-dependent CO_2 reductase	UFR	upstream flanking region
HPLC	High performance liquid chromatography	vs.	Versus
Hyd	electron bifurcating hydrogenase	WLP	Wood-Ljungdahl pathway

<u>Units</u>

µl	Microliter	ml	Milliliter
µM	Micromolar	mM	Millimolar
bp	Base pairs	mV	Millivolt
g	Gram	nm	Nanometer
h	Hours	P	p-value
kbp	Kilo base pairs	Pa	Pascal
l	Liter	rpm (g)	rounds per minute (gravitational force)
M	Molar	V	Volt
mg	Milligram	v/v	volume fraction
min	Minutes		

1 Introduction

1.1 Origin of life

After the earth's formation about 4.55 to 4.58 billion years ago (Manhes et al. 1980), Archaea and Bacteria were the first organisms to emerge and successfully colonize it. The Origin of Life on Earth is still uncertain. The oldest microfossils are about 3.5 billion years old, and there are also speculations that life on Earth has existed for more than 3.8 billion years (Mojzsis et al. 1996; Lunine 2006). However, roughly 4 billion years ago, the Earth's surface stabilized, and the atmosphere cooled, allowing gaseous water in the atmosphere released by volcanic activity to condense to liquid water (Lunine 2006). It is hypothesized that the first pioneer organisms were formed during this time in volcanically active areas known as hydrothermal fields (Kelley et al. 2005; Wächtershäuser 2006). In these hydrothermal fields, volcanic exhalations release metals, salts, and inorganic molecules such as H_2, N_2, H_2S, NH_3, CH_4, CO, CO_2, HCN, and P_4O_{10}. Simple molecular bioorganic compounds may have been formed through autocatalytic processes, some of which accumulated into organic structures similar to a cell membrane (Wächtershäuser 2006; Lane et al. 2010). These structures probably enabled the formation of vesicles, which separated a small part of the environment from the outside world (Lindahl and Chang 2001; Wächtershäuser 2006). Through diffusion, inorganic molecules, as well as metals and salts, penetrated into the separated environment and formed further structures like amino acids and nucleic acids through chemical and later biological processes. Such a membrane-protected environment can be considered an incubation chamber of life (Wächtershäuser 2006; Gill and Forterre 2016). Based on these theories, the concept of the last universal common ancestor (LUCA) of Bacteria and Archaea was developed, and it is assumed that acetogens and methanogens are the direct descendants of LUCA (Russell and Hall 2009; Lane et al. 2010). This assumption is consistent with studies on the acetyl-CoA pathway present in acetogens and methanogens, which identified enzymes that catalyze the same previously mentioned autocatalytic reactions leading to the formation of low carbon compounds by fixation of CO_2 (Martin and Russell 2007; Martin 2020). In further studies using genomic reconstruction analyses of sequenced prokaryotic genomes to find similarities and predict the physiology of LUCA, LUCA was defined as an anaerobic, CO_2-fixing, N_2-fixing, H_2-dependent and thermophilic organism containing genes for the acetyl-CoA pathway (Wood-Ljungdahl pathway; Weiss et al. 2016). Therefore, LUCA most likely lived in a hydrothermal environment and utilized H_2, N_2 and CO_2 released by volcanic activity to produce biomass and conserve energy (Lane et al. 2010; Weiss et al. 2016).

1.2 Acetogenesis

Today's acetogens are generally considered anaerobic microorganisms capable of fixating CO_2 through acetyl-CoA synthase via the Wood-Ljungdahl-pathway (WLP) (Drake et al. 2008). The first described acetogen was *Clostridium aceticum*, isolated from ditch mud by Wieringa (1939). The stain was able to consume H_2/CO_2 and produced acetic acid (acetate). Although this original strain was lost, it was later reisolated by Adamse (1980) and is considered the first isolated acetogen. Since then, more than 100 acetogens have been isolated from various geographic areas, as well as from the digestive tracts of animals and humans (Drake et al. 2008). The WLP is present in acetogens, sulfate reducing bacteria and is partially found in methanogens (Ragsdale and Pierce 2008; Borrel et al. 2016). As mentioned above, acetogens use CO_2 as a carbon source and fix it via the WLP, producing acetyl-CoA as a precursor of C3 molecules for further biochemical processes (Martin and Russell 2007; Martin 2020). In contrast, sulfate-reducing bacteria use acetate as a carbon source for building up biomass through reverse acetogenesis by oxidizing acetate to CO_2 and H_2 and simultaneously reducing sulfate to sulfide (Thauer et al. 1977; Ragsdale and Pierce 2008). In comparison, methanogens convert CO_2 and H_2 to methane

and biomass (Meuer et al. 2002; Ragsdale and Pierce 2008). In addition to the ability of acetogens to grow lithoautotrophically on H_2 + CO_2, some of them are also able to utilize carbon monoxide (CO). Furthermore, they utilize a versatile spectrum of substrates organotrophically (Table 1).

Table 1 Representative acetogens and substrates they utilize lithotrophically and organotrophically.

Organism	Substrate lithotroph	Substrate organotroph	Product	Reference
Acetobacterium woodii	H_2 + CO_2	fructose, glucose, lactate, glycerate, formate and methanol, ethanol, 1,2-propanediol, alanine, 2,3-butanediol, ethylene glycol, acetoin, lactate, glycerate, betaine and some methoxylated aromatic acids	Acetate	Balch et al. 1977; Braun and Gottschalk 1981; Heise et al. 1989; Schuchmann and Müller 2014; Dönig and Müller 2018
Clostridium ljungdahlii	H_2 + CO_2, CO	fructose, glucose, gluconate, arabinose, xylose, formate, pyruvate, malate, ethanol and more	Acetate	Tanner et al. 1993; Köpke et al. 2010
Moorella thermoacetica	H_2 + CO_2, CO	fructose, glucose, xylose, ethanol, n-propanol, n-butanol, oxalate, glyoxylate, glycolate, pyruvate and lactate	Acetate	Pierce et al. 2008
Thermoanaerobacter kivui	H_2 + CO_2, CO	glucose, mannose, fructose, mannitol, pyruvate, and formate	Acetate	Leigh et al. 1981; Weghoff and Müller 2016; Moon et al. 2019

Depending on the substrate, different redox carriers are reduced. For example, during the oxidation of sugars such as glucose or fructose through glycolysis, electrons are transferred to oxidized redox carriers such as NAD^+ and oxidized ferredoxin (Fd_{ox}) while also generating via substrate-level phosphorylation ATP in the process (Schuchmann and Müller 2016). During glycolysis, electrons are transferred to oxidized redox carriers such as NAD^+ and oxidized ferredoxin (Fd_{ox}) so that these are available in their reduced form (NADH and Fd_{red}). The reduced NADH and Fd_{red} are available for further biological processes and re-oxidized again in order to serve as electron acceptors for the oxidization of further carbon substrates. In the case of acetogens, a large part of the oxidation of the redox carriers takes place in the WLP since it is the terminal electron pathway (Drake et al. 2008; Ragsdale and Pierce 2008; Huang et al. 2012). Depending on the organism, different reducing agents are required in the WLP, which will be described later.

1.2.1 Wood-Ljungdahl-pathway (WLP)

The WLP of acetogens consists of two branches, the methyl-branch, where CO_2 is reduced to a methyl group and subsequently bound to tetrahydrofolate (THF) through stepwise reduction, and the shorter carbonyl-branch. At the end, the products of both branches are combined to form acetyl-coenzyme A, which is further converted to acetate (Figure 1).

For reduction of CO_2 to a methyl group, CO_2 is in the first step reduced to formate by a formate dehydrogenase (FDH; Figure 1, A). In *Acetobacterium woodii* and *Thermoanaerobacter kivui*, this CO_2 to formate reaction is catalyzed by a hydrogen-dependent CO_2 reductase (HDCR) using H_2 as a direct

electron donor (Schuchmann and Müller 2013; Dietrich et al. 2022). Due to the low redox potential of CO_2/formate (E°' = −420 mV), an electron donor with similar redox potential is required. Thus H^+/H_2 (E°' = −414 mV) or ferredoxin (E°' = −400 mV) are valid reducing agents, while NADPH (E°' = −320 mV) is required for the reduction of CO_2 to formate in *Moorella thermoacetica* (Thauer et al. 1977; Huang et al. 2012; Buckel and Thauer 2013). The HDCR (hydrogen-dependent CO_2 reductase) of *T. kivui* is described to use H_2 and ferredoxin (Fd) (Schwarz et al. 2018; Dietrich and Müller 2023).

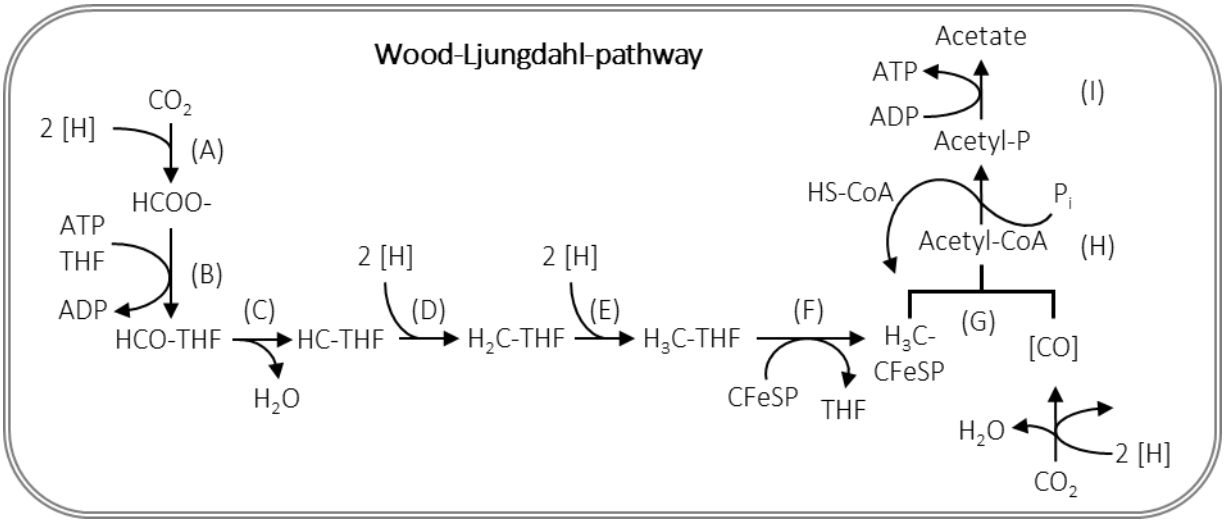

Figure 1 The Wood-Ljungdahl pathway as terminal electron accepting pathway of acetogenic bacteria. It consists of two branches the methyl-branch (A-G) and the carbonyl-branch (G). Enzymes involved in WLP are the FDH (formate dehydrogenase; HDCR in T. kivui and A. woodii) (A), formyl-THF synthase (B), formyl-THF cyclohydrolase (C), methylene-THF dehydrogenase (D), methylene-THF reductase (E), methyltransferase (F), CODH/ACS (G), phosphotransacetylase (H), and acetate kinase (I) (Schuchmann and Müller 2013, 2014).

After reduction of CO_2 to formate, it is bound to THF in the second step by an ATP-dependent formyl-THF synthase (Figure 1, B), resulting in formyl-THF (HCO-THF), which is subsequently dehydrated by formyl-THF cyclohydrolase (Figure 1, C) to methenyl-THF (HC-THF), in the third step (Ragsdale and Ljungdahl 1984). Afterward, as a fourth step, an additional reduction is carried out by an NADH- or NADPH-dependent methylene-THF dehydrogenase (Figure 1, D; Ragsdale and Ljungdahl 1984; Katsyv et al. 2021a). In this reaction, methenyl-THF (HC-THF) is reduced to methylene-THF (H_2C-THF), which is subsequently reduced to methyl-THF (H_3C-THF), in the fifth step. The fifth step is catalyzed by a NADH- or Fd-dependent methylene-THF reductase (MetFV; Figure 1, E; Schuchmann and Müller 2014; Katsyv et al. 2021a; Öppinger et al. 2022). For *T. kivui,* it was suggested that MetFV forms a complex with the membrane bound energy-converting hydrogenase (Ech) complex (Katsyv et al. 2021a). Due to the redox potential difference between methylene-/methyl-THF (E°' = −200 mV) (Wohlfarth and Diekert 1991) and Fd_{ox}/Fd_{red} (E_m = −387 mV) (Katsyv et al. 2023a), this reaction theoretically provides enough energy to allow the buildup of an ion gradient across the membrane (Schuchmann and Müller 2014; Öppinger et al. 2022). In the last step, the methyl-group is transferred from THF to the cobalt center of the corrinoid iron-sulfur protein (CFeSP) by a methyltransferase (Figure 1, F; Ragsdale and Pierce 2008). As mentioned above, the carbonyl-branch is a lot shorter and results in CO. For this, a second CO_2 has to be fixed by the CODH through the reduction of CO_2 to CO (E_0' = −540 mV; Ragsdale and Kumar 1996).This reaction requires Fd_{red} (Em = −387 mV; Katsyv et al. 2023a). Afterwards, the methyl-group merges with CO, which had been produced through the carbonyl-branch. This reaction is catalyzed by the bifunctional carbon monoxide dehydrogenase/acetyl-CoA synthase (CODH/ACS; Figure 1, G; Ragsdale and Kumar 1996). Next, the methyl-group from the methyl-branch and the CO from the carbonyl-branch are merged with

coenzyme A (CoA) to produce acetyl-CoA. The generated acetyl-CoA can be used for the generation of biomass (Ljungdahl 1986) or energy conservation by converting it to acetate, thereby gaining 1 ATP through phosphotransacetylase and acetate kinase (Ljungdahl 1986). Overall, the WLP generates acetyl-CoA by the reduction of 2 CO_2 coupled to the oxidation of different redox carriers, transferring a total of 8 electrons and thereby acting as an electron sink (Schuchmann and Müller 2016).

To recapture the Wood Ljungdahl pathway, it requires electron donors such as H_2, Fd_{red} and NADH or NADPH to reduce CO_2 to acetyl-CoA. It requires one ATP, which is regained in the conversion of acetyl-CoA to acetate by acetate kinase (Schuchmann and Müller 2016). To elaborate on how acetogens provide the necessary reducing agents to drive the WLP, conserve energy for biochemical processes and maintain their redox balance, the metabolic pathways of *A. woodii* and *T. kivui* are further explained.

1.3 *Acetobacterium woodii*

A. woodii was first isolated from the black sediment of a marine estuary in 1977 by Balch et al. this organism grows optimal at a temperature of 30 °C and is, therefore, a mesophilic acetogen. The organism grows heterotrophically (Table 1) on mineral medium with glucose, fructose, lactate, glycerate, formate, alcohols, methoxylated aromatic acids or methanol as substrate in the presence of CO_2, as well autotrophically with a H_2/CO_2 and CO (Balch et al. 1977; Braun and Gottschalk 1981; Ljungdahl 1986; Schuchmann and Müller 2014). As an example of the heterotrophic growth of an acetogen, the metabolic pathway of fructose utilization is depicted in Figure 2. The oxidation of fructose through glycolysis provides 4 ATP, 2 CO_2, 2 NADH, and 2 Fd_{red} (Wiechmann et al. 2020).

Since the WLP of *A. woodii* requires H_2, Fd_{red} and 2 NADH for the reduction of 2 CO_2 to acetate and 2 Fd_{red} and 2 NADH are provided by the glycolysis, H_2 has to be produced on a different pathway. The electron bifurcating hydrogenase (Figure 2; Hyd) enables *A. woodii* to reduce H^+ to H_2 by oxidation of Fd_{red} and NADH, so that H_2 is available in the cell for the reduction of CO_2 to formate by the HDCR (Figure 2). The oxidized NAD^+ and Fd_{ox} are then again reduced to NADH and Fd_{red} during glycolysis (Wiechmann et al. 2020; Katsyv et al. 2023b).

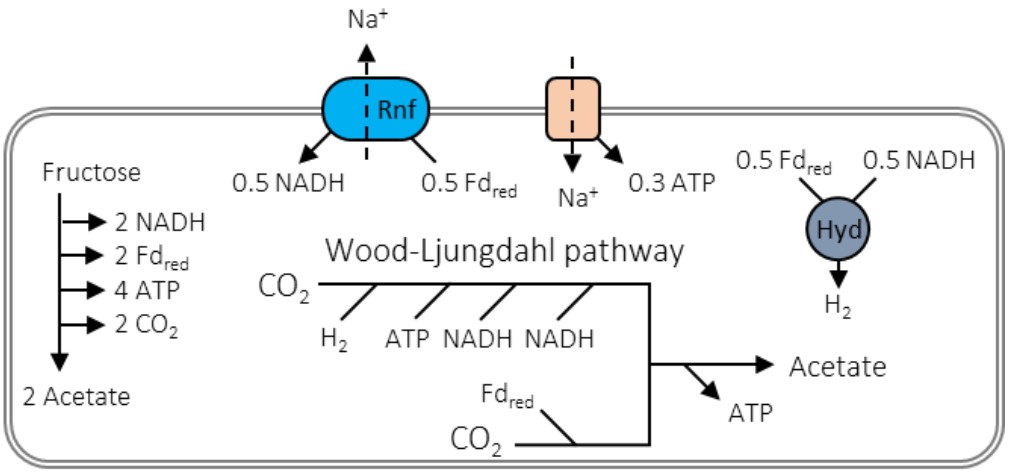

Figure 2 Model of homo-acetogenesis of *A. woodii* based on Westphal et al. (2018).
Shown are the enzymes involved in the metabolic redox balance during growth on fructose. Enzymes involved are the *Rhodobacter* nitrogen fixation complex (blue; Rnf complex), ATP synthase (orange) and the electron bifurcating hydrogenases (gray-blue; Hyd).

In contrast to organotrophic growth on fructose, where ATP is provided through glycolysis (Decker et al. 1970; Fuchs 2017), lithotrophic growth on H_2 and CO_2 requires energy conservation via membrane

bound enzymes (Figure 2; Rnf). These enzymes translocate protons or sodium ions across the membrane from the cytoplasm to the periplasm in order to build up an ion gradient that drives ATP synthase (Hackmann and Firkins 2015; Schoelmerich and Müller 2019; Kuhns et al. 2020). The translocation of ions requires energy, which comes from the exergonic electron transfer between two redox partners catalyzed by the membrane bound enzyme. In acetogens, there are two membrane bound enzymes that perform translocation of ions, the Rnf and the Ech complex. Only one of these two enzymes is present in any acetogen (Rosenbaum and Müller 2021). Representatives of these complexes are the before mentioned *A. woodii*, containing a Rnf complex, and *T. kivui*, containing two energy-converting Echs.

1.4 *Thermoanaerobacter kivui*

Thermoanaerobacter kivui was first described by Leigh et al. (1981) as *Acetogenium kivui* and later renamed after 16S rRNA sequencing (Rainey et al. 1993; Collins et al. 1994). *T. kivui* has a temperature range of 39 to 72 °C (Lehmann et al. 2023), with an optimum at 66 °C, making it a thermophilic acetogen. It grows in a pH range of 5.3 to 7.3. *T. kivui* contains genes for synthesizing all essential vitamins and does not depend on additives such as yeast extract or vitamin solution to grow (Leigh et al. 1981; Hess et al. 2014). Like *A. woodii*, *T. kivui* grows organotrophically by oxidizing hexoses such as glucose, mannose, fructose, pyruvate and formate (Leigh et al. 1981). Furthermore it is able to utilize the sugar alcohol mannitol (Moon et al. 2019). Moreover, it grows autotrophically on H_2/CO_2. *T. kivui* also has genes for CO metabolism and is able to utilize it in cell suspension experiments without adaption. To be able to grow on CO, *T. kivui* requires a longer adaption period (Leigh et al. 1981; Weghoff and Müller 2016; Schwarz et al. 2020).

Depending on the substrate, different metabolic routes conserve energy and maintain the redox balance (Katsyv et al. 2021a). Figure 3 shows the metabolism with four carbon and energy sources that *T. kivui* can utilize; the first one is glucose (Figure 3 A), which is converted through glycolysis and pyruvate oxidation to acetate, providing 4 ATP, 2 NADH, 2 Fd_{red} and 2 CO_2. Similar to *A. woodii*, *T. kivui* has to produce H_2 to reduce CO_2 to formate by the HDCR. Instead of NADH, *T. kivui* requires NADPH for the reduction of methenyl-THF to methylene-THF by the NADPH-dependent methylene-THF dehydrogenase (Figure 1). Furthermore, it is hypothesized that methylenetetrahydrofolate reductases (MetFV) form a complex with the energy-converting hydrogenase (Ech), referred as the Ech-MetFV complex, which is essential for explaining energy conservation in *T. kivui* under autotrophic growth conditions with H_2/CO_2 (Öppinger et al. 2022).

Four enzymes are involved to provide H_2 and NADPH, and to maintain the balance of the redox carriers. First, the transhydrogenase (NfnAB) catalyzes the reduction of 4 $NADP^+$ to 4 NADPH by oxidizing 2 NADH and 2 Fd_{red}, second the electron bifurcating hydrogenase (HydABC) oxidizes 3 NADPH and 3 Fd_{red} to reduce 12 H^+ to 6 H_2. The third is the energy-converting hydrogenase (Ech) oxidizes 5 H_2 to 10 H^+ and reduces 5 Fd_{ox} to 5 Fd_{red}, while utilizing the electrochemical membrane potential in the form of a proton gradient ($\Delta\mu_{H+}$). The fourth enzyme, ATP synthase, translocates protons out of the cell by consuming ATP to maintain the proton gradient (Hess et al. 2014; Katsyv et al. 2021a). The ATP synthase has an assumed H^+/ATP stoichiometry of 3.6 and it is assumed that Ech translocates one proton per redox reaction (Katsyv and Müller 2022). Therefore, the reduction of Fd_{ox} to Fd_{red} by Ech requires H_2 and one H^+ (≈ 0.28 ATP), while a maximum of 1.38 ATP is required for glucose metabolism to maintain the proton gradient, only 2.62 ATP are generated in the glucose metabolism (Katsyv et al. 2021a). However, it is assumed that the Ech-MetFV complex translocates protons out of the cell so that the amount of ATP required could be lower, but this has yet to be verified.

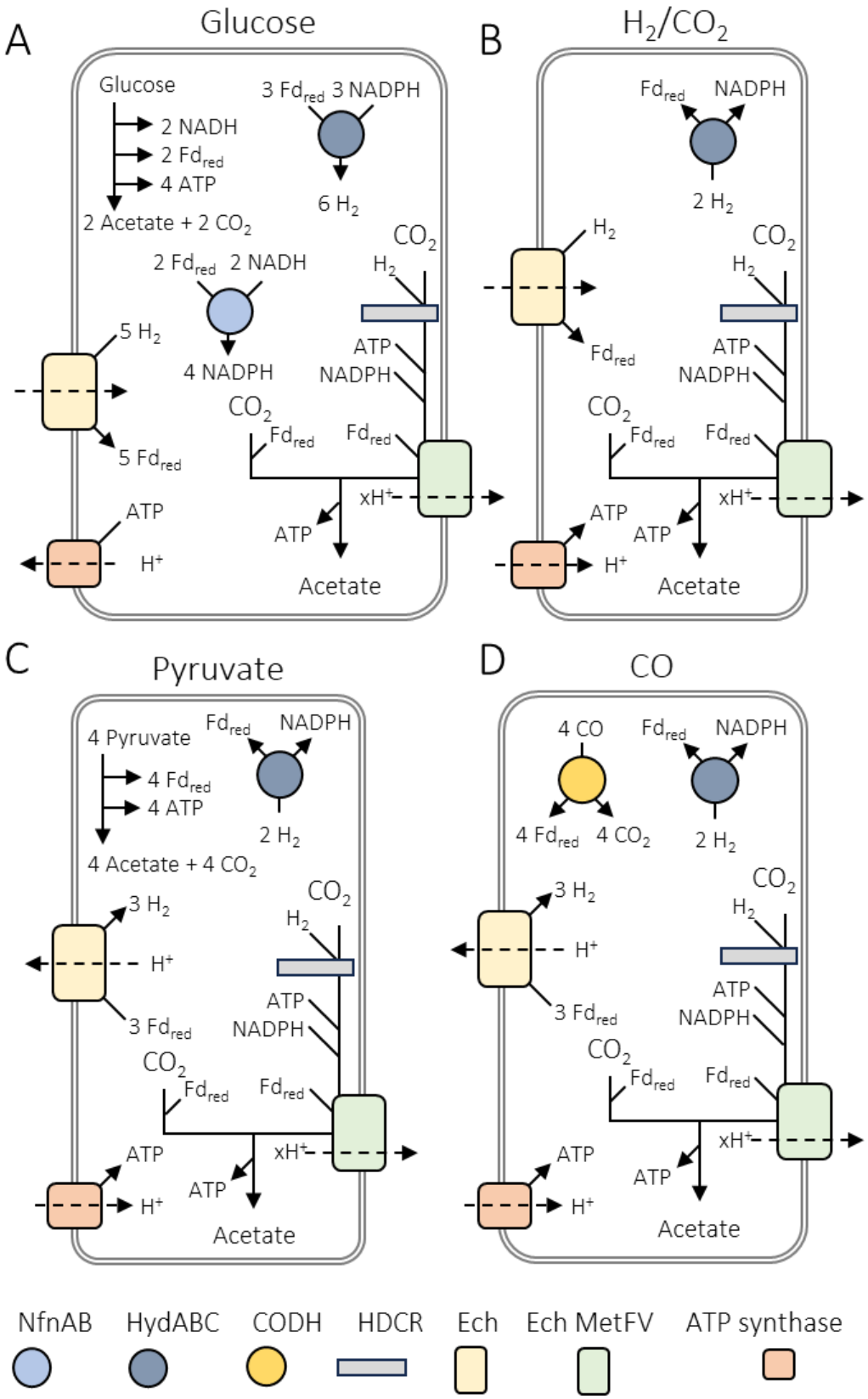

Figure 3 Model of acetogenesis in *Thermoanaerobacter kivui* based on Katsyv et al. (2021a).
Shown are the metabolic pathways for the utilization of glucose (A), H_2/CO_2 (B), pyruvate (C) and CO (D). Enzymes involved in the redox metabolism are an electron bifurcating transhydrogenase (NfnAB; light blue), an electron bifurcating hydrogenase (HydABC; blue-gray), a carbon monoxide dehydrogenase (CODH; yellow), a hydrogen dependent carbon dioxide reductase (HDCR; light gray), two energy converting hydrogenases (Ech1/Ech2; light yellow and Ech MetFV; light green) and an ATP synthase (light orange).

The second substrate for which the metabolic pathway is described in Figure 3 (B) is H_2/CO_2. The model suggests that some enzymes of the WLP (Ech, HydABC and the ATP synthase) are involved in the utilization of H_2/CO_2. According to Katsyv et al. (2021a) the HydABC oxidizes 2 H_2 to 4 H^+ while reducing $NADP^+$ to NADPH and Fd_{ox} to Fd_{red}, which are required for the WLP. Additionally, the Ech oxidizes H_2 to reduce Fd_{ox} to Fd_{red} for the WLP, translocating one proton in the cell. Since, as mentioned above, ATP must be generated to enable further metabolic processes, it is assumed that Ech-MetFV translocates protons out of the cell. However, under these conditions, the Ech-MetFV complex must translocate more than one proton to enable ATP synthase (Katsyv et al. 2021a).

Pyruvate (Figure 3 C) and CO (Figure 3 D) are Fd-dependent substrates. While the utilization of pyruvate provides Fd_{red} and CO_2 through pyruvate:ferredoxin oxidoreductase (Katsyv et al. 2021b) and ATP through acetate kinase (Hess et al. 2014; Fuchs 2017), CO provides Fd_{red} through the oxidation of CO by a CODH (CooS*; Jain et al. 2021*). Since the WLP requires H_2 and NADPH, both pathways reduce 6 H^+ to 3 H_2 by oxidizing 3 Fd_{red} through an Ech complex, translocating 3 protons outside the cell. To reduce $NADP^+$ to NADPH and Fd_{ox} to Fd_{red}, 2 H_2 are oxidized by the HydABC. The reduced electron carriers provided are used in the WLP to reduce CO_2 to acetate. An additional proton is translocated from the Ech-MetFV complex resulting in a total of four protons outside the cell. These protons are then utilized by the ATP synthase to produce 1.11 ATP (Katsyv et al. 2021a). For pyruvate, the ATP yield is slightly higher compared to CO, as ATP is additionally provided by acetate kinase.

In the following chapters, the mentioned enzymes Ech (Ech1 and Ech2), HydABC and NfnAB as well as the genetic system of *T. kivui* developed by Basen et al. (2018) are described in more detail.

1.5 Energy conservation in acetogens

Aerobic and anaerobic microorganisms contain membrane bound respiratory enzymes involved in energy metabolism (Ville and Wikström 2021). Under aerobic conditions, respiratory oxidases reduce dioxygen to water (O_2/H_2O; $E_{m,7}$ = + 815 mV; $E_{m,7}$ = redox midpoint potential at pH 7 relative to the normal hydrogen electrode; Ville and Wikström 2021) while translocating protons to generate a proton motive force ($\Delta\mu_{H+}$) used by an ATP synthase to synthesize ATP. An electron donor for the reduction of O_2 to H_2O can be NADH, which is oxidized to NAD^+ (NADH/NAD^+ [$Em_{,7}$ = -320 mV]) by a nitric oxide reductase or a NADH:ubiquinone oxidoreductase, whereby quinone is reduced as an intermediate electron carrier. The reduced quinone is then oxidized by an oxidase and O_2 is reduced to H_2O (Ville and Wikström 2021).

Under anaerobic conditions, also a proton ($\Delta\mu_{H+}$) or sodium motive force ($\Delta\mu_{Na+}$) is generated and used for ATP synthase, but with other electron acceptors than O_2. Exemplary anaerobic respiratory mechanisms are fumarate (Kröger et al. 2002), nitrite and nitrate (Cole and Richardson 2008) and sulfate respiration (Keller and Wall 2011; Fuchs 2017; Ville and Wikström 2021). In acetogens and methanogens, two respiratory enzyme complexes are known to be involved in energy conservation, the *Rhodobacter* nitrogen fixation complex (Rnf) or the energy-converting hydrogenase (Ech) complex (Li et al. 2006; Welte et al. 2010a; Schuchmann and Müller 2014; Rosenbaum and Müller 2021).

1.5.1 *Rhodobacter* nitrogen fixation complex (Rnf complex)

Rhodobacter nitrogen fixation (Rnf) genes were first described by Schmehl et al. (1993) for *Rhodobacter capsulatus*, using DNA sequence analysis, secondary structure predictions, and generation of *rnf* mutants. They assumed that the Rnf complex is membrane bound, contains [4Fe-4S] cluster, and is involved in the electron transfer to nitrogenase, thus being required for nitrogen fixation (Schmehl et al. 1993).

Genes similar to *rnf* genes of *Rhodobacter capsulatus* were found in the acetogen *Acetobacterium woodii* (Müller et al. 2008; Biegel and Müller 2010) and *Clostridium ljungdahlii* (Köpke et al. 2010; Tremblay et al. 2012), and in the methanogen *Methanosarcina acetivorans* (Li et al. 2006). In these organisms, Rnf complexes differ in their redox partner and in the ions they translocate. The Rnf complex of *M. acetivorans*, for example, is coupled to a heterodisulfide reductase (Hdr). Here, Rnf oxidizes Fd_{red} to reduce the inner membrane electron carrier methanophenazine. The reduced methanophenazine is then oxidized to reduce heterodisulfide (CoM-S-S-CoB) through the Hdr (Schlegel et al. 2012b). During this process, both Na^+ and H^+ ions are independently translocated out of the cell to establish a sodium and proton motive force through the cooperative Rnf and Hdr (Schlegel et al. 2012a; Schlegel et al. 2012b). The established sodium and proton motive force drives the ATP synthase of *M. acetivorans*, which, under physiological conditions, is coupled to the translocation of Na^+ and H^+ ions across the membrane (Schlegel et al. 2012a; Schlegel et al. 2012b). Deletion of *rnf* in *M. acetivorans* resulted in the inability to oxidize reduced ferredoxin and thus also the reduction of inner membrane carrier methanophenazine by the Rnf complex, which in turn would transfer its electrons to heterodisulfide by the Hdr. Therefore, the deletion of the Rnf complex led to the inability to translocate Na^+ and H^+ and conclusively, it was no longer capable of growth on acetate (Schlegel et al. 2012b).

In contrast to *M. acetivorans*, *C. ljungdahlii* has a Rnf complex to build up a proton motive force, which an ATP synthase utilizes for ATP synthesis. In addition, the Rnf complex of *C. ljungdahlii* reduces NAD^+ to NADH during the oxidation of Fd_{red} instead of an inner membrane electron carrier (Köpke et al. 2010; Tremblay et al. 2012). A *rnf* deletion mutant was no longer able to grow with H_2/CO_2 or produce ATP in cell suspensions with H_2 as an electron donor and CO_2 as an electron acceptor (Tremblay et al. 2012). In addition to that, organotrophic growth was slightly impaired, as evidenced by a lower growth rate and reduced ATP production when fructose was used in growth and cell suspension experiments (Tremblay et al. 2012). The Rnf complex of *A. woodii* was the first biochemically characterized Rnf complex (Müller et al. 2008) that oxidizes Fd_{red} to reduce NAD^+ to NADH and translocate Na^+ ions instead of protons out of the cell to establish a sodium motive force (Imkamp et al. 2007; Biegel and Müller 2010; Kuhns et al. 2020). One of the first studies regarding the sodium dependency of *A. woodii* by Heise et al. (1989) showed that the sodium concentration has a direct influence on heterotrophic and autotrophic growth. At the same time, biochemical evidence was provided for the presence of a sodium pump in acetogens, which was later identified as the Rnf complex (Heise et al. 1989; Imkamp et al. 2007). Deletion of the Rnf complex in *A. woodii* led to inability to grow autotrophically on H_2/CO_2, and resting cells showed a significant reduction in acetate production. No ATP was synthesized with H_2/CO_2 in the headspace, leading to the conclusion that the Rnf complex is essential for the utilization of H_2/CO_2 (Westphal et al. 2018). Furthermore, deletion of the Rnf complex did not appear to be essential for organotrophic growth on fructose, but the mutant showed a biphasic growth pattern on complex medium and reduced acetate production. In addition to the described phenotypes, low-energy substrates such as ethanol or lactate were only utilized in the presence of H_2, indicating an imbalance of reducing agents during growth at the thermodynamic limits (Westphal et al. 2018).

1.5.2 Energy-converting hydrogenase (Ech) complex

Hydrogenases are a large and diverse group of enzymes found in a variety of microorganisms. Vignais and Billoud (2007) categorized them depending on the transition metal into three groups: [Fe], [FeFe] and [NiFe] hydrogenases. Since the [NiFe] hydrogenases are the most numerous and diverse of the three groups, it was further subdivided into subgroups from 1 to 4 depending on their subunit composition and functionality (Vignais and Billoud 2007).

In acetogens and methanogens, energy-converting membrane-bound enzymes are [NiFe]-hydrogenase belonging to group 4 (H_2-evolving, energy-converting, membrane-associated hydrogenases; Vignais and Billoud 2007). Representatives of methanogens containing energy-converting hydrogenases are *Methanosarcina barkeri* and *Methanosarcina mazei*. *M. barkeri* has an energy-converting [NiFe]-hydrogenase (Ech), which has been suggested to produce H_2 and, therefore, an intermediate step in methanogenesis from acetate (Künkel et al. 1998; Meuer et al. 1999). Genetic analysis of *M. barkeri* revealed that Ech is able to reversibly reduce ferredoxin by oxidizing H_2, whereby a proton motive force is built up or consumed (Meuer et al. 2002; Kulkarni et al. 2018). An *ech* deletion mutant of *M. barkeri* was unable to grow on acetate or autotrophically on H_2/CO_2. Thus, the Ech complex has an essential role in methanogenesis on acetate and H_2/CO_2 (Meuer et al. 2002).

M. mazei also contains a functionally similar Ech complex as described for *M. barkeri* and enables the formation of H_2 by oxidation of reduced ferredoxin and the translocation of protons (Welte et al. 2010a; Welte et al. 2010b). Deletion of *ech* in *M. mazei* resulted in a strain that was unable to grow on acetate as the sole energy source. Furthermore, inverted vesicles of the *M. mazei* mutant, which contained all essential membrane-bound enzymes involved in energy conservation except Ech, did not show H_2 formation, whereas inverted vesicles of the wild type did (Welte et al. 2010b). Moreover, it was shown that the Ech complex translocates protons, whereas the ATP synthases also used only protons for ATP synthesis and no sodium ions. This had previously been described for the ATP synthase of *M. acetivorans* and *A. woodii* (Imkamp et al. 2007; Welte et al. 2010b; Schlegel et al. 2012b). Thus, like the Rnf complex, the Ech hydrogenases of *M. barkeri* and *M. mazei* are essential for the respective microorganisms, as they enable energy conservation by generating an ion motive force. At the same time, the metabolic redox balance between metabolically involved reducing agents is maintained.

Genome sequencing by Hess et al. (2014) revealed that *T. kivui* harbors two membrane-bound energy-converting hydrogenases Ech1 and Ech2 (Figure 4), belonging to group 4 of [NiFe]-hydrogenases (Vignais and Billoud 2007; Schoelmerich and Müller 2019). The analysis suggests that both Ech's have cofactors and catalytic domains required for proton (H^+) reduction to H_2 and ferredoxin oxidation and reduction while translocating protons over the membrane. However, on the amino acid level the identity of subunits between the two enzymes differs from 8 to 50 % (Hess et al. 2014). Since the first categorization of these hydrogenases, the group 4 of the [NiFe]-hydrogenases has been further divided into nine subgroups (Schoelmerich and Müller 2020).

Experiments by Schoelmerich and Müller (2019) with inverted membrane vesicles of *T. kivui* cells grown on CO revealed that Ech activity led to the translocation of H^+ and Na^+ ions across the cell membrane. The translocation of H^+ and Na^+ ions led to the assumption that both Ech complexes have the functionality of a Na^+/H^+ antiport. A comparison of the Ech subunits of *T. kivui* with corresponding subunits of other related complexes supported this assumption. It was revealed that the membrane-integral subunits of both Ech complexes have a high similarity in amino acid sequence to a Na^+/H^+ antiport (Schoelmerich and Müller 2019). The same study also showed that the ATP synthase only uses a proton and not a sodium gradient for ATP synthesis. Furthermore, transcriptional analysis of *T. kivui* grown on glucose, H_2/CO_2 or CO showed that the gene clusters of *ech1* and *ech2*, were strongly upregulated with H_2/CO_2 and CO compared to glucose. Expression levels were even more increased with CO than with H_2/CO_2. This upregulation of these two hydrogenases under CO probably promotes the adaptation to CO (Schoelmerich and Müller 2019). According to Schoelmerich and Müller (2020), the Ech1 complex belongs to group 4c, which contains CO-oxidizing energy-converting hydrogenases. The

Ech2 complex has been assigned to group 4g based on genomic predictions. It is thought to catalyze electron transfer from Fd_{red} to H^+ and the translocation of H^+ (Hess et al. 2014).

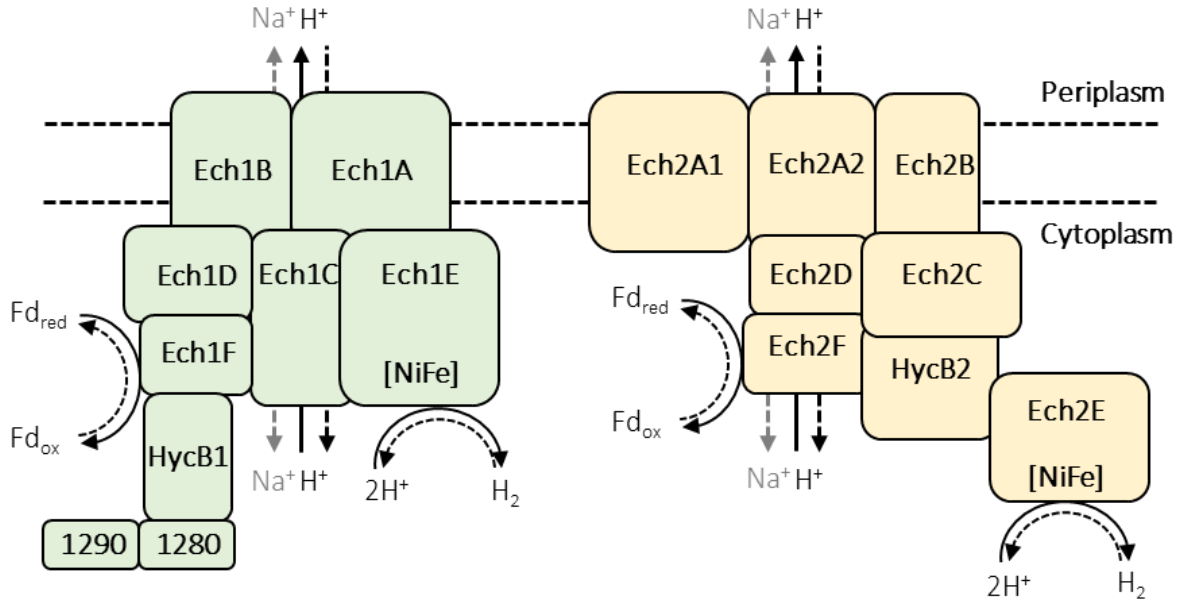

Figure 4 Model of the complexes Ech1 and Ech2.
Both Echs are able to reduce protons (H^+) by oxidizing ferredoxin (Fd_{red}) (black; continuous line) or reduce ferredoxin (Fd_{ox}) by oxidizing H_2 (black; dashed line), and thereby translocating protons (H^+) and sodium ions (Na^+) across the membrane (Schoelmerich and Müller 2019; Katsyv and Müller 2022).

While the function of the Ech1 complex in the metabolic system remains uncertain, it has been shown that Ech2 is able to build up an H^+ potential by oxidizing Fd_{red} and is thus probably involved in an energy-saving process in which only one H^+ is transferred by electron transfer (Katsyv and Müller 2022). Furthermore, it is suggested that methylene tetrahydrofolate reductase (MetFV) may interact with an Ech complex to oxidize Fd_{red} and reduce methylene tetrahydrofolate (H_2C-THF) to methyl tetrahydrofolate (H_3C THF; Öppinger et al. 2022).

1.6 Electron bifurcating hydrogenase and transhydrogenase

As mentioned above, the WLP of *T. kivui* requires the reduced electron carriers H_2, NADH, NADPH and Fd_{red} to reduce CO_2. To provide these, acetogens have an electron bifurcating hydrogenase HydABC and an electron bifurcating transhydrogenase NfnAB. These enzymes couple endergonic and exergonic redox reactions to provide the necessary redox agents, in particular, NAD(P)H and Fd_{red} from H_2 by the HydABC complex or NADPH form NADH and Fd_{red} by the NfnAB complex (Buckel and Thauer 2013; Peters et al. 2016; Wiechmann et al. 2020; Katsyv et al. 2023b).

Genomic analysis revealed that *T. kivui* (Hess et al. 2014) contains an electron bifurcating hydrogenase (Hyd) and an electron bifurcating transhydrogenase (Nfn). The transhydrogenase has two subunits, subunit A and B encoded by the genes TKV_c22270 (*nfnA*) and TKV_c22280 (*nfnB*). Both subunits together form the NfnAB complex. The electron bifurcating hydrogenase HydABC has the subunits A, B and C encoded by the genes TKV_c19580 (*hydA1*), TKV_c19590 (*hydB*) and TKV_c19600 (*hydC*) (Hess et al. 2014; Katsyv et al. 2023b). Both enzymes are thought to be important for heterotrophic growth on hexose and sugar alcohol (mannitol), while the HydABC is additionally required for autotrophic growth (Katsyv et al. 2021a).

1.6.1 Electron bifurcating transhydrogenase (NfnAB)

The electron bifurcating transhydrogenase (NfnAB) couples an endergonic and an exergonic redox reaction. This allows the endergonic reduction of NADPH by oxidation of NADH to be coupled to the exergonic reduction of NADPH by oxidation of Fd_{red} (Figure 5).

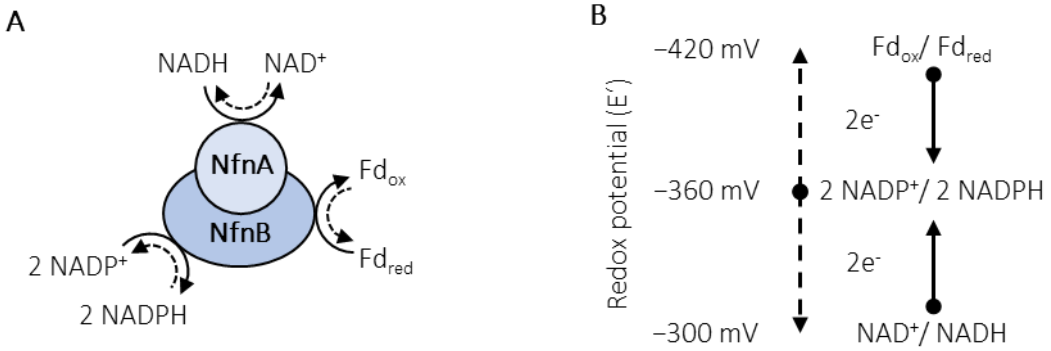

Figure 5 Model of the electron bifurcating transhydrogenase NfnAB.
A NfnAB catalyzes the oxidation of 2 NADPH and simultaneous reduction of NAD^+ and Fd_{ox} and vice versa. B Proposed electron flow of $NADP^+$/NADPH reduction and oxidation by NfnAB from *Clostridium kluyveri*. Model based on Wang et al. (2010).

Deletion mutants of the NfnAB complexes are rarely described in the literature. However, the first successful deletion of *nfnAB* was done by Lo et al. (2015) in *Thermoanaerobacterium saccharolyticum*. However, the deletion of the NfnAB complex did not result in any inhibition of growth, only in a decreased product yield, yet it demonstrated the need for electron transfer between redox agents for further metabolic reactions (Lo et al. 2015). The gene sequence of the *nfnA* and *nfnB* subunits of *T. saccharolyticum* is similar to those of *T. kivui*. Meaning, the gene sequence of subunit A of *T. saccharolyticum* (Tsac2086) shows a 64 % match with *T. kivui* (TKVc22270) and a 73 % match for subunit B (Tsac2085 vs. TKVc22280) based on the amino acid sequence (Lo et al. 2015). In contrast, P*yrococcus furiosus* has two distinct NADH-dependent ferredoxin $NADP^+$ oxidoreductases, NfnI and Xfn (Nguyen et al. 2017). Both enzymes are similar in function to the NfnAB complex of *T. kivui*. However, Xfn requires a not yet determined redox partner instead of NADH. The deletion mutants of *nfnI* and *xfn* showed a decreased growth in maltose sulfur medium, sulfur medium, or minimal peptide sulfur medium compared to the wild type (Nguyen et al. 2017). Therefore, it was concluded that NfnI and Xfn are crucial in *P. furiosus* to maintain the redox balance during sulfur and peptide metabolism. This indicates that the NfnAB and Nfn-like enzymes are important for the electron transfer between NADH/NAD^+, Fd_{red}/Fd_{ox} and NADPH/$NADP^+$ and therefore possibly vital to maintain balance.

1.6.2 Electron bifurcating hydrogenases HydABC

One of the first electron bifurcating hydrogenases (Hyd) was described in the late 2000s by Schut and Adams (2009) from the anaerobic, hyperthermophilic bacterium *Thermotoga maritima*. This [FeFe]-hydrogenase and is considered essential for the metabolic redox balance with regard to the regeneration of NAD^+ and Fd_{ox} by oxidation of H_2. Furthermore, it is suggested that it mainly evolves H_2, using the reducing agents Fd_{red} and NADH, which are reduced during glucose oxidation (Vignais and Billoud 2007; Schut and Adams 2009).

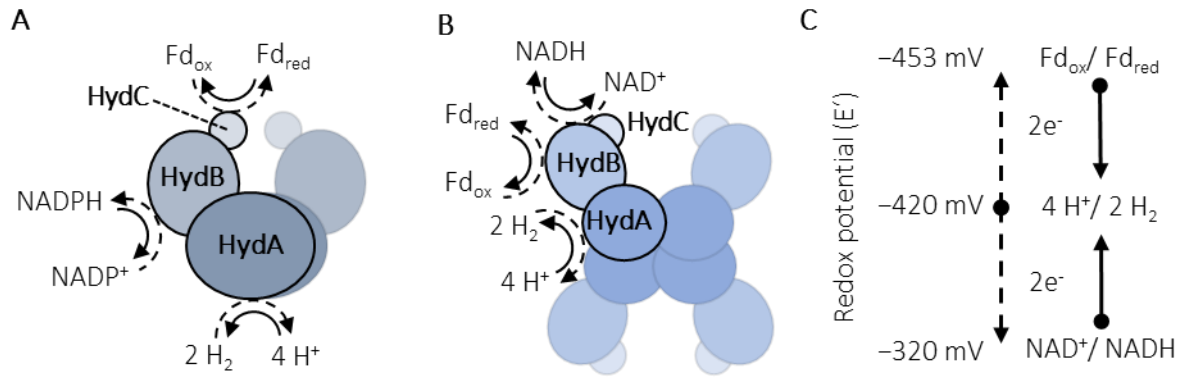

Figure 6 Model of electron bifurcating hydrogenases (HydABC) of *T. kivui* and *T. maritima*.
The HydABC of *T. kivui* (A) consists of a homodimer of heterotrimers (HydA, B and C) catalyzing the reversible oxidation of 2 H_2 and reduction of $NADP^+$ to NADPH and Fd_{ox} to Fd_{red}. The HydABC of *T. maritima* (B) consists of a homotetramer of heterotrimers (HydA, B and C) catalyzing the reversible oxidation of 2 H_2 and reduction of NAD^+ to NADH and Fd_{ox} to Fd_{red}. (C) Proposed electron flow of reduction of H_2 through oxidation of Fd_{red} and NADH (Schut and Adams 2009).

Several biochemical studies demonstrated the functionality of electron bifurcating hydrogenases. Activity assay of a His-HydABC of *T. kivui* demonstrated that H_2 was produced when NADPH and Fd_{red} were present (Figure 6 A). However, no H_2 was produced when NADH and Fd_{red} were used in the assay, proving that the HydABC of *T. kivui* is exclusively NADPH dependent. (Katsyv et al. 2023a; Katsyv et al. 2023b). In contrast, the HydABC of *T. maritima* showed NADH-dependency and H_2 formation occurred when NADH and Fd_{red} were present as electron donors in an assay (Figure 6 B; Schut and Adams 2009; Furlan et al. 2022). Also, the HydABCD of *A. woodii* showed a reduction of NAD^+ to NADH and Fd_{ox} to Fd_{red} if H_2 is present and that NAD^+ can only be reduced with Fd_{ox} in a stoichiometric ratio of 1 to 1 (Schuchmann and Müller 2012).

Deleting parts of the HydABCD complex of *A. woodii* inhibited growth while growing organotrophically. In contrast, growth was restored under mixotrophic growth conditions or when formate in addition to a sugar. Yet growth on H_2/CO_2 was not possible without the HydABCD. Therefore it was concluded that the HydABCD is required for internal hydrogen production during growth on an organic substrate and the reduction of NAD^+ and Fd_{ox} (Wiechmann et al. 2020).

The sulfate reducer *Solidesulfovibrio fructosivorans* (formerly *Desulfovibrio fructosovorans)* contains a [FeFe]-hydrogenase Hnd encoded by the *hndD* gene (Malki et al. 1997; Kpebe et al. 2023), now classified as electron bifurcating hydrogenase (Kpebe et al. 2023). Deletion of this hydrogenase resulted in reduced growth on fructose, pyruvate or lactate (Malki et al. 1997). Decades later, the strain SM4 (Δ*hndD*) was further studied by Kpebe et al. (2023). It has been shown that SM4 is not able to grow on ethanol, whereas the wild type is. It is hypothesized that the electron carriers NADH and Fd_{red}, which are reduced during the oxidation of ethanol to acetate, cannot be re-oxidized, leading to a metabolic redox imbalance. Another hypothesis is that the absence of Hnd prevents the formation of H_2, which may be necessary for sulfate respiration (Kpebe et al. 2023).

Therefore, electron bifurcating hydrogenases are essential for maintaining the metabolic redox balance by oxidation or reduction of reducing agents in these organisms. Additionally, electron bifurcating hydrogenase and transhydrogenase are probably directly involved under mixotrophic growth conditions, enabling growth by maintaining a balance between all involved redox carriers.

1.6.3 Genetic modification of *Thermoanaerobacter kivui*

Genetic modification of a microorganism is an important way to study metabolic pathways, optimize production yields of desired products or implement genes to produce a different product. Numerous *Thermoanaerobacter* species have been described as naturally competent for foreign DNA uptake and are used as model organisms, to study metabolic pathways or bioengineering applications (Shaw et al. 2010; Zeldes et al. 2015). Based on already existing genetic tools, developed for *Thermococcus kodakaraensis* (Sato et al. 2003) and *Caldicellulosiruptor bescii* (Lipscomb et al. 2016), a genetic system for *T. kivui* was developed by Basen et al. (2018). The genetic system is based on the disruption of the pyrimidine biosynthesis pathway by enforcing a deletion of the *pyrE* gene encoding orotate phosphoribosyltransferase or the *pyrF* gene encoding orotidine 5'-phosphate decarboxylase. For this purpose, cells were cultivated in the presents of 5-fluoroorotic acid/5-fluoroorotate (5-FOA). This substance, if utilized by one of the mentioned enzymes, is converted to 5-fluorouracil, which is a cytotoxin that leads to cell death. This selective pressure and natural occurring mutations may lead to the disruption of *pyrE* or *pyrF* in the organism. The resulting deletion mutants are uracil auxotrophs (Jund and Lacroute 1970; Krooth et al. 1979). To bypass the loss of *pyrE* or *pyrF*, uracil is added to the medium (Zeldes et al. 2015; Basen et al. 2018).

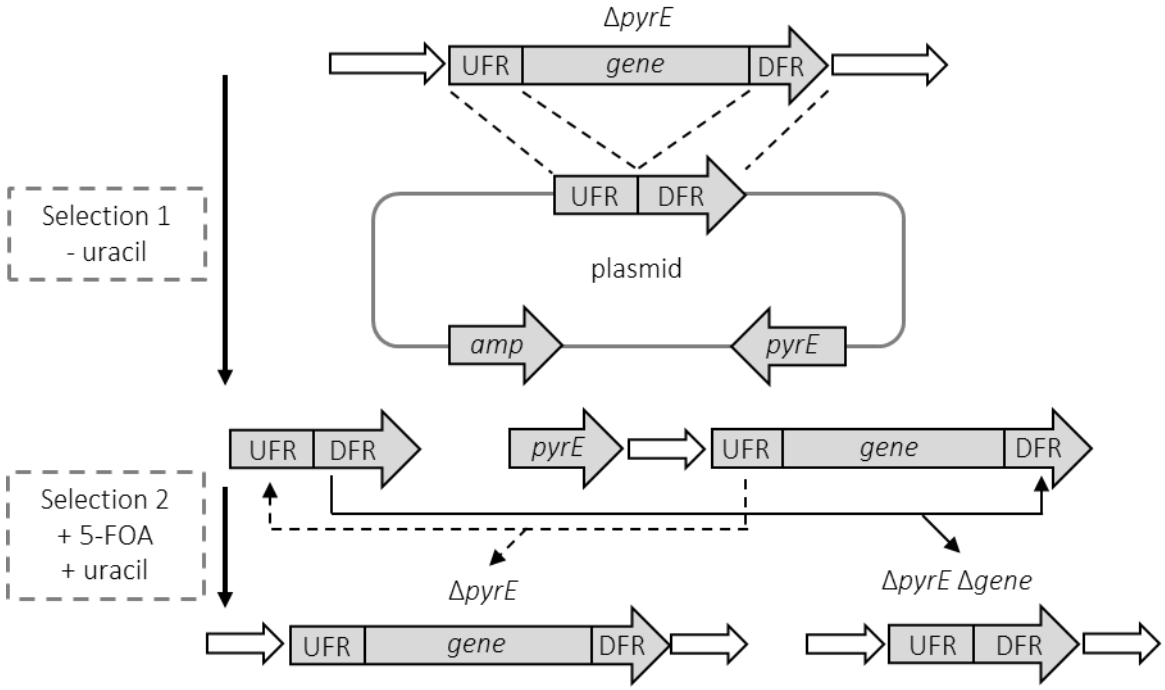

Figure 7 Visualization of the schematic deletion process in *T. kivui*.
The target gene or gene region in T. kivui was deleted using two independent homologous recombination events. The plasmid designed for this deletion includes the upstream flanking region (UFR), the downstream flanking region (DFR) of the gene of interest, the *pyrE* gene, and an ampicillin resistance gene (*amp*).

The Δ*pyrE* mutant strain of *T. kivui* (TKV002) was generated using a plasmid based on the pMU131 (Shaw et al. 2010; Basen et al. 2018). The plasmid pMU131 is a replicating shuttle plasmid containing genes for ampicillin resistance (Amp^r) for the selection in *Escherichia coli* and a thermostable kanamycin resistance gene (Kan^r). Furthermore, the plasmid has the pUC origin of replication in *E. coli*, and a thermostable origin of replication from a native plasmid of *Thermoanaerobacterium saccharolyticum*. The plasmid was modified by integrating upstream and downstream flanking regions of the *pyrE* gene, resulting in the plasmid pMBTkv002b, which allowed homologous recombination at the flanking region of the *pyrE* gene. The integration of the plasmid into the genome resulted in colonies of *T. kivui* that

were resistant to kanamycin (Kan^r). Transformants of *T. kivui* with pMBTkv002b were grown in the presence of 5-FOA and uracil to select for loss of the *pyrE* gene, the resulting Δ*pyrE* strain was named TKV002 (Basen et al. 2018).

For the generation of further deletion mutants, plasmids are required to contain the *pyrE* gene for reintegration, as well upstream and downstream flanking regions of the gene of interest (Figure 7). Subsequently, a two-step selections process is performed. First, the constructed plasmid is added to the growing cells of the Δ*pyrE* mutant. First, through a homologous recombination event the plasmid integrates into the genome of the mutant. The mutant is then able to grow on defined medium without uracil, due to the reintroduced *pyrE* gene. In the second selection step, cells from the first selection are cultivated in the presence of 5-FOA and uracil. Due to the mentioned selective pressure thought 5-FOA, the cells need to lose the inserted *pyrE* gene. As a result, a second homologous recombination event occurs, which may lead to deletion of the gene of interest and the *pyrE* gene (Figure 7). Thus, the Δ*pyrE* strain (TKV002) enables a markerless deletion of genes, as demonstrated for *fruk* (TKVc23150; 1-phosphofructosekinase; Basen et al. 2018) or the gene cluster encoding the HDCR (TKVc19990-19960) (Jain et al. 2020).

1.7 Aim of the thesis

As *Thermoanaerobacter kivui* gains importance in industrial applications, understanding its metabolic mechanisms, especially those involved in energy conservation and redox balance, becomes crucial. Despite its potential, several aspects of *T. kivui*'s metabolism remain unexplored, even though it is increasingly established as a model organism for thermophilic acetogens. This thesis aims to contribute to filling these gaps in knowledge.

The primary objective of my research was to investigate the metabolic function of both energy-converting hydrogenase complexes (Ech1 and Ech2) in *T. kivui*. To achieve this, I focused on generating deletion mutants for the genes encoding the Ech complexes and subsequent investigation of potentially resulting phenotypes and metabolic relevance. This investigation involved a series of growth experiments, resting cell experiments and gene expression studies.

Additionally, I aimed to gain a deeper understanding of the mixotrophic growth of *T. kivui,* especially considering that H_2 serves as an important intermediate and electron carrier. H_2 is used or produced by the hydrogenases, consequently affecting energy and redox metabolism of the metabolic system. To explore this aspect of my thesis, I conducted growth experiments with various substrates in the presence of H_2, accompanied by qPCR analyses and RNA sequencing, to determine changes due to the different growth conditions.

Finally, the thesis also investigates the NfnAB complex, which is known for its role in electron transfer between electron carriers in other microorganisms, to study its function in the catabolism of *T. kivui* on different substrates. I aimed to create a deletion mutant of the NfnAB complex genes and characterize this mutant through growth and resting cell experiments. In addition, qPCR analyses should determine how gene expression changes as a result of the deletion of the NfnAB complexes.

2 Material and Methods

2.1 Organisms

Microbial strains used in this study were provided by the research group (Microbiology, University of Rostock) or generated throughout this study (Table 2).

Table 2 Microorganisms used in this study.

Strain	Genotype	Reference
Thermoanaerobacter kivui DSM 2030	Wild type	Leigh et al. (1981)
Thermoanaerobacter kivui TKV_MB002	Δ*pyrE*	Basen et al. (2018)
Thermoanaerobacter kivui TKV_MB050 (Δ*ech2*)	Δ*pyrE* Δ*ech2* (Tkv_c19670 to Tkv_c19760)	This study
Thermoanaerobacter kivui TKV_MB144(P_{frc}*ech1*)	Fructose promoter exchange *ech1* promoter *pyrE* under control of gyrase promoter	This study
Thermoanaerobacter kivui TKV_MB52 (P_{frc}*ech1*Δ*ech2*)	Δ*ech2*, fructose promoter exchange Ech1 promoter, *pyrE* under control of gyrase promoter	This study
Thermoanaerobacter kivui TKV_MB60 (WT_CO1)	DSM 2030 adapted to CO	This study
Thermoanaerobacter kivui TKV_MB55 (Δ*nfnB*)	Δ*nfnB* (TKV_c22280), *pyrE* under control of gyrase promoter	This study
Escherichia coli DH5α	F, Φ80lacZΔ*M15*, *endA1*, *recA1*, *hsdR17*(r_k-m_k-), *supE44*, thi-1, λ-, *gyrA96*, *relA1*, Δ(*lacZYAargF*) U196	Hanahan (1983)

2.2 Medium composition, supplements and substrates

2.2.1 Chemicals

All chemicals used in this study were obtained from either one of the following companies: AppliChem GmbH (Darmstadt, Germany), Carl Roth GmbH + Co.KG (Karlsruhe, Germany), Fisher Scientific GmbH (Schwerte, Germany), Merck KGaA (Darmstadt, Germany) and Sigma-Aldrich Chemie GmbH (Merck KGaA).

2.2.2 Gasses

The gasses and gas mixtes Nitrogen (N_2), Protadur (CO_2/N_2; 20/80; v/v), H_2/CO_2 (66.6/33.3; v/v) and forming gas (H_2/N_2; 5/95; v/v) were purchased form Westfalen AG (Münster, Germany). Carbon monoxide (CO) gas was purchased form Linde GmbH (Pullach, Germany).

2.2.3 Medium for *Thermoanaerobacter kivui* cultivation

T. kivui was grown in carbonate buffered, anoxic defined medium without yeast extract or complex medium containing yeast extract (Table 5) modified after Leigh et al. (1981). The medium was prepared according to the procedure used by Hungate (1969). For the *T. kivui* medium, phosphate solution (500 mM $Na_2HPO_4 \cdot 2\ H_2O$, 500 mM $NaH_2PO_4 \cdot 2\ H_2O$, 12.6 mM K_2HPO_4, 16.2 mM KH_2PO_4), sulfate solution (167 mM $(NH_4)_2SO_4$, 36.6 mM $MgSO_4 \cdot 7\ H_2O$, 0.72 mM $FeSO_4 \cdot 7\ H_2O$) and chloride solution (759 mM NaCl, 579 mM NH_4Cl) were prepared with deionized water and stored at 4 °C. The $CaCl_2$ stock solution (0.42 mM $CaCl_2 \cdot 2H_2O$) was stored at room temperature.

Trace element solution DSMZ141 (Table 3) used for the medium of *T. kivui* (Table 3) was prepared by first resolving nitrilotriacetic acid in deionized water. The pH was adjusted to 6.5 with KOH, other trace

elements were added and finally, the pH of the solution was adjusted with KOH to a pH of 7.0. Subsequently, the trace element solution was sterile filtered and stored at 4 °C.

Table 3 Trace elements solution DSM141.

Component	Concentration
Nitrilotriacetic acid	7.85 mM
$MgSO_4 \cdot 7\ H_2O$	12.2 mM
$MnSO_4 \cdot H_2O$	2.96 mM
NaCl	17.2 mM
$FeSO_4 \cdot 7\ H_2O$	0.36 mM
$CoSO_4 \cdot 7\ H_2O$	0.64 mM
$CaCl_2 \cdot 2\ H_2O$	0.68 mM
$ZnSO_4 \cdot 7\ H_2O$	0.63 mM
$CuSO_4 \cdot 5\ H_2O$	40.1 µM
$KAl(SO_4)_2 \cdot 12\ H_2O$	42.2 µM
H_3BO_3	0.16 mM
$Na_2MoO_4 \cdot 2\ H_2O$	41.3 µM
$NiCl_2 \cdot 6\ H_2O$	0.13 mM
$Na_2SeO_3 \cdot 5\ H_2O$	1.14 µM
$Na_2WO_4 \cdot 2\ H_2O$	1.21 µM

The vitamin solution DSM141 (mod.; Table 4) used for the medium of *T. kivui* (Table 5) was prepared, sterile filtered and stored at 4 °C protected from light.

Table 4 Vitamin solution DSM141 (mod.).

Component	Concentration
Biotin	16.4 µM
Folic acid	9.1 µM
Pyridoxin-HCl	97.3 µM
Thiamin-HCl	29.7 µM
Riboflavin	26.6 µM
Nicotinic acid	81.2 µM
Ca-panthothenate	21.0 µM
p-Aminobenzoic acid	72.9 µM
Lipoic acid	48.5 µM
Vitamin B_{12}	147 nM

Table 5 Defined medium and complex medium with yeast extract as the only modification of the defined medium for cultivating *T. kivui*.

Component	Volume/amount per l
Phosphate solution	100 ml
Sulfate solution	10 ml
Chloride solution	10 ml
$CaCl_2$	1 ml
Vitamin solution DSMZ141	5 ml
Trace elements DSMZ141	10 ml
0.1 % resazurin	1 ml
Yeast extract (only complex medium)	2 g
$KHCO_3$	5.4 g
Cystein-$HCl \cdot H_2O$	0.5 g

Alle solutions (Table 5) were mixed and Cysteine-$HCl \cdot H_2O$ and $KHCO_3$ were added shortly before gassing the medium with Protadur (N_2/CO_2; 80 /20; v/v) to remove oxygen dissolved in the medium. After

preparation, either 5 or 10 ml medium were aliquoted into 16 ml-Hungate tubes (Glasgerätebau Ochs, Bovenden, Germany), or into 50, 100 and 200 ml serum bottles (Glasgerätebau Ochs, Bovenden, Germany) with 25, 40, 50 or 100 ml medium, respectively. Alternatively, 250 or 500 ml medium was filled into a 1 l bottle (Schott Ag, Mainz, Germany). To prevent oxygen input during aliquoting, all tubes and bottles were subsequently gassed with a N_2/CO_2 gas mix (Protadur; 80/20; v/v). Hungate tubes, serum bottles and 1 l bottles were sealed with rubber stoppers (Glasgerätebau Ochs Laborfachhandel e.K., Bovenden, Germany), fixed with plastic twist caps or aluminum caps and autoclaved.

2.2.4 Medium for cultivation of *Escherichia coli* cultivation

E. coli DH5α was cultivated in LB medium (lysogeny broth; Bertani 1951. For the preparation of LB plates, 1.5 % agar (w/v) was added. For plates containing antibiotics, 1 ml of ampicillin (50 mg l^{-1}) was added to 500 ml of medium after autoclaving to a final concentration of 100 µg ml^{-1}.

Table 6 Composition of LB medium for cultivation of *E. coli.*

Component	Concentration
tryptone	1 % [w/v]
Yeast extract	0.5 % [w/v]
NaCl	86 mM

For the transformation of *E. coli* DH5α, SOC medium (Table 7) was used.

Table 7 Composition of SOC medium for cultivation of *E. coli.*

Component	Concentration
Tryptone	1 % [w/v]
Yeast extract	0.5 % [w/v]
NaCl	10 mM
KCl	2.5 mM
$MgCl_2$	10 mM
$MgSO_4 \cdot 7\ H_2O$	10 mM
Glucose	20 mM

2.2.5 Antibiotics

Stock solutions of 50 mg ml^{-1} ampicillin (amp) were prepared and sterile filtered. Ampicillin was then added to the autoclaved medium to a final 100 µg ml^{-1} concentration.

2.3 Microbiological methods

If not stated otherwise, heat stable solutions and equipment were autoclaved before use. Solutions sensitive to heat were sterile filtered by using Filtropur V25 sterile filters (SARSTEDT AG & Co. KG, Nümbrecht, Germany) and stored at 4 °C. Buffers for FPLC and HPLC were made with ultra-pure water, sterile filtered and stored at room temperature. Non-autoclavable devices and equipment were cleaned with 70 % ethanol before use. All medium and equipment in contact with bacteria was autoclaved, cleaned with 70 % ethanol or flamed.

2.3.1 Cultivation of *T. kivui*

T. kivui was routinely grown in anoxic, defined or complex medium (Table 5) at 65 °C with 25 mM glucose, 25 mM fructose, 25 mM mannitol, 50-100 mM pyruvate, H_2/CO_2 ($3x10^5$ Pa; 66.6/33.3; v/v), $H_2/CO_2/CO$ ($3x10^5$ Pa; 44/22/33; v/v/v) or CO/N_2 ($3x10^5$ Pa; 10-50/90-50; v/v) as substrate. Depending on the experiment, *T. kivui* was grown in volumes between 5 and 500 ml.

For a better understanding of the atmospheric composition, the unit Pascal (Pa) is used, where $1x10^5$ Pa represents the pressure of 1 atmosphere. An overpressure of $1x10^5$ Pa or $2x10^5$ Pa means a total pressure of $2x10^5$ Pa or $3x10^5$ Pa, respectively.

2.3.2 Resting cell experiment

Resting cells of *T. kivui* were prepared as described previously (Schwarz et al. 2020) under strict anoxic conditions in an anoxic glove box (Coy Laboratory Products, Grass Lake, MI) containing a reducing gas atmosphere (H_2/N_2; 5/95; v/v). Cells were cultivated in 250−500 ml complex medium containing 25 mM glucose in 1000 ml bottles (SCHOTT AG, Mainz, Germany) and harvested in the late exponential growth phase by centrifugation at 4,000 rpm (1,503 g), 4 °C for 15 minutes. The cells were washed in imidazole buffer (50 mM imidazole, 20 mM $MgSO_4$, 20 mM KCl, 4 µM resazurin, 2 mM DTE, pH 7.0) or Tris-HCl buffer (50 mM Tris, 4 µM resazurin, 2 mM DTE, pH 7,5) and subsequently resuspended the corresponding buffer. The cells were transferred into 50 ml serum bottles and sealed with butyl robber stopper. The gas atmosphere (H_2/N_2; 5/95; v/v) in the serum bottles was replaced by flushing the bottles with N_2 gas. Finally, hexoses, carbonyl acids or gas was added to the bottles.

2.3.3 Determination of protein concentration of cells

The protein concentration of cell samples from experiments with resting cells was determined according to Schmidt et al. (1963). Therefore, samples of 0.5-1 ml were taken during the experiment and harvested at 13,000 rpm (15,871 g) for 10 minutes at 4 °C. The pellet was resuspended in 200 µl H_2O and 25 µl NaOH (4 M NaOH) was added. The mixture was heated to 100 °C for 10 minutes. Afterward, the mixture was cooled down and 80 µl Schmidt reagent (60 mM potassium sodium tartrate, 10 mM copper sulfate, 38 mM potassium iodide, 250 mM NaOH) was added and the mixture was incubated for 30 minutes at 37 °C. The mixture was centrifuged for 5 minutes at 13,000 rpm to remove cell debris and 200 µl sample was transferred on a 96-well-plate (SARSTEDT AG & Co. KG, Nümbrecht, Germany) and the absorption was measured at 546 nm in a plate reader (SpectraMax M2e, Molecular Devices, LLC., San Jose, California, USA). Bovine serum albumin (BSA) solution was used as a standard with a protein concentration of 0 to 1.5 mg ml^{-1} to determine the protein concentration. The standard was treated in the same way as the samples and water was used as blank.

2.3.4 Cultivation of *E. coli*

E. coli was routinely grown in 5 ml oxic LB medium (Table 6) in test tubes at 37 °C while shaking. For cloning, sterile ampicillin (50 mg ml^{-1}) was added to the medium before inoculation to select for ampicillin resistance. The final ampicillin concentration was 100 µg ml^{-1}.

2.3.5 Photometric determination of growth

Cell growth was determined by measuring the optical densities of cultures at a wavelength of 600 nm. The measurement was carried out in cuvettes with a light path of 10 mm (SARSTEDT AG & Co. KG, Nümbrecht, Germany) in a spectral photometer (NANOCOLOR VIS II, MACHEREY-NAGEL GmbH & Co. KG, Düren, Germany). Samples expected to have an optical density >0.3 were diluted 1:6 (*T. kivui*) or 1:10 (*E. coli*). Medium or diluted medium served as a blank, while water was used to test for differences in absorbance between batches of medium. In addition to the cuvette measurements, in some experiments, the optical density was determined directly in Hungate tubes.

2.3.6 Stock cultures

For long-term storage of cultures at −70°C, stock solutions were prepared with autoclaved glycerol/water (50/50; v/v). Aerobic stock cultures were prepared by mixing 0.5 ml 50 % glycerol and 0.5 ml cooled culture in sterile screw-capped reaction tubes (SARSTEDT AG & Co. KG, Nümbrecht,

Germany). Anoxic stock cultures were prepared by adding 3 ml of cooled culture to 3 ml of glycerol in to an autoclaved 10 ml injection vial sealed with a rubber stopper (Glasgerätebau Ochs, Bovenden, Germany) and a N_2 atmosphere.

2.4 Metabolite analysis

2.4.1 High-performance liquid chromatography

High-performance liquid chromatography (HPLC) was used to determine the concentrations of glucose, mannitol, fructose, pyruvate, formate and acetate. For sample preparation, cells were centrifugated at 13,000 rpm (15,871 g) for 10 minutes at 4 °C, 250 µl of supernatant was filled into a 1.5 ml polypropylene tube and 5 µl 50 % H_2SO_4 [v/v] was added. The sample was mixed and centrifuged at 13,000 rpm for 10 minutes at 4 °C to remove possible precipitates. Afterwards, 200 µl of the sample was transferred into an HPLC vial (Diagonal GmbH & Co. KG, Münster, Germany). Liquid chromatography was performed by using an organic acid resin 300 × 8 mm column (CS—Chromatography Service GmbH, Langerwehe, Germany). The system consisted of a Shimadzu (Kyoto, Japan) SIL-20AC autosampler (10 µL sample injection), LC-20AD pump (0.6 ml min^{-1} of 5 mM H_2SO_4), CTO-20AC column oven (30 °C), and RID-10A refractive index detector. The metabolites were quantified by comparison with standard calibration curve.

2.4.2 Gas chromatography

Acetate concentrations were determined by gas chromatography. For the sample preparation, cells were centrifugate at 13,000 rpm (15,871 g) for 10 minutes at 4 °C, 450 µl of supernatant was filled into a 1.5 ml polypropylene tube and 50 µl 2 M phosphor acid was added. The sample was mixed and centrifuged at 13,000 rpm for 10 minutes at 4 °C. Subsequently, 500 µl of the sample was transferred into an GC vial. Gas chromatography was performed using a 8860 GC System (Agilent, Santa Clara, United States). The GC system consisted of a HayeSep P 60/80 UM column (6 Ft 1/8 2 mm) and a flame ionization detector (FID). The FID operated at a temperature of 250 °C, with an airflow (synthetic air) of 300 ml min^{-1}, a H_2 flow of 30 ml min^{-1}, and a N_2 make-up flow of 25 ml min^{-1}. Pure N_2 with a flow rate of 10 ml min^{-1} was used as the carrier gas. For the measurement, a sample volume of 0.5 µl of was injected at 195 °C using a PPZ inlet with a flow rate of 10 ml min^{-1}. During the measurement a temperature gradient was applied by starting from 120 °C for 3 min followed by an increase of 5 °C min^{-1} to 145 °C for 3 min, followed by an increase of 10 °C min^{-1} to 170 °C for 0.5 min. To remove the last remnants of the samples, the temperature was increased by 30 °C min^{-1} to 200°C. OpenLAB CDS EZChrom software (Agilent, Santa Clara, United States) was used for data analysis.

2.4.3 Statistical analysis

Datasets were analyzed by t-test (one-tailed and two-sample unequal variance) using the software Microsoft Excel (Microsoft Corporation, Redmond, Washington, USA).

2.5 Molecular biological methods

2.5.1 Polymerase chain reaction (PCR)

PCR amplification of fragments for the construction of plasmids (Table 8) or colony PCR (Table 9) was routinely carried out with OneTaq® DNA Polymerase or Q5® High-Fidelity DNA Polymerase (New England Biolabs, Frankfurt am Main, Germany), according to protocol of the used polymerase. OneTaq® DNA Polymerase was used for the screening of cloning constructs and mutant strains, while Q5® High-Fidelity DNA Polymerase was used for amplification of plasmid backbone and DNA fragments for the cloning constructs. PCR thermal cycler Biometra TAdvanced of Analytik Jena GmbH+Co. KG (Jena,

Germany) or GeneExplorer 96 of Biozym Scientific GmbH (Hessisch Oldendorf, Germany) were used for PCR.

Table 8 List of oligonucleotides to construct the plasmids in this study.
The abbreviations for the primer directions (Dir.) are fwd (forward) and rev (reverse).

Plasmid	Nr.	Fragment	Dir.	sequence (5' à 3') Overlap + Binding	Melting temp (One Taq)
pEch1TK02	1E02a	*ech1* UFR	fwd	CCCGGGGATCCATGAC ATCCTTTATACCCATAATGTTAGTTTTATG	56.4 °C
	1E02b		rev	TTTAATTGTT TAAAATATGAAGAGATAGTGAACAATTCCCAAAAT	56.4 °C
	1E02c	*ech1* DFR	fwd	TCATATTTTA AACAATTAAAAATACTGAGATCATGTTTGGTCA	56.9 °C
	1E02d		rev	CAGGTCGACTCTAGA TTATCTCTCAGTACAAGAAATACATGGATCAAT	56.6 °C
pEch2TK02	2E02a	*ech2* UFR	fwd	CCCGGGGATCC TTGAAGAGTATGCCAACATGTGTTATT	56.0 °C
	2E02b		rev	AAATCATATT GGTGGGGGTGGGTAAGAAC	56.8 °C
	2E02c	*ech2* DFR	fwd	CACCCCCACC AATATGATTTGTCCCAAACCCTATATCTACA	56.4 °C
	2E02d		rev	CAGGTCGACTCTAGA ATTTTTCAATGGCAAGAAAAAGATTAACGT	56.4 °C
p144_NfnB	CB98	*nfnA* UFR	fwd	AGCTCGGTACCCGGGGATCC AGCTGGAGACTATATCCA	48.0 °C
	CB99		rev	CGGGAAGCAGGAAATTTTAA CATTCATGAGCTTCATTAAATC	48.5 °C
	CB100	*pyrE*	fwd	CCCTCGAAAGATTTAATGAAGCTCATGAATG TTAAAATTTCCTGCTTCCC	48.0 °C
	CB101		rev	ATACCAGTACGCCACCGGGT CCTATTTTTACTCTTCTTTCTGG	49.5 °C
	CB102	*nfnB* DFR	fwd	GTATTGCTTTAACCAGAAAGAAGAGTAAAAATAGG ACCCGGTGGCGTA	50.7 °C
	CB103		rev	GCCTGCAGGTCGACTCTAGA CTAAGCCTTCAGTGGC	49 °C

Primers for colony PCR (Table 9) were designed for testing for deletion of the target genes.

Table 9 List of oligonucleotides to check deletion of *ech1, ech2* and *nfnB* or promoter exchange (*p144*).

Check primer	Nr.	Dir.	sequence (5' → 3')	Melting temp (OneTaq)
Δech1	O1a	fwd	TTGCGGTATCAGGTATTTAAACTATTAGG	55.6 °C
	O1d	rev	TTATTCTCTATACTTAAAATCTTCATAGGAACAGC	55.9 °C
Δech2	O2a	fwd	CAATGCATTTTGCTAAGTTTAATGTATATTTTGA	55.6 °C
	O2d	rev	TGCAGATGTTTATTTTTCAATGGCAA	55.6 °C
ΔnfnB	CB104	fwd	GCTGTAAGTGACAGGATGTACG	55.6 °C
	CB105	rev	GGCTGCATCCATAGCTACATTG	56.3 °C
p144	BZ154	fwd	GTAGAAGCAGTGGATAAAGTCATACTG	55.0 °C
	BZ155	rev	GACCTATAATAGAGGCGCTTAAATAGATG	54.9 °C

Plasmids constructed and used to transform *Thermoanaerobacter kivui* strain TKV_MB002 in this study are listed in Table 10.

Table 10 List of plasmids and their genotype/phenotype used study.

Plasmid	Genotype/phenotype	Reference
pMBTkv022	*amp*, *pyrE*, restriction site UFR/DFR	Basen et al. 2018
pEch1TK02	*amp*, *pyrE*, restriction site, UFR/DFR e*ch1*	This study
pEch2TK02	*amp*, *pyrE*, restriction site, UFR/DFR e*ch2*	This study
p144	*amp*, *pyrE* under control of gyrase promoter, *ech1* under control of P_{frc} promoter, restriction site UFR/DFR *ech1*	Zeldes, unpublished
p144_NfnB	amp, restriction site UFR/pyrE/DFR NfnAB (deletion NfnB)	This study

2.5.2 PCR fragment clean-up

PCR fragments were cleaned-up by using the GeneJET Gel-Extraction Kit (Thermo Fisher Scientific Inc., Waltham, USA) or the Monarch DNA Gel Extraction Kit (New England Biolabs, Frankfurt am Main, Germany).

2.5.3 Quantification via Nanophotometry

DNA concentration of PCR fragments and plasmids was determined by measuring absorbance at wavelength of 260 nm using a NanoPhotometer (N50 touch, Implen GmbH, München, Germany). RNA- and DNA-free water served as blank.

2.5.4 DNA and RNA separation via agarose gel electrophoresis

DNA fragments were separated according to their lengths via agarose gel electrophoresis. DNA samples mixed with Gel Loading Dye, Purple (6X) (New England Biolabs, Frankfurt am Main, Germany), and a DNA Standard 1 kb DNA Ladder (New England Biolabs, Frankfurt am Main, Germany) were loaded on to an 1 % agarose gel (w/v) in 1x TAE buffer (1 mM EDTA, 40 mM Tris and 20 mM acetic acid, pH 8). The separation was carried out at 80–100 V in an electrophoresis chamber (Analytik Jena GmbH+Co. KG, Jena, Germany). The agarose gel was then stained in an ethidium bromide bath or pre-stained with Midori Green Advance (NIPPON Genetics EUROPE, Düren, Germany) by adding the dye to the liquid agarose gel (6 µl per 100 ml agarose). DNA fragments were visualized under UV light, documented with the dark hood DH50 (Bionis (biostep), Houdan, France) combined with a Canon EOS 700D (Canon Deutschland GmbH, Krefeld, Germany) and evaluated with the software Argus X1 (Bionis (biostep), Houdan, France).

2.5.5 Plasmid construction

Plasmids were constructed according to Basen et al (2018) and derived from pMBTKv0022 or p144. Upstream (UFR) and downstream (DFR) flanking regions of a gene cluster were amplified with a sequence size of around 900 to 1000 bp, using the primers described in Table 8. The PCR fragments were cleaned-up and UFR and DFR fragments were fused by overlap extensions using PCR. The resulting UFR/DFR fragment and pMBTKv0022 were digested with *Bam*HI and *Xba*I (New England Biolabs, Frankfurt am Main, Germany). Plasmid and fragment were ligated using T4 ligase (Thermo Fisher Scientific Inc., Waltham, USA), and the resulting plasmid was transformed into *E. coli* DH5α. Restriction and ligation was performed according to the protocol of the manufacturer.

Plasmid p144_NfnB was made by using NEBuilder HiFi DNA Assembly Cloning Kit (New England Biolabs, Frankfurt am Main, Germany). Primers were designed according to protocol of NEBuilder HiFi DNA Assembly Cloning Kit specifications. Q5® High-Fidelity DNA Polymerase was used to amplify UFR, DFR, the *pyr*E gene and the plasmid backbone (Table 8). The PCR fragments were cleaned-up and used to

perform DNA assembly as described in the protocol of the manufacturer. The resulting plasmid construct was then used to transform *E. coli* DH5α.

2.5.6 Production of chemically competent *E. coli* DH5α cells

For the production of chemically competent cells (Hanahan 1983, mod.), 100 ml LB medium (Table 6) was inoculated with *E. coli* DH5α to an OD_{600} of 0.05 and grown at 37 °C for 2 to 3 hours to an OD_{600} of 0.4 to 0.6, then the cells were cooled on ice for 10 to 15 minutes. The cold cells were centrifuged at 4 °C for 5 minutes at 4,000 rpm (1,503 g, Thermo ScientificTM SorvallTM RC 6 Plus, Thermo Fisher Scientific GmbH, Dreieich, Germany), the supernatant discarded, and the cells resuspended in 20 to 30 ml of ice-cold $CaCl_2$ buffer (100 mM $CaCl_2$, 20 % glycerol). Afterwards, they were incubated again on ice for 10 to 15 minutes. Subsequently, the cells were centrifuged, the supernatant was discarded again, and the pellet was resuspended in 1 to 2 ml of ice-cold $CaCl_2$ buffer. After further incubation on ice for 1 to 2 hours, the cells were finally aliquoted into 100-µl aliquots and stored at -70 °C.

2.5.7 Transformation via heat shock

For transformation of plasmids into *E. coli* DH5α, an aliquot of 100 µl chemically competent cells was thawed on ice for 10 minutes. The 100 µl aliquot was then divided into 2 x 50 µl and 1 to 5 µl of plasmid (approximately 100 ng) was added to the cells. The mixture was incubated on ice for 30 minutes. After incubation, a heat shock was performed for 30 seconds at 42 °C in a thermoblock (Eppendorf SE, Hamburg, Germany). Cells were then placed back on ice for 5 minutes followed by the addition of 950 µl SOC medium (Table 7). The cells were incubated at 37 °C for 60 minutes. Subsequently, 100 to 200 µl of the mixture was applied to LB plates containing ampicillin for selection and incubated overnight at 37 °C.

2.5.8 Plasmid isolation

To isolate plasmids from *E. coli*, 5 ml culture was harvested and centrifuged at 13,000 rpm (15,871 g) and room temperature for 2 minutes. The NucleoSpin® Plasmid Easy Pure Kit (Macherey-Nagel, Düren, Germany) was used to isolate the plasmids. Contrary to the description in the kit, the plasmids were eluted with 40-50 µL sterile deionized H_2O. The purity and amount of purified genomic DNA was examined using the NanoPhotometer N50 touch (Implen GmbH, Munich, Germany).

2.5.9 Transformation of *Thermoanaerobacter kivui*

For generation of *T. kivui* mutans, plasmids or PCR fragments were constructed according to Basen et al. (2018). Plasmid constructs were used to transform the Δ*pyrE* strain (TKV_MB002; Basen et al. 2018), for which about 1 µg of the construct was mixed with about 100 µl of the Δ*pyrE* culture. Then, the mixture was transferred to defined medium containing 25 mM glucose and 40 µM uracil. The cells were incubated for several hours. Once OD_{600} reached a value of around 1, the cells were subjected to one or two selection steps. In the first selection step, 100 µl of the grown cells of TKV_MB002 plus the contracted plasmid (pEch2TK02) were pipetted into a petri dish. Then, approximately 8 ml of liquid defined medium containing 1.5 % Bacto Agar (Becton, Dickinson and Company, Franklin Lakes, USA) and 25 mM glucose was poured over the cells. The agar plates, which were still liquid, were placed in an anoxic glove box (Coy Laboratory Products, Grass Lake, MI) and remained there until they were hard. The plates were then placed in an airtight incubator and removed from the anoxic glove box. The airtight incubator was then pressurized to $0.5x10^5$ Pa overpressure with N_2/CO_2 (80/20; v/v) and incubated at 65 °C for 3 to 4 days. After incubation, the incubator was opened under oxic conditions and colonies were transferred to Hungate tubes with defined medium containing glucose. The second selection step was performed once the cultures had grown from the colonies. For this purpose, 1 to 100 µl of the grown cells were pipetted into a petri dish and approximately 8 ml of liquid defined medium containing

1.5 % Bacto Agar, 25 mM glucose, 5 mM 5-FOA (5-fluoroorotic acid/5-fluoroorotate) and 40 mM uracil. Grown colonies were transferred to defined medium containing 40 mM uracil or complex medium and tested for loss of the gene of interest by PCR using primers binding outside of the gene of interest (Table 9). Only the first selection was performed for the generation of deletion or promoter exchange mutants. The grown colonies were transferred to defined medium containing glucose and afterwards screened by PCR for the loss of the gene of interest or the promoter exchange using primers binding outside the target area (Table 9).

2.5.10 Sequencing

Samples were sent to LGC genomics for sequencing to verify the deletion or integration of target DNA samples were prepared according to the description for "Ready 2 Run" samples (LGC Genomics GmbH, Berlin, Germany). Sequencing data was aligned via APE-plasmid editor (Davis and Jorgensen 2022), Clustal Omega (EMBL's European Bioinformatics Institute (EMBL-EBI), Hinxton, United Kingdom) or MAFFT (EMBL's European Bioinformatics Institute (EMBL-EBI), Hinxton, United Kingdom).

2.6 Quantifications of mRNA isolated from *Thermoanaerobacter kivui*

2.6.1 Cell harvest and RNA extraction

Cells for RNA extraction were harvested in the exponential growth phase between an OD_{600} of 0.2−0.35. Samples for RNA extraction and sequencing were chilled immediately after collection by transferring 2 ml of culture into a 2-ml polyether tube stored in an ice-water bath. The RNA extraction required approximately 2 ml of culture for qPCR applications, whereas, approximately 4-5 ml of the culture was needed for RNA-sequencing. Cells were centrifuged at 15,000 rpm (21,130 g) at 4 °C for 5 minutes. The supernatant was carefully removed, and the cell pellet was stored in a −70 °C freezer.

RNA extraction was performed as described in the protocol of the RNeasy Protect Kit (QIAGEN GmbH, Hilden, Germany) in combination with the RNase-Free DNase Set (QIAGEN GmbH, Hilden, Germany). For lysis of the cells, the Fastprep-24 5G (Fisher Scientific GmbH (Mpbio), Schwerte, Germany) was used. Deviating from the protocol of the RNase-Free DNase set, the samples were incubated with DNase for 45 minutes instead of 15 minutes. Subsequently, RNA quality was determined by preparing 4 µl of the sample as described in the RNA RiboRuler High Range RNA Ladder protocol (Thermo Fisher Scientific Inc., Waltham, USA) and separating it on a 1 % agarose gel. RNA concentration was determined by measuring the sample using NanoPhotometer N50 touch (Implen GmbH, Munich, Germany). The extracted RNA was stored in a −70 °C freezer.

2.6.2 DNase treatment

An additional DNase treatment was carried out if an RNA extract had a high DNA content. This additional purification was done with the DNase TURBO DNA-free™ Kit from Thermo Fisher Scientific Inc. (Waltham, USA) as described in the protocol.

2.6.3 cDNA synthesis

For cDNA synthesis, the extracted RNA was prepared as described in the protocol of the Biozym cDNA synthesis kit (Biozym Scientific GmbH, Hessisch Oldendorf, Germany). For all cDNA reactions, hexamer primers were used.

2.6.4 Real Time Quantitative PCR (RT-qPCR or qPCR)

Master mixes containing a primer pair for the amplification of the gene of interest (Table 11) were prepared for 10 µl per reaction according to the protocol of Biozym Blue S'Green qPCR Kit Separate ROX (Biozym Scientific GmbH, Hessisch Oldendorf, Germany), For RT-qPCR, 1 µl of cDNA sample was pipetted

into a well of a 96-well plate and 9 µl of master mix was added. The 96-well PCR plate (Biozym Scientific GmbH, Hessisch Oldendorf, Germany) was sealed with adhesive clear qPCR Seal (Biozym Scientific GmbH, Hessisch Oldendorf, Germany) and centrifuged in a 96-well plate centrifuge (Benchmark Scientific, Sayreville, United States). RT-qPCR was performed using qTOWER³ (Analytik Jena GmbH, Jena, Germany) according to the manufacturer's instructions for the master mixes. Data analysis was performed using qPCRsoft4.1 software (Analytik Jena GmbH, Jena, Germany).

Table 11 List of RT-qPCR Primer used in this study.

Name	Dir.	Sequence	DNA target
gyrB_for_qRT	fwd	CCAGTTGTGCTTCCTTCTCGATTTCC	DNA gyrase subunit B
gyrB_rev_qRT	rev	GCGACAATGCCATCTATGACTTCTCC	(*gyrB* - TKV_c00090)
Ech1A_for_qRT T.k.	fwd	CCTCCTTTGCCGGTGTAATGAGTAAGG	Ech1 complex
Ech1A_rev_qRT T.k.	rev	AAGCATGGTAAACGCACCCAAC	(*ech1A* - TKV_c01230)
Ech2D_for_qRT T.k.	fwd	CAATTGAAGCCTGAGATGTC	Ech2 complex
Ech2D_rev_qRT T.k.	rev	AGCAGAATGGGCAGAAAG	(*ech2D* - TKV_c19750)
BZq19	fwd	CTGTGGACAGGATAGTACCGAATGTAG	Mannitol-1-phosphate dehydrogenase
BZq20	rev	CAAGGTCAGCGACAAGTTCCAC	(*mtlD* - TKV_c02860)
BZq21	fwd	GACATAATTAGAGAAATAAAAAGCGGCG	1-Phosphofructosekinase
BZq22	rev	CTACTGCATCTTCTAACTCCTGC	(*fruK* - TKV_c23150)
BZq27	fwd	CAT TAAATAGATTCCCGACAGACACAG	Formyl-tetrahydrofolate synthetase
BZq28	rev	CTCTTTTGCAAGCTCAATTCCAC	(*fhs1* - TKV_c19930)
BZq31	fwd	GTTTATGTCGACCAAGACGAATGC	Ferredoxin
BZq32	rev	GACAAGAGCTCATTGCATCTTGC	(*fd1* - TKV_c16450)
BZq33	fwd	AGAGAAGGTGCAGGTGCATT	Electron bifurcating hydrogenases
BZq34	rev	GTTCAAAACCGTTGGCATCT	(*hydB* - TKV_c19590)
BZq35	fwd	CTTTGTTGGGCCTTTAGGTG	NfnA transhydrogenase subunit A
BZq36	rev	TCTACCCCCTGCTGATGAAG	(*nfnA* - TKV_c22270)
BZq55	fwd	ACGCGTCATTGTAGCTGTATGA	Hydrogen dependent carbon
BZq56	rev	GCATATGTGATGAAGGGGCTGA	dioxide reductase (*fdhF* - TKV_c19990)
BZq61	fwd	AGCAGAAGTCGAAGTTCCTGTT	Glyceraldehyde 3-phosphate
BZq62	rev	CTGTCGTCTCCTTTGAAGTCCA	dehydrogenase (*gap*- TKV_c16340)
BZq76	fwd	ACAACGCAGAATTTGGTCTTGG	Pyruvate-ferredoxin/flavodoxin
BZq77	rev	TTTTGCCGTCCATCATGTTGTC	oxidoreductase (PFOR1) (*nifJ1*- TKV_c04340)
BZq78	fwd	GAGATGGATGGGCGTATGACAT	Pyruvate-ferredoxin/
BZq79	rev	GGCGTAGATTTTGAGGATTGCC	flavodoxin oxidoreductase (PFOR2) (*nifJ2* - TKV_c21450)
BZq80	fwd	TGAGGTTACAGCTTACATGGCA	Oxoglutarate/2-oxoacid ferredoxin
BZq81	rev	TGGAAGTCATAACACGAGCTCC	oxidoreductase subunit alpha (OGOR) (*2OxFOR* - TKV_c19280)
Rex _Fwd	fwd	GGTTGTTTGGGCTTAAAATCAG	Redox-sensing transcriptional repressor
Rex _Rex	rev	TCCTGCCTTCACTAATCTGTCA	(*rex* - TKV_c05420)
CB104	fwd	GCTGTAAGTGACAGGATGTACG	NfnB transhydrogenase subunit B
CB105	rev	GGCTGCATCCATAGCTACATTG	(*nfnB* - TKV_c22280)

2.6.5 Data analyses qPCR

The measured Ct values were calculated according to Schmittgen and Livak (2008) to calculate the ΔCt (A), ΔΔCt (B) and the fold change (x-fold; C).

A) $\Delta\mathrm{Ct} = \mathrm{Ct\ value\ gene\ of\ interrest} - \mathrm{Ct\ value\ gyrase}\ (gyrB)$

B) $\Delta\Delta\mathrm{Ct} = \Delta\mathrm{Ct\ value\ gene\ of\ intrrest\ (test)} - \Delta\mathrm{Ct\ value\ gene\ of\ interrest\ (calibrator)}$

C) $\Delta\Delta\mathrm{Ct} = -\mathrm{x} \rightarrow \mathrm{fold\ change} = 2^{-\Delta\Delta\mathrm{Ct}}$

Formula 1 Analyses of qPCR data. A) Calculation of the ΔCt value. Reflects the abundancy of the gene of interest in relation to the housekeeping gene (gyrase). B) Calculation of the ΔΔCt value from the ΔCt values. C) Calculation of the fold change (x-fold) value from the ΔΔCt value.

The resulting fold change is positive for a negative ΔΔCt value and reflects a x-fold up regulation in relation to the calibrator ΔΔCt value, while a positive ΔΔCt value reflects a x-fold down regulation in relation to the calibrator ΔΔCt value. A fold change of 1 or −1 is regarded as no up or downregulation, values above a fold change of 4 or below a fold change of −4 were regarded as four times up or downregulation in relation to the calibrator gene.

A value above a 4-fold change and below −4 was considered a significant expression change and therefore these values were set as the threshold.

2.6.6 Transcriptome analysis (mRNA sequencing)

The mRNA sequencing data provided contains the number of mRNA copies (reads) for each gene. Using the data, the ratio and subsequently the log2(x) was calculated to easily visualize the expression of whether a gene was up or downregulated (Formula 2). The threshold was set to a $\log_2(x)$ value of 2 or −2, which corresponds to a 4-fold up or downregulation.

$$\log_2(\mathrm{x})\ \mathrm{values} = \log_2\left(\frac{\mathrm{test\ condition}}{\mathrm{calibrator\ condition\ (control)}}\right)$$

Formula 2 Analysis of the RNA data. Calculation of the log2(x) value from the mRNA read ratio between the test and calibration conditions.

3 Results

3.1 Deletion of the energy-converting hydrogenase Ech2

3.1.1 Generation of a Δ*ech2* strain

In order to resolve whether Ech1 or Ech2 is responsible for energy conservation and turnover of ferredoxin (Fd_{red} → Fd_{ox}; Fd_{ox} → Fd_{red}). A markerless deletion of the entire gene cluster encoding the Ech2 complex (TKV_c19680 to TKV_c19750). Strain *T. kivui* TKV002 (Δ*pyrE*) was transformed with the plasmid pEch2TK02 (Figure 8), which contained the upstream flanking region (UFR, 900 bp) and the downstream flanking region (DFR, 1000 bp) of *ech2* gene cluster for homologues recombination of the plasmid into the genome and *pyrE* as a selective marker as described in Basen et al. (2018)

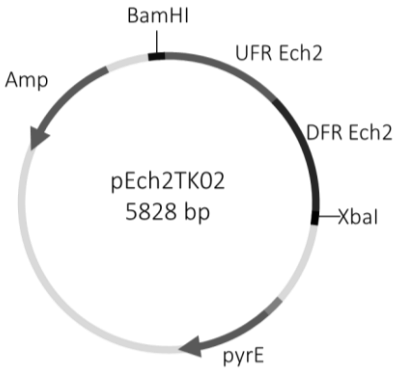

Figure 8 Plasmid map of pEch2TK02.
The plasmid has two regions (UFR and DFR) homologous to the chromosome of *T. kivui*, targeting a genome region between TKV_c19670 and TKV_c19760. The plasmid contains an ampicillin resistance cassette (Amp) for selection in *E. coli* and the *pyrE* gene for selection in *T. kivui*.

For the generation of the deletion mutant, two selection steps were performed. In the first step, the plasmid was integrated into the genome by single homologous recombination of either UFR or DFR, allowing transformed cells to grow on defined media without uracil. In the second step, 5-FOA was used for selective pressure. Colonies grown on plates containing 5-FOA and uracil did not contain *pyrE*. Out of 10 colonies, 7 were revertants, meaning they transformed back to *T. kivui* TKV002 and, the other 3 had lost the *ech2* gene cluster (Figure 9). The deletion of *ech2* gene cluster was verified by PCR using the primers O2a and O2d, which are binding in the flanking regions outside the deletion (Figure 9; Table 9) and sequencing of the PCR product.

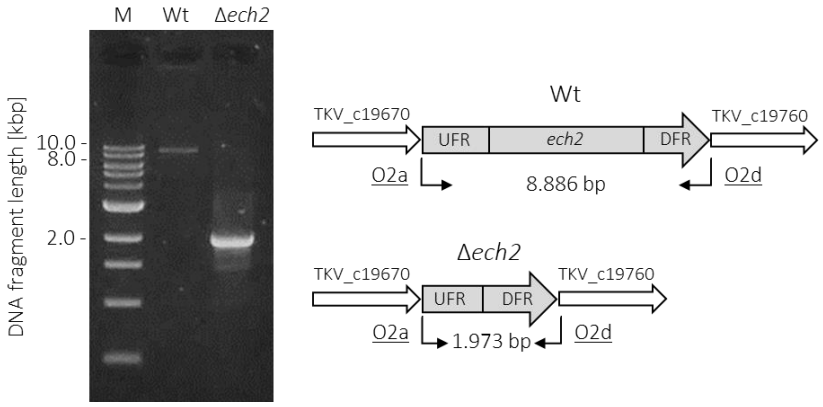

Figure 9 Verification of loss of *ech2* gene cluster.
The loss of the *ech2* (6770 bp) gene cluster was verified by PCR using primers binding outside of the *ech2* cluster (O2a and O2d; Table 9). Electrophoretic separation of the DNA fragments from the PCRs using cells of *T. kivui* wild type (WT; strain DSM 2030; expected fragment size, 8.8 kbp) and Δ*ech2* strain (expected fragment size, 2.0 kbp). The agarose gel was stained with midori green.

The newly generated Δ*ech2* strain (*ech2* mutant) was uracil autotroph due to the lack of the *pyrE* gene and only grew if yeast extract or uracil were supplied in the medium. The mutant was used for further genetic modifications, as shown later in the study.

3.2 Growth of the Δ*ech2* strain on sugar substrates and on H_2/CO_2

3.2.1 Growth of the Δ*ech2* strain on sugars glucose, mannitol and fructose

The expected metabolic function of Ech2 is to catalyze the reversible oxidation of Fd_{red} with protons as electron acceptors and vice versa (Figure 3). Reduced electron carriers, such as Fd_{red} and H_2, derived from the oxidation of sugars, must be re-oxidized to keep the metabolism going. Ech2 has been shown to carry out the oxidation of Fd_{red} by coupling the oxidation of Fd_{red} with proton reduction, suggesting that the Ech2 complex is important for metabolic equilibrium (Katsyv and Müller 2022).

For characterization of the Δ*ech2* strain, the growth rate and doubling time (Table 12) of the Δ*ech2* strain and the wild type (DSM 2030) were determined on complex and defined containing glucose, mannitol, fructose or gas mix of hydrogen and carbon dioxide (H_2/CO_2) in the atmosphere.

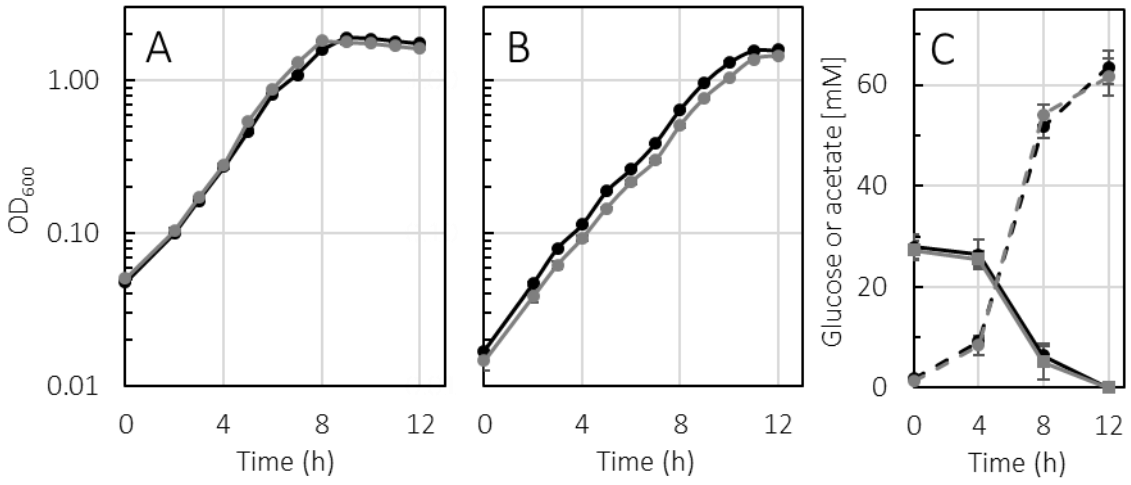

Figure 10 Growth of Δ*ech2* strain on glucose.
Representative growth curves of the Δ*ech2* strain (gray) and the wild type strain DSM 2030 (black) in the presence of 25 mM glucose (A) complex medium or (B) defined medium containing uracil (40 µM). (C) Glucose (continuous lines) or acetate (dashed lines) concentrations [mM] of *T. kivui* grown on complex medium containing glucose (A). All experiments were performed at 65 °C and 160 rpm (n = 3).

The *ech2* mutant grew in complex medium and defined medium containing 25 mM glucose. The determined growth rate of the mutant in a complex medium containing 25 mM glucose was 0.55 h^{-1} and of the wild type, it was 0.54 h^{-1} (Figure 10 A; Table 12). In defined medium containing 25 mM glucose and 40 µM uracil was the growth rate of the mutant 0.43 h^{-1} and of the wild type 0.44 h^{-1} (Figure 10 B; Table 12).The final OD_{600} of the mutant on complex medium was 1.61 and of the wild type 1.89 (Figure 10 A), while the final OD_{600} on defined medium was 1.45 for the mutant and 1.58 for the wild type (Figure 10 B). Both strains utilized glucose (wild type −5.0 mM h^{-1}± 0.5 mM h^{-1} and Δ*ech2* strain −5.1 mM h^{-1} ± 1.3 mM h^{-1}) and produced acetate (wild type 10.6 mM h^{-1}± 0.5 mM h^{-1} and Δ*ech2* strain 11.4 mM h^{-1} ± 1.2 mM h^{-1}) at almost same rate between hour 4 and 8 (Figure 10 C). Growing cells of the wild type and the *ech2* mutant produced 2.43 ± 0.23 mol and 2.43 ± 0.28 mol acetate from one mol glucose, respectively.

Growth experiments with 25 mM mannitol and 25 mM fructose were performed. Mannitol is more reduced than glucose and fructose, providing one additional mole NADH per mole substrate during metabolism.

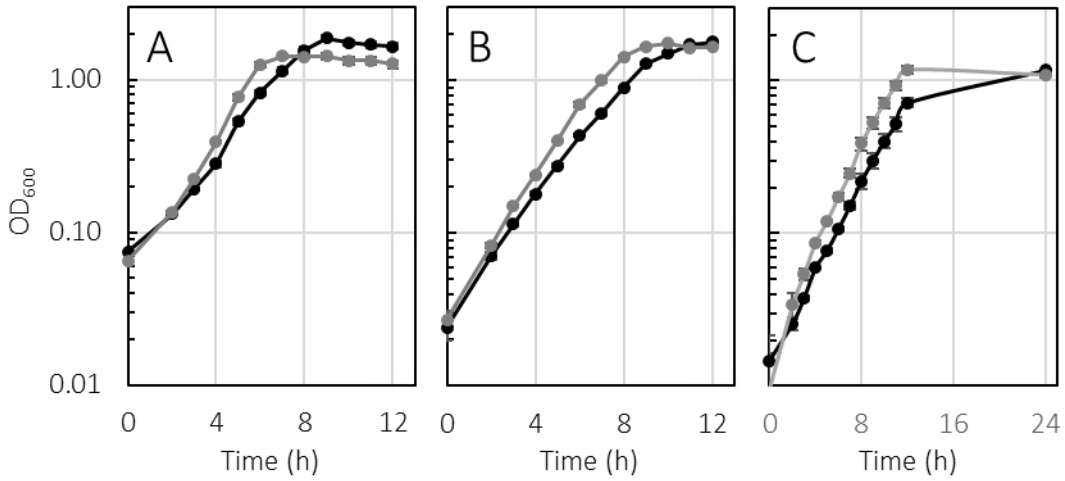

Figure 11 Growth of Δ*ech2* strain on fructose and mannitol.
Representative growth curves of Δ*ech2* strain (gray) and the wild type strain DSM 2030 (black) grown on complex medium containing (A) 25 mM fructose and (B) 25 mM mannitol. (C) Wild type and Δ*ech2* strain grown on defined medium containing 25 mM mannitol and uracil (40 µM). All experiments were performed at 65 °C and 160 rpm; (n = 3).

The Δ*ech2* strain grew in complex medium and defined medium containing 25 mM mannitol. The growth rate of the mutant was 0.48 h^{-1} and of the wild type 0.40 h^{-1} on complex medium (Figure 11 B; Table 12), while on the defined medium, the growth rate of the mutant was 0.40 h^{-1} and the of wild type 0.35 h^{-1} (Figure 11 C; Table 12). The final OD_{600} for the Δ*ech2* strain was on the complex medium 1.76 ± 0.03 and on defined medium 1.18 ± 0.06, and the wild type had a final OD_{600} of 1.79 ± 0.03 on the complex medium and 1.17 ± 0.02 on the defined medium.

On 25 mM fructose, the Δ*ech2* strain had a growth rate of 0.57 h^{-1} ± 0.02 h^{-1} and reached a final OD_{600} of 1.42 ± 0.07, while the wild type had a growth rate of 0.47 h^{-1} ± 0.01 h^{-1} and reached a final OD_{600} of 1.87 ± 0.07 (Figure 11 A; Table 12).

The Δ*ech2* strain showed growth patterns similar to the wild type when grown heterotrophically on glucose, fructose and mannitol, showing slightly faster growth on fructose and mannitol on the complex medium (Table 12). The final OD_{600} of the mutant was slightly lower for glucose and fructose than of the wild type, while the final OD_{600} was the same for mannitol for both strains.

3.2.2 Growth of the Δ*ech2* strain on H_2/CO_2

In addition to heterotrophic substrates, autotrophic growth of the Δ*ech2* strain was also investigated. The models of Katsyv et al. (2021a) indicate that the Ech2 complex is important for the buildup of the proton gradient while growing on H_2 and CO_2. Therefore, growth and resting cell experiments were performed with H_2/CO_2 to investigate possible changes in the metabolic turnover of H_2/CO_2 to acetate.

Growth experiments on complex medium showed that both strains grew similarly on H_2/CO_2. The wild type had a growth rate of 0.57 h^{-1} and the Δ*ech2* strain had a growth rate of 0.53 h^{-1} (Figure 12 A; Table 12). Measuring the acetate concentration showed that both strains build up acetate at different rates during the exponential phase. The wild type produced 10.4 mM h^{-1} ± 1.0 mM h^{-1} acetate, while the Δ*ech2* strain produced 17.3 mM h^{-1} ± 2.7 mM h^{-1} acetate (Figure 12 B), which is 1.7 times more than the wild type. The final acetate concentration was also different, 118.5 mM ± 7.5 mM acetate were measured in the wild type and 146.7 mM ± 16.2 mM acetate in the Δ*ech2* strain.

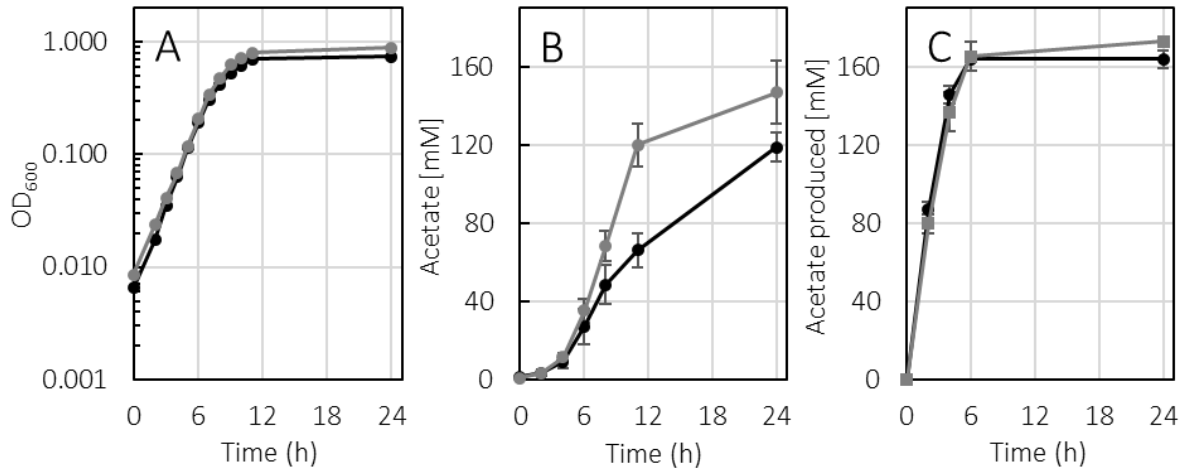

Figure 12 Growth of Δ*ech2* strain on H_2/CO_2.
(A) Representative growth curve of the Δ*ech2* strain (gray) and the wild type strain DSM 2030 (black) in the presence of 3x10^5 Pa H_2/CO_2. After hour 2, H_2/CO_2 was refilled every hour to a pressure of 3x10^5 Pa. (B) Acetate production of the mutant (gray) and the wild type (black) over time grown on H_2/CO_2. All experiments were performed in complex medium at 65 °C and 160 rpm; (n = 4). (C) Acetate production of the Δ*ech2* strain (gray) and the wild type (black) in a resting cell experiment. Incubated for 24 h in defined medium with 3x10^5 Pa H_2/CO_2 (66/33, v/v) at 65 °C and 160 rpm; (n = 3).

Resting cells of the wild type and the Δ*ech2* strain produced the same amount of acetate from 3x10^5 Pa H_2/CO_2 and had a similar production rate of 36.5 mM h^{-1} ± 1.2 mM h^{-1} and 34.5 mM h^{-1} ± 2.6 mM h^{-1}, acetate respectively (Figure 12 C).

The growth experiments on H_2/CO_2 indicated that the deletion of the Ech2 complex leads to a higher conversion rate of H_2/CO_2 to acetate in the mutant and to the assumption that in order to achieve the same growth rate, the mutant may consume more H_2 than the wild type (Figure 12, B).

In summary, the Δ*ech2* strain grew on all substrates and media tested, with no major differences to the wild type (Table 12). The mutant showed a slightly lower final OD_{600} on glucose and fructose, while it grew slightly faster on fructose and mannitol compared to wild type. Metabolically, the Δ*ech2* strain showed a 1.7-fold higher acetate conversion rate during growth on H_2/CO_2 compared to the wild type.

Table 12 Growth rate and doubling time (h) of *T. kivui* wild type (DSM 2030) and the Δ*ech2* strain.
Comparison of the growth of the wild type and the Δ*ech2* strain grown on complex or defined medium containing different sugars or H_2/CO_2 (3x10^5 Pa; 66/33; v/v).

	Substrate	Growth rate (h^{-1})		Doubling time (h)	
		Wild type	Δ*ech2* strain	Wild type	Δ*ech2* strain
Complex medium	Glucose	0.54 ± 0.05	0.55 ± 0.03	1.29 ± 0.12	1.27 ± 0.08
	Fructose	0.47 ± 0.01	0.57 ± 0.02	1.49 ± 0.03	1.21 ± 0.03
	Mannitol	0.40 ± 0.03	0.48 ± 0.04	1.75 ± 0.14	1.47 ± 0.13
	H_2/CO_2	0.57 ± 0.04	0.53 ± 0.02	1.35 ± 0.19	1.38 ± 0.11
Defined medium	Glucose	0.43 ± 0.01	0.44 ± 0.00	1.57 ± 0.01	1.60 ± 0.05
	Mannitol	0.35± 0.03	0.40 ± 0.04	2.01 ± 0.17	1.77 ± 0.20

After the investigation of the growth behavior of *T. kivui*, the expression of specific genes in both the mutant and the wild type was analyzed to confirm any gene expression changes resulting from the loss of the Ech2 complex. For this purpose, samples for RNA extraction were taken during the exponential growth of *T. kivui* (OD_{600} of 0.2 to 0.25; Figure 10 A; Table 12 A) and analyzed using qPCR.

3.2.3 Expression of metabolic relevant genes of the wild type and Δ*ech2* strain

Previous studies have shown a 6- and 16-fold upregulation of *ech1* and *ech2*, respectively, in cells grown in complex medium and H_2/CO_2 compared to cells grown in complex medium and glucose (Schoelmerich and Müller 2019). Deleting the *ech2* operon could lead to a shift in the expression of various genes. Therefore, a small number of representative genes involved in the H_2/CO_2 metabolism were selected for gene expression studies using qPCR. These include the genes encoding the Ech1 complex (*ech1A*), the Ech2 complex (*ech2D*), the formyl tetrahydrofolate synthetase (*fhs*) of the Wood-Ljungdahl pathway and the electron bifurcating hydrogenase (*hydB*).

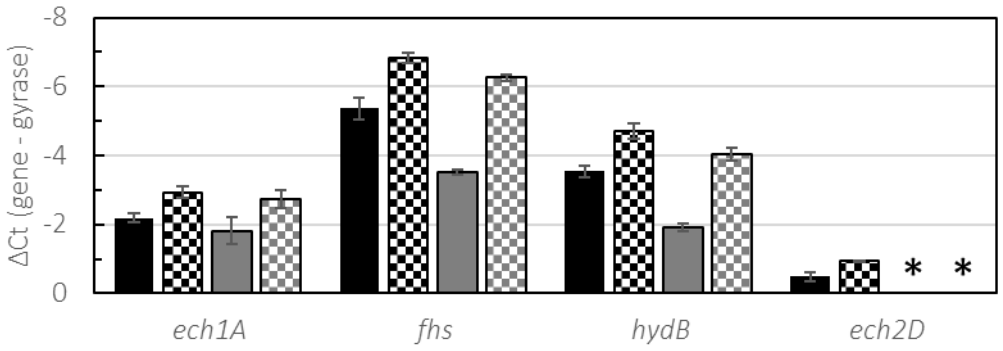

Figure 13 Expression of metabolic relevant genes of the wild type and Δ*ech2* strain.
Wild type strain DSM 2030 (black) and Δ*ech2* strain (gray) grown on complex medium in the presence of 25 mM glucose (filled columns) or 2x10^5 Pa H_2/CO_2 (checkered columns) medium at 65 °C and 160 rpm. The mRNA levels were normalized (ΔCt = gene – *gyrB*) to the abundance of gyrase (*gyrB*). Gene expression was determined for *ech1* (Ech1 complex), *fhs* (formyl-tetrahydrofolate synthetase), *hydB* (electron bifurcating hydrogenase) and *ech2* (Ech2 complex). RNA was extracted from cells that were harvested in the exponential growth phase. The gene *ech2D* was not expressed in the Δ*ech2* strain (*). Biological replicates for glucose cultures (n = 1) and for H_2/CO_2 (n = 2); were tested with varying technical replicates (n=2-4).

Data analysis of the qPCR showed that the ΔCt values of the genes *ech1D*, *fhs* and *hydB* were lower on H_2/CO_2 compared to glucose in both the wild type and the Δ*ech2* strain normalized against *gyrB* (ΔCt; Figure 13), meaning a higher amount of mRNA in the sample of the gene (Schmittgen and Livak 2008). For further comparisons between substrates and strains, the fold change of the ΔΔCt was determined according to Schmittgen and Livak 2008 (Table 13).

Table 13 Fold change values of qPCR of *T. kivui* wild type and Δ*ech2* strain.
Calculated fold change values of *T. kivui* grown on complex medium with glucose or 3x10^5 Pa H_2/CO_2. Comparison of gene expression of H_2/CO_2 (test) to glucose (calibrator) or Δ*ech2* strain (test) to wild type strain DSM 2030 (calibrator). The upregulation of the gene is indicated by blue and downregulation by red. The threshold value for upregulation is 4-fold and for downregulation −4-fold and indicated by darker color.

		Fold change			
Comparison		Wild type	Δ*ech2* strain	Glucose	H_2/CO_2
Test		H_2/CO_2	H_2/CO_2	Δ*ech2* strain	Δ*ech2* strain
Calibrator		Glucose	Glucose	Wild type	Wild type
Gene	*ech1A*	1.7	1.9	−1.3	−1.1
	fhs	2.8	6.7	−3.6	−1.5
	hydB	2.3	4.3	−3.1	−1.6
	ech2D	1.4	*	*	*

The calculated fold change for the condition H_2/CO_2 (test) against glucose (calibrator) of the wild type and the Δ*ech2* strain showed that the *fhs* and *hydB* were upregulated in both strains if grown on H_2/CO_2 but only in the Δ*ech2* strain *fhs* and *hydB* above the threshold of 4. The genes *ech1A* and *ech2D* were not upregulated in both strains during growth with H_2/CO_2 (Table 13). When comparing the Δ*ech2* strain (test) with the wild type (calibrator) under glucose or H_2/CO_2, all genes are slightly downregulated in the Δ*ech2* strain, with *fhs* and *hydB* being the most downregulated but above the threshold of −4 (Table 13).

Only minor changes below the threshold were observed between the regulation of the tested genes in the two strains. However, in the mutant, deletion of the *ech2* gene cluster resulted in lower expression of *fhs* and *hydB* when grown on glucose compared to the wild type grown on glucose. This also results in a higher expression difference above the threshold of *fhs* and *hydB* when comparing growth on H_2/CO_2 to growth on glucose in the mutant (Figure 13, Table 13).

3.3 Growth of the Δ*ech2* strain on Fd-dependent substrates

T. kivui is able to utilize pyruvate and carbon monoxide. Both substrates provide reduced ferredoxin as a reducing agent, which has to be re-oxidized by Ech2 or Ech1 complex according to an assumed pathway model (Katsyv et al. 2021a). Thus, deletion of *ech2* may lead to redox imbalance and inhibited growth, if the Ech1 complex or another ferredoxin dependent enzyme cannot take over its function.

3.3.1 Growth of the Δ*ech2* strain on pyruvate

To answer this question for pyruvate utilization, complex medium cultures of the wild type and the Δ*ech2* strain previously grown on glucose were transferred to complex medium containing 50 mM pyruvate or 25 mM glucose. After inoculation, the wild type grew immediately on glucose and pyruvate, while the Δ*ech2* strain only began to grow immediately on glucose. On pyruvate the mutant did not grow for 48 hours but began growing afterwards. A final OD_{600} of 0.464 ± 0.045 was reached after 96 hours (Figure 14 A). In another adaptation experiment, the Δ*ech2* strain grew after 100 to 120 hours after incubation with pyruvate as substrate (Figure A-1). However, after several passages on pyruvate, the Δ*ech2* strain showed a similar growth rate of 0.46 h^{-1} ± 0.13 h^{-1} (doubling time of 1.53 h) as the wild type 0.44 h^{-1} ± 0.00 h^{-1} (doubling time of 1.61 h; Figure 14 B).

In summary, the Δ*ech2* strain was able to grow with pyruvate as substrate, after an adaption period of 2 to 5 days, while the wild type needed no adaption. In the further course of the study, resting cell experiments were carried out to investigate whether the Δ*ech2* strain metabolizes pyruvate without adaptation and if so, whether there are differences in product formation.

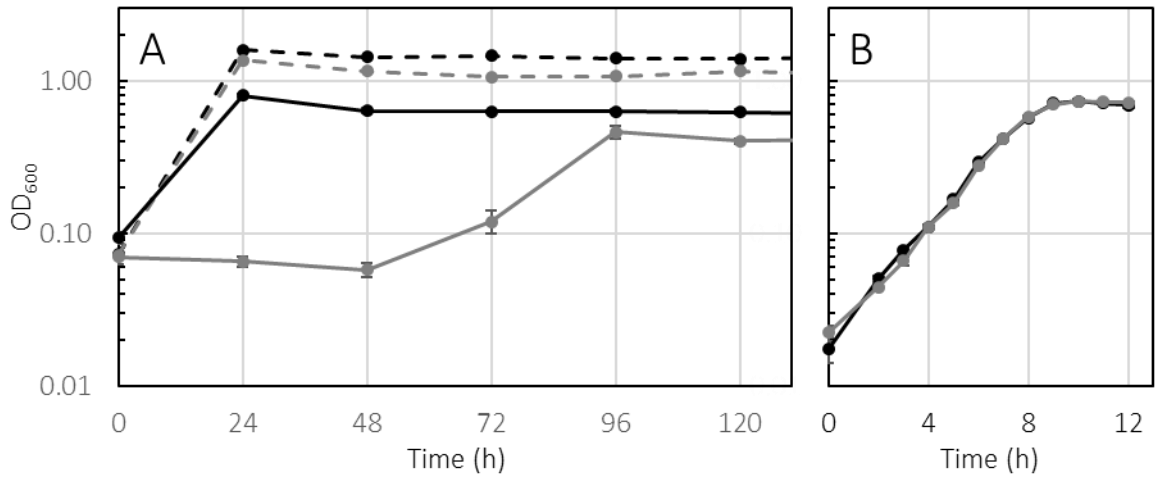

Figure 14 Growth of Δ*ech2* strain on pyruvate.
(A) Representative growth curves of the first transfer of Δ*ech2* strain (gray) and the wild type strain DSM 2030 (black) grown on glucose to medium containing 50 mM pyruvate (lines) or 25 mM glucose (dashed lines). The experiment was performed in Hungate tubes with 5 ml complex medium at 65 °C (n = 3). (B) Growth of the fourth passage on pyruvate of the Δ*ech2* strain (gray) and the wild type (black) in the presence of 50 mM pyruvate. The experiment was performed on complex medium at 65 °C and 160 rpm (n = 3).

3.3.2 Resting cell experiment with the Δ*ech2* strain and the wild type

To test the pyruvate utilization capacity of Δ*ech2* strain cells without adaption to pyruvate, a resting cell experiment was performed. For this purpose, the mutant and the wild type cells were grown on glucose, harvested, washed and concentrated in Tris-HCl buffer to an OD_{600} of around 2. Samples were taken hourly for the first 3 hours, and a final sample after 24 hours. The substrate usage of pyruvate, the production of formate and acetate (Figure 15 A and B) and the protein concentration (Figure 15 C) were monitored.

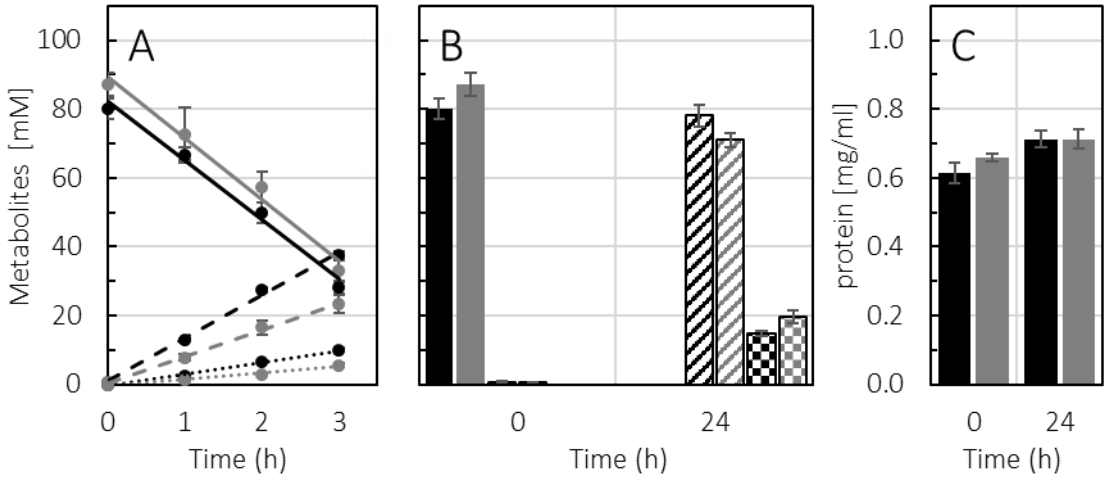

Figure 15 Resting cell experiment of the *T. kivui* wild type DSM 2030 and Δ*ech2* strain.
The wild type (black) and Δech2 strain (gray) of *T. kivui* strains were incubated for 24 hours in 50 mM Tris-HCl buffer with ca. 100 mM pyruvate at 65 °C. A) Concentration changes of pyruvate (solid lines), acetate (dashed lines) and formate (dotted lines) over 3 hours. B) Concentration at the beginning and after 24 hours of pyruvate (filled columns), acetate (striped column) and formate (checkered column). C) Protein concentration at the beginning and after 24 hours (n = 3).

The pyruvate consumption was similar for the wild type (−17.23 mM h^{-1} ± 0.59 mM h^{-1}) and the Δ*ech2* strain (−17.72 mM h^{-1} ± 0.38 mM h^{-1}). However, differences were seen in the acetate (12.45 mM h^{-1} ±

0.4 mM h^{-1} vs. 7.68 mM h^{-1} ± 0.9 mM h^{-1}; respectively) and formate production (3.43 mM h^{-1} ± 0.16 mM h^{-1} vs. 1.84 mM h^{-1} ± 0.14 mM h^{-1}; respectively; Figure 15 A). After 24 hours, pyruvate was completely consumed by the wild type (80.16 mM ± 2.90 mM) and the Δ*ech2* strain (87.11 mM ± 3.24 mM), whereas the acetate production of the wild type (78.09 mM ± 3.30 mM) and the Δ*ech2* strain (71.05 mM ± 2.01 mM) did not correspond to the starting concentration of the pyruvate (Figure 15 B). Formate was produced by the wild type (14.73 mM ± 0.86 mM) and the mutant (19.50 mM ± 1.80 mM). The protein concentration for the wild type was 0.61 mg ml^{-1} ± 0.03 mg ml^{-1} and increased to 0.71 mg ml^{-1} ± 0.03 mg ml^{-1} after 24 hours; while the Δ*ech2* strain started at 0.66 mg ml^{-1} ± 0.01 mg ml^{-1} and after 24 hours increased to 0.71 mg ml^{-1} ± 0.03 mg ml^{-1}. This indicates a slight growth of both strains during the experiment (Figure 15 C).

Moreover, 1 mM acetate requires 1.02 mM pyruvate in the wild type, whereas in the Δ*ech2* strain, 1.23 mM of pyruvate was needed to produce 1 mM acetate. A general loss of carbon during pyruvate utilization could be assumed due to slightly increased protein concentration. In another experiment, no formate production was observed in the wild type during growth on pyruvate (Figure 30).

In summary, resting cells of the *Δech2* strain did utilize pyruvate without adaptation but must be adapted to grow with pyruvate. Also, the wild type produces more acetate from pyruvate (1.02 pyruvate/1 acetate) than the *Δech2* strain (1.23 pyruvate/ 1 acetate). It is not clear why the electron balance of the mutant, in particular, is not closed. No other products were found in HPLC. The fast acetate buildup and higher acetate/pyruvate ratio of the wild type may indicate that the mutant is not able to oxidize Fd_{red}, but all acetate is produced oxidatively, while part of the acetate in the wild type was produced in the WLP.

3.3.3 Growth of the *Δech2* strain on $H_2/CO_2/CO$ and carbon monoxide (CO)

Based on previous studies by Weghoff and Müller (2016), adaptation experiments to synthesis gas and later to CO were performed for the wild type of *T. kivui* and the *Δech2* strain.

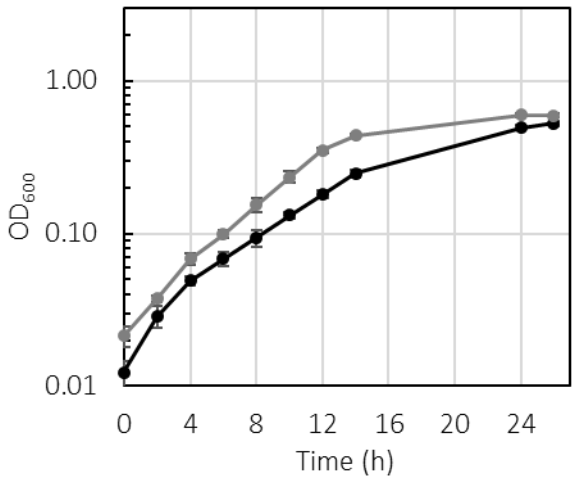

Figure 16 Growth of *T. kivui on* synthesis gas.
Representative growth curve of the wild type strain DSM 2030 (black) and *Δech2* strain (gray) in the presence of 3x10^5 Pa synthesis gas. All experiments were performed on complex medium at 65 °C and 160 rpm. Synthesis gas consisted of $H_2/CO_2/CO$ (44/22/33; v/v/v; [2x10^5 Pa H_2/CO_2 (66/33; v/v) plus 1x10^5 Pa pure CO] (n = 3).

For the adaption of *T. kivui* to synthesis gas, precultures of the wild type and the mutant grown on H_2/CO_2 were transferred to complex medium with a synthesis gas atmosphere (3x10^5 Pa; $H_2/CO_2/CO$; 44/22/33; v/v/v; [2x10^5 Pa H_2/CO_2 (66/33; v/v) plus 1x10^5 Pa CO]). After adaption to synthesis gas, growth experiments (Figure 16) were performed on 3x10^5 Pa synthesis gas containing $H_2/CO_2/CO$

(44/22/33; v/v/v). Both strains grew slower on synthesis gas compared to growth on H_2/CO_2 ($3x10^5$ Pa). The *ech2* strain had a growth rate of 0.21 $h^{-1} \pm 0.00$ h^{-1}, while the wild type had a lower growth rate of 0.16 $h^{-1} \pm 0.01$ h^{-1} (Figure 16).

Afterwards, wild type and Δ*ech2* strain cultures, grown on $H_2/CO_2/CO$ were transferred to complex medium with a CO/N_2 atmosphere ($3x10^5$ Pa; 14/86 v/v) and cultivated for several days at 65 °C at 160 rpm (Figure 17).

In the first transfer (Figure 17; solid line), the wild type grew to an OD_{600} of 0.06 after fourteen days, whereas the Δ*ech2* strain remained at 0.02. After 23 days, the wild type and mutant were passaged (Figure 17; light gray arrow), and the wild type grew to an OD_{600} of 0.12, whereas the mutant stopped growing at around 0.03. The observed growth of the mutant probably due to the yeast extract added to the medium. Thus, the *ech2* strain could not be adapted to carbon monoxide, while the adaption of the wild type occurred.

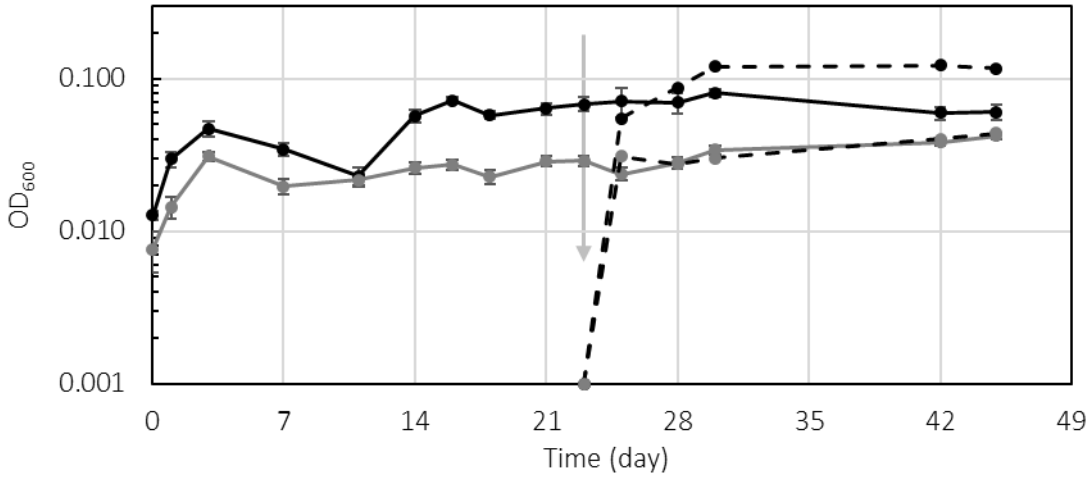

Figure 17 Adaption to CO of *T. kivui* pre-adapted to $H_2/CO_2/CO$.
The Δ*ech2* strain (gray; passage 1 solid lines; passage 2 dashed lines) and the wild type strain DSM 2030 (black; passage 1 solid lines; passage 2 dashed lines) in the presence of CO/N_2 ($3x10^5$ Pa; 14/86 v/v). Inoculation of passage 2 from passage 1 of the wild type and the Δ*ech2* strain (light gray arrow). The experiment was performed on complex medium at 65 °C and 160 rpm (passage 1, n = 3 and passage 2, n = 2).

To test whether the Δ*ech2* strain utilized carbon monoxide, a resting cell experiment was performed. Towards that, the Δ*ech2* strain, the wild type and the wild type after adaption to CO (Figure 17) were cultivated on glucose, harvested, washed and concentrated in imidazole buffer. The concentrated cells were transferred to serum bottles and the atmosphere was exchanged to CO/N_2 ($3x10^5$ Pa; 14/86 v/v) or $H_2/CO_2/CO$ ($3x10^5$ Pa; 44/22/33; v/v/v). Afterwards the cells were incubated for 24 hours at 65 °C and 160 rpm.

The wild type (9.3 mM ± 0.9 mM) and the CO adapted wild type (12.1 mM ± 0.3 mM) produced around 10 mM acetate after 24 hours, whereas the Δ*ech2* strain only produced 1.3 mM ± 1.0 mM acetate. It should be noted that only one of the three samples had produced 2.6 mM, while the other two had produced less than 1.0 mM acetate (Figure 18 A).

In contrast to the resting cell experiment conducted with a 14 % CO atmosphere, the $H_2/CO_2/CO$ atmosphere resulted in varying acetate production for all tested strains. The *Δech2* strain was found to produce the most acetate (91.5 mM ± 0.0 mM), followed by the wild type (76.6 mM ± 2.6 mM) and finally, the CO-adapted wild type (23.3 mM ± 3.6 mM).

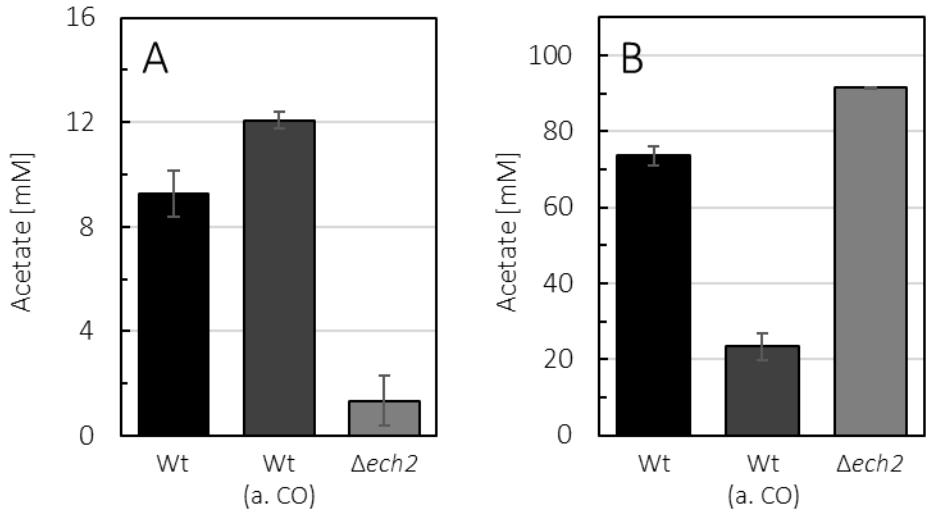

Figure 18 Resting cell experiment of the *T. kivui* with a CO or $H_2/CO_2/CO$ atmosphere.
The wild type strain DSM 2030 (Wt; black), CO adapted wild type (Wt a. CO; dark gray) and Δ*ech2* strain (Δ*ech2*; gray) were incubated for 24 hours in imidazole buffer with A) CO/N_2 ($3x10^5$ Pa; 14/86 v/v) or B) $H_2/CO_2/CO$ ($3x10^5$ Pa 44/22/33; v/v/v) in the atmosphere at 65 °C and 160 rpm (n = 3).

In summary, the Δ*ech2* strain can neither be adapted to CO, nor convert CO to acetate in the cell resting experiment. However, the Δ*ech2* strain grew on $H_2/CO_2/CO$, suggesting it may be tolerant to CO, while H_2/CO_2 was utilized. Interestingly, the wild type produced around 9 mM acetate and with $3x10^5$ Pa CO/N_2 (14/86; v/v) in the atmosphere, and with $3x10^5$ Pa $H_2/CO_2/CO$ (44/22/33; v/v/v) around 77 mM acetate. Meanwhile, the wild type adapted to CO produced a similar amount of acetate with CO (12 mM) but three times less the amount of acetate on $H_2/CO_2/CO$ (23 mM) compared to the wild type indicating that the CO adapted wild type may have lost the ability to utilize H_2.

3.3.4 Promoter exchange of the *ech1* gene cluster

The successful deletion of the entire *ech2* gene cluster showed that the Ech2 complex is not essential for the growth on sugar, sugar alcohols and H_2/CO_2 but is important during utilization of pyruvate and CO. The next logical step was to attempt to delete the entire *ech1* gene cluster using the same method used to generate the Δ*ech2* strain. A plasmid similar to pEch2TK02 but with flanking regions of the *ech1* gene cluster was constructed pEch1TK02 and used to transform strain TKV002 (Δ*pyrE*). The deletion of the *ech1* gene cluster was not successful, and after eight unsuccessful attempts (Table A-1), it was concluded that deletion of *ech1* may not be possible.

To address the issue of energy conservation and ferredoxin turnover by the Ech1 complex, attempts were made to downregulate the expression of the *ech1* by replacing the *ech1* promoter with a fructose inducible promoter (P_{frc}). This fructose promoter was characterized by Benjamin Zeldes (University personal communication; Zeldes et al. 2024), who had performed expression analyses of various promoters suitable for use in *T. kivui*. Therefore, strain *T. kivui* TKV002 (Δ*pyrE*) and the Δ*ech2* strain were transformed with PCR fragments of plasmid p144 (Zeldes et al. 2024). The used PCR fragments of p144 contained a fructose promoter (P_{frc}) and the *pyrE* gene under the control of the gyrase promoter of Thermoanaerobacter sp. strain X514 (Basen et al. 2018) between the UFR and DFR promoter region of the *ech1A* gene (Figure 19).

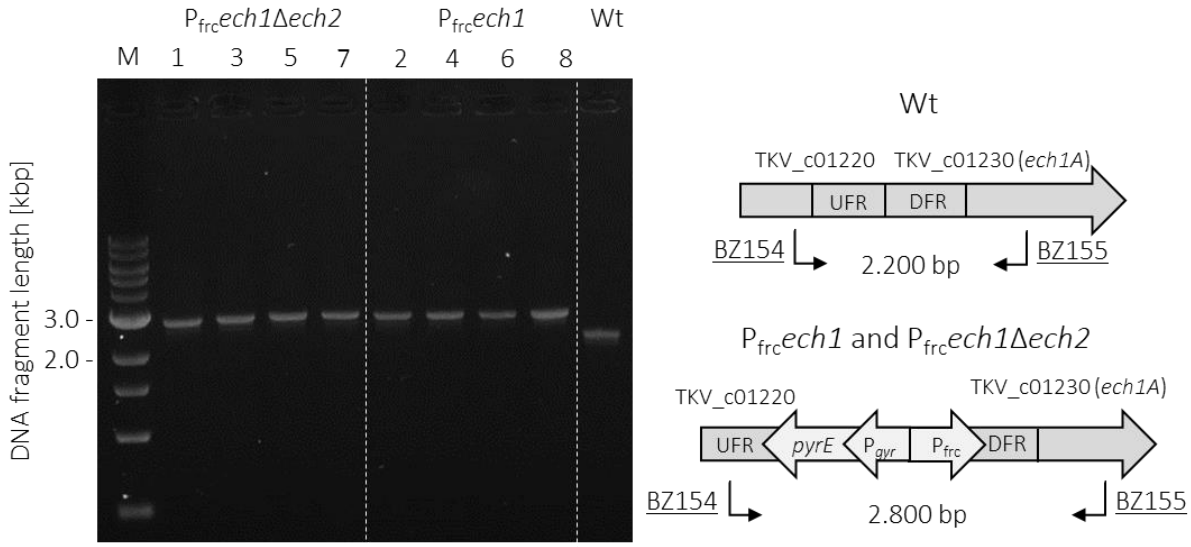

Figure 19 Verification of *ech1* promoter exchange.
The promoter exchange was verified by PCR using primers binding outside of the *ech1A* promoter region. Shown are the amplified DNA fragments of *T. kivui* wild type (Wt; DSM 2030; fragment size, 2.2 kbp), P$_{frc}$*ech1* and P$_{frc}$*ech1*Δ*ech2* (fragment size, 2.8 kbp). The integration of the *pyrE* gene under control of a gyrase promoter (P$_{gyr}$) plus the promoter P$_{frc}$ led to a fragment extension of about 600 bp. The agarose gel was stained with midori green.

The integration of the *pyrE* gene and the successful exchange of the *ech1* promoter with the fructose promoter (P$_{frc}$) was verified by PCR and sequencing of the PCR fragment. For further studies, one of each promoter mutant was chosen and designated as strain P$_{frc}$*ech1* and P$_{frc}$*ech1*Δ*ech2*.

3.3.5 Characterization of strain P$_{frc}$*ech1* and P$_{frc}$*ech1*Δ*ech2*

Growth experiments with glucose and fructose were performed on defined medium, and samples for RNA extraction were collected during exponential growth (OD$_{600}$ 0.2 to 0.3) to examine differences in gene expression of the genes *ech1A, ech2D* and *fruK*.

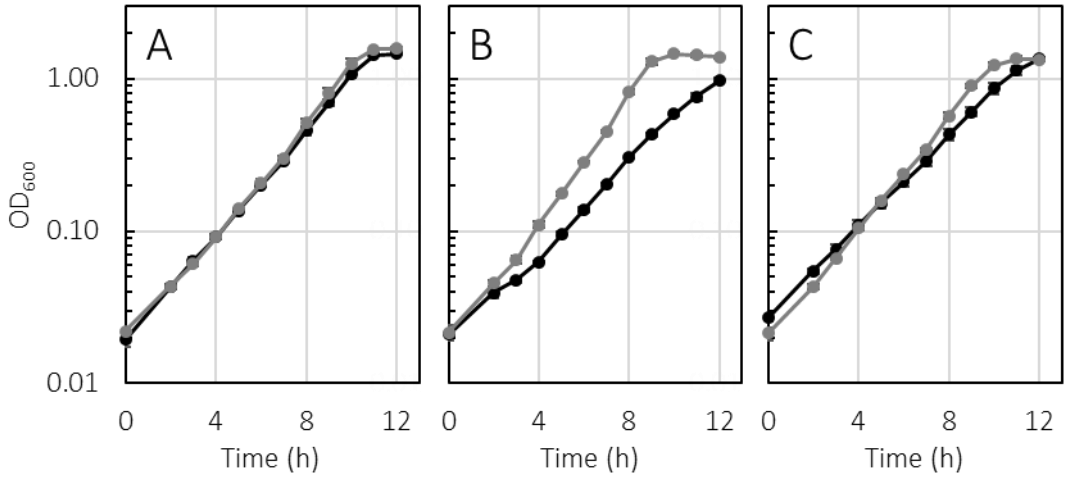

Figure 20 Growth of P$_{frc}$*ech1* and P$_{frc}$*ech1*Δ*ech2* strain strains on glucose and fructose.
Representative growth curve of the A) wild type (DSM 2030), B) P$_{frc}$*ech1* and C) P$_{frc}$*ech1*Δ*ech2* in the presence of 25 mM glucose (black) or 25 mM fructose (gray). The experiment was performed on defined medium at 65 °C and 160 rpm. Biological replicates (n = 3).

The *ech1* promoter exchange strains grew at almost the same rate on glucose than the wild type (DSM 2030). The mutant P$_{frc}$*ech1* grew even slightly faster on fructose than the wild type, whereas P$_{frc}$*ech1*Δ*ech2* grew slightly slower than the wild type and the P$_{frc}$*ech1* mutant (Figure 20 and Table 14).

Table 14 Growth rate (h^{-1}) and doubling time (h) of *T. kivui* promoter mutant strains.
Comparison of growth rate and doubling time (h) of the wild type, P_{frc}*ech1* and P_{frc}*ech1Δech2* strain grown on defined medium and 25 mM Glucose or 25 mM fructose.

Strain	Growth rate (h^{-1})		Doubling time (h)	
	Glucose	Fructose	Glucose	Fructose
Wild type (DSM 2030)	0.42 ± 0.01	0.46 ± 0.01	1.64 ± 0.04	1.51 ± 0.03
P_{frc}*ech1*	0.36 ± 0.00	0.50 ± 0.01	1.90 ± 0.01	1.40 ± 0.03
P_{frc}*ech1Δech2*	0.35 ± 0.00	0.43 ± 0.01	1.98 ± 0.03	1.60 ± 0.03

The slower growth of the promoter mutants on glucose compared to the wild type might be due to the *ech1* operon being expressed less than in the wild type on glucose. To verify whether the expression of *ech1A* in the promoter mutant's changes depending on the sugar present, qPCR was performed with RNA extracted from cells harvested during the exponential growth phase at an OD_{600} of around 0.2 (Figure 21).

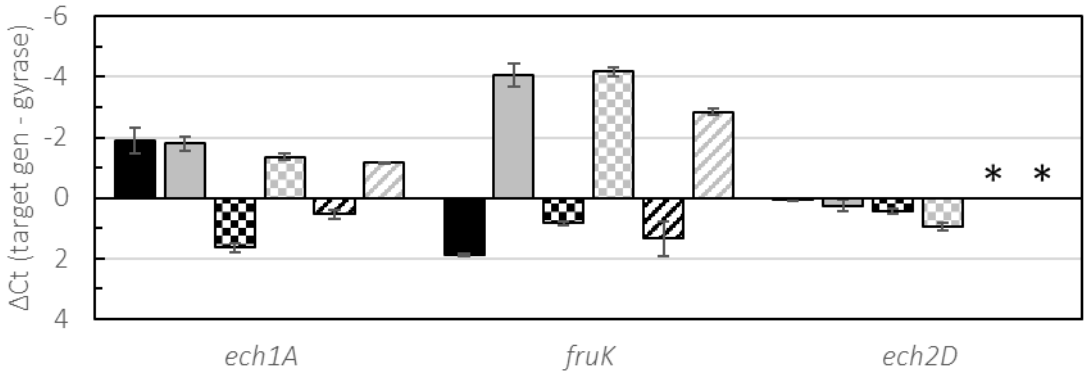

Figure 21 Gene expression of on glucose and fructose of the *ech1* promoter exchange strains.
Gene expression of the wild type (filled column), P_{frc}*ech1* (checkered column) and P_{frc}*ech1Δech2* (striped column) grown on glucose (black) or on fructose (light gray). The mRNA levels were normalized to the abundance of gyrase (*gyrB*). Gene expression was determined for *ech1A* (Ech1 complex), *ech2D* (Ech2 complex) and *fruK* (1-phosphofructosekinase). The RNA was extracted from cells harvested during the exponential growth phase. The associated growth experiment was performed on defined medium at 65 °C and 160 rpm. Multiple biological replicates (n =2) and technical replicates (n = 3) were tested. The gene *ech2D* is not depicted for P_{frc}*ech1Δech2* (*).

As expected, the expression of *ech1A* was lower when the *ech1* promoter mutants were grown with glucose compared to the wild type. When grown on fructose, the expression of *ech1A* increased in the mutants but was overall still below the expression of *ech1A* in the wild type. Meanwhile, in the wild type, the expression of *ech1A* was equally high for both sugars (Figure 21; Table 15).

Table 15 Fold change values of qPCR of *ech1* promoter mutants grown on glucose or fructose (Figure 21).
Calculated fold change values of the *T. kivui* wild type (DSM 2030), strain P_{frc}*ech1* and strain P_{frc}*ech1Δech2* grown on defined medium with 25 mM glucose or 25 mM fructose. Comparison of gene expression fructose (test) compared to glucose (calibrator) or P_{frc} mutant (test) compared to wild type (calibrator). The upregulation of the gene is indicated by blue and downregulation by red. The threshold value for upregulation is 4-fold and for downregulation −4-fold and indicated by darker color.

		Fold change				
Test		Wild type Fructose	P_{frc}*ech1* Glucose	P_{frc}*ech1* Fructose	P_{frc}*ech1Δech2* Glucose	P_{frc}*ech1Δech2* Fructose
Calibrator		Wild type glucose				
Gene	*ech1A*	−1.1	−11.5	−1.5	−5.4	−1.7
	fruK	60.7	2.1	66.8	1.5	26.5
	ech2D	−1.1	−1.3	−1.8	*	*

The calculated fold change showed that on glucose, *ech1A* was downregulated by −11.5-fold in P_{frc}*ech1* and −5.36-fold in P_{frc}*ech1*Δ*ech2* compared to the wild type (Table 15). When the mutants were grown on fructose, *ech1A* was higher expressed than on glucose, but still lower than in the wild type on fructose or glucose.

Since *ech1A* was still expressed, indicating growth on glucose or other high-energy substrates is still possible, this method does not seem sufficient to mimic the deletion of *ech1* gene cluster. However, the low expression of *ech1A* could lead to impaired growth on low-energy substrates such as pyruvate or H_2/CO_2. Thus, transfer experiments were performed from glucose to pyruvate or H_2/CO_2.

3.3.6 Transfer experiment of P_{frc}*ech1* and P_{frc}*ech1*Δ*ech2* from glucose to pyruvate or H_2/CO_2

The Δ*ech2* strain showed a phenotype when transferred to pyruvate for the first time (Figure 14), and a similar phenotype was expected for the P_{frc}*ech1*Δ*ech2* strain. If the Ech1 complex is required for re-oxidation of reduced ferredoxin (Fd_{red}), the two-promotor exchange mutants should exhibit different phenotypes compared to the wild type, the Δ*ech2* strain, and each other (Figure 22).

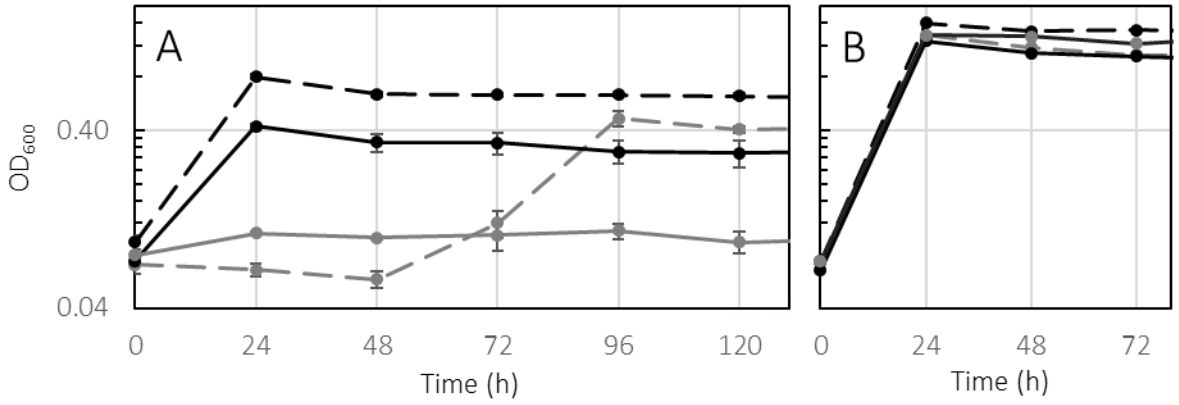

Figure 22 First transfer of *T. kivui* strains from glucose to pyruvate.
Growth of the *T. kivui* wild type (black, dashed), strain P_{frc}*ech1* (black; solid), strain Δ*ech2* (gray; dashed) and strain P_{frc}*ech1*Δ*ech2* (gray; solid) in the presence of A) 100 mM pyruvate or B) 25 mM glucose. The experiment was carried out in Hungate tubes with 5 ml complex medium at 65°C (n = 3).

All four tested strains grew on glucose immediately after inoculation (Figure 22 B), as did the wild type and the P_{frc}*ech1* mutant on pyruvate. While the wild type reached a final OD_{600} of 0.8 on pyruvate, the P_{frc}*ech1* mutant only reached of final OD_{600} of 0.42. As mentioned before, the Δ*ech2* strain did not grow on pyruvate for the first 48 hours, but reached a final OD_{600} of around 0.46 after 96 hours (Figure 14 A; Figure 22). In contrast to the Δ*ech2* strain, the P_{frc}*ech1*Δ*ech2* strain showed a small increase of the OD_{600} from 0.08 to 0.11 after 24 hours. However, the strain stayed at this OD_{600} for the duration of the experiment (Figure 22 A).

As both Ech complexes are assumed to be involved in energy conservation during growth on H_2/CO_2, a growth phenotype under these conditions was expected. Therefore, a transfer experiment from glucose to H_2/CO_2 was conducted with the mutants. The transfer experiment showed that P_{frc}*ech1*Δ*ech2* took over 144 hours to grow on H_2/CO_2, while the wild type and P_{frc}*ech1* mutant took 96 to 116 hours to grow (Figure A-2). These preliminary data suggest that the mutants are capable of growth on H_2/CO_2. However, it is unclear how growth on H_2/CO_2 occurred with *ech1* being downregulated, so further experiments need to confirm the results.

Based on these results, it can be concluded that both promoter strains show a phenotype of reduced growth on pyruvate. While the presence of the Ech2 complex allows immediate growth to a lower final

OD_{600}, the loss of the Ech2 complex leads to a long adaptation time (Δ*ech2* strain) and the additional downregulation of *ech1* to growth inhibition. This implies that both the Ech1 and Ech2 complexes are needed for growth on pyruvate without growth impairment. This suggests that both complexes are partially required for the re-oxidation of reduced ferredoxin (Fd_{red}) and, thus, also for energy conservation.

3.4 Mixotrophic growth of *T. kivui* (DSM 2030)

3.4.1 Mixotrophic growth of *T. kivui* with pure H_2 in the atmosphere

Hydrogen (H_2) is one of the redox partners in the metabolic pathway of *T. kivui*, which can be utilized by the Ech complexes, electron bifurcating hydrogenase (HydABC) and hydrogen-dependent carbon dioxide reductase (HDCR). In case of growth on glucose (Figure 3), an Ech complex is presumed to oxidize H_2 to H^+ and to reduce Fd_{ox} to Fd_{red} at the expense of the proton gradient. HydABC reduces H^+ to H_2 and oxidizes NADPH to $NADP^+$ and Fd_{red} to Fd_{ox} and the HDCR oxidizes H_2 to H^+ and reduces CO_2 to formate based on the model for glucose utilization of *T. kivui* (Figure 3; Katsyv et al. 2021a). Thus, excess H_2 could disturb the metabolic redox balance in *T. kivui* during growth on organotrophic substrates such as glucose. Several growth experiments with hydrogen in the atmosphere were carried out to investigate this hypothesis.

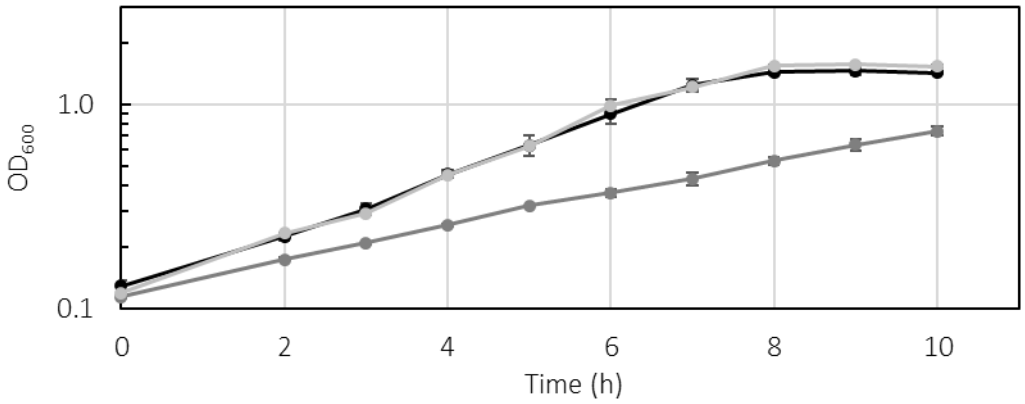

Figure 23 Mixotrophic growth of *T. kivui* (DSM 2030).
Representative growth curve of *T. kivui* in the presence of 25 mM glucose (black), glucose plus H_2 (dark gray) and glucose plus N_2 (light gray). Before inoculation, $1x10^5$ Pa pure H_2 or N_2 was added to the serum bottles (Total pressure $2x10^5$ Pa). The experiment was performed on defined medium at 65 °C and 160 rpm (n = 2).

First, a growth experiment was carried out on defined medium containing 25 mM glucose and different atmosphere conditions (Figure 23), inoculated with a preculture grown on glucose and an N_2/CO_2 atmosphere ($1x10^5$ Pa; 80/20; v/v). The first condition was N_2/CO_2 ($1x10^5$ Pa; 80/20; v/v), the second, was N_2/CO_2 ($2x10^5$ Pa; 90/10; v/v/v) and the third, was $N_2/CO_2/H_2$ ($2x10^5$ Pa; 40/10/50; v/v/v). The cultures with 80/20 N_2/CO_2 atmosphere and glucose had a growth rate of 0.35 h^{-1} ± 0.01 h^{-1} (doubling time 1.99 h), with the 90/10 N_2/CO_2 the growth rate was 0.35 h^{-1} ± 0.01 h^{-1} (doubling time 1.95 h) and with 40/10/50 $N_2/CO_2/H_2$ atmosphere the growth rate was 0.18 h^{-1} ± 0.01 h^{-1} (doubling time 3.84 h). The growth of *T. kivui* was impaired only when H_2 was in the atmosphere but not when the CO_2 ratio changed. In addition to the altered growth with H_2 in the atmosphere, the gene expression of hydrogenases or other enzymes of *T. kivui* could have changed. For more insights, samples were taken during the exponential growth phase (OD_{600} of 0.4 to 0.5) of *T. kivui* for RNA extraction. Afterwards, qPCR analysis (Figure 24) to determine the expression of genes encoding for Ech1 complex (*ech1A*), Ech2 complex (*ech2D*), electron bifurcating hydrogenase (*hydB*) and ferredoxin (*fd1*; TKV_c16450) were conducted.

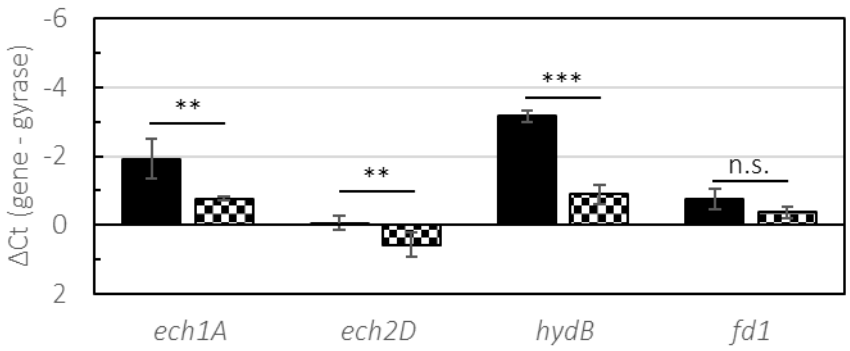

Figure 24 Expression of metabolic relevant genes of *T. kivui* (DSM 2030).
Gene expression in *T. kivui* in the presence of 25 mM Glucose with a N_2/CO_2 ($1x10^5$ Pa; 80/20; v/v) atmosphere (filled columns) or 25 mM Glucose with a $N_2/CO_2/H_2$ ($2x10^5$ Pa; 40/10/50; v/v/v) atmosphere (checkered columns; Figure 24). The Ct values of *ech1A* (Ech1), *ech2D* (Ech2), *hydB* (electron bifurcating hydrogenase; HydABC) and *fd1* (ferredoxin; TKV_c16450) were normalized to the abundance of gyrase (*gyrB*). The RNA was extracted from cells harvested during the exponential growth phase. The associated growth experiment was performed on defined medium at 65 °C and 160 rpm. Multiple biological replicates (n = 2) and technical replicates (n = 3) were tested. The P(T<=t) (n.s. = P > 0.05, * = P ≤0.05, ** = P ≤0.01 or P ≤0.001) was calculated by t-test (one-tailed and two-sample unequal variance).

When comparing the qPCR analyses (Figure 13; Figure 21; Figure 24), it is noticeable that the ΔCt value for *ech1A* was about −2 when *T. kivui* grew on glucose, regardless of whether complex or defined medium was used. This shows that *ech1A* was in the same ratio to gyrase regardless of how much RNA was extracted or at what OD_{600} range from 0.2 to 0.5, indicating that the amount of RNA did not matter once the ΔCt was calculated. Based on the ΔCt values (Figure 24) and the fold change values (Table 16), all genes are slightly downregulated when H_2 was present in the atmosphere. In particular, the expression of the HydABC (*hydB*) was more than −4-fold downregulated.

Table 16 Fold change values of qPCR of wild type.
Calculated fold change values of *T. kivui* grown on glucose and a N_2/CO_2 or a $N_2/CO_2/H_2$ atmosphere (Figure 24). Change of gene expression of glucose plus H_2 (test) compare to glucose (calibrator). The upregulation of the gene is indicated by blue and downregulation by red. The threshold value for upregulation is 4-fold and for downregulation −4-fold and indicated by darker color.

		Fold change			
Test	Calibrator	*ech1A*	*ech2D*	*hydB*	*fd1*
Glucose plus H_2	Glucose	−2.2	−1.5	−4.8	−1.3

These results demonstrate that exposure to H_2 inhibits growth and alters the expression of certain genes in organotrophically growing cells of *T. kivui*. Further growth experiments with glucose, mannitol and pyruvate were performed to verify this effect in the presence of other organotrophic substrates. For example, when mannitol is used as a substrate, a higher amount of the electron carrier NADH is provided, while only Fd_{red} is provided when pyruvate is used as a substrate.

3.4.2 Mixotrophic growth of *T. kivui* with H_2/CO_2 in the atmosphere

For better comparison, the atmosphere composition of 40/10/50 $N_2/CO_2/H_2$ ($2x10^5$ Pa; v/v/v) was changed to 40/26.6/33.3 $N_2/CO_2/H_2$ ($2x10^5$ Pa; v/v/v), to mimic a CO_2 concentration similar to growth on H_2/CO_2 (66.6/33.3; v/v).

Furthermore, apart from growth on glucose, the substrates mannitol and pyruvate were investigated and it was tested to see if adaptation to H_2/CO_2 was possible. To accomplish H_2 adaption, cultures of *T.*

kivui were pre-grown on the respective substrate with 40/26.6/33.3 $N_2/CO_2/H_2$ atmosphere and then used in growth experiments.

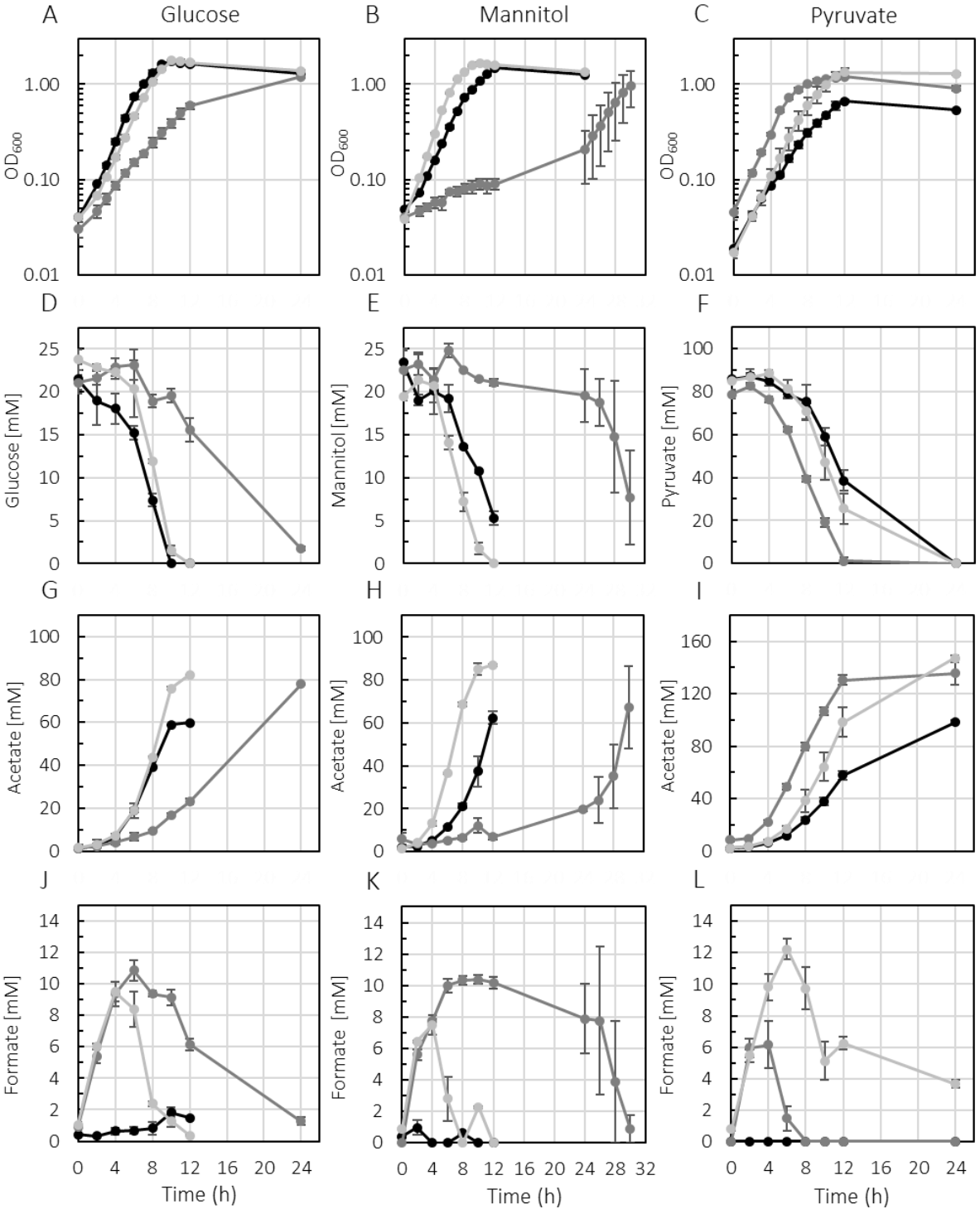

Figure 25 Growth of *T. kivui* (DSM 2030) on substrate with and without H_2/CO_2.
Pre cultures of *T. kivui* grown in the presence or absence of H_2 were used to inoculate complex medium containing 25 mM glucose (A), 25 mM mannitol (B) or 100 mM pyruvate (C). Serum bottles containing $1x10^5$ Pa N_2/CO_2 atmosphere (80/20; v/v) were gassed before use with an overpressure of $1x10^5$ Pa N_2/CO_2 (80/20; v/v) or H_2/CO_2 (66.6/33.3; v/v). Shown is the growth of unadapted cells without (black) and with (dark gray) H_2/CO_2 in the atmosphere and H_2 adapted cells with (light gray) H_2/CO_2 in the atmosphere. The OD_{600} and the concentrations of glucose (D), mannitol (E), pyruvate (F), acetate (G, H and I) and formate (J, K and L) were measured. All experiments were performed at 65 °C and 160 rpm. Three biological replicates with glucose or pyruvate and two biological replicates with mannitol were investigated.

The cultures grown on glucose and mannitol with an N_2/CO_2 atmosphere (Figure 25, black) grew similarly to the cultures in previous growth experiments (Table 12; Table 17). The pyruvate cultures grew slightly slower than previously observed (doubling time 2.06 h vs. 1.61 h). In all cultures, the substrates were completely utilized within 24 hours, no formate was produced during exponential growth, and the final product was acetate (Figure 25, black).

In contrast, the cultures grown with H_2/CO_2 atmosphere (Figure 25, A and B), which were not previously adapted to H_2 (Figure 25, gray), were inhibited in their growth on glucose and mannitol. The glucose cultures grew with a doubling time of 2.31 hours (Figure 25, A; Table 17), but the mannitol cultures only doubled every 10 hours until hour 24, after which the cultures continued to grow with a doubling time of 2.20 hours. The pyruvate cultures (Figure 25, C) were not inhibited by H_2 in the atmosphere and even grew to a higher final OD_{600} than without H_2 (Table 17). All cultures produced up to 11 mM formate as intermediate (Figure 25, J, K and L). In the glucose and pyruvate cultures, formate was produced in the beginning and then decreased continuously with increasing OD_{600}. In the mannitol cultures, formate remained at a high concentration (10 mM) for a longer period until the OD_{600} increased after 24 hours, after which the formate concentration decreased. In all cultures with the H_2/CO_2 atmosphere, the final acetate concentration was higher than those without H_2/CO_2.

The H_2 adapted cultures pre-grown on glucose, mannitol or pyruvate and H_2/CO_2 atmosphere (Figure 25; A, B and C, light gray) grew differently than the unadapted cultures (Figure 25; dark gray). The H_2 adapted glucose cultures showed no visible growth inhibition, while the H_2 adapted mannitol cultures grew even a little faster in the presence of H_2/CO_2 than without. On pyruvate, the H_2 adapted cultures grew similarly to the unadapted cells (Table 17). Formate production was observed but it was consumed faster than in the unadapted cultures (Figure 25, J and K).

Cell growth of H_2 adapted pyruvate cultures showed a different formate consumption pattern than the unadapted cells. About 12 mM formate was produced, which was consumed until the formate concentration reached about 6 mM, then the formate concentration remained at 6 mM, and after 24 hours, the final formate concentration was 4 mM. The acetate concentration produced by the H_2 adapted cells was similar to that of the unadapted cells when grown on a substrate with H_2/CO_2 in the atmosphere.

Table 17 Doubling time (h) of unadapted and H_2 adapted *T. kivui* cells.
Doubling time of *T. kivui* grown on 25 mM glucose, 25 mM mannitol or 100 mM pyruvate with and without $1x10^5$ Pa H_2/CO_2 overpressure in the atmosphere (40/26.6/33.3; $N_2/CO_2/H_2$; v/v/v; Figure 25) on complex medium.

	Doubling time (h)		
	Unadapted cells		H_2 adapted cells
Substrate	Substrate	Substrate and H_2/CO_2	Substrate and H_2/CO_2
Glucose	1.29 ± 0.01	2.31 ± 0.19	1.48 ± 0.02
Mannitol	1.78 ± 0.03	10.06 ± 0.57	1.33 ± 0.01
Pyruvate	2.06 ± 0.08	1.47 ± 0.08	1.57 ± 0.04

In summary, the inhibition effect of H_2 in the atmosphere occurred only in cultures grown on glucose and mannitol but not on pyruvate. This experiment also showed that *T. kivui* pre-adapted to H_2, resulted in no growth inhibition, but the same doubling times or even a reduction in doubling times in the case of mannitol were observed.

3.4.3 Hydrogen shock during exponential growth of *T. kivui* on complex medium

To investigate the immediate reaction to H_2, cultures grown on glucose, mannitol and pyruvate were shocked during exponential growth with H_2/CO_2 (overpressure $1x10^5$ Pa) at an OD_{600} of 0.25 to 0.35, and samples for gene expression analyses were taken 5 minutes before and 15 minutes after the shock.

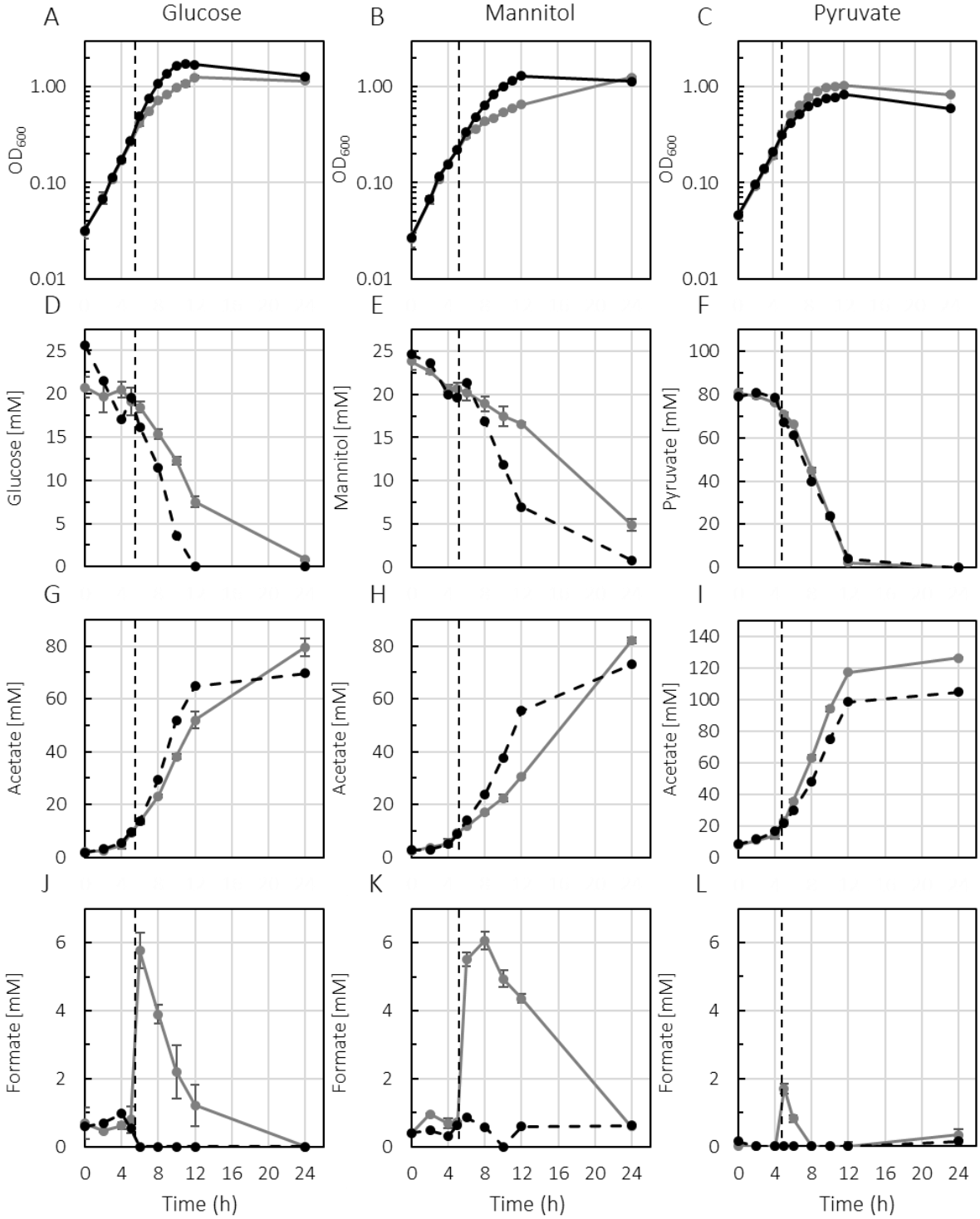

Figure 26 Hydrogen shock of *T. kivui* (DSM 2030) during exponential growth on different substrates. Representative growth curve of *T. kivui* grown on glucose (A), mannitol (B) or pyruvate (C; black) and wild type on glucose (A), mannitol (B) or pyruvate (C) shocked with H_2 (gray). Cultures were shocked with $1x10^5$ Pa H_2/CO_2 overpressure after hour 5 of the experiment (black dashed line). Samples for RNA extraction were taken 5 minutes before and 15 minutes after the H_2 shock. Shown are the OD_{600} and the concentration of glucose (D), mannitol (E), pyruvate (F), acetate (G, H and I) and formate (J, K and L). All experiments were performed on complex medium at 65 °C and 160 rpm (n = 3).

Cultures grown on glucose and mannitol were inhibited shortly after the addition of H_2/CO_2 in the atmosphere during the exponential growth phase, while the pyruvate cultures continued to grow. Before the addition of H_2/CO_2, the glucose cultures had a doubling time of 1.61 hours and after the shock with H_2/CO_2, the doubling time was 3.26 hours (Table 18; Figure 26, A), while the doubling time of the mannitol cultures was 1.61 hours before and 5.65 hours after the shock with H_2/CO_2 (Table 18; Figure 26, B). The pyruvate cultures showed similar growth before and after the shock (Table 18; Figure 26, C). Thus, the H_2/CO_2 shock did not affect the growth rate of *T. kivui* on pyruvate but resulted in a higher final $OD_{600,}$ as observed for the mixotrophic cultures before.

Table 18 Doubling time (h) of *T. kivui* (DSM 2030) before and after hydrogen shock.
Shown is the doubling time of *T. kivui* grown on complex medium containing 25 mM glucose, 25 mM mannitol or 100 mM pyruvate before and after shocked with H_2/CO_2 ($1x10^5$ Pa overpressure). The control cultures were not shocked with H_2/CO_2.

	Doubling time (h)					
Substrate	Glucose		Mannitol		Pyruvate	
Culture	H_2 shock	control	shock	control	shock	control
before H_2 shock	1.61 ± 0.12		1.61 ± 0.11		1.89 ± 0.10	
after H_2 shock	3.26 ± 0.16	1.74	5.65 ± 0.47	2.31	2.03 ± 0.14	2.8

Formate was produced immediately after the H_2/CO_2 shock with all three substrates (Figure 26, J, K and L). The glucose and mannitol cultures showed a formate production of up to 6 mM, after which the formate concentration decreased over time. Moreover, formate utilization was faster in the glucose cultures (−0.77 mM h^{-1}) than in the mannitol cultures (−0.33 mM h^{-1}). The pyruvate cultures produced only around 2 mM, which was consumed within 3 hours (Figure 26, L).

Table 19 Substrate consumption rate of *T. kivui* after the H_2 shock.
The consumption rate of *T. kivui* of glucose, mannitol and pyruvate after the shock with H_2/CO_2 is shown compared to consumption rates of unshocked cultures.

	Substrate consumption rate (mM h^{-1})	
Substrate	H_2 shock culture	Control culture
Glucose	−1.80	−2.82
Mannitol	−0.89	−2.41
Pyruvate	−10.68	−9.42

After the addition of H_2, the substrate consumption was decreased by 1 mM h^{-1} for glucose and by 1.5 mM h^{-1} for mannitol, while the consumption rate increased on pyruvate by around 1 mM h^{-1} compared to the control cultures (Table 19; Figure 26, D, E and F).

Similar observations were made for the acetate production after the H_2 shock: In the glucose and mannitol cultures, the acetate production rate decreased after adding H_2/CO_2 compared to the control culture, yet the final acetate concentration was higher. In contrast to that, the pyruvate cultures had a slightly higher acetate production rate compared to the control culture (Table 20; Figure 26, G, H and I). Furthermore, the shocked pyruvate cultures showed a short-term reduction of pyruvate consumption direly after the addition of H_2/CO_2 (hours 5 to 6; Figure 26, F).

In summary, unadapted cells responded similarly to H_2, when it was present in the atmosphere prior to inoculation or when H_2 was added during the exponential growth phase. The main difference between the addition during growth (Figure 26) and the addition before inoculation (Figure 25) was the inhibitory effect on the glucose and mannitol cultures. The cultures on glucose showed a doubling time of 3.26 hours after the H_2 shock (Table 18) and had doubling time of 2.31 hours when H_2 was the atmosphere

prior to inoculation (Table 17), whereas the cultures on mannitol showed a doubling time of 5.65 hours after shock (Table 18) and of 10.06 hours when H_2 was the atmosphere prior to inoculation (Table 17).

Table 20 Acetate production rate of *T. kivui* after the H_2 shock.
Shown is the acetate production rate of *T. kivui* grown on glucose, mannitol or pyruvate after the shock with H_2/CO_2 compared to consumption rates of unshocked cultures.

Acetate production rate (mM h^{-1})		
Substrate	H_2 shock culture	Control culture
Glucose	6.16	8.30
Mannitol	2.99	6.56
Pyruvate	13.70	11.05

I anticipated that this inhibitory effect on growth with glucose or with mannitol induced by the addition of H_2 is associated with a change in gene expression of metabolically important genes. To gain further insights, samples were taken for RNA extraction during the exponential growth phase at an OD_{600} of 0.3 to 0.4 for qPCR analyses (Figure 27), to determine the expression of genes encoding for Ech1 complex (*ech1A*), Ech2 complex (*ech2D*), formyl-tetrahydrofolate synthetase (*fhs*), HDCR (*fdhF*), transhydrogenase subunit A (*nfnA*), electron bifurcating hydrogenase (*hydB*), glyceraldehyde 3-phosphate dehydrogenase (*gap*), mannitol-1-phosphate dehydrogenase (*mtlD*), ferredoxin (*fd1*; TKV_c16450), PFOR1 (*nifJ1*), PFOR2 (*nifJ2*) and 2-oxoacid:ferredoxin oxidoreductases (*2OxFOR*; TKV_c19280).

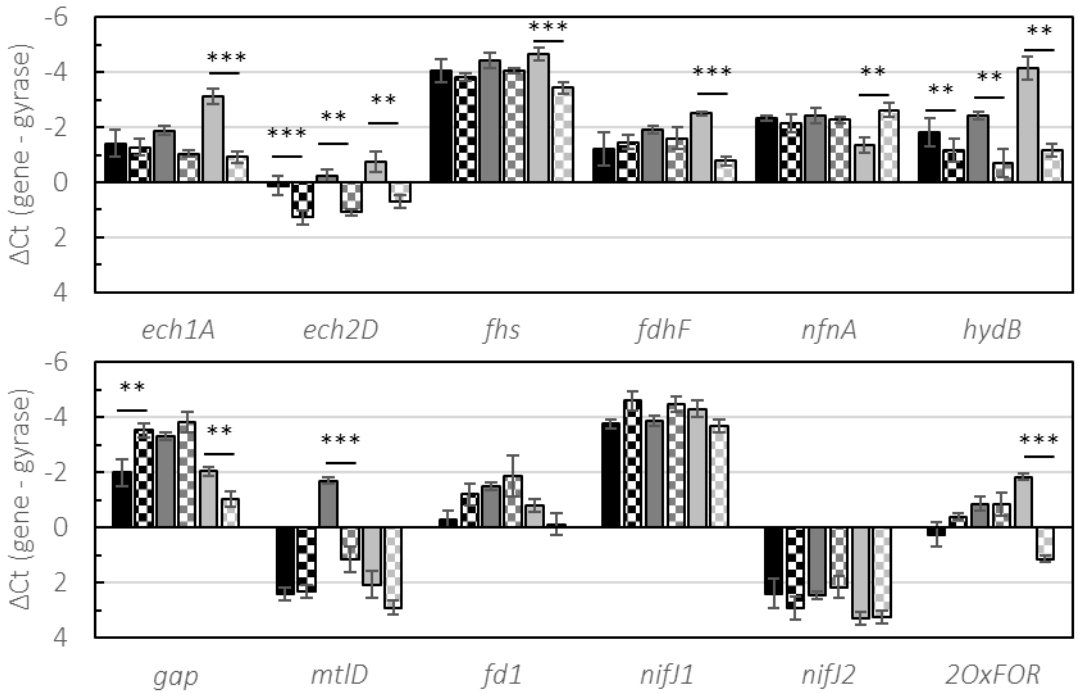

Figure 27 Expression of metabolic relevant genes of *T. kivui* (DSM 2030) before and after H_2 shock (Figure 26).
Gene expression before (filled column) and after H_2 shock (checkered column) of the wild type in the presence of glucose (black), mannitol (dark gray) and pyruvate (light gray). The mRNA levels were normalized to the abundance of gyrase (*gyrB*). Gene expression was determined for *ech1A* (Ech1 complex), *ech2D* (Ech2 complex), *fhs* (formyl-tetrahydrofolate synthetase), *fdhF* (HDCR), *nfnA* (transhydrogenase subunit A), *hydB* (electron bifurcating hydrogenase), *gap* (glyceraldehyde 3-phosphate dehydrogenase), *mtlD* (mannitol-1-phosphate dehydrogenase) *fd1* (ferredoxin; TKV_c16450), *nifJ1* (PFOR1), *nifJ2* (PFOR2), *2OxFOR* (2-oxoacid:ferredoxin oxidoreductases; TKV_c19280). The RNA was extracted from cells harvested during the exponential growth phase 5 minutes before and 15 minutes after the H_2 shock. The associated growth experiment was performed on complex medium at 65 °C and 160 rpm. Multiple biological replicates (n = 2) and technical replicates (n = 2) were tested. The P(T<=t) (n.s. = P > 0.05, * = P ≤0.05, ** = P ≤0.01 or P ≤0.001) was calculated by t-test (one-tailed and two-sample unequal variance).

The calculated ΔCt values (Figure 27) and the fold change (Table 21) showed that after the H_2 addition the expression of most of the genes did change but above the threshold of 4-fold or below −4-fold.

On glucose, all genes did not show any major gene expression change after the addition of H_2/CO_2 above or below the threshold with *gap* showing the highest upregulation with a 2.9-fold. While on mannitol *mtlD* was significantly downregulated after the addition of H_2/CO_2 (−7.3-fold), explaining the lower consumption rate (Figure 26; Table 19). On pyruvate the genes *ech1A*, *hydB* and *2OxFOR* responded to the H_2 addition, resulting in a significant downregulation below the threshold, while the other genes only showed a slight up- or downregulation (Table 21). It seems that *hydB* was downregulated to different extents depending on the substrate (Table 21; fold change = −1.6/−3.4/−7.9; glucose/mannitol/pyruvate).

Table 21 Fold change values of qPCR of H_2 shock experiment with *T. kivui* (Figure 27).
Calculated fold change values of *T. kivui* (DSM 2030) and grown on complex medium with 25 mM glucose, 25 mM mannitol or 100 mM pyruvate before H_2 shock (b. H_2) and after H_2 shock (a. H_2). Change of gene expression of after H_2 shock (test) compare to before H_2 shock (calibrator). The upregulation of the gene is indicated by blue and downregulation by red. The threshold value for upregulation is 4-fold and for downregulation −4-fold and indicated by darker color.

		Fold change		
Test		Glucose a. H_2	Mannitol a. H_2	Pyruvate a. H_2
Calibrator		Glucose b. H_2	Mannitol b. H_2	Pyruvate b. H_2
Gene	*ech1A*	−1.1	−1.8	−4.6
	ech2D	−2.2	−2.5	−2.7
	fhs	−1.2	−1.3	−2.4
	fdhF	1.2	−1.2	−3.3
	nfnA	−1.2	−1.1	2.4
	hydB	−1.6	−3.4	−7.9
	gap	2.9	1.4	−2.1
	mtlD	1.1	−7.3	−1.8
	fd1	1.9	1.3	−1.6
	nifJ1	1.8	1.5	−1.5
	nifJ2	−1.5	1.2	1.1
	2OxFOR	1.6	1.0	−7.9

In conclusion, the addition of H_2 to the cultures during exponential growth resulted in minor gene expression changes on glucose and mannitol, except for the strong downregulation of *mtlD* on mannitol, while, on pyruvate *ech1A*, *hydB* and *2OxFOR* were strongly downregulated.

3.4.4 Addition of organic substrate to *T. kivui* during growth on H_2/CO_2.

Thus, growth inhibition in the presence of H_2 was demonstrated. For further conclusions, the experimental setup was reversed. In this experiment, wild type cells grown lithotrophically on H_2/CO_2 were shocked with 25 mM glucose, 25 mM mannitol or 50 mM pyruvate.

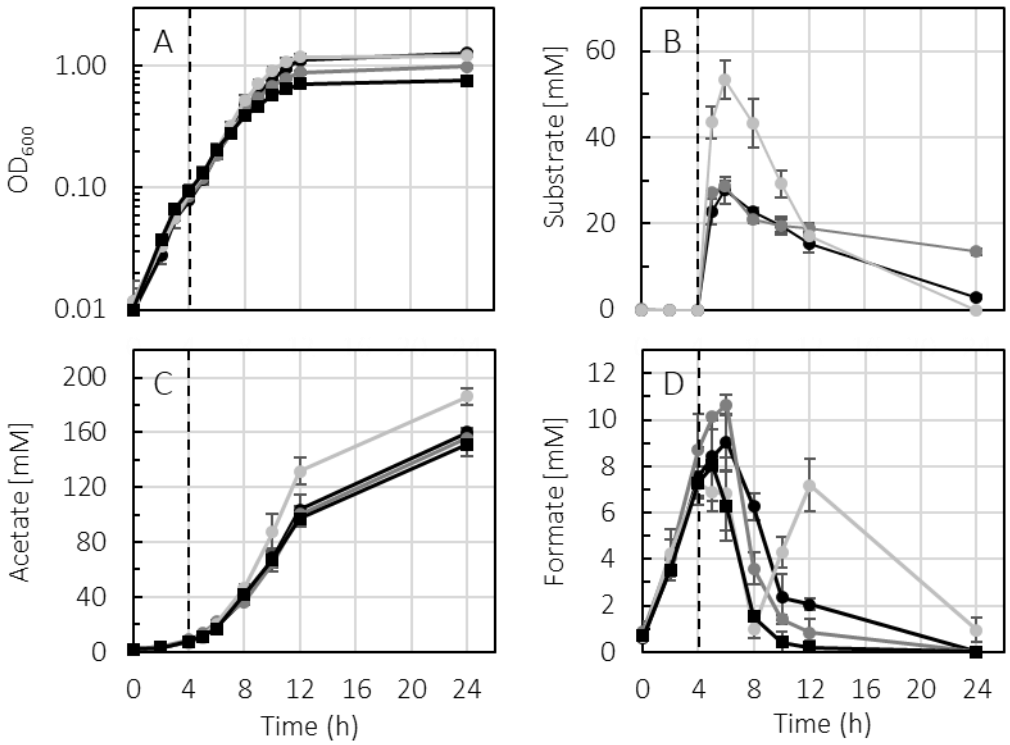

Figure 28 Addition of heterotrophic substrate to *T. kivui* during growth on H_2/CO_2.
Representative growth curves of *T. kivui* wild type grown on H_2/CO_2 (black square) and grown on H_2/CO_2 shocked after hour 4 (black dashed line) with 25 mM glucose (black circle), 25 mM mannitol (dark gray circle) or 50 mM pyruvate (light gray circle). Shown are the OD_{600} (A) and the concentration of glucose (B), mannitol (B), pyruvate (B), acetate (C) and formate (D). All experiments were performed on complex medium at 65 °C and 160 rpm. H_2/CO_2 was refilled every hour to a pressure of $2x10^5$ Pa (n = 3).

All cultures grew with the same growth rate on H_2/CO_2 until the organic substrates were added. No growth inhibition was observed when the substrates were added; instead, the growth rates increased compared to growth on H_2/CO_2 alone (Table 22). Correspondingly, the final OD_{600} was higher in cultures with additional substrate than with H_2/CO_2 alone (Table 22). Formate production occurred in all cultures, with the highest formate concentration at hour 6. After that, formate was consumed, but additional formate production occurred in cultures grown with H_2/CO_2 and pyruvate with a concentration of 7.18 mM formate after 12 hours. Glucose, mannitol and pyruvate were consumed immediately after addition to growing cells, but the consumption rate between hours 6 and 12 was different for each substrate (Table 22). The glucose consumption rate was −2.04 mM h^{-1}, of mannitol −0.46 mM h^{-1} and of pyruvate −6.14 mM h^{-1} (Table 22). In addition, around 3 mM glucose and 13.4 mM mannitol were still present after 24 hours of incubation (Figure 28; B). The final acetate concentration was for glucose cultures 160 mM, mannitol cultures 156 mM, pyruvate cultures 186 mM and pure H_2/CO_2 cultures 151 mM acetate (Figure 28; C).

Table 22 Substrate shock to *T. kivui* (DSM 2030) pre-grown on H_2/CO_2 (66/33; v/v).
Doubling time and substrate consumption rate were determined between hours 5 to 9 (Figure 28). The highest OD_{600} value of the growth curve (Figure 28) was taken as the final OD_{600}.

Substrate	Doubling time (h)	final OD_{600}	Consumption rate
Glucose	1.66 ± 0.04	1.28 ± 0.04	−2.04 mM h^{-1}
Mannitol	1.77 ± 0.01	0.99 ± 0.02	−0.46 mM h^{-1}
Pyruvate	1.59 ± 0.07	1.22 ± 0.03	−6.14 mM h^{-1}
H_2/CO_2	2.19 ± 0.04	0.76 ± 0.03	n.d.

Overall, growth was not inhibited when autotrophically growing cells came into contact with glucose, mannitol or pyruvate during the exponential growth phase. Compared to the pure H_2/CO_2 cultures, the final OD_{600} and the growth rate increased after adding these substrates.

Table 23 Summary of glucose, mannitol and pyruvate consumption rate (Figure 26; Figure 28).
The consumption rate of glucose, mannitol and pyruvate of *T. kivui* is shown when growing on substrate only, substrate and H_2/CO_2 added and H_2/CO_2 and substrate added. All experiments were performed on complex medium at 65 °C and 160 rpm (n = 3).

Substrate	Substrate only	Substrate and H_2/CO_2 (added)	H_2/CO_2 and Substrate (added)
Glucose	−2.82 mM h^{-1}	−1.80 mM h^{-1}	−2.04 mM h^{-1}
Mannitol	−2.41 mM h^{-1}	−0.89 mM h^{-1}	−0.46 mM h^{-1}
Pyruvate	−9.42 mM h^{-1}	−10.68 mM h^{-1}	−6.14 mM h^{-1}

The glucose consumption rate was slightly lower after the addition of H_2/CO_2 and in the H_2/CO_2 cultures with glucose added later. In comparison, the cultures with H_2/CO_2 and pyruvate added showed a lower consumption rate, which was unexpected. Mannitol consumption was expectedly even lower with H_2/CO_2 and mannitol added compared to the cultures with mannitol and H_2/CO_2 added or mannitol only, as *mtlD* was probably not expressed in the H_2/CO_2 culture.

Thus, depending on how *T. kivui* was pre-grown, it responded differently when exposed to H_2/CO_2 or an organic substrate, leading to the assumption of metabolic imbalance when organotrophically growing cells were exposed to H_2 and, to a lesser extent, lithotrophically growing cells were exposed to an organictrophic substrate.

3.4.5 Hydrogen shock of *T. kivui* during growth on defined medium containing glucose

To verify and extend previous results additional H_2 shock experiments were carried out on defined medium. The reason why defined medium was used instead of complex medium was to reduce the possible influence of yeast extract on the gene expression. Also, the cultures were shocked with $1x10^5$ Pa or $2x10^5$ Pa H_2/CO_2 (66/33; v/v) overpressure at an OD_{600} 0.25-0.35 in the exponential growth phase. The different pressures of H_2/CO_2 were used to investigate whether there is a correlation between the amount of H_2 and the inhibition of growth and gene expression. For this purpose, cell samples for RNA extraction were taken 5 minutes before and 15 minutes after the H_2 shock.

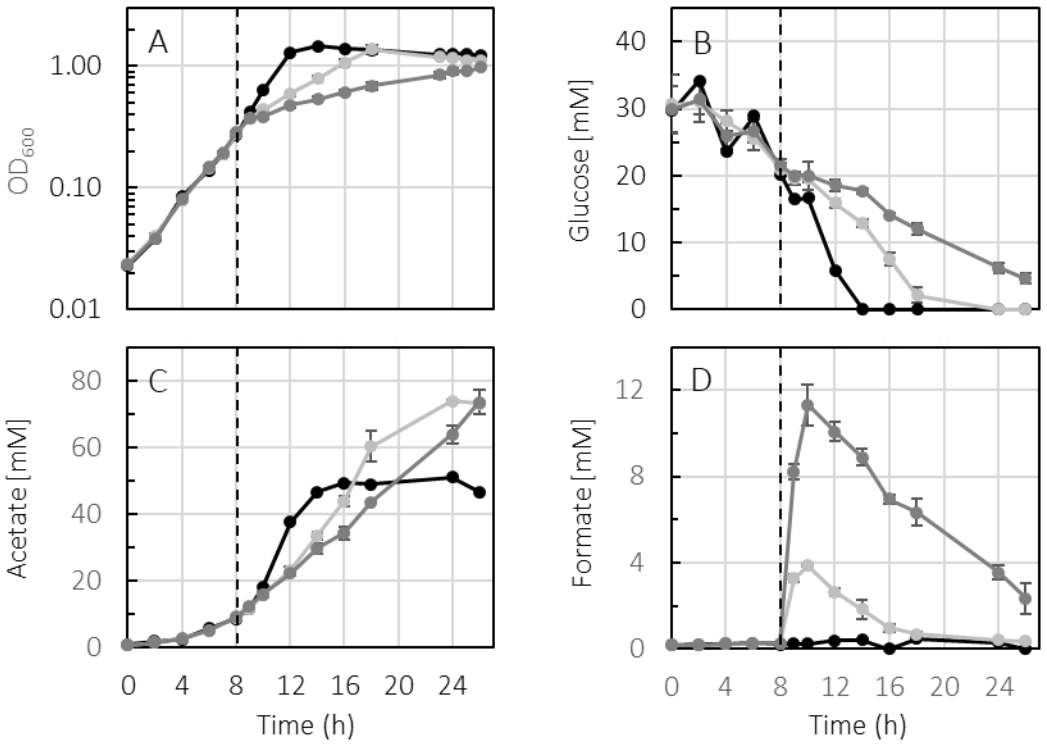

Figure 29 H_2 shock of *T. kivui* (DSM 2030) during growth on defined medium containing glucose. Representative growth curve of *T. kivui* wild type grown on 25 mM glucose (black), shocked with $1x10^5$ Pa H_2/CO_2 overpressure (light gray) and shocked with $2x10^5$ Pa H_2/CO_2 overpressure (dark gray). Cultures were shocked after 8 hours (black dashed line). Samples for RNA extraction were taken 5 minutes before and 15 minutes after the H_2 shock. Shown are the OD_{600} (A) and the concentration of glucose (B), acetate (C) and formate (D). All experiments were performed on defined medium at 65 °C and 160 rpm. Biological replicates glucose (n = 1), glucose and H_2/CO_2 (n = 3).

All cultures grew at a doubling time of 2.11 (Table 24) before the H_2 shock on defined medium containing 25 mM glucose. The unshocked culture, reached a final OD_{600} of 1.46 after 14 hours. At this time point all glucose (29.7 mM) was consumed. After 24 hours 50.6 mM acetate and no formate were produced. The H_2 shock was performed after 8 hours at an OD_{600} of approximately 0.27. After the H_2 shock, the doubling time increased as a result; at an overpressure of $1x10^5$ Pa to 4.98 h and at $2x10^5$ Pa to 11.53 h (Table 24). Furthermore, at the overpressure of $1x10^5$ Pa, the final OD_{600} of 1.36 was reached after 18 hours and at f $2x10^5$ Pa the final OD_{600} of 0.97 was reached after 26 hours (Figure 29; A).

Glucose consumption was at −0.45 mM h^{-1} between 0 and 8 hours and increased after the addition H_2/CO_2 to −0.95 mM h^{-1} in the $1x10^5$ Pa cultures and −0.53 mM h^{-1} in the $2x10^5$ Pa cultures, while the control culture consumed −3.46 mM h^{-1} (Figure 29; B).Different amounts of formate were produced depending on the overpressure, with $1x10^5$ Pa H_2/CO_2 3.9 mM ± 0.1 mM and with $2x10^5$ Pa H_2/CO_2 11.3 mM ± 0.9 mM formate were produced after the addition of H_2/CO_2. However, the consumption of formate was similar for both conditions with a rate of −0.42 mM h^{-1} for $1x10^5$ Pa and −0.55 mM h^{-1} for $2x10^5$ Pa H_2/CO_2 (Figure 29; D).The acetate production rate between 9 and 12 hours differed in the two conditions compared to the control; after the H_2 shock with $1x10^5$ Pa H_2/CO_2 the production rate was 3.84 mM h^{-1} acetate, with $2x10^5$ Pa H_2/CO_2it was 3.2 mM h^{-1} acetate and the control culture 8.83 mM h^{-1} was produced. The final acetate concentration in the control was 46.6 mM, while in the $1x10^5$ Pa H_2/CO_2 culture 73.2 mM and in the $2x10^5$ Pa H_2/CO_2 culture 73.5 mM were reached (Figure 29; C).

Table 24 Comparison of the doubling time of *T. kivui* after adding H_2/CO_2.
The doubling time of *T. kivui* grown on complex medium (Figure 26) or defined medium (Figure 29) containing 25 mM glucose before and after the H_2 shock with an overpressure of $1x10^5$ Pa or $2x10^5$ Pa H_2/CO_2 (66/33; v/v).

Doubling time (h)					
	Complex medium		Defined medium		
Condition	Control	$1x10^5$ Pa H_2/CO_2	Control	$1x10^5$ Pa H_2/CO_2	$2x10^5$ Pa H_2/CO_2
before shock	1.61 ± 0.12		2.11 ± 0.05		
after shock	-	3.26 ± 0.16	-	4.98 ± 0.35	11.53 ± 0.32

It has been shown that the medium has an influence on the growth inhibitory effect of H_2/CO_2 when the cultures were shocked with $1x10^5$ Pa H_2/CO_2. The difference of doubling time indicates that *T. kivui* tolerates the elevated H_2 concentration in the atmosphere more in complex medium than in defined medium. Furthermore, a higher H_2/CO_2 overpressure resulted in greater growth inhibition in the defined medium (Table 24).

Table 25 Summary of consumption and production rate of glucose, formate and acetate of *T. kivui*.
T. kivui grown on complex medium (Figure 26) or defined medium (Figure 29) containing 25 mM glucose before and after the H_2 shock with an overpressure of $1x10^5$ Pa or $2x10^5$ Pa H_2/CO_2 (66/33; v/v).

Consumption and production rate					
	Complex medium		Defined medium		
Condition	Control	$1x10^5$ Pa H_2/CO_2	Control	$1x10^5$ Pa H_2/CO_2	$2x10^5$ Pa H_2/CO_2
Glucose	−2.82 mM h^{-1}	−1.80 mM h^{-1}	−3.46 mM h^{-1}	−0.95 mM h^{-1}	−0.53 mM h^{-1}
Formate	-	−0.77 mM h^{-1}	-	−0.42 mM h^{-1}	−0.55 mM h^{-1}
Acetate	8.3 mM h^{-1}	6.16 mM h^{-1}	8.83 mM h^{-1}	3.84 mM h^{-1}	3.20 mM h^{-1}

It can therefore be stated that glucose consumption and acetate production also decreased with increasing overpressure, and the decrease also depended on the medium in which *T. kivui* was cultured (Table 25). On complex medium, glucose consumption and acetate production were higher than on defined medium, where the values were only half. Formate consumption was similar in all tested conditions. Further experiments were performed with pyruvate as substrate and an overpressure of $2x10^5$ Pa H_2/CO_2 (66/33; v/v).

3.4.6 Hydrogen shock of *T. kivui* during growth on defined medium containing pyruvate

In addition to the H_2 shock on defined medium with glucose, another experiment was performed with pyruvate instead of glucose to describe further the effect of H_2 in cultures grown on pyruvate. The H_2 shock was performed with an overpressure of $2x10^5$ Pa H_2/CO_2.

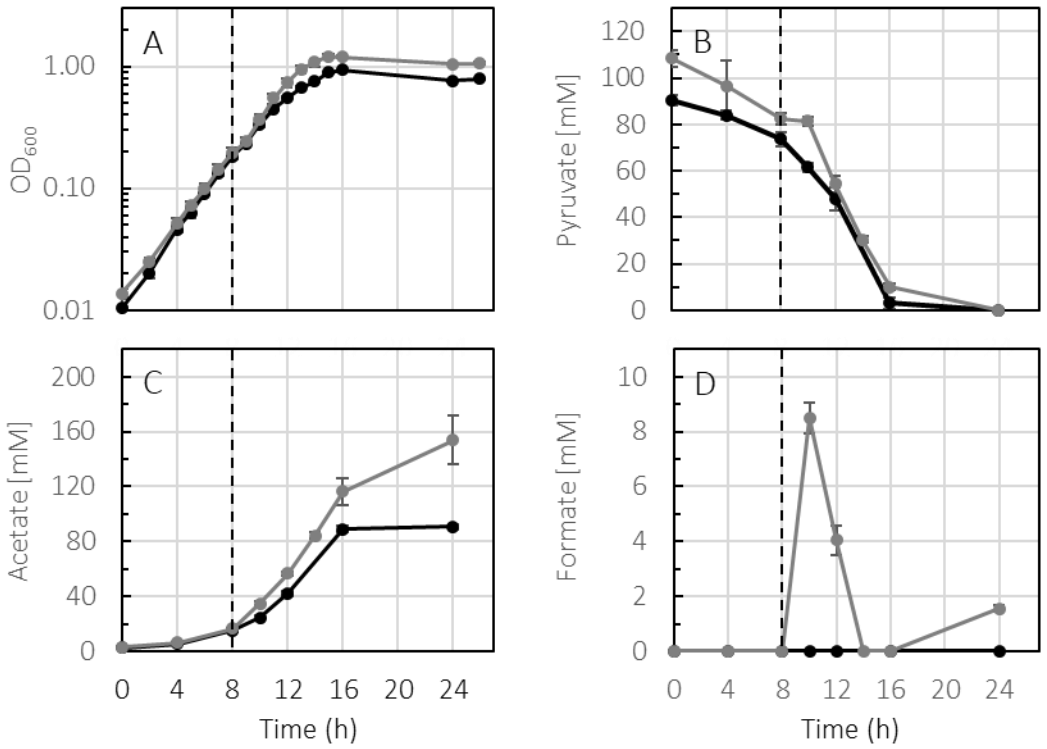

Figure 30 H_2 shock of *T. kivui* (DSM 2030) during growth on defined medium containing pyruvate. Representative growth curve of *T. kivui* grown on 100 mM pyruvate (black) and shocked with $2x10^5$ Pa H_2/CO_2 overpressure (gray). Cultures were shocked after 8 hours (black dashed line). Samples for RNA extraction were taken 5 minutes before and 15 minutes after the H_2 shock. Shown are the OD_{600} and the concentration of glucose, acetate and formate. All experiments were performed on defined medium at 65 °C and 160 rpm (n = 3).

All pyruvate cultures grew with a doubling time of 1.98 h in the first 8 hours, before the H_2 shock was performed. After the H_2 shock between, the doubling time of the unshocked cultures increased to 2.66 h, while the of the shocked cultures remained unchanged with a doubling time of 2.02 h. The unshocked cultures reached a maximal OD_{600} of 0.93 after 16 hours, while the shocked cultures reached a maximal OD_{600} of 1.21 after 15 hours (Figure 30; A).

The initial pyruvate concentration in the unshocked cultures was 90.6 mM ± 2.2 mM and in the cultures that were shocked 108.5 mM ± 3.6 mM pyruvate. The consumption rate of pyruvate between 10 to 16 hours was for the unshocked cultures −9.95 mM h^{-1} and for shocked cultures −11.9 mM h^{-1} (Figure 30; B). Only in the shocked cultures, formate (8.5 mM ± 0.6 mM) was produced due to the additional H_2, and it was later consumed at a rate of −2.13 mM h^{-1} (Figure 30; D). The produced formate was completely consumed after 14 hours, but 1.6 mM ± 0.1 mM were detected after 24 hours. The production rate of acetate between hour 10 to 16 was 9.46 mM h^{-1} in the unshocked cultures and 12.45 mM h^{-1} in the shocked cultures, and the final acetate concentration of the unshocked cultures was 90.8 mM ± 2.0 mM and of the shocked cultures was 153.8 mM ± 17.8 mM (Figure 30; C).

In addition, pyruvate utilization was stopped for about 2 hours after the H_2 shock, during which time formate was produced and acetate production was increased. After 4 hours after the H_2 shock, the pyruvate concentration decreased to the concentration measured in the unshocked cultures. These results are consistent with the observations made on complex medium, where growth time, pyruvate consumption and acetate production were increased after the H_2 shock under both conditions compared to the control cultures (Figure 26; Figure 30).

In summary, it was shown that the addition of H_2/CO_2 on defined medium containing glucose resulted in stronger growth and metabolic inhibition than on complex medium, and that a higher pressure of $2x10^5$ Pa H_2/CO_2 resulted in greater inhibition than $1x10^5$ Pa H_2/CO_2. For pyruvate, the additional H_2/CO_2 did not lead to growth inhibition but to a short-term reduction of the pyruvate consumption in the first to second hour after the H_2 shock on complex and defined medium, followed by an increased pyruvate consumption after the third hour.

3.4.7 Growth of *T. kivui* autotrophically with H_2/CO_2 on defined medium

An additional growth experiment was performed with H_2/CO_2 on defined medium to compare later the differences in gene expression between shocked and unshocked cells grown on glucose or pyruvate and cells grown exclusively on H_2/CO_2. Therefore, RNA samples were taken at an OD_{600} of about 0.2 of the H_2/CO_2 cultures (Figure 31).

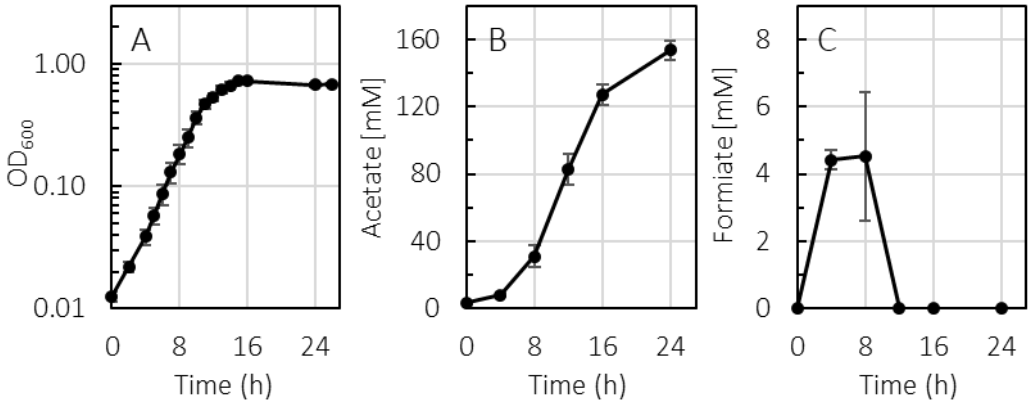

Figure 31 Growth of *T. kivui* (DSM 2030) on H_2/CO_2.
Representative growth curve of *T. kivui* DSM 2030 (black) in the presence of $2x10^5$ Pa H_2/CO_2 overpressure (3 atm), after 2 hours, H_2/CO_2 was refilled every hour to an overpressure of $2x10^5$ Pa. Shown is the OD_{600} (A), the acetate (B) and formate (C) concentration over time. All experiments were performed on defined medium at 65 °C and 160 rpm (n = 3).

T. kivui growing autotrophically with $2x10^5$ Pa H_2/CO_2 had a doubling time of 1.87 h on the defined medium (Figure 31; A). The acetate production rate was 12.04 mM h^{-1} and the final acetate concentration was 153.5 mM ± 5.5 mM (Figure 31; B). Formate was produced between 0 to 8 hours, the highest concentration was 4.5 mM ± 1.9 mM, after 8 hours the produced formate was completely consumed.

3.4.8 Gene expression comparison of qPCR Data of *T. kivui* cells shocked with H_2

Comparing the growth inhibitory effect of H_2 on complex and defined medium showed that on defined medium the response to the added H_2 was stronger. Therefore, samples were taken for RNA extraction during the experiments to investigate whether there is also a stronger change in gene regulation. The cell samples were taken 5 minutes before and 15 minutes after H_2 shock with defined medium and glucose (Figure 29) or pyruvate (Figure 30), with an OD_{600} of approximately 0.2 at the time of H_2 shock in both growth experiments. In addition, samples of H_2/CO_2 cultures (Figure 31) were taken at an OD_{600} of approximately 0.2 for comparison with the other conditions.

The gene expression was determined for the genes encoding for Ech1 complex (*ech1A*), Ech2 complex (*ech2D*), formyl-tetrahydrofolate synthetase (*fhs*), HDCR (*fdhF*), transhydrogenase subunit A (*nfnA*), electron bifurcating hydrogenase (*hydB*), glyceraldehyde 3-phosphate dehydrogenase (*gap*), redox-sensing transcriptional repressor (*rex*), ferredoxin (*fd1*; TKV_c16450), PFOR1 (*nifJ1*), PFOR2 (*nifJ2*) and 2-oxoacid:ferredoxin oxidoreductases (*2OxFOR*; TKV_c19280).

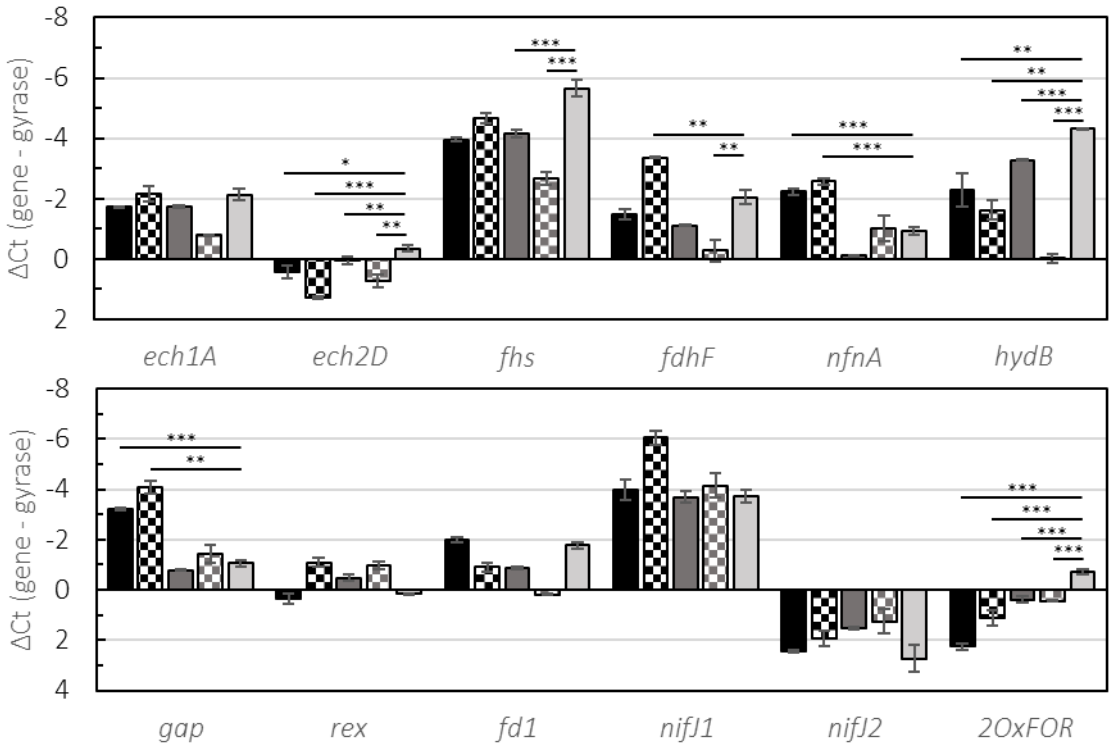

Figure 32 Expression of metabolic relevant genes of *T. kivui* (DSM 2030) before and after the H_2 shock.
Gene expression before (filled column) and after H_2 shock (checkered column) of *T. kivui* in the presence of glucose (black), pyruvate (dark gray) and H_2/CO_2 (light gray). The mRNA levels were normalized to the abundance of gyrase (*gyrB*). Gene expression was determined for *ech1A* (Ech1 complex), *ech2D* (Ech2 complex), *fhs* (formyl-tetrahydrofolate synthetase), *fdhF* (HDCR), *nfnA* (transhydrogenase subunit A), *hydB* (electron bifurcating hydrogenase), *gap* (glyceraldehyde 3-phosphate dehydrogenase), *rex* (redox-sensing transcriptional repressor) *fd1* (ferredoxin; TKV_c16450), *nifJ1* (PFOR1), *nifJ2* (PFOR2), *2OxFOR* (2-oxoacid:ferredoxin oxidoreductases; TKV_c19280). RNA was extracted from cells that were harvested in the exponential growth phase 5 minutes before and 15 minutes after the H_2 shock. The experiment was performed on defined medium at 65 °C and 160 rpm. Multiple biological replicates (n = 2) and technical replicates (n = 3) were tested. The P(T<=t) (n.s. = P > 0.05, * = P ≤0.05, ** = P ≤0.01 or P ≤0.001) was calculated by t-test (one-tailed and two-sample unequal variance).

Comparison of the defined medium with the complex medium containing glucose showed that all tested genes were expressed similar, indicating that there is no strong effect of the two media on gene regulation on glucose. Still, *2OxFOR* was close to the threshold of −4-fold and could be considered as expressed less on defined medium (Table 26). This observation was supported by the comparison of gene regulation on defined and complex medium containing pyruvate, were only *2OxFOR* was downregulated, (−4.69-fold) indicating a significant downregulation on defined medium.

This suggests that the 2-oxoacid:ferredoxin oxidoreductases is relevant on complex medium. While strong gene regulation changes did not occur on complex medium after the addition of H_2/CO_2 to *T. kivui* cells grown on glucose, changes were observed on defined medium showing upregulation of *nifJ1* (PFOR1) and of *fdhF* (HDCR), close to the threshold of 4-fold. On pyruvate, downregulation of *ech1A* and *2OxFOR* on complex medium were observed as reported earlier, whereas *hydB* was strongly downregulated on both media.

In conclusion, the regulation of genes was slightly different depending on the medium used, which must be considered when interpreting gene regulation.

Table 26 Comparison of fold change of gene expression level in the H_2 shock experiment with *T. kivui* (DSM 2030) grown on complex and defined medium (Figure 27; Figure 32).

Calculated fold change values of *T. kivui* (DSM 2030) and grown on complex (com.) or defined (def.) medium containing glucose or pyruvate before H_2 shock (b. H_2) and after H_2 shock (a. H_2). Comparison between defined (test) and complex medium (calibrator) with glucose or pyruvate before and after the H_2 shock and comparison between after the H_2 shock (test) and before the H_2 shock (calibrator) on complex or defined medium with glucose or pyruvate. The upregulation of the gene is indicated by blue and downregulation by red. The threshold value for upregulation is 4-fold and for downregulation −4-fold and indicated by darker color. The fold change was calculated using Ct values obtained from qPCR analysis.

		Fold change					
Test		Glucose b. H_2 def.	Pyruvate b. H_2 def.	Glucose a. H_2 com.	Glucose a. H_2 def.	Pyruvate a. H_2 com.	Pyruvate a. H_2 def.
Calibrator		Glucose b. H_2 com.	Pyruvate b. H_2 com.	Glucose b. H_2 com.	Glucose b. H_2 def.	Pyruvate b. H_2 com.	Pyruvate b. H_2 def.
Gene	*ech1A*	1.2	−2.6	−1.1	1.4	−4.6	−1.9
	ech2D	−1.2	−1.7	−2.2	−1.8	−2.7	−1.6
	fhs	−1.1	−1.4	−1.2	1.6	−2.4	−2.8
	fdhF	1.2	−2.6	1.2	3.7	−3.3	−1.8
	nfnA	−1.1	−2.4	−1.2	1.3	2.4	1.9
	hydB	1.4	−1.8	−1.6	−1.6	−7.9	−9.7
	gap	2.4	−2.4	2.9	1.8	−2.1	1.6
	fd1	3.2	1.1	1.9	−2.1	−1.6	−2.1
	nifJ1	1.2	−1.5	1.8	4.2	−1.5	1.4
	nifJ2	−1.0	3.4	−1.5	1.4	1.1	1.2
	2OxFOR	−3.9	−4.7	1.6	2.2	−7.9	−1.0

Since H_2/CO_2 was added to the atmosphere of *T. kivui* cultures growing on glucose or pyruvate in a defined medium, all tested conditions were compared to the gene expression of cells growing lithographically on H_2/CO_2 alone (Table 27).

Table 27 Comparison of fold change of gene expression of *T. kivui* (DSM 2030) grown on glucose, pyruvate or H_2/CO_2 (Figure 32).

Calculated fold change values of the *T. kivui* and grown on defined medium with glucose or pyruvate before H_2 shock (b. H_2) or after H_2 shock (a. H_2) compared to H_2/CO_2 (calibrator). The upregulation of the gene is indicated by blue and downregulation by red. The threshold value for upregulation is 4-fold and for downregulation −4-fold and indicated by darker color. The fold change was calculated using Ct values obtained from qPCR analysis.

		Fold change			
Test		Glucose b. H_2	Glucose a. H_2	Pyruvate b. H_2	Pyruvate a. H_2
Calibrator		H_2/CO_2			
Gene	*ech1A*	-1.3	1.0	-1.3	-2.5
	ech2D	-1.7	-3.1	-1.3	-2.1
	fhs	-3.2	-2.0	-2.8	-7.9
	fdhF	-1.5	2.5	-1.9	-3.4
	nfnA	2.5	3.1	-1.8	1.1
	hydB	-4.1	-6.6	-2.1	-20.0
	gap	4.5	8.0	-1.2	1.3
	fd1	1.2	-1.8	-1.9	-3.9
	nifJ1	1.2	4.9	-1.0	1.3
	nifJ2	1.2	1.8	2.3	2.8
	2OxFOR	-7.9	-3.6	-2.2	-2.3
	rex	-1.1	2.4	1.6	2.2

This comparison revealed that the gene expression of *T. kivui* was similar when grown on pyruvate before the addition of H_2/CO_2 compared to H_2/CO_2 alone. However, following the addition of H_2/CO_2, *hydB* was downregulated by −20.04-fold and *fhs* by −7.88-fold, while all other genes showed changes in expression that were either below or above the threshold (Table 27).

In cultures grown on glucose and H_2/CO_2, *hydB* and *2OxFOR* were expressed below the −4-fold threshold, whereas *gap* was expressed above the 4-fold threshold. After adding H_2/CO_2 to the glucose cultures, *hydB* was further downregulated, and *gap* was further upregulated. Additionally, *2OxFOR* was slightly upregulated, surpassing the −4-fold threshold, while *nifJ1* was upregulated to 4.92-fold (Table 27).

In summary, the addition of H_2/CO_2 to a pyruvate culture resulted in lower expression of *fhs* and *hydB*, suggesting that the formyl-tetrahydrofolate synthetase (*fhs*) and HydABC (*hydB*) are less required in the presence of pyruvate and H_2/CO_2. Growth on glucose showed lower expression of *hydB* and *2OxFOR* and higher expression of *gap* compared to H_2/CO_2, suggesting that HydABC is less required for growth on glucose than on H_2/CO_2. Meanwhile, *gap* is needed, as it is part of glycolysis. Furthermore, adding H_2/CO_2 to glucose-grown cells stimulated the expression of glycolysis-related genes, including *gap* and *nifJ1* (*PFOR1*), while reducing *hydB* expression.

3.4.9 RNA sequencing of *T. kivui* cells grown on glucose shocked with H_2/CO_2

Additionally, samples from cells grown in a defined medium containing glucose (Figure 29) were sent in for mRNA sequencing (transcriptome analysis). Samples were taken 5 minutes before and 15 minutes after the addition of H_2/CO_2. To investigate the change in general gene expression through H_2/CO_2 addition, *T. kivui* cells growing on glucose were shocked with different H_2/CO_2 overpressures.

First impressions of the principal component analysis of the transcriptome dataset (Figure A-3) showed a clear separation of the conditions before (pre_1bar and pre_2bar) and after (after_1bar and after_2bar) the addition of H_2/CO_2 to principal component 1 (PC1), furthermore, a clear separation of the two conditions after the addition to component 2 (PC2) was visible, while the samples without H_2/CO_2 were in between.

The transcriptome data showed that the change in gene expression after the addition of $2x10^5$ Pa H_2/CO_2 did not result in changes in gene expression below or above the threshold of $\log_2(x) = 2$ or $\log_2(x) = -2$ of the genes investigated in the qPCR analysis (Table A-4, Table A-5). Compared to the qPCR data (Table 26; test Glucose a. H_2 def./ Calibrator glucose b. H_2 def.) the only difference was that *nifJ1* (PFOR1) was slightly upregulated in the qPCR data, while all other genes were below or above the threshold of 4-fold or −4-fold. The comparison of transcriptome and qPCR data showed that the gene response of glucose grown cultures shocked with $2x10^5$ Pa H_2/CO_2 was found similarly by both analysis methods and therefore do not contradict each other. In conclusion, the genes for the WLP (*fhs* and *fdhF*), energy conservation (*ech1* and *ech2*) or redox balance (*hydABC and nfnAB*) were not affected by the addition of H_2/CO_2 when *T. kivui* grew on glucose. Moreover, the expression of genes encoding proteins of the Embden-Meyerhof-Parnas pathway (Table A-8) and ferredoxins (Table A-6) were not affected by the addition of H_2/CO_2.

Instead of changes in the expression of genes investigated by qPCR, the transcriptome data showed other changes in gene expression: Genes for glycosyltransferase, transposase, glycogen biosynthesis, phosphoenolpyruvate synthase (*PpsA*), CRISPR subtype III (*Cmr2*/*Cas10*) and bacteriocin ABC transporter were upregulated (Table 28; Table A-2), while genes for pyrimidine biosynthesis (*pyrB*, *pyrC*,

pyrE and *pyrF*), arginine biosynthesis (*ArgB*, *ArgD*), iron complex transporters and ribosomal proteins were downregulated (Table 28; Table A-3).

Table 28 Transcriptome analysis of *T. kivui* shocked with H_2/CO_2.
Shown are $log_2(x)$ values of the transcriptome analysis of *T. kivui* (DSM 2030) grown on defined medium containing glucose before (b. H_2) and after (a. H_2) the addition of H_2/CO_2 (Figure 29). Shown is the change in expression of representative genes for up and downregulation after adding H_2/CO_2 to the atmosphere with an overpressure of $1x10^5$ Pa (1) or $2x10^5$ Pa (2). The ratio of mRNA reads was calculated and the log_2(ratio [test/calibrator]) was determined. The upregulation of the gene is indicated by blue and downregulation by red. The threshold value for upregulation is 2-fold and for downregulation −2-fold and indicated by darker color.

			$log_2(x)$ values	
		Test	Glucose a. H_2 (1)	Glucose a. H_2 (2)
		Calibrator	Glucose b. H_2	
Locus tag / Annotation	TKV_c00720	glycosyltransferase	3.15	4.18
	TKV_c00710	glycosyltransferase	2.95	4.04
	TKV_c08210	transposase	2.17	3.89
	TKV_c11030	C4-alpha-glucan branching enzyme GlgB	2.68	3.64
	TKV_c11040	glucose-1-phosphate adenylyltransferase GlgC	2.44	3.40
	TKV_c11050	glycogen biosynthesis protein GlgD	2.16	3.17
	TKV_c11060	glycogen synthase GlgA	1.91	2.79
	TKV_c10530	phosphoenolpyruvate synthase PpsA	1.75	2.66
	TKV_c23560	CRISPR subtype III-B-associated RAMP protein Cmr2/Cas10	2.34	2.52
	TKV_c08020	putative bacteriocin ABC transporter	2.06	2.51
	TKV_c01670	S-layer domain-containing protein	0.70	0.89
	TKV_c19970	hydrogen dependent carbon dioxide reductase subunit HycB4	-0.03	0.50
	TKV_c01400	acetyltransferase	-0.12	0.00
	TKV_c00040	DNA replication and repair protein RecF	0.13	-0.11
	TKV_c14000	ATPase	-0.33	-0.60
	TKV_c00100	DNA gyrase subunit A	-0.78	-1.00
	TKV_c20460	50S ribosomal protein L24	-1.68	-3.02
	TKV_c22220	acetylglutamate kinase ArgB	-2.70	-3.63
	TKV_c22210	acetylornithine aminotransferase ArgD	-2.89	-3.70
	TKV_c22200	carbamoyl-phosphate synthase small chain	-2.91	-3.78
	TKV_c10330	glutathione-binding protein GsiB	-3.22	-4.29
	TKV_c16530	ABC-type Fe_3^+-hydroxamate transport system	-2.80	-4.33
	TKV_c14380	orotate phosphoribosyltransferase PyrE	-4.82	-5.20
	TKV_c14400	dihydroorotate dehydrogenase B	-5.72	-6.63
	TKV_c14420	dihydroorotase PyrC	-7.83	-8.08
	TKV_c14430	aspartate carbamoyltransferase PyrB	-8.50	-9.10

Furthermore, the intensity of the expression change depended on the applied overpressure. An overpressure of $1x10^5$ Pa H_2/CO_2 leads to a lower expression change than $2x10^5$ Pa H_2/CO_2. Almost all $log_2(x)$ values were higher (upregulation) or lower (downregulation) compared to the $1x10^5$ Pa condition. However, there are also exceptions, genes encoding the S-layer domain-containing protein (TKV_c01670), subunit HycB4 of the HDCR (TKV_c01400), acetyltransferase (TKV_c00100), DNA

replication and repair protein (TKV_c00040), ATPase (TKV_c14000) and DNA gyrase subunit A (TKV_c00100) responded only slightly to the addition of H_2/CO_2 and showed no significant change due to the increased pressure (Table 28).

In summary, the addition of H_2/CO_2 to cells growing heterotrophically on glucose resulted in growth inhibition, a reduction of glucose consumption and thereby, acetate production (Figure 29, Table 24 and Table 25). qPCR and transcriptome analyses showed that the expression of genes related to glucose and H_2/CO_2 utilization did not strongly increase or decrease, nor did genes encoding proteins to maintain redox balance (Table 26, Table A-4, Table A-5 and Table A-8). Meanwhile, pyrimidine and arginine biosynthesis genes were downregulated, while glycogen biosynthesis genes were upregulated (Table 28, Table A-2 and Table A-3).

3.5 Generation and characterization of a *nfnB* mutant

According to the metabolic model of Katsyv et al. (2021a), the electron bifurcating transhydrogenase complex NfnAB is assumed to be necessary for the glucose metabolism of *T. kivui*. Deletion mutants of *nfnAB* analogs in *T. saccharolyticum* and *P. furiosus* suggest that it is essential for NADPH metabolism and maintaining redox balance (Lo et al. 2015; Nguyen et al. 2017). Thus, depending on the metabolized substrate, deletion of *nfnB* in *T. kivui* could lead to an unbalanced redox equilibrium and, therefore, poor or no growth if the organism cannot bypass the function of the NfnAB complex.

3.5.1 Generation of a *nfnB* mutant

To investigate the loss of the NfnAB complex in *T. kivui*, an *nfnB* mutant was generated using the previously mentioned methods to generate the Δ*ech2* strain. The generated plasmid P144_NfnB is based on the plasmid p144 (by B. Zeldes). The backbone and the *pyrE* gene, under the control of a gyrase promoter, were amplified from the plasmid P144. The UFR (*nfnA*) and DFR (*nfnB*) were amplified from the genomic DNA of *T. kivui* strain DSM 2030. The fragments were assembled to the plasmid p144_NfnB (Figure 33) using the DNA assembly Cloning Kit and cloned in *E. coli*. Afterwards, the strain *T. kivui* TKV002 (Δ*pyrE*) was transformed with the plasmid p144_NfnB.

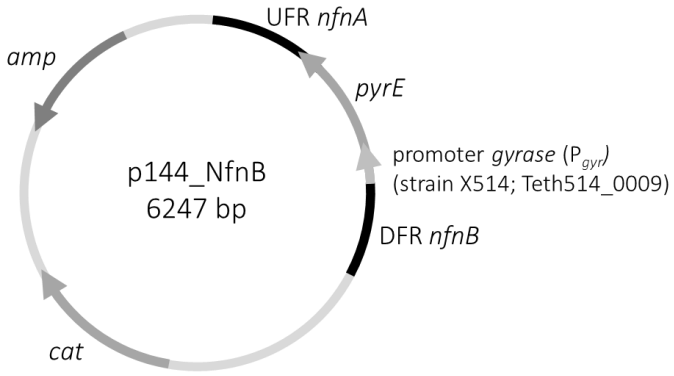

Figure 33 Plasmid map of P144 NfnB.
The non-replicating plasmid has two homologous regions (UFR and DFR) to the chromosome of T. kivui, targeting a genome region between TKV_c22260 and TKV_c22290. Between the UFR and DFR is the *pyrE* gene, which is under control, a gyrase promoter of *Thermoanaerobacter sp*. X514 (Teth514_0009) is used for selection on a defined medium. This plasmid possesses an ampicillin resistance cassette (*amp*) for selection in *E. coli* and a kanamycin resistance cassette (*cat*) for selection in *T. kivui*.

Only one selection step was necessary to generate the *nfnB* mutant on a defined medium containing 25 mM glucose, although it was assumed that the NfnAB complex is essential for growth on glucose.

The *nfnA-pyrE-nfnB* fragment was directly integrated into the target gene region (TKV_c22270 - TKV_c22280) to exchange *nfnB* with *pyrE* (Figure 34). Thus, only *nfnB* mutant colonies could grow on defined medium without uracil. The deletion of *nfnB* and integration of *pyrE* was verified by PCR (Figure 34) and sequencing of the PCR product. The primers Oa (CB104) and Ob (CB105) bound in the gene region TKV_c22270 - TKV_c22280 and amplified fragments with a size of 1318 bp for the wild type strain DSM 2030 or 1656 bp for the *nfnB* mutant. The fragment size for the integrated *pyrE* gene and gyrase promoter was 897 bp, compared to 559 bp for the original *nfnB* fragment. Consequently, the amplified fragment in the *nfnB* mutant was 338 bp larger than that of the wild type (Figure 34).

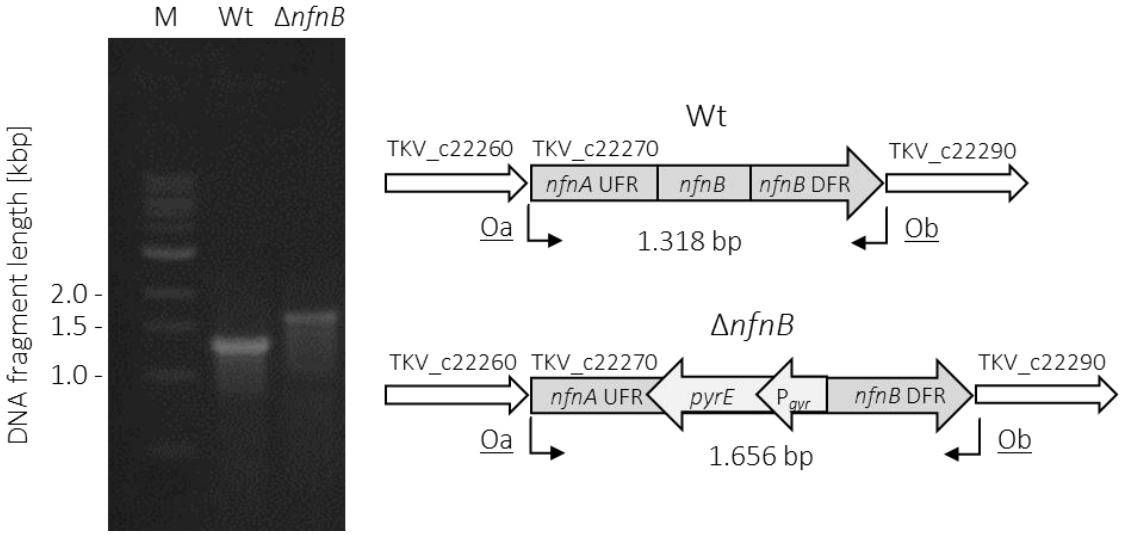

Figure 34 Verification of the loss of *nfnB* and integration of *pyrE*.
The deletion of *nfnB* and integration of *pyrE* was verified by PCR using primers binding outside of *nfnA* (TKV_c22270) and *nfnB* (TKV_c22280). Shown is the electrophoretic separation of the DNA fragments from the PCR using cells of *T. kivui* wild type (WT; strain DSM 2030; expected fragment size, 1.318 bp) and *nfnB* mutant (expected fragment size, 1.656 bp). The agarose gel was stained with Midori green.

The growth of the *nfnB* mutant on defined medium was enabled by the integration of the *pyrE* gene, which means that the mutant cannot be used for further genetic modifications without removing the *pyrE* gene. Subsequently, the *nfnB* mutant was cultivated on defined medium containing glucose, fructose, mannitol, pyruvate or H_2/CO_2.

3.5.2 Growth of the *nfnB* mutant stain.

The initial characterization of the *nfnB* mutant strain was conducted through growth experiments on defined medium containing 25 mM glucose, 25 mM mannitol or 25 mM fructose (Figure 35).

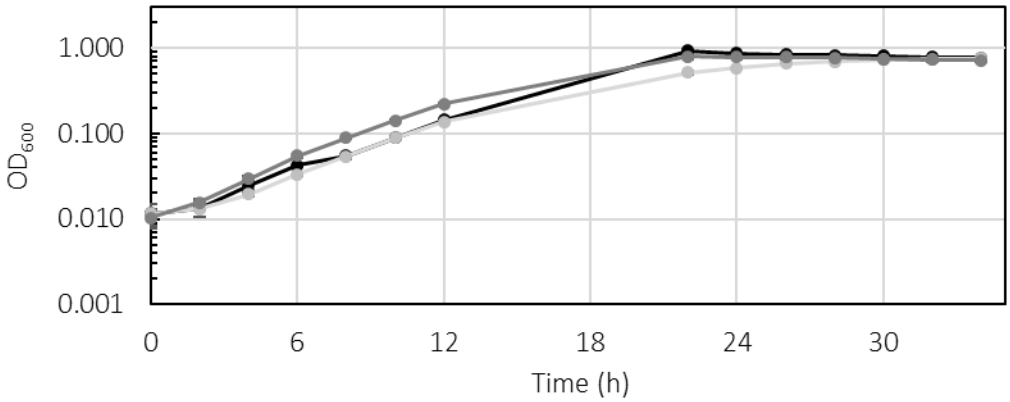

Figure 35 Growth of *nfnB* mutant on glucose, fructose and mannitol.
Representative growth curves of the *nfnB* strain in the presence of 25 mM glucose (black), 25 mM fructose (gray) and 25 mM mannitol (light gray). All experiments were performed on defined medium at 65 °C and 160 rpm (n = 3).

The doubling time of the *nfnB* mutant grown on defined medium with 25 mM glucose was 3.26 h, with 25 mM mannitol 2.94 h and with 25 mM fructose 2.79 h. Moreover, the final OD_{600} of 0.93 on glucose was reached after 22 hours, 0.75 on mannitol after 34 hours, and 0.79 on fructose cultures after 22 hours (Figure 35; Table 29). Thus, the doubling time of the *nfnB* mutant was 1.5 to 2 times higher compared to the wild type when grown on the tested substrates. Additionally, the final OD_{600} of the mutant was reduced by 35–50 % depending on the substrate.

Table 29 Doubling times and final OD_{600} of *T. kivui nfnB* mutant compared to the wild type strain DSM 2030.
Both strains grew on defined medium containing 25 mM glucose, 25 mM mannitol or 25 mM fructose (Figure 10; Figure 11; Figure 20; Figure 35).

Substrate	Doubling time (h)		Final OD_{600}	
	Wild type	*nfnB* mutant	Wild type	*nfnB* mutant
Glucose	1.57 ± 0.01	3.26 ± 0.27	1.58 ± 0.02	0.926 ± 0.023
Mannitol	2.01 ± 0.17	2.94 ± 0.10	1.17 ± 0.02	0.752 ± 0.011
Fructose	1.51 ± 0.03	2.79 ± 0.11	1.57 ± 0.03	0.788 ± 0.042

The observed growth is interesting since glucose, fructose, and mannitol metabolism through glycolysis generates NADH, which must be re-oxidized. It was assumed that the NfnAB complex plays a crucial role in re-oxidation to maintain redox balance. The fact that growth was seen on all NADH-producing substrates suggests that NfnB is not essential for growth on these substrates or for the primary re-oxidation of NADH. Instead, the NfnAB complex could have a supporting role in maintaining the redox balance.

Further experiments were carried out with glucose and pyruvate to investigate how the mutant grows on a Fd-dependent/low-energy substrate (Figure 36).

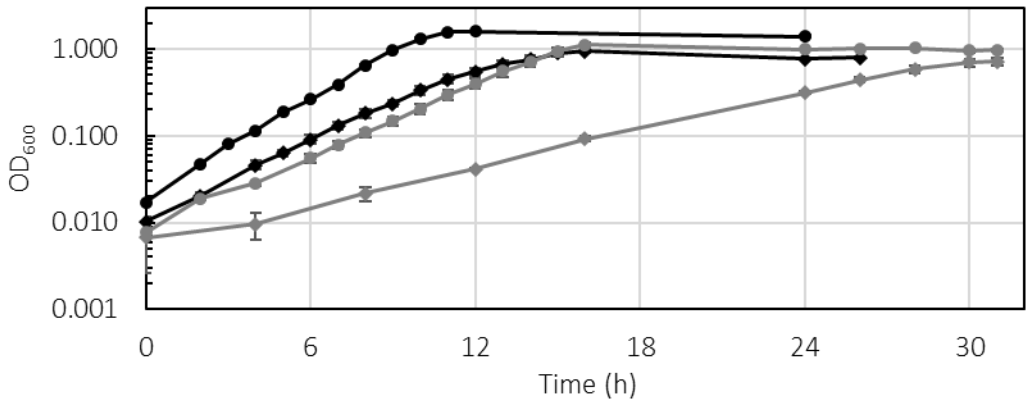

Figure 36 Growth of *nfnB* mutant on glucose and pyruvate.
Representative growth curves of *T. kivui* wild type (strain DSM 2030; black) and the *nfnB* mutant (gray) in the presence of 25 mM glucose (circles) or 100 mM pyruvate (diamonds). All experiments were performed on defined medium at 65 °C and 160 rpm (n = 3).

The *nfnB* mutant grew in defined medium containing either glucose or pyruvate (Figure 36), with a doubling time of 2.12 h with 25 mM glucose and 4.13 h with 100 mM pyruvate. The final OD_{600} was 1.11 with glucose and 0.72 with pyruvate. Compared to the wild type strain DSM 2030, the *nfnB* mutant showed slower growth and reached a lower final OD_{600} on both substrates (Table 30). However, in this experiment, the growth of the *nfnB* mutant with glucose was slightly faster than in the previous growth experiment (Figure 35).

Table 30 Doubling time of the *T. kivui nfnB* mutant grown on glucose or pyruvate.
Comparison of the doubling time of the *T. kivui nfnB* mutant and the wildtype strain DSM 2030 (glucose Figure 10 and pyruvate Figure 30) grown on defined medium containing glucose or pyruvate (Figure 36).

Substrate	Doubling time (h)		Final OD_{600}	
	Wild type	*nfnB* mutant	Wild type	*nfnB* mutant
Glucose	1.57 ± 0.01	2.12 ± 0.14	1.58 ± 0.02	1.11 ± 0.08
Pyruvate	1.98 ± 0.12	4.13 ± 0.25	0.93 ± 0.02	0.72 ± 0.06

The mutant grew 1.35 times slower on glucose and reached a final OD_{600} that was 30% lower than the wild type, though it grew faster and achieved a higher final OD_{600} than in the previous experiment. On pyruvate, the mutant was 2 times slower and had a 23 % lower final OD_{600} compared to the wild type.

The faster growth and the higher OD_{600} with glucose as carbon source could indicate an adaptation of the mutant to the substrate, promoted by further passage of the culture on glucose containing defined medium.

Additionally, autotrophic growth on H_2/CO_2 was investigated by transferring glucose-grown cultures to defined medium with an H_2/CO_2 atmosphere. After three attempts to adapt the mutant to H_2/CO_2, the mutant grew to an OD_{600} of about 0.18 (Figure A-4), suggesting potential growth, which has yet to be reproduced.

In summary, the *nfnB* mutant was able to metabolize sugars like glucose and fructose, the sugar alcohol mannitol, and pyruvate, although with a slower growth rate and a lower final OD_{600} compared to the wild type stain DSM 2030. Additionally, attempts to reliably adapt the mutant to growth on H_2/CO_2 were unsuccessful, possibly suggesting an impaired redox balance or indicating a shortage of NADH, which is crucial for biomass build-up during anabolism.

3.5.3 Utilization of glucose, pyruvate or H_2/CO_2 by resting cells of the *nfnB* mutant strain

Previous experiments showed that the loss of *nfnB* resulted in slower growth on all substrates tested. To confirm these results and to investigate a potential disrupted redox balance during the utilization of glucose, pyruvate or H_2/CO_2, a resting cell experiment was performed.

The resting cell experiment (Figure 37), was conducted using cells grown on complex medium containing 25 mM glucose, as they had shown growth on glucose in previous experiments to a final OD_{600} of around 1. However, the main cultures for the resting cell experiment only reached a final OD_{600} of about 0.16, nevertheless the cells were harvested and processed as described.

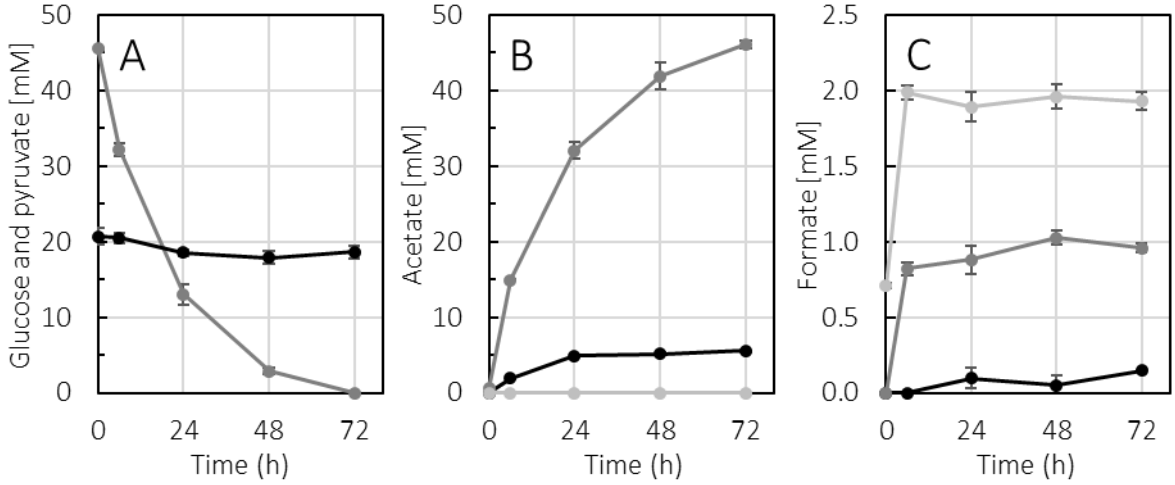

Figure 37 Resting cell experiment of the *nfnB* mutant.
Cell suspensions were incubated for 72 hours in 50 mM Tris-HCl buffer at 65°C with 25 mM glucose (black), 50 mM pyruvate (dark gray) or $3x10^5$ Pa H_2/CO_2 (light gray; 66/33 v/v). Shown is the concentration of glucose (A), pyruvate (A), acetate (B) and formate (C) over 72 hours. The cells were grown on complex medium containing 25 mM glucose (n = 3).

Protein determination showed that the initial protein concentration in the cell suspension was 0.20 mg ml^{-1} ± 0.03 mg ml^{-1}. After 24 hours, the protein concentration decreased in all cultures, with final protein concentrations of 0.15 mg ml^{-1} on glucose, 0.16 mg ml^{-1} on pyruvate, and 0.16 mg ml^{-1} on H_2 /CO_2, indicating that no growth occurred. Pyruvate was fully consumed after 72 hours, resulting in the production of 46.12 mM acetate and 0.96 mM formate (Figure 37; A, B and C). Consequently, the mutant requires 1 mM pyruvate to produce 1 mM acetate, similar to the wild type strain DSM 2030 (Figure 15).

Table 31 Pyruvate consumption and acetate production of resting cells of the *nfnB* mutant.
The cells were incubated for 72 hours in 50 mM Tris-HCl buffer at 65 °C with 50 mM pyruvate (n = 3). The resting cells were grown on complex medium containing 25 mM glucose.

Time (h)	Pyruvate consumption (mM/h)	Acetate production (mM/h)
0-6	−2.24 ± 0.18	2.39 ± 0.01
6-24	−1.06 ± 0.03	0.95 ± 0.07
24-48	−0.42 ± 0.05	0.41 ± 0.05
48-72	−0.13 ± 0.02	0.18 ± 0.08

Additionally, between 0 and 6 hours, the pyruvate consumption rate was −2.24 mM h^{-1} and acetate production rate was 2.39 mM h^{-1}. But both the pyruvate consumption rate and the acetate production rate decreased by half every 24 hours (Table 31).

Given that the protein concentration was approximately one-third of that in the previous resting cell experiment with the wild type (0.61 mg ml; Figure 15) a lower consumption rate was anticipated. However, the calculated pyruvate consumption and acetate production rate of the wild type DSM 2030 showed different rates compared to the *nfnB* mutant for the protein concentration of 0.20 mg ml^{-1}.

With a protein concentration of 0.20 mg ml^{-1}, the pyruvate consumption rate would be −3.5 mM mg^{-1} h^{-1} for the wild type, compared to −0.46 mM mg^{-1} h^{-1} of the mutant. The acetate production rate would be 2.54 mM mg^{-1} h^{-1} for the wild type compared to 0.49 mM mg^{-1} h^{-1} of the *nfnB* mutant. Thus, the mutant has a slower pyruvate consumption and a lower acetate production rate relative to the protein concentration compared to the wild type. Notably, in the mutant, the rates of pyruvate consumption and acetate production were directly proportional (Figure 31), unlike in the wild type, which consumed −17.23 mM h^{-1} while producing 12.45 mM h^{-1} (Figure 15; Figure 37).

Unexpectedly, the resting cells of the mutant consumed only 2.1 mM ± 1.3 mM of 20.7 mM ± 1.4 mM glucose over 72 hours, resulting in the production of 5.6 mM ± 0.1 mM acetate (Figure 37; A and B). Furthermore, the mutant produced about 1.9 mM ± 0.1 mM formate and no acetate with H_2/CO_2 in the atmosphere (Figure 37; C). Therefore, the *nfnB* mutant did not utilize glucose but was able to utilize pyruvate, indicating that glucose can only be metabolized during growth. The limited formate production and the absence of acetate in the H_2/CO_2 cultures suggest that the *nfnB* mutant grown on glucose cannot utilize H_2/CO_2.

In contrast, previous experiments with resting cells of the wild type pre-grown on glucose showed the production of acetate with only H_2/CO_2 in the atmosphere (Figure 12). Further experiments were conducted to investigate the physiological and gene expression response of the *nfnB* mutant to H_2/CO_2.

3.5.4 Hydrogen shock of the *nfnB* mutant during growth on defined medium containing glucose

To investigate the inability of resting cells to convert H_2/CO_2 to acetate and the difficulty of growing the *nfnB* mutant on H_2/CO_2, growth experiments on defined medium containing glucose or pyruvate were performed. Therefore, the cultures were shocked with H_2/CO_2 during the exponential growth phase by adding H_2/CO_2 with an overpressure of $2x10^5$ Pa (Figure 38; Figure 40).

The *nfnB* mutant grew with a doubling time of 2.12 on defined medium containing 25 mM glucose and the final OD_{600} of the unshocked cultures were around 1.11 after 16 hours of growth (Figure 38). Most of the glucose (28.27 mM ± 2.10 mM) in the unshocked cultures was consumed after 16 hours, with a consumption rate of −3.81 mM h^{-1} between 12 and 16 hours (Figure 38; A). Up to 1.70 mM ± 0.07 mM formate was produced after 12 hours and was subsequently consumed. Acetate was produced at a rate of 4.62 mM h^{-1} between 8 and 16 hours and the final acetate concentration was 47.18 mM ± 2.11 mM (Figure 38; B).

Half of the *nfnB* mutant cultures were shocked with $2x10^5$ Pa H_2/CO_2 overpressure after 9 hours of growth at an OD_{600} of approximately 0.16. Afterwards, the cells grew to an OD_{600} of only 0.29 within 7 hours with a doubling time 9.83 h. Growth then stalled, maintaining an OD_{600} of around 0.28 for 32 hours (hour 16 to 48). Over the following 48 hours (hour 48 to 96) the mutant grew then to a final OD_{600} of 0.83.

The glucose consumption rate was −0.15 mM h^{-1} between 10 to 48 hours, and after 96 hours, all glucose was consumed. After the addition of H_2/CO_2, formate was produced, with the highest concentration of 14.80 mM ± 0.18 mM. The produced formate was subsequently consumed at a rate of −0.13 mM h^{-1} between hour 10 and 48, and 0.95 mM ± 0.2 mM formate remained after 96 hours. The acetate production changed after the H_2 shock from 4.62 mM h^{-1} (unshocked) to 1.22 mM h^{-1} (shocked)

between 8 to 16 hours, decreased further between 16 to 48 hours to 0.49 mM h^{-1} and when the cells started to grow again, the acetate production rate increased to 1.32 mM h^{-1} (48 to 96 hours). The final acetate concentration was 93.16 mM ± 2.63 mM (Figure 38; C).

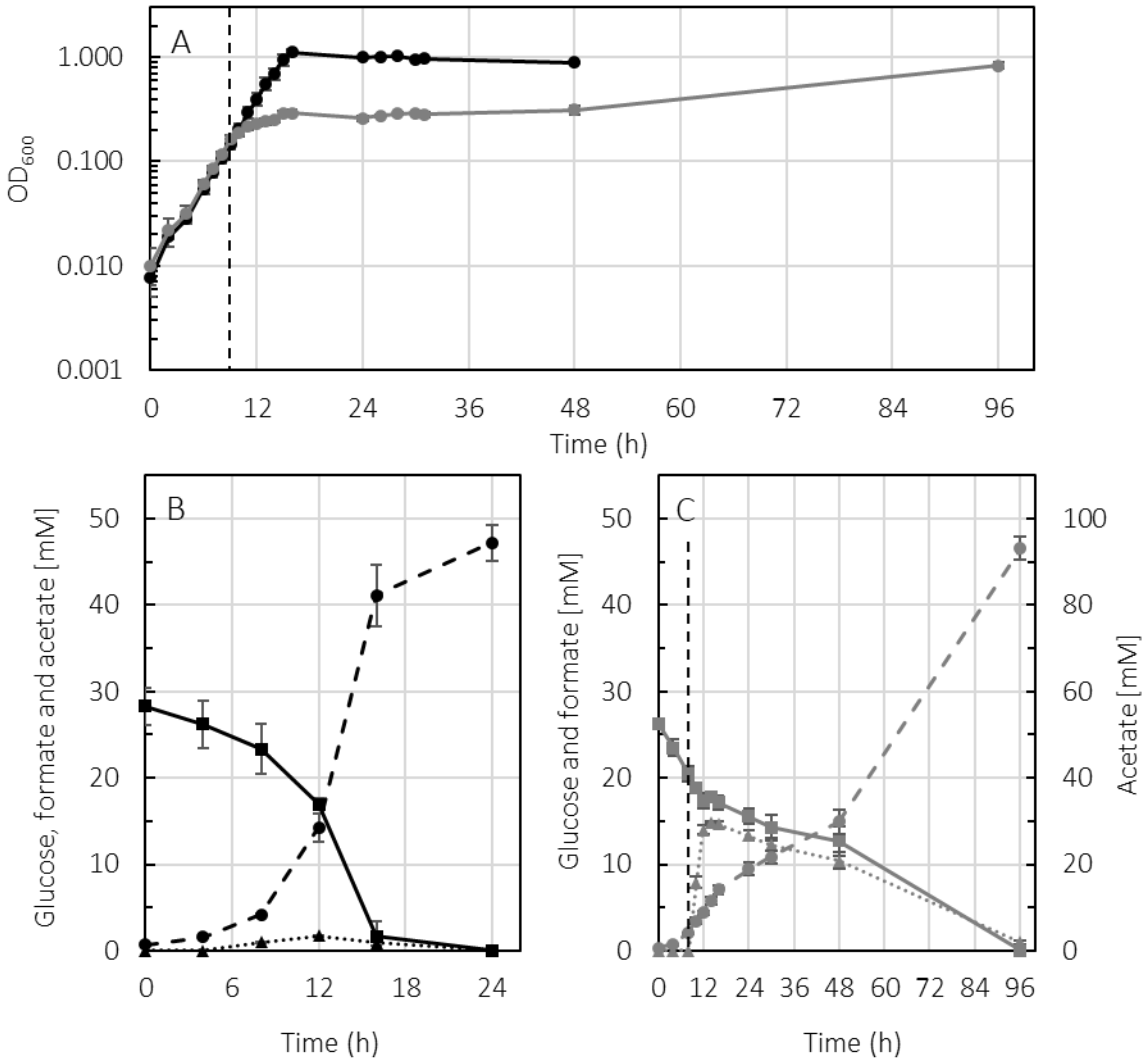

Figure 38 H_2 shock of the *nfnB* mutant during growth on defined medium containing glucose.
Representative growth curve (A) of the *nfnB* mutant on 25 mM glucose (black) and shocked with H_2/CO_2 (dark gray) after 9 hours (black dashed line). Cultures were shocked with $2x10^5$ Pa H_2/CO_2 overpressure. Substrate concentration was determined for the *nfnB* mutant on glucose (B; black) and glucose shocked with H_2/CO_2 (C; dark gray) for glucose (squares; continuous line), formate (triangles; dotted line), and acetate (circles; dashed line). All experiments were performed on defined medium at 65 °C and 160 rpm (n = 3).

The addition of H_2/CO_2 during the exponential growth phase resulted in a significant inhibition of growth for 48 hours, along with a reduction in glucose consumption. Glucose and formate consumption was coupled as in the wild type (strain DSM 2030), and the final concentration of acetate was similar to the wild type under both conditions (Figure 29). However, the wild type still had some glucose in the shocked cultures, resulting in a slightly lower acetate concentration. Furthermore, the acetate concentration in the cultures with additional H_2/CO_2 was about 46 mM higher, indicating that the mutant was able to utilize H_2/CO_2 under these conditions.

Further analyses of gene expression of the genes encoding for Ech1 complex (*ech1A*), Ech2 complex (*ech2D*), formyl-tetrahydrofolate synthetase (*fhs*), HDCR (*fdhF*), electron bifurcating hydrogenase (*hydB*), glyceraldehyde 3-phosphate dehydrogenase (*gap*), ferredoxin (*fd1*; TKV_c16450), PFOR1 (*nifJ1*),

PFOR2 (*nifJ2*) and 2-oxoacid:ferredoxin oxidoreductases (*2OxFOR*; TKV_c19280). This analysis could reveal how the *nfnB* mutant responds to the presence of additional H_2/CO_2 in the atmosphere during heterotrophic growth on glucose and whether there were any differences in gene regulation between the mutant and the wild type strain DSM 2030 in general.

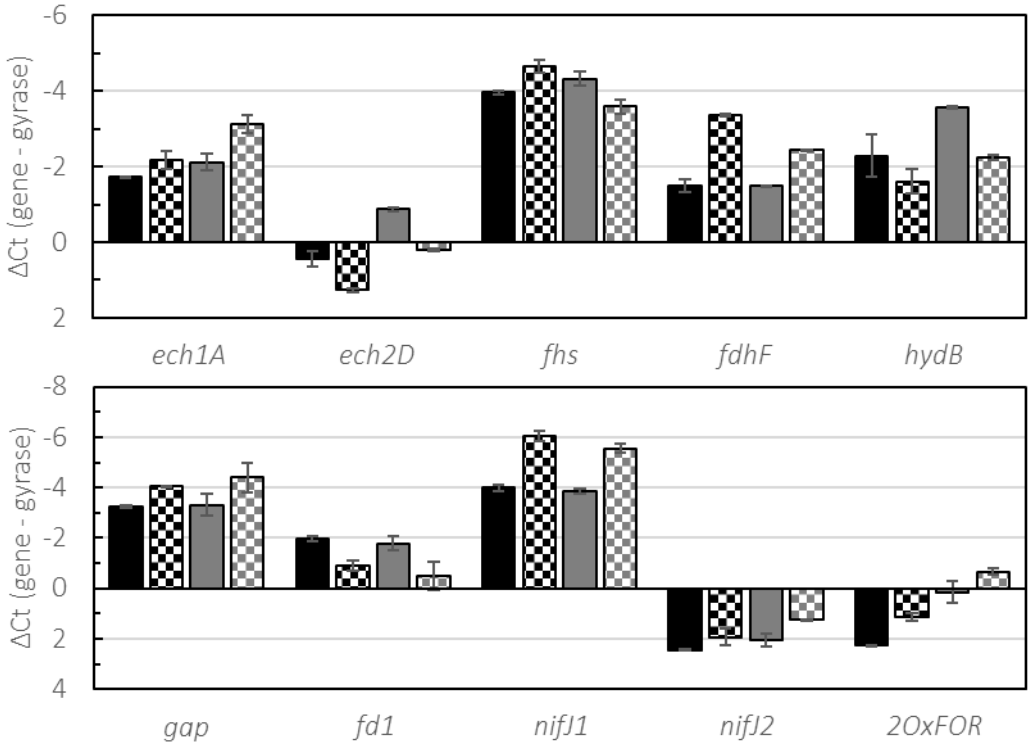

Figure 39 Expression of metabolic relevant genes of the *nfnB* mutant and the wild type grown on glucose and shocked with H_2/CO_2 (Figure 29, Figure 38).
Gene expression before (filled column) and after the H_2 shock (checkered column) of the wild type (black) and *nfnB* mutant (gray) in the presence of glucose. The mRNA levels were normalized to the abundance of gyrase (*gyrB*). Gene expression was determined for *ech1A* (Ech1 complex), *ech2D* (Ech2 complex), *fhs* (Formyl-tetrahydrofolate synthetase), *fdhF* (HDCR), *hydB* (electron bifurcating hydrogenase), *gap* (glyceraldehyde 3-phosphate dehydrogenase), *fd1* (ferredoxin; TKV_c16450), *nifJ1* (PFOR1), *nifJ2* (PFOR2), *2OxFOR* (2-oxoacid:ferredoxin oxidoreductases; TKV_c19280). RNA was extracted form cells that were harvested in the exponential growth phase 5 minutes before and 15 minutes after the H_2 shock. The associated growth experiment was performed on defined medium at 65 °C and 160 rpm. Multiple biological replicates (n = 2) and technical replicates (n = 3) were tested.

A comparison of glucose cultures between the *nfnB* mutant and the wild type before the addition of H_2/CO_2 (b. H_2) revealed no significant changes in gene expression in the mutant beyond the 4-fold or −4-fold threshold, except for *2OxFOR* (2-oxoacid:ferredoxin oxidoreductases; TKV_c19280; Figure 39, Table 32). There was a slight upregulation of the *ech2D* and *hydB* genes by a 2-fold change, while all other genes remained unchanged (Figure 39, Table 32).

Comparing the gene expression in the mutant and the wild type after the addition of H_2/CO_2 (a. H_2) all genes were below or above the threshold, indicating that the mutant responded to H_2 shock in a way similar as the wild type.

When comparing gene expression before (b. H_2) and after (a. H_2) the addition of H_2/CO_2 (Table 32), the mutant did not show significant changes in gene expression. A slight upregulation of *nifJ1* by 3.3-fold was also observed in the mutant, although this was below the 4-fold value. In contrast to that, the wild type showed upregulation above the threshold of *nifJ1*, as previously noted (Table 26, Table 32).

Table 32 Fold change values of qPCR of *T. kivui* wild type and *nfnB* mutant (Figure 39).
Calculated fold change values of the *nfnB* mutant and the wild type strain DSM 2030 grown on defined medium with glucose before the H_2 shock (b. H_2), after the H_2 shock (a. H_2). Comparisons of the *nfnB* mutant gene expression and wild type in different combinations. The upregulation of the gene is indicated by blue and downregulation by red. The threshold value for upregulation is 4-fold and for downregulation −4-fold and indicated by darker color.

		Fold change			
		Glucose b. H_2	Glucose a. H_2	Wild type	*nfnB* mutant
Test		*nfnB* mutant	*nfnB* mutant	Glucose a. H_2	Glucose a. H_2
Calibrator		Wild type	Wild type	Glucose b. H_2	Glucose b. H_2
Gene	*ech1A*	1.3	1.9	1.4	2.0
	ech2D	2.5	2.1	−1.8	−2.1
	fhs	1.3	−2.1	1.6	−1.7
	fdhF	1.0	−1.9	3.7	1.9
	hydB	2.4	1.5	−1.6	−2.5
	gap	1.1	1.3	1.8	2.1
	fd1	−1.1	−1.3	−2.1	−2.5
	nifJ1	−1.1	−1.4	4.2	3.3
	nifJ2	1.3	1.6	1.4	1.8
	2OxFOR	4.2	3.4	2.2	1.8

In summary, the loss of *nfnB* did not result in a significant change in gene expression of the genes investigated. The mutant responded to the addition of H_2/CO_2 like the wild type, although the physiological response was stronger. This suggests that other genes might be involved or that the observed phenotype could be due to a metabolic bottleneck caused by the loss of *nfnB* combined with the addition of H_2/CO_2.

3.5.5 Hydrogen shock of the *nfnB* mutant during growth on defined medium containing pyruvate

The observed response of the *nfnB* mutant, grown on defined medium containing glucose, to the addition of H_2/CO_2 during exponential growth (Figure 38) revealed significant impairment in growth. To determine whether this growth inhibition also occurs when the mutant is grown on pyruvate or if growth is promoted as seen in the wild type (Figure 30), additional experiments were conducted using defined medium containing pyruvate, with H_2/CO_2 added during exponential growth.

The *nfnB* mutant grew on defined medium containing 100 mM pyruvate with a doubling time of 4.13 h and the cultures reached a final OD_{600} of 0.72 after 31 hours (Figure 40; A). In the unshocked cultures, pyruvate (102.89 mM ± 10.12 mM) was almost completely consumed after 30 hours, with a consumption rate of −7.49 mM between 24 to 30 hours (Figure 40; B). After 48 hours, 100.1 mM ± 5.79 mM acetate was produced with a rate of 7.45 mM between 24 to 30 hours (Figure 40; B), while no formate was produced.

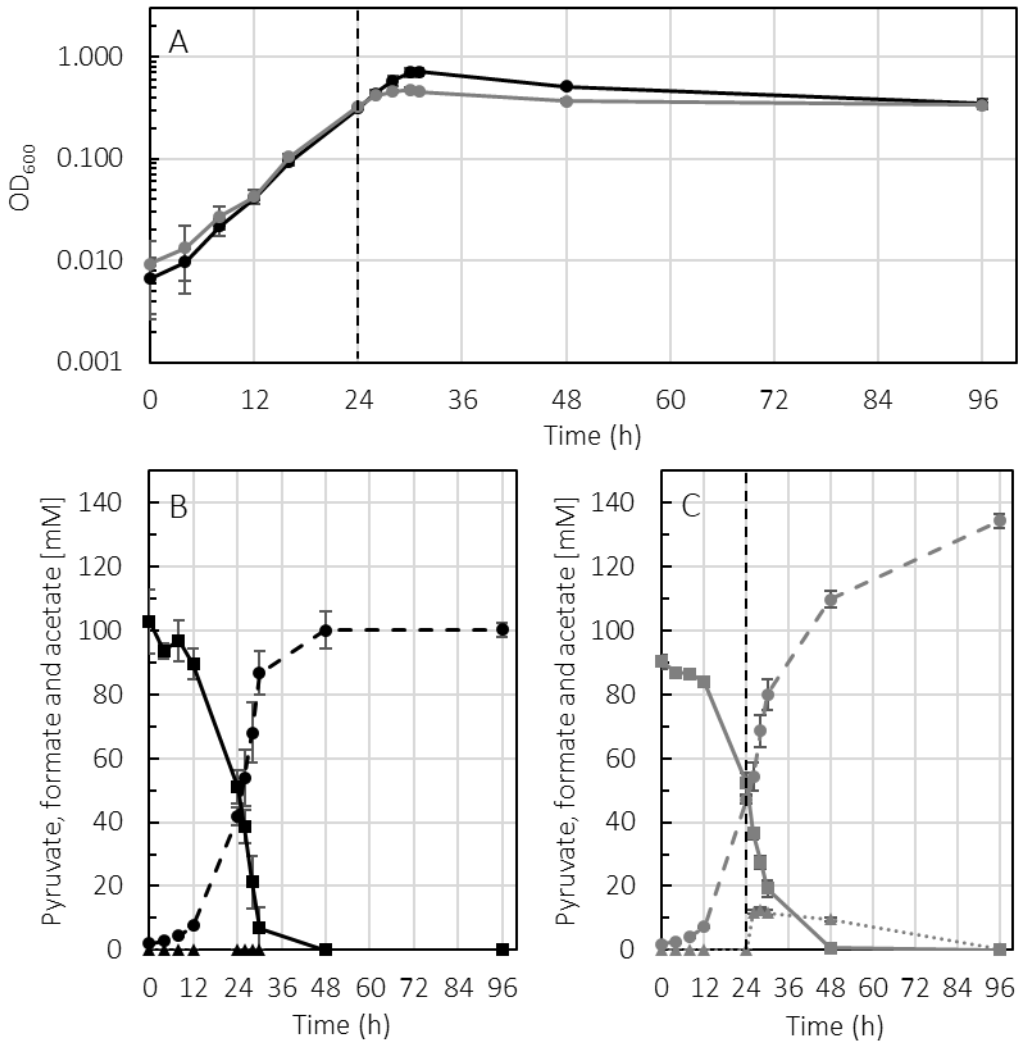

Figure 40 H_2 shock of the *nfnB* mutant during growth on defined medium containing pyruvate.
Representative growth curve of *nfnB* mutant on pyruvate (black) and shocked with H_2/CO_2 (dark gray) after 24 hours (black dashed line). Cultures were shocked with $2x10^5$ Pa H_2/CO_2 overpressure. Substrate concentration was determined for the *nfnB* mutant on pyruvate (black) and on pyruvate shoecked with H_2/CO_2 (dark gray) for glucose (square; continuous line), format (triangle; dotted line) and acetate (circle; dashed line). All experiments were performed on defined medium at 65 °C and 160 rpm (n = 3).

The *nfnB* mutant cultures were shocked with $2x10^5$ Pa H_2/CO_2 overpressure after 24 hours of growth at an OD_{600} of around 0.32. Following the shock, the mutant continued to grow for 6 hours, reaching an OD_{600} of 0.478 with a doubling time of 20.78 h. Growth then stopped, and the OD_{600} gradually decreased over time, similar to the unshocked cultures (Figure 40; A). Between 24 to 30 hours, 90.19 mM ± 2.11 mM pyruvate was consumed at a rate of −5.38 mM h^{-1} (Figure 40; C), while acetate was produced at a rate of 5.65 mM h^{-1} during this period, resulting in a final acetate concentration of 134.37 mM ± 2.19 mM. After the addition of H_2/CO_2, formate was produced, with the highest concentration of 12.66 mM ± 0.53 mM after 28 hours and was consumed at a rate of −0.18 mM h^{-1} between 28 to 96 hours and by hour 96 all formate had been consumed.

Thus, growth of the *nfnB* mutant was inhibited after the addition of H_2/CO_2 when grown on either pyruvate or glucose. However, unlike glucose consumption, pyruvate consumption was not coupled to formate consumption. Moreover, in the shocked cultures, pyruvate consumption and acetate production were reduced by about 2 mM h^{-1} compared to the unshocked cultures. In contrast to that, in the wild type, both pyruvate consumption and acetate production increased by about 2 mM h^{-1} after

the H_2/CO_2 shock (Figure 30; Figure 40). Formate consumption was also lower in the shocked cultures of the *nfnB* mutant compared to the wild type (−0.18 mM h^{-1} vs −2.13 mM h^{-1}, respectively). Similar to the experiment with glucose, the pyruvate cultures with additional H_2/CO_2 showed an increase of about 34 mM acetate compared to the unshocked cultures, indicating that the *nfnB* mutant was capable of utilizing H_2/CO_2 under both growth conditions.

Similar to the glucose cultures, gene expression in the pyruvate cultures of the *nfnB* mutant was analysed and compared to that of the wild type. The gene expression of the genes encoding for Ech1 complex (*ech1A*), Ech2 complex (*ech2D*), formyl-tetrahydrofolate synthetase (*fhs*), HDCR (*fdhF*), electron bifurcating hydrogenase (*hydB*), glyceraldehyde 3-phosphate dehydrogenase (*gap*), ferredoxin (*fd1*; TKV_c16450), PFOR1 (*nifJ1*), PFOR2 (*nifJ2*) and 2-oxoacid:ferredoxin oxidoreductases (*2OxFOR*; TKV_c19280) were investigated.

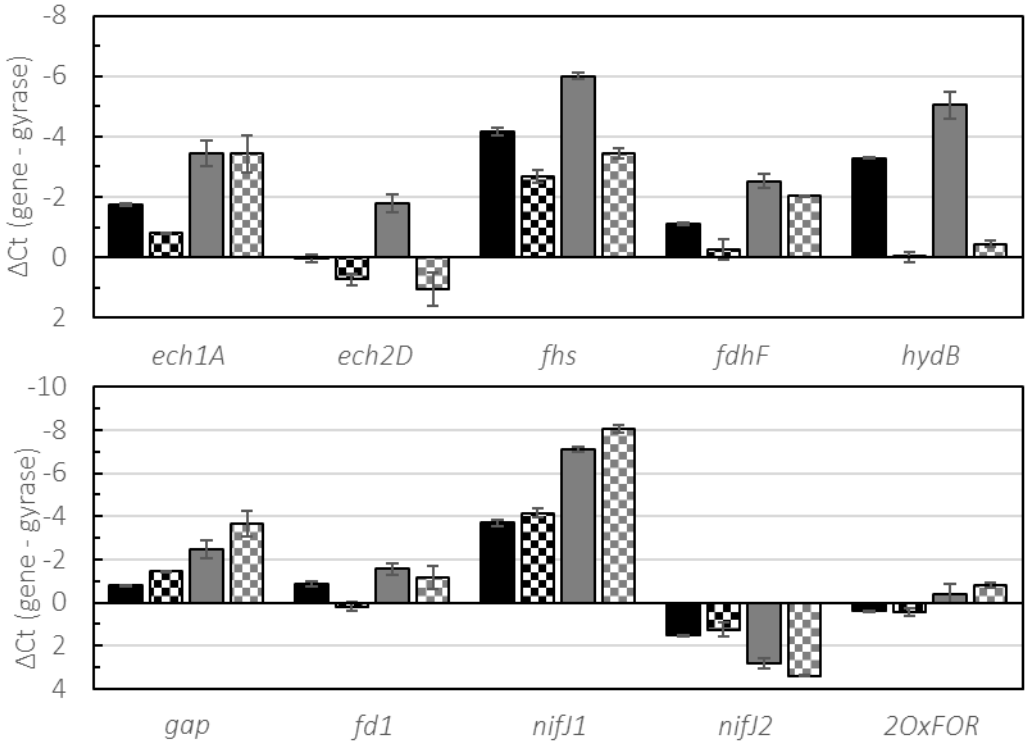

Figure 41 Expression of metabolic relevant genes of *T. kivui* wild type and *nfnB* mutant grown on pyruvate and shocked with H_2/CO_2 (Figure 30, Figure 40, Figure 38).
Gene expression before (filled column) and after H_2 shock (checkered column) of the wild type (black) and *nfnB* mutant (dark gray) in the presence of pyruvate. The mRNA levels were normalized to the abundance of gyrase (*gyrB*). Gene expression was determined for *ech1A* (Ech1 complex), *ech2D* (Ech2 complex), *fhs* (Formyl-tetrahydrofolate synthetase), *fdhF* (HDCR), *hydB* (electron bifurcating hydrogenase), *gap* (glyceraldehyde 3-phosphate dehydrogenase), *fd1* (ferredoxin; TKV_c16450), *nifJ1* (PFOR1), *nifJ2* (PFOR2), *2OxFOR* (2-oxoacid:ferredoxin oxidoreductases; TKV_c19280). RNA was extracted form cells that were harvested in the exponential growth phase 5 minutes before and 15 minutes after the H_2 shock. The associated growth experiment was performed on defined medium at 65 °C and 160 rpm. Multiple biological replicates (n = 2) and technical replicates (n = 3) were tested.

Comparison of the pyruvate cultures of the *nfnB* mutant to the wild type before the addition of H_2/CO_2 (b. H_2) revealed a slight upregulation for *ech1A*, *ech2D*, *fhs*, *fdhF*, *hydB*, and *gap*, with increases ranging from just above 2-fold but below 4-fold. Notably, *nifJ1* was strongly upregulated by 10.57-fold (Figure 41; Table 33).

When comparing the conditions after the addition of H_2/CO_2 (a. H_2), the *nfnB* mutant showed an upregulation of *fdhF* just below the threshold and upregulation above the threshold for the genes *ech1A*, *gap* and *nifJ1* compared to the wild type. While the *ech2D* shifted from being slightly upregulated to slightly downregulated and *nifJ2* was strongly downregulated compared to the wild type (Figure 41; Table 33).

The comparison of gene expression before (b. H_2) and after (a. H_2) the addition of H_2/CO_2 (Table 33) showed, that *hydB* was downregulated by −9.7-fold in the wild type (Table 26). In the *nfnB* mutant, *hydB* showed an even stronger downregulation of −24-fold, accompanied by downregulation of *ech2D* and *fhs*, which was not observed in the wild type. Other genes remained unchanged.

Table 33 Fold change values of qPCR of *T. kivui* wild type and *nfnB* mutant (Figure 41).
Calculated fold change values of the *T. kivui nfn*B mutant and wild type strain DSM 2030 grown on defined medium with pyruvate before H_2 shock (b. H_2), after H_2 shock (a. H_2) with H_2/CO_2. Comparison of gene expression of after H_2 shock (test) compared to before H_2 shock (calibrator) or *nfnB* mutant (test) compared to wild type (calibrator). The upregulation of the gene is indicated by blue and downregulation by red. The threshold value for upregulation is 4-fold and for downregulation −4-fold and indicated by darker color.

		Fold change			
		Pyruvate b. H_2	Pyruvate a. H_2	Wild type	*nfnB* mutant
Test		*nfnB* mutant	*nfnB* mutant	Pyruvate a. H_2	Pyruvate a. H_2
Calibrator		Wild type	Wild type	Pyruvate b. H_2	Pyruvate b. H_2
Gene	*ech1A*	3.2	6.2	−1.9	−1.0
	ech2D	3.6	-1.3	-1.6	−7.2
	fhs	3.6	1.7	-2.8	−5.9
	fdhF	2.6	3.4	-1.8	−1.4
	hydB	3.4	1.4	−9.7	−24.1
	gap	3.2	4.7	1.6	2.3
	fd1	1.6	2.6	-2.1	-1.3
	nifJ1	10.6	15.0	1.4	2.0
	nifJ2	-2.4	−4.4	1.2	-1.5
	2OxFOR	1.8	2.4	-1.0	1.3

In summary, the *nfnB* mutant showed growth inhibition when grown with pyruvate after the addition of H_2/CO_2, a response that differed from that of the wild type. Furthermore, the gene expression changes were stronger for *hydB*, *ech2* and *fhs*. The mutant also showed upregulation of *nifJ1* during normal growth compared to the wild type and after the addition of H_2/CO_2, *nifJ1*, *ech1A* and *gap* were highly upregulated compared to the wild type. This suggests that the mutant requires Ech1 and PFOR1 (*nifJ1*) to maintain energy conservation and allow growth on pyruvate, while the addition of H_2/CO_2 likely leads to a redox imbalance resulting in growth inhibition and only a slight reduction in pyruvate consumption, as well as downregulation of *hydB*, *ech2D* and *fhs*.

4 Discussion

4.1 H_2 and redox metabolism in *T. kivui*

Thermoanaerobacter kivui is one of the few *Thermoanaerobacter* strains that are genetically accessible to date due to the natural tendency to take up DNA and integrate it under selective pressure. This characteristic makes it an ideal organism for research and industrial applications (Shaw et al. 2010; Basen et al. 2018; Zeldes et al. 2023). Since the genome analyses conducted by Hess et al. (2014), several studies have investigated the functionality and structure of enzymes involved in the autotrophic and heterotrophic acetogenesis of *T. kivui* (Figure 3).

This research work focuses on the deletion of enzymes that are involved in maintaining metabolic redox balance by transferring electrons between redox partners. Among these enzymes are the membrane-bound Ech1 and Ech2 hydrogenases complexes, which couple the oxidation and reduction of the redox carriers like ferredoxins (Fd_{red}/Fd_{ox}) and hydrogen ($H_2/2\ H^+$), to build up or consume a proton gradient across the membrane (Rosenbaum and Müller 2021). Furthermore, the electron bifurcating transhydrogenase complex NfnAB is considered to be important for maintaining redox balance (Lo et al. 2015). The genes encoding the NfnAB complex are annotated in the genome of *T. kivui* (Hess et al. 2014). The NfnAB complex catalyzes the endergonic reduction of NADPH by the oxidation of NADH coupled with the exergonic reaction of the reduction of NADPH by the oxidation of Fd_{red} (Peters et al. 2016).

In this context, the Ech1, Ech2, and NfnAB complexes are likely crucial mediators of the redox balance in *T. kivui*. Deleting either an Ech complex or the NfnAB complex could result in a redox imbalance, depending on the form of the redox carriers provided by the utilized substrate. This imbalance could inhibit growth if the organism cannot adapt to the loss of the enzyme. The heterotrophic metabolism of glucose is described below to understand the importance of maintaining the redox equilibrium and the electron transfer between the electron carriers by these enzymes (Figure 3). ATP, NADH, and Fd_{red} are available to the organism during glucose utilization. Glucose is taken up by PTS systems of *T. kivui* (Hess et al. 2014; Moon et al. 2019) and afterwards oxidized via glycolysis to acetate and CO_2. The glycerinaldehyde-3-P dehydrogenase (*gap*; TKV_c16340) provides NADH and the pyruvate-ferredoxin oxidoreductase (PFOR1; *nifJ1*; TKV_c04340) oxidizes pyruvate to acetyl-CoA and CO_2, while reducing Fd_{ox} to Fd_{red} (Katsyv et al. 2021b). Subsequently, NADH and Fd_{red} as electron carries must be re-oxidized, to provide the necessary oxidized electron carriers for further oxidation of glucose. Therefore, the transhydrogenase NfnAB provides two NADPH by oxidizing NADH and Fd_{red}, one for the WLP and one for the electron bifurcating hydrogenase (HydABC). The HydABC in turn provides H_2 by oxidizing NADPH and additional Fd_{red}, and subsequently H_2 can be converted to Fd_{red} by the Ech complexes. In theory, the Ech and NfnAB complexes are essential to balance all relevant electron carriers required by the WLP during growth on glucose (Figure 3; Katsyv et al. 2021a).

The Ech2 complex of *T. kivui* was characterized and described by Katsyv and Müller (2022) to oxidize Fd_{red} to reduce H_2 and build up a transmembrane proton gradient, while it is also able to reduce Fd_{ox} by oxidizing H_2 and at the expense of the proton gradient. Moreover, it seems that that the oxidation of Fd_{red} and reduction of H_2 is more favorable compare to the oxidation of H_2 and reduction of Fd_{ox} (10.4 ± 3.4 U mg^{-1} vs. 1.6 ± 0.3 U mg^{-1}, respectively; Katsyv and Müller 2022). The characterization of the Ech1 complex has not yet been carried out.

Although the Ech2 complex has been characterized, the metabolic function of the Ech2 complex in *T. kivui* has not yet been clarified. Consequently, characterizing the Ech2 deletion mutant, along with the deletion mutants of the Ech1 and NfnAB complexes, was of great importance.

4.2 Metabolic function of Ech2

4.2.1 Utilization of sugars and H_2/CO_2 of the Δ*ech2* strain

As described, the Ech2 complex is assumed to be required for the oxidative status of Fd_{ox}/Fd_{red} and $H_2/2\ H^+$. Therefore, deleting the *ech2* operon would, theoretically, sensitively disturb the redox balance depending on the growth substrate.

No difference between the wild type strain DSM 2030 and the Δ*ech2* strain was seen during organotrophic growth on the sugar's glucose and fructose, neither on complex nor on defined medium containing uracil (Table 34). However, an exception was observed with the sugar alcohol mannitol. The Δ*ech2* strain grew significantly better on complex medium (P = 0.0006 [P ≤0.05]) but not on defined medium (P = 0.19 [P ≤0.05]). Growth experiments with defined media and various substrates showed that the Δ*ech2* strain did not require additional substrates besides uracil to achieve growth comparable or better than the wild type strain DSM 2030. Previous studies regarding the growth of *T. kivui* on complex medium achieved doubling times of 1.24 h to 2.4 h on glucose (Jain et al. 2020; Dietrich et al. 2022), 1.3 h on fructose (Basen et al. 2018) and 2 h on mannitol (Moon et al. 2019). Therefore, the growth rates observed in this study were within the same range, with a slightly faster on mannitol. In addition, the cells of wild type and Δ*ech2* strain metabolized glucose in a homoacetogenic manner, with 2.43 mol ± 0.23 mol vs. 2.43 mol ± 0.28 mol acetate produced from one mol glucose on complex medium, respectively. This agrees with the reported conversion of one mol glucose to 2.5 mol ± 0.24 mol (Leigh et al. 1981) and 2.6 mol ± 0.1 mol acetate (Moon et al. 2020). Other acetogens, such as *Moorella thermoacetica* (Fontaine et al. 1942) and *Acetobacterium woodii* (Heise et al. 1989) produced between 2.5 mol and 2.7 mol acetate per glucose and fructose, respectively. Acetogens like *A. woodii* and *Clostridium ljungdahlii* containing a Rnf complex instead of one Ech complex, showed metabolic phenotypes on fructose when the *rnf* gene cluster was removed. The *rnf* mutant of *A. woodii* produced only 2.06 moles of acetate from 1 mole of fructose, indicating impairment of the WLP. Additionally, two growth phases on complex medium were observed, while the mutant grew just like the wild type on defined medium (Westphal et al. 2018). Meanwhile, the *rnf* mutant of the acetogen *C. ljungdahlii* showed a 24.7 % decrease in ATP synthesis utilizing fructose, resulting in growth inhibition of approximately 2 hours compared to wild type (Tremblay et al. 2012).

The growth on glucose, fructose and mannitol and the ratio of sugar to acetate indicate that the Ech2 complex is not essential for *T. kivui* under these conditions, suggesting that the Ech complex shown in the metabolic models of *T. kivui* (Figure 3; Katsyv et al. 2021a; Öppinger et al. 2022), may be exclusively the Ech1 complex, which redox balancing and H_2 oxidation during growth on sugars.

It is remarkable that the wild type grew at a similar rate on complex medium and H_2/CO_2 as on glucose or fructose (Table 34), as the utilization of H_2/CO_2 has a lower energy output per produced mole acetate than glucose or fructose. Based on the models for heterotrophic growth of *T. kivui*, each glucose molecule provides 2.62 ATP and 3 acetate molecules, corresponding to 0.87 ATP per acetate. In contrast, models for autotrophic growth on H_2/CO_2 predict a negative ATP yield unless the Ech complex translocates more than one proton (Katsyv et al. 2021a; Öppinger et al. 2022). Theoretically, this would be possible if the Ech complex forms a complex with methylenetetrahydrofolate reductase (MetFV) and the final electron acceptor is methylene-THF instead of H_2, which would increase the free energy from

$\Delta G_0' = -6.9$ kJ mol^{-1} to $\Delta G_0' = -48.3$ kJ mol^{-1}, allowing the translocation of more than one proton (Katsyv et al. 2021a).

Table 34 Summary of the doubling times (h) for different *T. kivui* strains.
The strains were cultivated on either complex or defined media containing organic substrates like 25 mM glucose, 25 mM fructose, 25 mM mannitol, or 50-100 mM pyruvate, as well as gas mixtures of H_2/CO_2 or $H_2/CO_2/CO$. Strains not grown under certain conditions are considered as not determined (n.d.).

Medium	Substrate	Wild type	Δ*ech2*	P_{frc}*ech1*	P_{frc}*ech1*Δ*ech2*
Complex	Glucose	1.29 ± 0.12	1.27 ± 0.08	n.d.	n.d.
	Fructose	1.49 ± 0.03	1.21 ± 0.03	n.d.	n.d.
	Mannitol	1.75 ± 0.14	1.47 ± 0.13	n.d.	n.d.
	Pyruvate	1.61 ± 0.03	1.53 ± 0.05	n.d.	n.d.
	H_2/CO_2	1.35 ± 0.19	1.38 ± 0.11	n.d.	n.d.
	$H_2/CO_2/CO$	4.30 ± 0.32	3.29 ± 0.05	n.d.	n.d.
Defined	Glucose	1.61 ± 0.04	1.60 ± 0.05	1.90 ± 0.01	1.98 ± 0.03
	Fructose	1.51 ± 0.03	n.d.	1.40 ± 0.03	1.60 ± 0.03
	Mannitol	2.01 ± 0.17	1.77 ± 0.20	n.d.	n.d.
	Pyruvate	1.98 ± 0.02	n.d.	n.d.	n.d.
	H_2/CO_2	1.87 ± 0.02	n.d.	n.d.	n.d.

If *T. kivui* translocates an additional proton, the ATP acetate ratio would be 0.28 ATP per acetate. Consequently, *T. kivui* would need to produce 3.1 times more acetate when growing on H_2/CO_2 than on glucose to generate the same amount of ATP. Yet, the acetate production of the wild type during exponential growth was nearly identical on glucose (10.6 mM h^{-1} ± 0.5 mM h^{-1}; Figure 10) and H_2/CO_2 (10.4 mM h^{-1} ± 1.0 mM h^{-1}; Figure 12).

This suggests that more than one additional proton must be translocated through the Ech-MetFV complex to maintain equivalent growth on H_2/CO_2, assuming ATP production is directly linked to growth. The exact number of protons translocated by the presumed Ech-MetFV complex, which are crucial for energy conservation and allow growth comparable to that on glucose, remains an unresolved question. It is also unclear if one of the two Ech complexes in the wild-type DSM 2030 of *T. kivui* potentially forms a super-complex with MetFV. There is no direct evidence supporting the formation of such an Ech-MetFV complex. It could be possible that the Ech complexes and the MetFV complex function independently, as biochemical evidence showed that the Ech2 complex and the MetFV complex can oxidize Fd_{red} separately (Katsyv et al. 2021a; Katsyv and Müller 2022; Öppinger et al. 2022). Nonetheless, if an Ech-MetFV complex were to form, it would likely involve Ech1 in the Δ*ech2* strain, given that Ech2 has been deleted.

The current model for autotrophic growth on H_2/CO_2 suggests that only Ech-MetFV translocates protons outside the membrane, while another Ech complex reduces Fd_{red} by oxidizing H_2 and using the proton gradient, resulting in a balanced metabolism. This suggests that Ech2 may be involved in the reduction of ferredoxin. In *Methanosarcina barkeri*, loss of the only Ech complex resulted in growth inhibition during autotrophic growth on H_2/CO_2, showing that the deleted Ech complex is essential for the organism when growing on H_2/CO_2 (Meuer et al. 2002). Yet, the Δ*ech2* strain of *T. kivui* had the same growth rate as the wild type on H_2/CO_2 in complex medium, with a doubling time of around 1.20 h to 1.54 h (Table 34). This is slightly faster growth than the first description of *T. kivui,* which demonstrated doubling times of 1.75 h to 2.5 h on H_2/CO_2 (Leigh et al. 1981). It can, therefore, be assumed that the Ech2 complex is not essential for autotrophic growth.

Although the wild type and mutant grew at the same growth rate on H_2/CO_2 the acetate production rates were different. The mutant produced 1.7 times more acetate in the exponential phase (Figure 12 B) as the wild type, and the final concentration of acetate was significantly ($P = 0.01$ [$P \leq 0.05$]) higher in the cultures of the Δ*ech2* strain. Experiments with resting cells showed that acetate production rate and final concentration were the same when a fixed amount of H_2/CO_2 was utilized (Figure 12). Minor variations in the concentration of acetate are probably due to the filling of the serum bottle with H_2/CO_2. In conclusion, the Δ*ech2* strain has a higher turnover rate of H_2 and CO_2 to maintain the same growth rate as the wild type, based on the production of acetate during growth and the higher final acetate concentration (Figure 12).

Different conversion rates of substrate to product and biomass were observed with *Escherichia coli* and *Pseudomonas taiwanensis*. *E. coli* has three terminal cytochrome oxidases that are relevant for establishing a proton gradient. A study by Bekker et al. (2009) showed that mutants of these three oxidases lead to a change in the metabolic flux regarding substrate-to-product ratio, depending on which oxidase is still present in the organism. They concluded that oxidases can be uncoupled from the respiratory chain, which leads to ATP being synthesized exclusively by substrate level phosphorylation and not additionally by electron transport phosphorylation (Bekker et al. 2009). This allows a flexible metabolic system capable of adjusting to different environmental conditions (Bekker et al. 2009). While *P. taiwanensis* possesses three NADH dehydrogenases (Ndh-1, Ndh-2 and Nuo), deletion of all three appears to result in non-viable cells. However, deletion of one or two of the NADH dehydrogenases resulted in phenotypes and metabolic turnovers that differ from or resemble the wild type depending which dehydrogenase was deleted (Nies et al. 2020). Deletion of the NADH dehydrogenase Ndh-1 and Ndh-2 leads to a biphasic growth pattern, whereas deletion of Nuo leads to overexpression of Ndh-2 but not Ndh-1, and a higher gluconate accumulation, while growth is similar to wild type (Nies et al. 2020). Therefore, a high metabolic flexibility is shown in this organism as well if one or two NADH dehydrogenase are missing (Nies et al. 2020). Both examples show that the loss of an energy-converting complex can be compensated for, suggesting that the loss of Ech2 could also be compensated for by the Ech1 complex or another enzyme that can oxidize H_2 and reduce ferredoxins.

Thus, in *P. taiwanensis* mutants, the deletion of dehydrogenases resulted in altered gene expression; however, this was not observed in the Δ*ech2* strain, the expression of *ech1A* (TKV_c01230) was the same compared to the wild type on both glucose and H_2/CO_2 (Table 13). Yet, different genes in the mutant changed in their expression. The genes *fhs* (formyl-tetrahydrofolate synthetase; TKV_c19930) and *hydB* (electron bifurcating hydrogenases; TKV_c19590) were less strongly expressed in the mutant on glucose than in the wild type. When comparing the conditions H_2/CO_2 (test) and glucose (calibrator), the mutant showed an upregulation above the threshold of 4-fold for both genes, while the wild type showed an upregulation but below the threshold (Table 13). This observation was supported by qPCR data regarding mixotrophic growth of the wild type. Both genes are downregulated on glucose (test) compared to H_2/CO_2 (calibrator) by −3 to −4-fold (Figure 32 and Table 27).

This suggests that both genes were less relevant for *T. kivui* when it grew on glucose than on H_2/CO_2, which seems to apply even more to the mutant. It could be hypothesized that the internal H_2 concentration is lower in the mutant due to the absence of the Ech2 complex. The lower H_2 concentration might lead to lower expression of *fhs* and *hydB,* as H_2-responsive signaling pathways have been shown to regulate gene expression of hydrogenases in *Ralstonia eutropha* (Lenz and Friedrich 1998; Schwartz et al. 2013). However, H_2-responsive signaling pathways have not been explored in *T. kivui* to date, making them a potential area of interest for future research. Additionally, the qPCR

analyses should be repeated, and a broader range of genes should be examined, with a particular focus on the expression of HDCR (e.g., formate dehydrogenase subunit FdhF; *fdhF* - TKV_c19990).

The higher turnover rate of H_2/CO_2 to acetate is, therefore, an indication of the uncoupling of catabolism from ATP synthesis. This indicates that the Δ*ech2* strain conserves energy less efficiently from H_2/CO_2 than the wild type but still produces enough ATP to support similar growth rates. Growth and acetate production on organic substrates remain unaffected, as ATP is primarily generated through substrate level phosphorylation (glycolysis) rather than through electron transport phosphorylation. The current model cannot easily explain these observations (Figure 3; Katsyv et al. 2021a). Further investigations are therefore required, in particular a proteomic study would be necessary, as the expression of *ech1A* has not changed, but the amount of Ech1 complex in the cell could be increased to compensate for the absence of the Ech2 complex.

4.2.2 Ferredoxin-dependent substrates

While the Δ*ech2* strain was not impaired in growth by the utilization of sugars or H_2/CO_2 (Table 34) and showed a higher acetate production on H_2/CO_2, these observations suggest that the mutant is able to maintain the redox balance without the Ech2 complex. Since sugars provide ATP, NADH and Fd_{red} via glycolysis, pyruvate was selected for further investigations as it is an intermediate of glycolysis that provides only reduced ferredoxin as a reducing agent and ATP if it is further converted to acetate (Furdui and Ragsdale 2000). *T. kivui* utilizes pyruvate by pyruvate oxidoreductases (PFOR). Two of those enzymes are annotated as *nifJ1* (PFOR1; TKV_c04340) and *nifJ2* (PFOR2; TKV_c21450), whereas *nifJ1* is about 100-fold higher expressed than *nifJ2* (Table A-4). Additionally, PFOR1 from *T. kivui* was purified and characterized, demonstrating pyruvate oxidation coupled with ferredoxin reduction. Consequently, it is regarded as the main PFOR in *T. kivui* (Katsyv et al. 2021b). PFORs oxidize pyruvate to acetyl-CoA and CO_2 while reducing Fd_{ox} to Fd_{red} or synthesize pyruvate for anabolic reactions using Fd_{red}, acetyl-CoA and CO_2. Acetyl-CoA is converted to acetate by a phosphotransacetylase (PTA) and an acetate kinase (ACK), generating ATP (Furdui and Ragsdale 2000; Sawers and Clark 2004; Katsyv et al. 2021b).

In addition to pyruvate, *T. kivui* is able to grow with CO, a second substrate depending on Fd as a sole electron carrier, as carbon and energy source. However, the organism must first be adapted to CO (Weghoff and Müller 2016). CO is utilized by two CO dehydrogenases, which are annotated in *T. kivui*, as a monofunctional carbon monoxide dehydrogenase (CooS; TKV_c08080) and a CO dehydrogenase (CODH; TKV_c19820) forming a complex with an acetyl-CoA synthase (CODH/ACS) (Jain et al. 2021). CooS has been shown to be responsible for CO oxidation and ferredoxin reduction (Jain et al. 2021), while the CODH/ACS complex the key enzyme of the WLP that links the methyl branch to the carbonyl branch. While the CODH reduces CO_2 to CO by oxidizing Fd_{red}, the resulting CO is merged by the ACS with the methyl group of the carbonyl branch to form acetyl-CoA. (Ragsdale and Kumar 1996; Ragsdale and Pierce 2008).

Thus, the utilization of pyruvate or CO provides only reduced ferredoxin as an electron carrier (Figure 3). Assuming that the Ech2 complex mainly converts Fd_{red} to H_2 and Ech1 forms a complex with MetFV as previously hypothesized, the function of providing H_2 for the reduction of $NADP^+$ to NADPH by the electron bifurcating hydrogenase (HydABC) could be essential for WLP (Jain et al. 2020; Katsyv et al. 2021a). Therefore, the loss of the Ech2 complex might lead to a redox imbalance and thus to an impairment or inhibition of growth with Fd-dependent substrates if the loss of the Ech2 complex cannot be compensated for.

First transfer experiments from cultures grown on glucose to pyruvate showed that the Δ*ech2* strain could not grow immediately with pyruvate as substrate, whereas the wild-type strain DSM 2030 did. Yet, adaptation of the Δ*ech2* strain to pyruvate was possible, and growth was observed after more than 48 hours of incubation (Figure 14). In comparison, *ech* deletion in of *M. barkeri* and *M. mazei* resulted in the inability to grow on acetate (Meuer et al. 2002; Welte et al. 2010b). Acetate in both organisms provide Fd_{red} through the acetyl-CoA decarbonylase/synthetase, which is used for energy conservation via the electron transport chain involving Ech. Since *M. barkeri* and *M. mazei* only contain one Ech complex, its deletion leads to the complete shutdown of the energy conservation via proton translocation and therefore also of ATP synthesis (Meuer et al. 2002; Welte et al. 2010a; Welte et al. 2010b).

Pyruvate conversion to acetate via PFOR, PTA and ACK provide ATP, which may enable the *T. kivui* Δ*ech2* strain to maintain sufficient energy to sustain cell activity and redox balance. This may give the mutant enough time to adapt to pyruvate through altered gene expression. Alternatively, a subpopulation with beneficial mutations in the genome might be selected over time. The fact that the mutant eventually grew on pyruvate and showed a similar growth rate as the wild type after multiple passages (Table 34) suggests that the Ech2 complex in the pyruvate metabolism of *T. kivui* might be compensated by the activity of other Fd-dependent enzymes.

The ability to metabolize pyruvate was also reflected in resting cells of the mutant, which utilized pyruvate without adaptation. Interestingly, pyruvate was consumed at the same rate in the mutant and wild type ($P = 0.17$; $P \leq 0.05$), but production rates are significantly lower in the mutant by 1.62-fold ($P = 0.0004$; $P \leq 0.05$) for acetate and by 1.87-fold ($P = 0.0004$; $P \leq 0.05$) for formate. Furthermore, the wild type produced 1.02 mol pyruvate per 1 mol acetate in the resting cell experiment (Figure 15) and when grown on defined medium, 1.00 mol pyruvate per 1 mol acetate (Figure 30), while a previous study showed that 0.93 mM pyruvate is required for 1 mol acetate (Leigh et al. 1981). According to the metabolic model, theoretically, only 0.8 mol of pyruvate would be required to produce 1 mol of acetate (Figure 3 C). Therefore, *T. kivui* showed, in general, an incomplete carbon and electron balance during pyruvate conversion, probably due to unidentified products and in part, the observed increase in protein concentration (Figure 15). Nevertheless, the mutant requires 1.23 mol of pyruvate per 1 mol of acetate, i.e. 20 % more than the wild type, indicating an additional loss of carbon or less efficient energy conservation. Since pyruvate was consumed at the same rate by the wild type and the Δ*ech2* strain, sufficient Fd_{ox} must be available to allow the constant oxidation of pyruvate by the PFOR so that the re-oxidation of Fd_{red} cannot be impaired, which could mean that enzymes other than the Ech2 complex re-oxidize Fd_{red} in the mutant.

While the lower acetate production in the Δ*ech2* strain indicates impaired metabolism, inhibition of phosphotransacetylase (TKV_c13970) and acetate kinase (TKV_c13960) is unlikely, as ferredoxin is not required for the conversion of acetyl-CoA to acetate. Therefore, the WLP might be impaired, which could explain the reduced formate production leading to lower acetate production (Figure 15). The enzyme responsible for formate production is the HDCR (Jain et al. 2020), which reduces CO_2 to formate by oxidizing H_2. A model by Schuchmann and Müller (2013) of the HDCR of *A. woodii* assumes that Fd_{red} or H_2 are oxidized to reduce CO_2 to formate. Since the process from formate to H_2 is reversible, a direct electron transfer from Fd_{red} to H^+ or H_2 to Fd_{ox} could also be possible (Schuchmann and Müller 2013; Lemaire et al. 2020). This cannot be proven with certainty, but the reduced formate production in the Δ*ech2* strain suggests that the HDCR may be involved in other biochemical reactions, such as the reduction of 2 H^+ to H_2 by the oxidation of Fd_{red}, in the absence of the Ech2 complex.

Furthermore, as mentioned, *T. kivui* is able to grow on CO through adaptation (Weghoff and Müller 2016). The same adaptation experiments were performed with the Δ*ech2* strain and an non-adapted wild type strain (DSM 2030). For adaptation, both strains were first adapted to a gas mixture containing H_2, CO_2, and CO in a ratio of 44/22/33; both strains grow on this gas mixture, with the mutant growing faster than the wild type but much slower than on H_2/CO_2 (Table 34). The slower growth is probably the consequence of inhibition of [FeFe]- and [NiFe]-hydrogenases though CO (Goldet et al. 2009; Baffert et al. 2011; Matsumoto et al. 2011).

Surprisingly, the mutant grew faster than the wild type on the gas mixture (Table 34), as if it had been less affected by CO. This suggests that Ech2 is involved in CO metabolism and that loss of the Ech2 complex leads to tolerance to CO. Subsequently, both strains were transferred to CO/N_2 atmosphere ($3x10^5$ Pa;14/86; v/v) and incubated for several days, the wild type showed growth in the first and second passage but the Δ*ech2* strain did not (Figure 17). Resting cell experiments were performed with the wild type DSM 2030, the newly isolated CO-adapted wild type and the Δ*ech2* strain in a CO/N_2 or a $H_2/CO_2/CO$ atmosphere (Figure 18), confirming that the Δ*ech2* strain could not utilize CO, while the other strains could, as previously reported for the Δ*ech2* strain by Schwarz et al. (2020).

Of significance, the CO-adapted wild type did not produce as much acetate on $H_2/CO_2/CO$ as the wild type or the Δ*ech2* strain, suggesting that the CO-adapted wild type was no longer able to utilize H_2 at high rates. While the mutant tolerated CO in the atmosphere and utilized only H_2/CO_2, the unadapted wild type was inhibited by CO, resulting in lower acetate production compared to the mutant (Figure 18; B), supporting the assumption of CO tolerance upon loss of Ech2. Based on the data shown, it can be assumed that the Ech2 complex has an important role in CO metabolism. To prove this hypotheses, H_2, CO_2 and CO concentrations should be monitored in the resting cell experiment and in the growth experiment, and gene expression should be investigated to determine whether there are significant differences in gene expression between the two strains.

The impaired growth of the mutant when utilizing pyruvate and CO, as well as the experiments with resting cells, clearly show that the Ech2 complex is involved in ferredoxin metabolism in some way, leading to two theories about how *T. kivui* may or may not compensate for the loss of the Ech2 complex.

4.2.3 Two theories

The current metabolic model of *T. kivui* (Katsyv et al. 2021a) only partially explains the observations made in this study. According to the model, one of the Ech's forms a complex with the MetFV complex oxidized Fd_{red} to reduce methylene-THF to methyl-THF, while protons are translocated across the membrane. Thus, it is part of the Wood-Ljungdahl pathway, which leads to the assumption of the indispensability of this Ech. While the same, the other or both Ech´s oxidizes H_2 or Fd_{red} to reduce Fd_{ox} or 2 H^+ translocating protons across the membrane, consuming or generating a proton gradient, depending on the substrate utilized (Figure 3; Katsyv et al. 2021a; Öppinger et al. 2022). Regarding the functionality of the Ech complexes, it has recently been shown that the Ech2 complex is able to transport protons across the membrane by oxidizing Fd_{red} and reducing 2 H+ to H_2, but this has not yet been demonstrated for the Ech1 complex (Katsyv and Müller 2022). Although a ferredoxin dependence of the MetFV complex has been demonstrated, the formation of the Ech-MetFV complex is only an assumption that has yet to be proven (Katsyv et al. 2021a; Öppinger et al. 2022). Thus, it was biochemically confirmed that Ech2 has the described function, yet the loss of Ech2 did not result in impairment of growth on sugars or H_2/CO_2. Therefore, Ech2 is either not essential under these conditions, or its loss can be compensated for.

Given that *T. kivui* possesses two Ech complexes, it is plausible that Ech1 could replace Ech2 or serve as the primary Ech complex responsible for maintaining redox balance and proton translocation in *T. kivui*. This implies that Ech1 might be bifunctional within the cell and potentially be part of the proposed Ech-MetFV complex to generate a proton gradient while also functioning independently to enable electron transfer between H_2 and Fd_{ox} or Fd_{red} and 2 H^+. Consequently, Ech1 could be essential for *T. kivui*, and its deletion could have similar effects on the organism as observed in *M. barkeri* (Meuer et al. 2002). The greater importance of Ech1 over Ech2 is indicated by the 10-fold higher expression of *ech1A* (TKV_c01230) compared to *ech2A* (TKV_c19720) during growth on glucose (Table A-5). The fact that it has not yet been possible to delete the ech1 gene cluster using established methods underlines its critical role in the metabolism of *T. kivui*.

This theory is supported by a promoter exchange study by Zeldes et al. 2024; parts of this work were carried out in this study. Since deletion of *ech1* was not possible, an attempt was made to generate knockdown mutants in which the *ech1* promoter was replaced with a fructose promoter, resulting in two new strains P_{frc}*ech1* and P_{frc}*ech1*Δ*ech2*. The inserted fructose promoter should enable the targeted expression of the *ech1* operon so that the expression of the *ech1* genes can be switched off when the new strains are grown on substrates other than fructose.

Unexpectedly, the mutant strains only grew slightly slower on glucose than on fructose (Table 34). Still, the *ech1A* expression in the P_{frc}*ech1* mutant was significantly downregulated by −11.5-fold and in the P_{frc}*ech1*Δ*ech2* strain by −5.4-fold compared to the wild type grown on glucose (Table 15). Although *fruk* expression was slightly upregulated in the mutants on glucose, it remained below the 4-fold threshold. The fructose promoter (P_{frc}) used in this study, therefore, only leads to downregulation and not to a knockdown of the *ech1* genes, which in turn enables growth similar to that of the wild type, even if the mutants grew 15-20 % slower on glucose (Table 34).

According to the transcriptome analysis data (Table A-4; Table A-8) of the wild type grown on glucose, the *fruK* gene (1-phosphofructokinase; TKV_c23150) showed minimal expression with approximately 10 mRNA reads, in contrast to 1552 reads for the *glcK* gene (glucokinase; TKV_c00920). Assuming that the qPCR represents the same expression level of the *fruK* gene for the wild type as the RNA sequencing data, a slight upregulation of the *fruK* gene can be observed in the mutants on glucose. This suggests that *fruK* is also expressed in the absence of fructose, which could also result in the expression of *ech1A* (Figure 21; Table 15). The promoter P_{frc} is, therefore, not sufficient to completely suppress the expression of *ech1*. Another reason for the expression of *fruK* could be that fructose was present in the cell as a naturally occurring sugar. It cannot be ruled out that small amounts of fructose were present as an intermediate product of glycolysis in the form of fructose-6-phosphate or fructose-1,6-bisphosphate in the cell, which may have led to the expression of *fruK* and *ech1A* in the mutants, but this is not indicated by the expression of *fruK* in the wild type. Since the fructose promoter used was not suitable for the generation of a knockdown mutant, a different promoter system should be used, which is induced by a less common or artificial substrate. For example, a mannitol promoter system studied by Zeldes et al. (2024) in place of the Ech1 promoter showed a promising phenotype, but no clear downregulation of *ech1A* was observed. With regard to promoter systems for knockdown applications, further research is needed to find promoter systems to downregulate potentially important genes to the point where a clear phenotype can be described.

Nevertheless, different phenotypes were observed during growth on pyruvate for the Δ*ech2*, the P_{frc}*ech1*Δ*ech2* and partially for the P_{frc}*ech1* mutant. The Δ*ech2* strain, as mentioned earlier, showed a long adaptation time of over 48 hours to pyruvate, whereas the P_{frc}*ech1*Δ*ech2* strain showed no

significant growth throughout the experiment (Figure 22). The P_{frc}*ech1* mutant grew on pyruvate but only to half of the final OD_{600} of the wild type. Therefore, all mutants show clear signs of impaired pyruvate utilization. Since the PFOR (*nifJ1*, pyruvate-flavodoxin oxidoreductase) oxidizes pyruvate to acetyl-CoA, CO_2, and Fd_{red}, the re-oxidation of Fd_{red} could be the cause of the described phenotypes in all mutants. In *T. kivui*, four genes are annotated as potential ferredoxins (Hess et al. 2014; Katsyv et al. 2023a) but only TKV_c16450 (*fd1*) and TKV_c09620 are reduced by the PFOR1 (Katsyv et al. 2023a). MetFV and Ech2 showed enzyme activity with both ferredoxins, with Ech2 showing slightly higher activity with TKV_c09620. However, this has not yet been proven for Ech1 (Katsyv et al. 2023a).

The Δ*ech2* strain required adaption to grow on pyruvate, and P_{frc}*ech1*Δ*ech2* did not grow, while P_{frc}*ech1* showed a reduced final OD_{600}, suggesting that both Ech´s are important for the pyruvate metabolism and, consequently, for the re-oxidation of reduced ferredoxin. These observations support the hypothesis that Ech1 may compensate for the loss of Ech2. The downregulation of *ech1* genes in response to pyruvate could be more distinct in the P_{frc}*ech1* mutants, since fructose-6-phosphate or fructose-1,6-bisphosphate, are not produced as intermediates during pyruvate utilization

Thus, Ech2 might re-oxidize Fd_{red} in P_{frc}*ech1*, which only resulted in a lower OD_{600}, while P_{frc}*ech1*Δ*ech2* was unable to compensate for the downregulation of Ech1. Further experiments should be conducted to determine if the mutants adapt to pyruvate in a manner similar to the Δech2 strain. The pyruvate consumption along with acetate and formate production should be determined as these analyses could help identify potential metabolic bottlenecks.

A conservative interpretation of the results is that Ech1 might replace Ech2 and simultaneously form the assumed Ech1-MetFV, suggesting a bifunctionality of Ech1 in *T. kivui*. However, it can be assumed that the formation of the Ech-MetFV complex occurs with the Ech1 complex, since the mutant and the wild type produce the same acetate concentrations on glucose, which would not be the case if the WLP were restricted.

Recent unpublished findings from a purified tagged Ech1 complex suggest that Ech1 does not utilize reduced ferredoxins or other natural reducing agents (personal communication Prof. Dr. Müller, Johann Wolfgang Goethe University Frankfurt am Main). These results imply that the Ech1 complex alone would be insufficient to replace Ech2 unless it forms a complex with another enzyme that provides the necessary binding sites for the oxidation and reduction of ferredoxins and H_2/2 H^+, enabling energy conservation with the Ech1 complex.

Another enzyme is evidently the more promising replacement candidate for the Ech2 complex than the Ech1 complex. The HDCR of *T. kivui* was found to be a hexamer protein complex consisting of six subunits one formate dehydrogenase (FdhF), two hydrogenases (HydA2) connected to three iron–sulfur proteins two HycB4 and one HycB3 (Dietrich et al. 2022). These hexamers form long oligomeric filaments with HycB4 and HycB3 as central connection between the hexamers. It was also found that the filament structure is membrane-associated (Dietrich et al. 2022; Dietrich and Müller 2023). While a complete deletion of HDCR resulted in a strain that required formate as an additional electron acceptor (Jain et al. 2020).

Mutant strains of the HDCR of *T. kivui* were still able to grow on glucose after the deletion of the subunits HycB4, HydA2 or both. Deletion of HycB4, HydA2 and HycB3 led to inhibition of growth on glucose (Dietrich and Müller 2023). Furthermore, enzyme assays with His-tag HDCR variants in which HydA2 or HydA2 and HycB4 were deleted showed enzyme activity when reduced ferredoxin was present (Dietrich and Müller 2023). The HDCR, therefore, not only oxidizes H_2 to reduce CO_2 to formate but is able to

oxidize reduced ferredoxin. Moreover, a model by Schuchmann and Müller (2013) of the HDCR of *A. woodii* assumes that Fd_{red} or H_2 are oxidized to reduce CO_2 to formate. Since the reaction of formate to H_2 is reversible, a direct electron transfer from Fd_{red} to H^+ or H_2 to Fd_{ox} could be possible (Schuchmann and Müller 2013; Lemaire et al. 2020).

It is therefore plausible that the HCDR of *T. kivui* could mediate electron transfer between H_2 and ferredoxins. The redox potentials of the ferredoxins TKV_c09620 and TKV_c16450 (Em = −386 mV; Katsyv et al. 2023a) and H^+/H_2 ($E^{\circ\prime}$ = −414 mV; Thauer et al. 1977) are close enough to suggest that energy-neutral electron transfer might be possible. However, these redox potentials can shift due to environmental factors such as temperature, pH, or concentration (Pueyo et al. 1991; Petersen et al. 2023). As a result, the actual redox potential within a living cell could differ more than initially anticipated. Nevertheless, it is assumed that the Ech complexes for the reduction of ferredoxins requires the oxidation of H_2 and an additional driving force such as a transmembrane electrochemical ion gradient generate and consumed by the Ech complexes (Schoelmerich and Müller 2019).

The fact that the HDCR is membrane-associated suggest that the reduction of ferredoxin could also be driven by membrane gradient, although the required membrane-spanning motif has not yet been demonstrated to be part of the HDCR complex. In addition, the filament structure contains several [4Fe4S]-clusters that enable electron flow between the subunits (Dietrich et al. 2022). These could serve as an electron store allowing an electron potential to be established that enables the reduction of ferredoxins by the oxidation of H_2 without the required proton translocation by an Ech complexes.

In addition, the observed higher acetate production of the mutant during growth on H_2/CO_2 may be due to the thermodynamically unfavorable reduction of ferredoxins by the oxidation of H_2. Ech and Rnf complexes require an additional driving force such as a transmembrane electrochemical ion gradient, for the reduction of ferredoxins (Schoelmerich and Müller 2019; Rosenbaum et al. 2021). Therefore, another driving force could enable the thermodynamic shift (Abu and Woodley 2015) towards the reduction of ferredoxins by increasing the internal concentration of H_2.

Since cultivation with H_2/CO_2 involves high concentrations of H_2, this could potentially drive ferredoxin reduction when multiple H_2 molecules are oxidized to reduce one ferredoxin. If this is the case, this would support the assumption of an uncoupled catabolism in the mutant, which likely leads to increased acetate formation per biomass due to the higher electron and metabolic flux.

Furthermore, SNP analyses showed that CO-adapted *T. kivui* strains have a mutation in the *hycB3* gene which results in disruption of the oligomeric filament structure of HDCR. The disruption is the consequence of a frameshift at the codons 164 and 168 of the *hycB3* gene, leading to single hetero-hexametric subunits of HDCR (Baum et al. 2024). Therefore, the adaptation of *T. kivui* to CO probably results in the HDCR being fragmented and no longer membrane-associated, which excludes a potential proton translocation across the membrane via the HDCR. The theoretical establishment of an electron potential in the filamentous HDCR complex is also less likely due to fragmentation, as fewer [4Fe4S] clusters would be present in the overall structure of the individual HDCR complexes. Moreover, adaptation studies with *A. woodii* on CO showed that mutations also occurred in the HycB2 subunit of the HDCR, which could potentially enable growth on CO and result in a similar hypothesized structural change of the HDCR as in *T. kivui* (Moon et al. 2024).

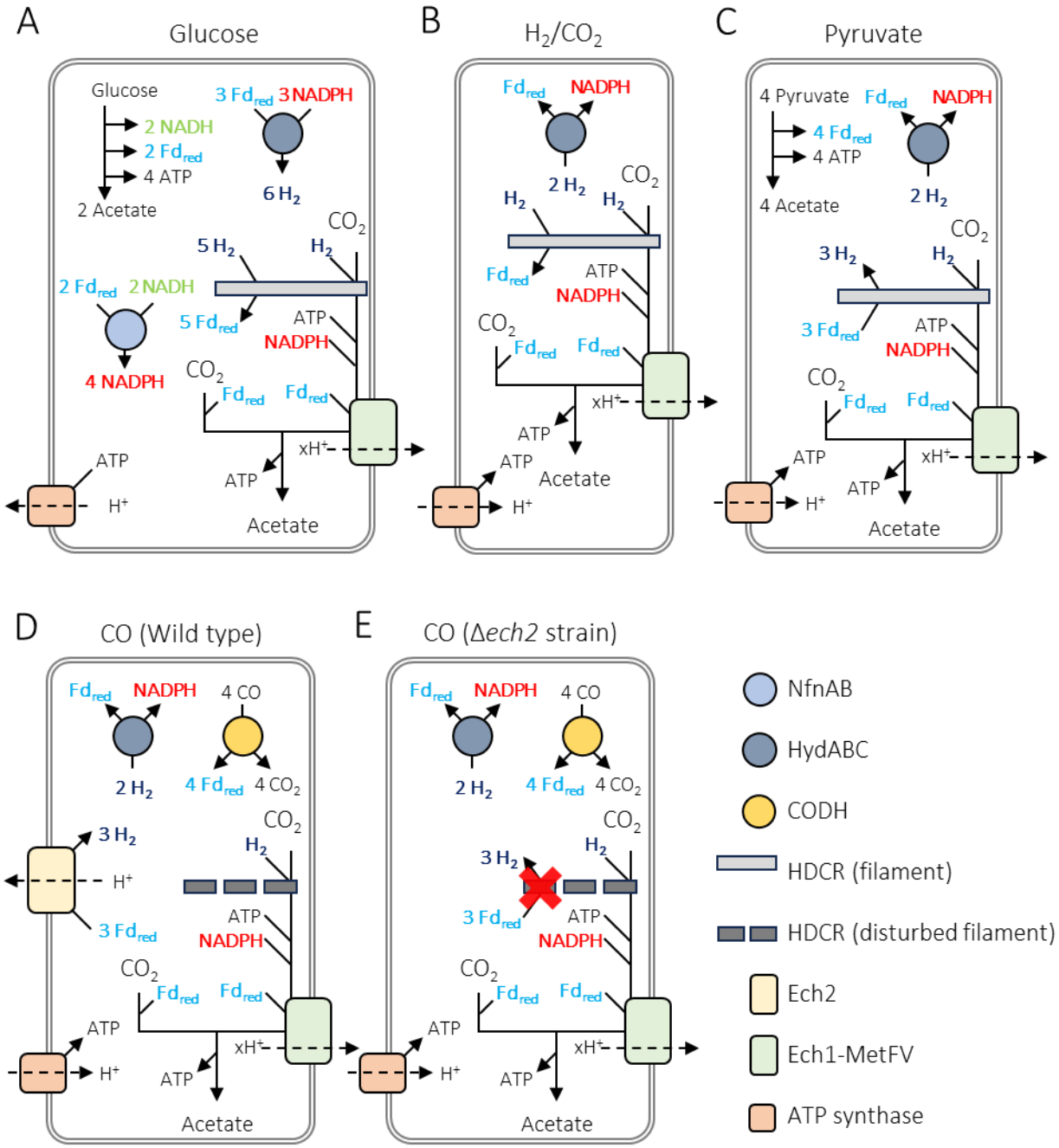

Figure 42 Proposed metabolic pathway of the Δ*ech2* strain of *T. kivui* (Baum et al. 2024).
Shown is the utilization of glucose (A), H_2/CO_2 (B), pyruvate (C) and the proposed CO utilization of the *T. kivui* CO adapted wild type strain (DSM 2030) and the inability of the Δ*ech2* strain to utilize CO. Depicted are enzymes involved in the redox metabolism; an electron bifurcating transhydrogenase (NfnAB; light blue), an electron bifurcating hydrogenase (HydABC; blue-gray), a carbon monoxide dehydrogenase (CODH; yellow), two energy converting hydrogenases (Ech2; light yellow and Ech1-MetFV; light green), an ATP synthase (light orange) and a hydrogen dependent carbon dioxide reductase (HDCR) in two structural forms for *T. kivui* wild type DSM 2030 (filament; light gray) and the CO adapted wild type strain (disrupted filament; dark gray), in which the HDCR HycB3 fragmentation likely disables the Fd_{red} oxidation and consequently growth on CO.

Therefore, the frame shift in the *hycB3* gene may have altered the protein structure such that HycB3 can no longer reduce or oxidize ferredoxins, which would make the HDCR unable to compensate for the loss of the Ech2 complex, making the Ech2 complex essential in CO-adapted *T. kivui* strains. The

structural change of HycB3 has yet to be proven and a His-tag HDCR of an CO adapted *T. kivui* strain could clarify whether the HycB3 is still able to oxidize or reduce ferredoxins.

Consequently, the HDCR is a promising compensator for Fd_{red} oxidation in the Δ*ech2* strain due to the demonstrated ability for ferredoxin oxidation (Dietrich and Müller 2023), the observed frameshift in *hycB3* in all *T. kivui* strains analyzed, and the observed inability to adapt the mutant to CO when Ech2 is absent in *T. kivui* (Baum et al. 2024). Based on the findings of this study (Baum et al. 2024; Zeldes et al. 2024), a different metabolic model was developed for the Δ*ech2* strain to take into account all the findings of both studies (Figure 43).

I propose the following model (Figure 43) for the metabolism of glucose, H_2/CO_2, pyruvate, and CO in the Δ*ech2* strain. In this model, the HDCR replaces the Ech2 complex following its deletion, while Ech1 interacts with MetFV and forms the Ech-MetFV complex, enabling proton translocation to generate a proton motive force.

The main difference compared to the previous models (Katsyv et al. 2021a), in the Δ*ech2* strain no protons are translocated through the HDCR, suggesting that the ATP yield could be higher when utilizing glucose or H_2/CO_2 (Figure 43, A and B) compared to wild type. Yet on pyruvate, the ATP yield could be lower (Figure 43, C), as no protons are translocated through the Ech2 complex inside or outside the cell.

Since it is unclear how many protons are translocated through the assumed Ech1-MetFV, the final ATP yield cannot be predicted, but it can be said that the loss of Ech2 does not lead to a growth deficit on glucose, fructose or mannitol. While pyruvate required adaptation. Yet, it is unclear why the mutant requires adaptation to pyruvate, as ATP and Fd_{red} are generated during the utilization of pyruvate, which should allow the reduction of H^+ to H_2 by the HDCR.

Contradicting the proposed model is the mutant higher acetate to biomass ratio when growing on H_2/CO_2, suggesting less efficient energy conservation and potential uncoupling of the catabolism compared to the wild type. Furthermore, the SNP analyses has been shown that the HDCRs of CO-adapted *T. kivui* strains are subject to fragmentation and structural change (Baum et al. 2024). This ultimately means that the Ech2 complex is irreplaceable for growth on CO as it cannot be replaced by the HDCR.

4.3 Redox balancing by the NfnAB complex

Electron bifurcation allows microorganisms to bypass thermodynamic obstacles by simultaneously coupling an exergonic and an endergonic redox reaction and thereby is part of the energy conservation by reducing the loss of energy (Peters et al. 2016). Several bifurcating enzymes are known, two of these are the electron bifurcating hydrogenase HydABC and the transhydrogenase NfnAB (Peters et al. 2016; Buckel and Thauer 2013). The electron bifurcating hydrogenase HydABC catalyzes the reduction of Fd_{ox} and $NADP^+$ through the oxidation of H_2 in *T. kivui*. In contrast, the transhydrogenase complex NfnAB catalyzes is thought to be required for the reversible reduction of ferredoxin and NAD^+ through the oxidation of 2 NADPH and vice versa (Demmer et al. 2015; Katsyv et al. 2023b).

The current metabolic model of *T. kivui* growing on glucose (Figure 3) includes both the HydABC complex and the NfnAB complex, while NfnAB is not considered to be involved if *T. kivui* grows on H_2/CO_2, CO or pyruvate (Figure 3). Theoretically, the deletion of *nfnB* should specifically impact the catabolism of glucose and other organic substrates that provide NADH. This is due depiction of NfnAB as the main enzyme involved in the re-oxidation of NADH in the current metabolic models of *T. kivui* (Katsyv et al. 2021a; Öppinger et al. 2022; Baum et al. 2024).

The *nfnB* mutant is capable of growing on glucose. However, its growth rate was nearly twice as slow as the growth rate of the wild type on glucose. The same trend was observed for growth on pyruvate (Table 35). Additionally, the mutant had a lower final OD_{600} for each substrate tested than the wild type (Table 35). To be more specific, the final OD_{600} was around 30 % lower on glucose and 23 % lower on pyruvate compared to the wild type (Figure 36, Table 35).

These observations indicate that the NfnAB complex is not essential for the growth on glucose or on pyruvate. Still, an impairment of growth cannot be denied when *nfnB* was deleted, suggesting a redox imbalance or a metabolic bottleneck.

Table 35 Summary of doubling time and final OD_{600} of the wild type strain DSM 2030 and the *nfnB* mutant. Both strains grew on defined medium containing glucose, fructose, mannitol or pyruvate (Figure 35; Figure 36).

Substrate	Wild type		*nfnB* mutant	
	Doubling time (h)	Final OD_{600}	Doubling time (h)	Final OD_{600}
Glucose	1.57 ± 0.01	1.58 ± 0.02	3.26 ± 0.27 (2.12 ± 0.14)	0.93 ± 0.02 (1.11 ± 0.08)
Fructose	1.51 ± 0.03	1.57 ± 0.03	2.79 ± 0.11	0.79 ± 0.04
Mannitol	2.01 ± 0.17	1.17 ± 0.02	2.94 ± 0.10	0.75 ± 0.01
Pyruvate	1.98 ± 0.02	0.93 ± 0.02	4.13 ± 0.25	0.72 ± 0.06

Remarkably, the *nfnB* mutant had a slightly higher glucose consumption rate than the wild type, although the mutant grew slower on glucose. Furthermore, the strains had different conversion rates of glucose to acetate during growth. The mutant only produced 1.21 mol acetate per 1 mol glucose, while the wild type produced 2.55 acetate per 1 mol glucose during growth but the final acetate concentration was around 1.6 mol acetate per 1 mol glucose for both strains on defined medium (Table 36). In contrast, pyruvate utilization was similar in both strains. The mutant had a slightly lower consumption rate of pyruvate than the wild type, probably due to the lower growth rate. Still, the conversion rate of pyruvate to acetate was 1 to 1 in both strains during growth and the final acetate yield per pyruvate was also 1 to 1 (Table 36). Furthermore, resting cells of the mutant could not fully utilize glucose, only 2.08 mM glucose was converted to 5.56 mM acetate over a duration of 72 hours, while pyruvate was completely consumed during this time (Figure 37).

These observations suggest that a metabolic bottleneck occurs during glucose oxidation via glycolysis. Glucose is oxidized to 2 pyruvates, yielding 2 ATP and 2 NADH, and subsequently, the 2 pyruvates are oxidized to 2 acetates, yielding 2 ATP and 2 Fd_{red} (Fuchs 2017). Therefore, only the redox carriers NADH and Fd_{red} are introduced into the metabolic system, which might accumulate, resulting in the observed phenotypes.

Yet, only glucose to acetate conversion was affected by the deletion of *nfnB* and not pyruvate to acetate, which strongly suggests that the deletion of *nfnB* impairs the re-oxidation of NADH produced by the glyceraldehyde-3-phosphate dehydrogenase, affecting the overall redox balance in growing and resting cells, which even leads to a stop of glucose utilization in resting cells.

Table 36 Glucose and formate consumption and acetate production of the *T. kivui* wild type strain (DSM 2030) and the *nfnB* mutant.

The production (pro.) and consumption (con.) rates were determined for both the wild type and the *nfnB* mutant on glucose and pyruvate (Figure 29; Figure 30; Figure 38; Figure 40). The acetate (pro.) to glucose (con.; pyruvate) ratio represents the rate during growth, while the final acetate-to-glucose (pyruvate) ratio is the acetate yield after all glucose (pyruvate) has been consumed.

Consumption and production (mM/h)		
Substrate	Wild type	*nfnB* mutant
Glucose (con.)	−3.46	−3.81
Acetate (pro.)	8.83	4.62
Acetate (pro.) to glucose (con.) ratio	2.55	1.21
final acetate-to-glucose ratio	1.57	1.67
Pyruvate (con.)	−9.95	−7.49
Acetate (pro.)	9.46	7.45
Acetate (pro.) to pyruvate (con.) ratio	0.95	0.99
final acetate-to-pyruvate ratio	1.00	0.98

Deletion of the NfnAB complex led to a change in the NADH/NAD^+ ratio, as previously demonstrated for the *nfnAB* mutant of *Thermoanaerobacterium aotearoense* (Li et al. 2019). After 6 hours of incubation with glucose, the mutant had about 21.9 % more NADH than the wild type in the cell, but over time, the NADH/NAD^+ ratio of the mutant converged to that of the wild type. Consequently, a shift of NADH/NAD^+ ratio may also be possible for the *nfnB* mutant of *T. kivui* while utilizing glucose.

Thus, growing cells can probably re-oxidize NADH with an unidentified NADH-dependent enzyme. Several NADH-dependent enzymes are annotated in *T. kivui* (Table A-7; Hess et al. 2014), which are thought to be involved in amino acid and lipid synthesis, potentially enabling re-oxidation of NADH only during growth. For further insight, proteomics analyses should be conducted to evaluate which NADH-depend enzyme could possibly compensate for the loss of NfnAB.

In addition, similar observations were made with *nfnAB* mutants of *Thermoanaerobacterium saccharolyticum*. A reduced growth rate was observed in the two *nfnAB* mutants of *T. saccharolyticum* compared to the wild type and all mutants lost NADPH-linked ferredoxin oxidoreductase activity in cell extracts (Lo et al. 2015). Confirming the loss of the NfnAB complex, one mutant (LL1144) showed no change in ethanol yield, while the other (LL1220) showed a reduced yield when gowning on cellobiose and yeast extract (Lo et al. 2015). Biochemical analyses showed that an NADPH-linked alcohol dehydrogenase was active in LL1220, whereas an NADH-linked alcohol dehydrogenase was active in LL1144. Therefore, they concluded that an undefined NADH:ferredoxin oxidoreductase was involved in providing NADH to reduce acetyl-CoA to ethanol (Lo et al. 2015; Leavitt et al. 2017).

It is therefore plausible that the growth of *T. kivui* was affected by the deletion of *nfnB*, but not the acetate final concentration, as the WLP requires NADPH for the reduction of methenyl-THF to methylene-THF by the methylene-THF dehydrogenase. Thus, *T. kivui* had to generate NADPH to allow acetate production similar to the wild type in a defined medium containing glucose. Although acetate production did not reach the theoretical yield of 3 acetate per glucose, there should still be observable differences when the WLP was impaired. Nevertheless, the mutant and wild type had the same final ratio of acetate per glucose (Table 36). Thus, it can be assumed that HydABC supplies the necessary NADPH. This would imply that H_2 needs to be provided, which, based on the current metabolic model for glucose (Figure 3 A), would have to be generated by HydABC itself or the Ech complexes.

Based on these observations, I propose a model of glucose utilization for the *nfnB* mutant (Figure 43), Ech2 provides H_2, while HydABC reduces $NADP^+$ to NADPH and thus enables the reduction of methenyl-THF in the WLP. Although the proposed model for the *nfnB* mutant (Figure 43 B) includes an unidentified enzyme, its inclusion is necessary since NADH would not be re-oxidized without it. This helps to visualize and explain the observed conversion ratio of glucose to acetate during growth and the findings from the resting cell experiments.

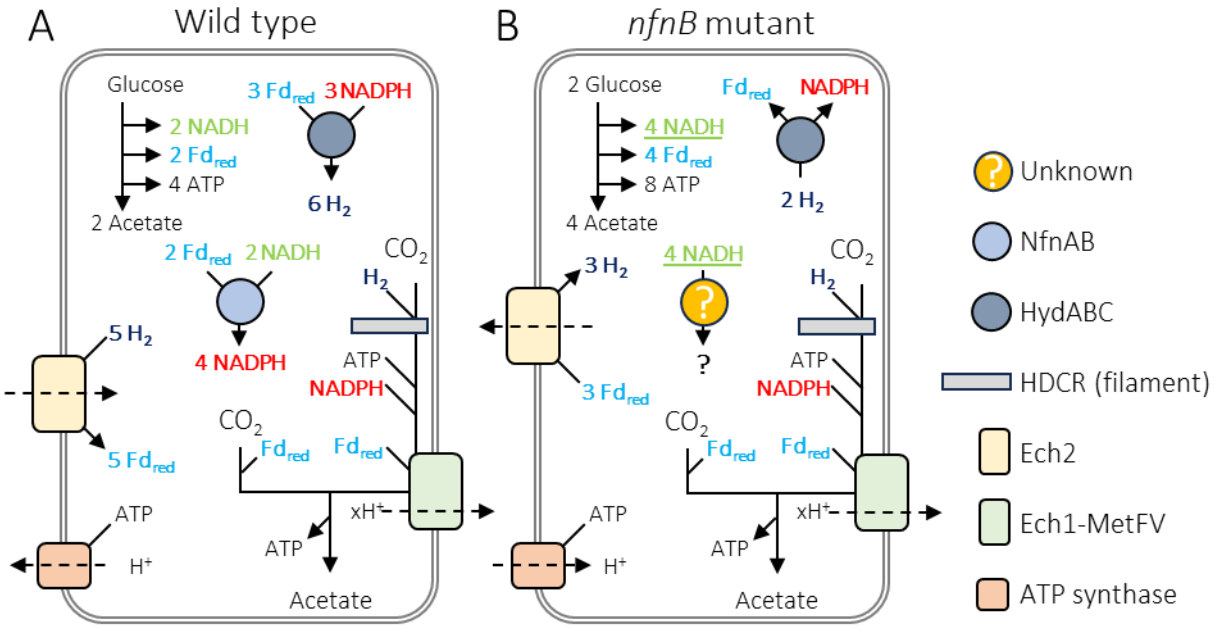

Figure 43 Proposed metabolic pathway for glucose utilization of the *nfnB* mutant of *T. kivui*.
Shown are the metabolic pathways for the utilization of glucose of the wild type (A) and the *nfnB* mutant (B). Depicted are enzymes involved in the redox metabolism; an electron bifurcating transhydrogenase (NfnAB; light blue), an electron bifurcating hydrogenase (HydABC; blue-gray), two energy converting hydrogenases (Ech2; light yellow and Ech1-MetFV; light green), an ATP synthase (light orange), a hydrogen dependent carbon dioxide reductase (HDCR; light gray) and an unknown enzyme re-oxidizing NADH to NAD^+(orange).

Furthermore, conducted qPCR analyses of cells grown on glucose only showed slight upregulation of *ech2D* (Ech2) and *hydB* (HydABC); these changes were above 2-fold, yet below the threshold of 4-fold while *2OxFOR* (TKV_c19280) was the only gene significantly upregulated compared to the wild type (Table 32). The 2OxFOR is encoded by the gene cluster TKV_c19260 to TKV_c19290 (Hess et al. 2014) and belongs to the 2-oxoglutarate:ferredoxin oxidoreductase (OFOR) enzyme family, which also includes pyruvate:ferredoxin oxidoreductase (PFOR; Gibson et al. 2016). Since the function of 2OxFOR in *T. kivui* has not yet been demonstrated, it can only be assumed that it may catalyze the oxidation of pyruvate to acetyl-CoA or the conversion of 2-oxoglutarate and succinyl-CoA (Katsyv et al. 2021b). Nevertheless, it can be assumed that the oxidation and reduction of ferredoxins take place in both cases (Gibson et al. 2016).

Strikingly, on pyruvate, most genes in the mutant, compared to the wild type, were upregulated by more than 3-fold but still below the 4-fold threshold, whereas *nifJ1* (PFOR1) was upregulated 10-fold (Table 33). This was surprising as *nifJ1* is, as mentioned, to be considered the main PFOR and was expected to be highly expressed anyway based on previous studies (Katsyv et al. 2021b) and RNA sequencing (Table A-4). The 10-fold increase in expression in the mutant indicates a high requirement for PFOR1 and, consequently, a high requirement for Fd_{red}, yet the consumption rate of pyruvate was lower in the mutant than in the wild type. Nevertheless, the high *nifJ1* and slight upregulation of Fd-dependent

enzymes such as *ech1A*, *ech2D* and *hydB* are an indication of a metabolic shift due to the deletion of the NfnAB complex and support the proposed model for glucose utilization (Figure 43) even if NfnAB is considered unnecessary during growth on pyruvate.

Furthermore, the reduced growth rate of the *nfnB* mutant on pyruvate suggests that NfnAB is needed to provide NADH directly for amino acid and lipid synthesis, suggesting that anabolism is NfnAB-dependent and catabolism is NfnAB-independent.

While the growth and resting cell behavior of the *nfnB* mutant can be explained for glucose and pyruvate, its behavior with H_2/CO_2 is puzzling. The lack of NfnAB complex could potentially result in no growth as no NADH would be provided for the anabolism. Nevertheless, it was initially assumed that resting cells of the *nfnB* mutant could still utilize H_2/CO_2. However, this assumption was disproven in resting cell experiments, where the cells failed to produce significant amounts of acetate or formate. Neither the lack of acetate production or formate production can be explained using the model for H_2/CO_2 (Katsyv et al. 2021a; Figure 3 B) since the NfnAB complex is not needed to provide all the required redox carriers for the WLP. However, the absence of formate is particularly striking since the HDCR only requires H_2 to reduce CO_2 to formate (Dietrich et al. 2022). In contrast, the resting cell experiments with the wild type of *T. kivui* and a protein concentration of 0.6 mg ml^{-1} showed a high conversion rate of H_2 to formate (Burger et al. 2022). Thus, even when the protein concentration was reduced in the resting cell experiment with the *nfnB* mutant (0.2 mg ml^{-1}), this might slow down the conversion rate but should not completely prevent formate production (Figure 37). This raises the question of the role of the NfnAB complex in H_2/CO_2 catabolism, which cannot be answered yet but is of interest to understand the metabolic system of *T. kivui*.

In summary, it could be shown that the deletion of *nfnB* results in a clear phenotype during growth and in resting cells, which indicates a major role of the NfnAB complex in upkeeping metabolic balance and especially the re-oxidation of NADH and in supplying NADH on pyruvate and H_2/CO_2 for growth. Characterizing the *nfnB* mutant requires further investigation since it is unclear how the growing cell re-oxidizes NADH. An analysis of the NADH/NAD^+ ratio, as described by Li et al. (2019) during the utilization of glucose in growing and resting cells, should show whether the deletion of the NfnAB complex leads to a metabolic bottleneck or not. Since qPCR is not suitable to investigate a general change in gene expression, RNA sequencing of the mutant should be performed to show which potential genes encoding NADH-dependent enzymes are upregulated on glucose, pyruvate or H_2/CO_2 compared to wild type if adaptation for H_2/CO_2 is possible.

4.4 Mixotrophy growth of *T. kivui*

4.4.1 Inhibitory effect of H_2

Some acetogens like *A. woodii* (Balch et al. 1977) and *T. kivui* (Leigh et al. 1981) can grow organotrophically on sugars, as well as lithotrophically on H_2/CO_2 (Table 1). Additionally, these microorganisms are capable of mixotrophic growth when provided with organic substrates along with H_2/CO_2 or gas mixtures containing H_2 (Braun and Gottschalk 1981; Peters 1998; Maru et al. 2018). For *A. woodii*, mixotrophic growth has been reported on fructose or lactate in the presence of H_2/CO_2 in the atmosphere. In both cases, the growth rate increased compared to conditions without H_2 in the atmosphere (Braun and Gottschalk 1981; Peters 1998).

In the case of *T. kivui* wild type DSM2030, the growth in a fermenter system with fructose along with synthesis gas ($CO/H_2/CO_2/N_2$; 55/20/10/15; v/v/v/v) in the atmosphere showed a slight increase in acetate production compared to growth with fructose along with an N_2 atmosphere, although overall

growth was reduced (Maru et al. 2018). This reduction in growth was likely due to CO in the gas mixture, as CO is known to inhibit hydrogenase activity (Goldet et al. 2009; Baffert et al. 2011; Matsumoto et al. 2011).

Therefore, the mixotrophic growth of *T. kivui* on organic substrates combined with H_2/CO_2 has not been thoroughly investigated, making this study a valuable contribution to addressing initial questions in this area.

It is evident that H_2 acts as a central redox carrier for both organisms. It can be supplied extracellularly as a substitute, but it is also produced internally by the organisms during the utilization of organic substrates, thereby enabling intracellular electron transfer between electron carriers via enzymes like the electron bifurcating hydrogenase of *A. woodii* and *T. kivui* (Wiechmann et al. 2020; Katsyv et al. 2021a; Burger et al. 2022; Katsyv et al. 2023b).

The essentiality of H_2 was shown in deletion mutants of *A. woodii* and *T. kivui*. The deletion of major subunits of electron bifurcating hydrogenase (HydABCD) in *A. woodii* resulted in the inability to grow on organic substrates such as fructose, lactate, ethanol and formate, while the addition of H_2 restored the ability to grow on organic substrates, with the exception of formate (Wiechmann et al. 2020). This demonstrates that the reduced redox carriers, such as NADH and Fd_{red}, generated through the oxidation of organic substrates, are re-oxidized by the HydABCD complex, which provides H_2 to the cell to enable growth.

The deletion of the HDCR gene in *T. kivui*, which is responsible for reducing CO_2 to formate by oxidizing H_2, resulted in the mutant being unable to grow on organic substrates without adding formate (Jain et al. 2020). Biochemical studies of the enzymes HydABC and Ech2 of *T. kivui* showed that H_2 is used as a reductant even though Ech2 is not essential for autotrophic growth (Katsyv et al. 2021a; Katsyv and Müller 2022; Katsyv et al. 2023b; Baum et al. 2024). Consequently, H_2 is crucial in the redox metabolism of *T. kivui*, and imbalances between H_2 and other reduced redox carriers might significantly influence the growth and catabolic conversion of organic substrate to acetate.

Initial experiments with cells grown on defined medium and glucose showed clear impairment of growth after the passage to medium containing glucose and H_2 in the atmosphere ($2x10^5$ Pa; $N_2/CO_2/H_2$; 40/10/50; v/v/v), while additional N_2 in the atmosphere ($2x10^5$ Pa; N_2/CO_2; 90/10; v/v) did not cause any inhibition compared to the control culture ($1x10^5$ Pa; N_2/CO_2; 80/20; v/v, Figure 23).

It was unlikely that the reduced CO_2 concentration in the atmosphere did not lead to impairment of growth since the medium was carbon buffered. Yet, an influence of the $N_2/CO_2/H_2$ ratio could not be excluded since *A. woodii* showed growth impairment when cultivated on fructose along with an H_2 atmosphere containing no CO_2 (Braun and Gottschalk 1981). Since the partial pressure of CO_2 remained constant while only its concentration changed, the growth impairment of *T. kivui* was likely caused by the addition of H_2 to the atmosphere. Nevertheless, to ensure that a reduced CO_2 concentration did not influence the growth of *T. kivui*, gas mixtures of N_2/CO_2 and H_2/CO_2 were used with a gas ratio of $N_2/CO_2/H_2$ of 40/26.6/33.3 (v/v/v) with an overpressure of $1x10^5$ Pa or 26.7/28.9/44.4 (v/v/v) with an overpressure of $2x10^5$ Pa. Furthermore, different conditions were tested: a preset atmosphere containing H_2/CO_2 and adding H_2/CO_2 during growth (H_2 shock).

Regardless of condition and H_2 concentration, growth impairment was always observed when grown on glucose. Yet, the data suggest that a higher H_2 concentration and partial pressure resulted in a stronger response of *T. kivui*. In the preset atmospheres of $N_2/CO_2/H_2$ with a 40/10/50 ratio (v/v/v; Figure 23) resulted in a doubling time of 3.8 h, while a $N_2/CO_2/H_2$ with a 40/26.6/33.3 ratio (v/v/v; Figure 25 A)

resulted in a doubling time of 2.3 h (Figure 25 A). This correlation was confirmed in the H_2 shock experiment on defined medium and glucose (Figure 29). An overpressure of $2x10^5$ Pa H_2/CO_2 led to a stronger growth impairment than $1x10^5$ Pa H_2/CO_2 (Table 24). It can be concluded that a higher partial pressure and concentration of H_2 result in a stronger growth impairment, while *T. kivui* utilizes glucose.

Based on these observations, I propose a metabolic model for the mixotrophic growth of *T. kivui* on glucose plus H_2/CO_2 with different glucose to H_2/CO_2 ratios (Figure 44). The oxidation of glucose to 2 acetate and 2 CO_2 provides 2 NADH, 2 Fd_{red} and 4 ATP. NADH and Fd_{red} are subsequently re-oxidized through the NfnAB complex, reducing $NADP^+$ to NADPH. NADPH is then re-oxidized by NADPH-dependent methylene-THF dehydrogenase within the WLP or by the HydABC in combination with Fd_{red} (Figure 44 A). The addition of H_2/CO_2 alters the glucose to H_2/CO_2 ratio, potentially shifting the direction of the HydABC-catalyzed reaction. For instance, at a 1 glucose to 12 H_2/6 CO_2 ratio (Figure 44 B) HydABC may remain inactive. However, increasing the ratio to 1 glucose to 24 H_2/12 CO_2 (Figure 44 C) could reverse the enzymatic reaction, leading to $NADP^+$ being reduced to NADPH by oxidizing H_2.

This reversal could create a metabolic bottleneck, as all the generated NADPH would need to be re-oxidized only by the NADPH-dependent methylene-THF dehydrogenase. Additionally, the increased amount of NADPH could potentially inhibit the re-oxidation of NADH via the NfnAB complex, leading to feedback inhibition of glyceraldehyde 3-phosphate dehydrogenase and, consequently, a reduction in glucose consumption. According to the proposed model, no additional ATP is consumed or produced by adding H_2/CO_2; however, an increased glucose to H_2/CO_2 ratio would lead to more acetate production.

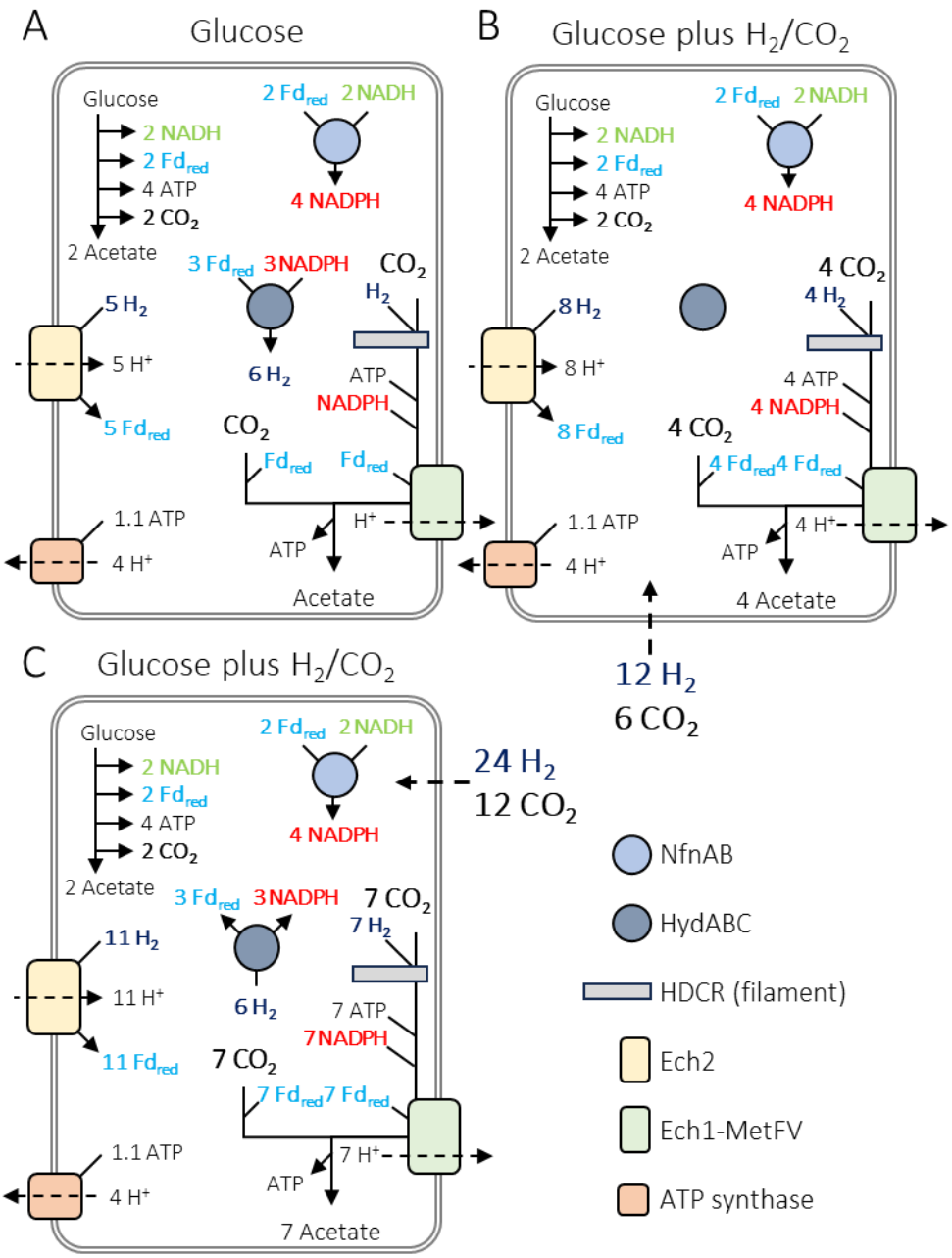

Figure 44 Proposed model for mixotrophic of *T. kivui* growth with glucose and H_2/CO_2.
The model shows the utilization of glucose (A) and glucose combined with H_2/CO_2 (B and C), with different glucose to H_2/CO_2 ratios: (A) with 1 glucose to 12 H_2 and 6 CO_2, and (B) with 1 glucose to 24 H_2 and 12 CO_2. Depicted are enzymes involved in the redox metabolism; an electron bifurcating transhydrogenase (NfnAB; light blue), an electron bifurcating hydrogenase (HydABC; blue-gray), two energy-converting hydrogenases (Ech2; light yellow and Ech1-MetFV; light green), an ATP synthase (light orange) and a hydrogen dependent carbon dioxide reductase (HDCR; light gray). As the amount of H_2 increases, the direction of the enzymatic reaction of the HydABC shifts from H_2 reduction to H_2 oxidation. In contrast to previous models (Katsyv et al. 2021a; Baum et al. 2024), the Ech1-MetFV complex translocates exactly one proton, rather than an undefined amount, to realize a balanced system. For the calculation of the ATP required for the translation of one proton, approximately 0.28 ATP is assumed.

The initial screening of gene expression in cells grown on glucose under an $N_2/CO_2/H_2$ atmosphere (40/10/50; v/v/v; Figure 23) revealed significant downregulation of *hydB* (HydABC) compared to cells grown under an N_2/CO_2 atmosphere (80/20; v/v; Figure 24; Table 16). This suggests that the expression of *hydB* is affected by the high H_2 concentration. However, in cells shock with H_2/CO_2 ($N_2/CO_2/H_2$; 40/26.6/33.3; v/v/v) on complex or defined medium containing glucose, no significant downregulation

of *hydB* was detected (Table 21; Table 26). Additionally, *nfnA* did not show significant expression change, whereas the *gap* was slightly upregulated, though not significantly, after adding H_2 to glucose cultures (Table 21; Table 26).

Thus, gene regulation and growth inhibition are influenced by the concentration of H_2 in the atmosphere. RNA sequencing data showed a clear difference in gene regulation between H_2/CO_2 overpressures of $1x10^5$ Pa and $2x10^5$ Pa (Table 28; Table A-2; Table A-3). This suggests that the degree of *hydB* downregulation is likely also dependent on H_2 concentration. However, gene expression could also be influenced by the timing of sample collection and the initial experimental conditions. For instance, in the preset condition (Figure 23), samples were taken 6 hours after the cells were first exposed to H_2, whereas in the shock experiments (Figure 26; Figure 29), only 15 minutes had passed. This implies that the downregulation of *hydB* might also represent an adaptation to H_2. Therefore, further studies regarding gene expression change over time should be considered, allowing the observation of the adaptation to H_2 in real time.

Interestingly, the response of adding H_2 differed depending on the carbon substrate. The impairment of growth on mannitol was even stronger than on glucose, while growth on pyruvate was not affected by the additional H_2 (Table 17; Figure 25 A, B and C). The different responses are probably due to the different redox agents and the amount provided when utilizing the carbon substrates. For example, mannitol provides 3 NADH and 2 Fd_{red} compared to the 2 NADH and 2 Fd_{red} from glucose and pyruvate provides only Fd_{red} (Figure 3 A and C; Moon et al. 2020; Katsyv et al. 2021b). Therefore, the homeostasis of redox agents such as NADH/NAD^+, NADPH/$NADP^+$, Fd_{red}/Fd_{ox} and H_2/2 H^+ in the cell differs depending on the utilized substrate and so also the flexibility of the metabolism to respond to changes.

The disturbance of the metabolic system by the addition of H_2 was indicated by the consumption rate of produced formate. Formate production after adding H_2/CO_2 was expected as the HDCR is highly active and directly reduces the CO_2 in the medium to formate when H_2 is present (Schwarz et al. 2018; Dietrich et al. 2022). In cultures growing on H_2/CO_2, formate accumulation consistently occurred during the early growth phase but was quickly consumed once a higher OD_{600} was reached (Figure 28 D; Figure 31 C).

Therefore, formate was detected in all cultures with additional H_2 in the atmosphere. Depending on when H_2 was added, formate was produced and afterward consumed. So, cultures with preset H_2 atmosphere showed slower production of formate (Figure 25 J, K, and L) compared to the instant formate production in cultures where H_2 was added during exponential growth (Figure 26 J, K, and L). The instant formate production occurred due to the higher OD_{600}. Consequently, CO_2 could be reduced directly by HDCR to formate (Schwarz and Müller 2020).

However, it turned out that the formate consumption was dependent on the carbon substrate, suggesting that the metabolism was disrupted. Formate was quickly consumed on pyruvate, but on glucose and mannitol, this was not the case (Figure 25 and Figure 26 J, K, and L). The consumption of formate was coupled to glucose or mannitol consumption, while pyruvate consumption was independent of formate consumption (Figure 25 and Figure 26 G, H, F, J, K, and L).

This observation supports the hypothesis of a metabolic shift for NADH-providing substrates plus H_2/CO_2 (Figure 44), likely resulting in a metabolic bottleneck. Additionally, I propose a model for the utilization of pyruvate with H_2/CO_2. Unlike glucose consumption, where NADH must be re-oxidized, on pyruvate, the presence of additional H_2 allows *T. kivui* to reduce $NADP^+$ to NADPH by the HydABC, bypassing the need to oxidize Fd_{red} to reduce 2 H+ to H_2 by the Ech2 complex. As a result, the additional H_2/CO_2 increases acetate production from 1.25 mol acetate per mol of pyruvate to 1.63 mol acetate.

Furthermore, the calculated ATP output would increase slightly from 1.2 to 1.3, assuming one translocated proton represents 0.28 ATP and the Ech1-MetFV complex translocates only one proton.

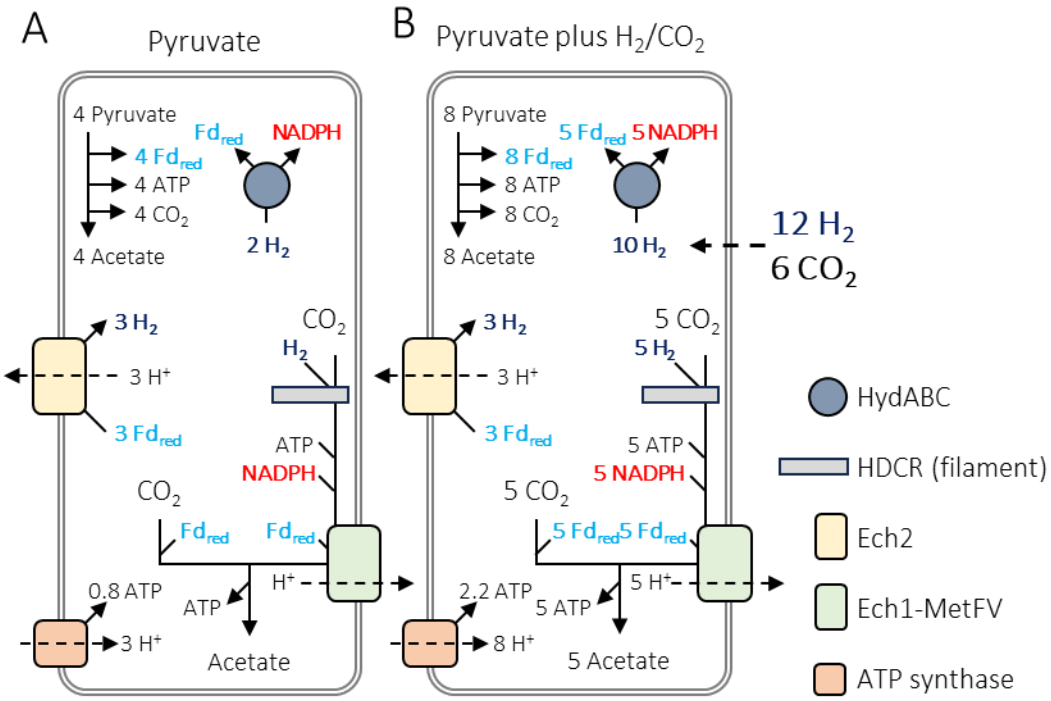

Figure 45 Proposed model for mixotrophic of *T. kivui* growth with pyruvate and H_2/CO_2.
The model shows the utilization of pyruvate (A) and pyruvate combined with H_2/CO_2 (B). Depicted are enzymes involved in the redox metabolism; an electron bifurcating hydrogenase (HydABC; blue-gray), two energy-converting hydrogenases (Ech2; light yellow and Ech1-MetFV; light green), an ATP synthase (light orange) and a hydrogen dependent carbon dioxide reductase (HDCR; light gray). In contrast, in the model of glucose combined with H_2/CO_2, the increasing amount of H_2 does not alter the direction of the enzymatic reaction catalyzed by HydABC. It is assumed that the Ech1-MetFV complex translocates one proton, rather than an undefined amount, to maintain a balanced system. For the calculation for ATP generation by the ATP synthase, it is estimated that the translation of one proton provides approximately 0.28 ATP.

Furthermore, it is unlikely that additional H_2 in the presence of pyruvate leads to feedback inhibition of NfnAB as observed with glucose. This is because NADH does not need to be re-oxidized but rather needs to be reduced for cellular anabolism.

However, *hydB* was significantly downregulated on pyruvate after adding H_2 (Table 21; Table 26). This downregulation suggests that the HydABC complex was less needed, as the additional H_2 pushes the catalytic reaction of HydABC towards H_2 oxidation and reduction of Fd_{red} and NADPH. As a result, the reduction of HydABC in the cell might help maintain redox balance. At the same time, *nfnA* was slightly upregulated, though not significantly, indicating that NADPH needed to be re-oxidized to accommodate the increased metabolic throughput of NADPH (Table 21; Table 26).

Interestingly, *hydB* was almost as highly expressed on only pyruvate as on H_2/CO_2 alone (Table 27). On pyruvate and H_2/CO_2, HydABC is assumed to oxidize H_2. HydABC is likely needed under these conditions to maintain redox balance and allow metabolic flexibility since only H_2 or Fd_{red} are provided as redox carriers.

The hypothesis regarding the downregulation of *hydB* was further supported by H_2 shock experiments conducted with the *nfnB* mutant. Strikingly, pyruvate cultures of the *nfnB* mutant exhibited growth impairment after adding H_2/CO_2 as the glucose cultures (Figure 38 A; Figure 40 A). Despite the

impairment of the growth, pyruvate consumption was only slightly slower than in the wild type (Figure 40 B and C). Interestingly, the produced format took over 2 days to be depleted after all pyruvate had been consumed (Figure 40 C), which was odd since the consumption of glucose and formate in the mutant was coupled as in the wild type (Figure 29 B and C; Figure 38 C).

Furthermore, the *nfnB* mutant showed no significant changes in gene expression for glucose upon adding H_2, even though *nifj1* (PFOR1) was slightly upregulated, similar to the wild type (Table 32). However, on pyruvate, adding H_2/CO_2 resulted in a significant downregulated of hydB stronger than in the wild type (Table 33). The downregulation of *hydB* was accompanied by a significant decrease in the expression of *ech2D* and *fhs* (Table 33).

Therefore, due to the deletion of *nfnB* and the resulting loss of the NfnAB complex, NADPH could not be re-oxidized metabolic bottleneck, leading to a significant downregulation of *hydB*. This downregulation likely prevents further reduction of NADPH by HydABC to overcome the redox imbalance, which probably caused the growth impairment on pyruvate.

The overall gene regulation response to adding H_2 is of particular interest. RNA sequencing data from glucose cultures revealed that similar to qPCR results, the expression of metabolic genes remained relatively unchanged after the addition of H_2/CO_2 (Table A-4). However, there were notable changes in the expression of other genes. Specifically, genes involved in glycosyltransferase, transposase, glycogen biosynthesis, CRISPR subtype III and phosphoenolpyruvate synthase were upregulated (Table 28; Table A-2). Conversely, genes associated with pyrimidine and arginine biosynthesis, as well as ribosomal proteins were downregulated (Table 28; Table A-3).

The upregulation of transposase and CRISPR subtype III indicates a general stress response, enabling rapid adaptation to unknown conditions (Siguier et al. 2014; Kolesnik et al. 2021). Similarly, the increased expression of genes involved in glycogen biosynthesis, phosphoenolpyruvate synthase and glycosyltransferase suggest glycogen formation. This typically occurs when an organism's growth is restricted, but excess organic substrates are available (Preiss 2014). This situation occurs from a deficiency of a critical nutrient or, in this instance, a redox imbalance caused by the addition of a redox carrier.

The downregulation of ribosomal proteins is likely a response to reduced growth rates, as the cell needs to translate less protein. By reducing the production of ribosomal proteins, the cell conserves resources and adapts its ribosomal capacity to the reduced demands of protein synthesis. The pyrimidine and arginine biosynthesis are essential for all organisms and are tightly regulated with various regulatory mechanisms, yet none of the descript regulators is described as H_2 sensitive (Turnbough and Switzer 2008). Therefore, the downregulation of the pyrimidine and arginine biosynthesis genes is the consequence of growth inhibition and not the cause.

This raises the question of whether *T. kivui* contains any H_2-sensitive regulators. While the H_2-sensitive protein regulator HoxA (Lenz et al. 2002) has been studied in *Ralstonia eutropha* (also known as *Cupriavidus necator*), BLAST analyses have been unsuccessful in identifying a similar H_2 regulator in *T. kivui*.

However, in *T. kivui*, the transcriptional regulatory redox-sensing protein Rex has been annotated (Hess et al. 2014; TKV_c05420; Table A-9). This transcriptional regulator responds to intracellular NADH/NAD^+ ratio changes, regulating NADH-dependent enzymes to maintain redox balance (Wietzke and Bahl 2012). Rex specifically responds to changes in the NADH/NAD^+ ratio and not in the NADPH/$NADP^+$ ratio (Wietzke and Bahl 2012; Bitoun and Wen 2016). In contrast, a different transcriptional regulator from

the LysR family has also been annotated in *T. kivui* (Hess et al. 2014; TKV_c19570; Table A-9). It is hypothesized that LysR may respond to changes in the NADPH/$NADP^+$ ratio; however, this has not been conclusively proven (Keulen et al. 1998).

Therefore, it is plausible that Rex and LysR responded to changes in the NADH/NAD^+ and NADPH/$NADP^+$ ratios following the addition of H_2, leading to regulatory changes. This is supported by the fact that both regulators were slightly upregulated, though not significantly (Table A-9).

Given the complexity of metabolic systems and the potential for unaccounted side reactions, further studies are required. Hence, it cannot be said with certainty how *T. kivui* responded at the protein level to the addition of H_2/CO_2. Proteomic analyses should be performed to clarify whether the quantity of HydABC, NfnAB or an unidentified enzyme changed. In addition, the ratio of NADH/NAD^+ and NADPH/$NADP^+$ should be determined to establish which of the two redox agents accumulates under which conditions. Moreover, the NfnAB complex seems vital for mixotrophic growth and could be involved in the H_2 metabolism even if it does not directly reduce or oxidize H_2. Therefore, further characterization of this enzyme could be of great importance for understanding the metabolic processes during the mixotrophic growth of *T. kivui*.

4.4.2 Adaption to mixotrophic conditions

Although adding H_2 to some organic substrates initially impaired the growth of *T. kivui*, it was observed that after one passage, *T. kivui* could adapt to the additional H_2 in the atmosphere (Figure 25 A, B and C). Once adapted, the cells showed growth rates similar to, or even slightly higher than, those of the unadapted cells grown only on the organic substrate, particularly when grown on mannitol with H_2/CO_2 (Table 17). A similar pattern was observed in the consumption rates of the organic substrate (Figure 25 D, E and F).

In the adapted cells, the consumption of glucose and mannitol was coupled with formate consumption, as observed in the unadapted cells (Figure 25 D, E, J and K). Notably, when grown on pyruvate, unadapted cells consumed formate faster than pyruvate, while adapted cells still had formate remaining after all the pyruvate was consumed (Figure 25 F and L). Additionally, all cultures with added H2/CO2 had a higher final acetate concentration than those grown only on the organic substrate. (Figure 25 G, H and I).

These findings demonstrate that *T. kivui* is capable of growing mixotrophically, as evidenced by the simultaneous consumption of organic substrates and formate (H_2/CO_2), as well as the increased final acetate concentration in cultures supplemented with additional H_2 and the enhanced acetate production in adapted cells. Furthermore, the inhibitory effect of H_2 on *T. kivui* is not permanent, and an adaptation period of approximately one day was sufficient for the organism to adapt to H_2.

For this reason, it was interesting to investigate the changes in gene expression during the first passage. It can be assumed that mutations are unnecessary to enable the simultaneous metabolism of glucose and H_2/CO_2, as adaptive processes involving genetic changes typically require longer periods, such as those needed to adapt to lower temperatures or CO (Lehmann et al. 2023; Baum et al. 2024).

The same experimental approach with *T. kivui* pre-grown of H_2/CO_2 and adding glucose, mannitol, or pyruvate in the early exponential growth phase resulted in growth impairment (Figure 28). The consumption rate of the added substrate was slower than cells pre-grown on the substrate (Table 23). Interestingly, substrate and formate consumption were not coupled.

Cells adapted to autotrophic growth on H_2/CO_2 were not adversely affected by the sudden addition of organic substrates. This is probably due to the slower uptake of the sugars into the cell (Fuhrer et al. 2005) compared to the H_2 uptake (Pinske and Sawers 2016), as well as the stepwise oxidation process of the sugar enabling the cell to maintain redox balance.

Additionally, the H_2 shock experiments with mannitol (Table 21) revealed significant downregulation of *mtlD*, which encodes mannitol-1-phosphate dehydrogenase. This enzyme catalyzes the $NAD(P)^+$-dependent oxidation of mannitol-1-phosphate to fructose-6-phosphate (Moon et al. 2019). The downregulation of *mtlD* corresponds to the reduced consumption rate of mannitol. On H_2/CO_2, *mtlD* was likely not expressed, resulting in less effective utilization of mannitol than cells pre-grown on mannitol. Other genes involved in organic substrate oxidation, such as *gap* (glyceraldehyde-3-phosphate dehydrogenase) and *nifJ1* (pyruvate-ferredoxin/flavodoxin oxidoreductase; PFOR1), were neither significantly upregulated nor downregulated on mannitol or glucose (Table 21). In addition, mRNA sequence analysis showed that the expression of genes involved in glycolysis were not affected by adding H_2 to cultures growing on glucose (Table A-8). Therefore, the expression of *mtlD* is regulated, as demonstrated by Zeldes et al. (2024), in contrast to genes encoding glycolytic enzymes, which remained consistently expressed even when growth was impaired.

In summary, the inhibition effect of H_2 is observed only upon initial contact when *T. kivui* is pre-cultured on organic substrates such as glucose or mannitol, which provide NADH. Moreover, adaptation to mixotrophic conditions improves both growth and acetate production rates. Although initial changes in gene expression after adding H_2 have been demonstrated and are partially understood, the precise gene regulatory mechanisms driving *T. kivui*'s adaptation to mixotrophic conditions remain speculative. To gain a deeper understanding of the adaptation process of *T. kivui* to mixotrophic conditions, further investigations into gene and protein expression changes in H_2-adapted strains are needed, using RNA sequencing and proteomic analyses.

5 Conclusions and Outlook

Even with progressing technologies and expanded knowledge, one important question that still needs to be elucidated is the origin of life on Earth. Based on our current understanding, the first organisms colonizing the Earth were most likely thermophilic archaea and bacteria. Direct descendants of this last universal common ancestor (LUCA) are supposedly acetogens and methanogens.

Acetogenic and methanogenic organisms are living at the thermodynamic edge by utilizing simple molecules like H_2 and CO_2 for production of biomass and formation of low carbon compounds. One acetogen that gained more and more importance as a model organism for these conversions is the thermophile *Thermoanaerobacter kivui*.

In this study, I focused primarily on energy and redox metabolism of *T. kivui*, as these investigations are crucial for advancing our understanding of the biochemical and regulatory mechanisms in thermophilic acetogens, and thereby providing valuable insights into the earliest metabolic processes. For this purpose, different genetic, as well as metabolic approaches were chosen.

By successfully creating a deletion mutant for the energy conserving hydrogenase Ech2, but not Ech1, I was able to demonstrate the importance of Ech1. Additionally, I used a novel method developed by Benjamin Zeldes (University of Rostock), to replace the *ech1* promoter, allowing targeted downregulation of *ech1*. By this means, I showed that both Ech1 and Ech2 contribute to growth on ferredoxin-dependent substrates like pyruvate.

Furthermore, I was able to shed light on the metabolic role of the NfnAB complex, which is essential for NADH re-oxidation. By deleting the gene cluster, a metabolic bottleneck is created under specific conditions, emphasizing the importance of NADH redox balance in *T. kivui*.

In addition to genetic approaches, metabolic studies were carried out and this study represents the first investigation of mixotrophy in *T. kivui*, demonstrating inhibitory effects of H_2 on *T. kivui* growth. These findings raise important questions about the regulatory mechanisms and adaptive strategies of T. kivui under redox stress, which should be further investigated in the future.

Further research focussing on key energy-converting and electron-bifurcating enzymes is an important aspiration and the development of a more refined genetic tool for promoter control, as well as more intensive investigation regarding the maintenance of redox homeostasis will hopefully give more insight.

In conclusion, the research here provides fundamental insights into the regulatory mechanisms regarding energy and redox metabolism of *T. kivui*. Gaining deeper insights into this organism is essential not only for understanding the origins of life but also for its potential biotechnological applications.

Publication bibliography

Abu, R.; Woodley, J. M. (2015): Application of enzyme coupling reactions to shift thermodynamically limited biocatalytic reactions. In *ChemCatChem* 7 (19), pp. 3094–3105. DOI: 10.1002/cctc.201500603.

Baffert, C.; Bertini, L.; Lautier, T.; Greco, C.; Sybirna, K.; Ezanno, P. et al. (2011): CO disrupts the reduced H-cluster of FeFe hydrogenase. A combined DFT and protein film voltammetry study. In *J. Am. Chem. Soc.* 133 (7), pp. 2096–2099. DOI: 10.1021/ja110627b.

Balch, W. E.; Schoberth, S.; Tanner, R. S.; Wolfe, R. S. (1977): Acetobacterium, a new genus of hydrogen-oxidizing, carbon dioxide-reducing, anaerobic bacteria. In *Int. J. Syst. Bacteriol.* 27 (4), pp. 355–361. DOI: 10.1099/00207713-27-4-355.

Basen, M.; Geiger, I.; Henke, L.; Müller, V. (2018): A genetic system for the thermophilic acetogenic bacterium *Thermoanaerobacter kivui*. In *Appl. Environ. Microbiol.* 84 (3). DOI: 10.1128/AEM.02210-17.

Baum, C.; Zeldes, B. M.; Poehlein, A.; Daniel, R.; Müller, V.; Basen, M. (2024): The energy-converting hydrogenase Ech2 is important for the growth of the thermophilic acetogen *Thermoanaerobacter kivui* on ferredoxin-dependent substrates. In *Microbiol. Spectr.*, e0338023. DOI: 10.1128/spectrum.03380-23.

Bekker, M.; Vries, S.; Beek, A.; Hellingwerf, K. J.; Mattos, M. J. T. (2009): Respiration of *Escherichia coli* can be fully uncoupled via the nonelectrogenic terminal cytochrome bd-II oxidase. In *J. Bacteriol.* 191 (17), pp. 5510–5517. DOI: 10.1128/JB.00562-09.

Bertani, G. (1951): Studies on lysogenesis. I. The mode of phage liberation by lysogenic *Escherichia coli*. In *J. Bacteriol.* 62 (3), pp. 293–300. DOI: 10.1128/jb.62.3.293-300.1951.

Biegel, E.; Müller, V. (2010): Bacterial Na^+-translocating ferredoxin:NAD^+ oxidoreductase. In *Proc. Natl. Acad. Sci. USA* 107 (42), pp. 18138–18142. DOI: 10.1073/pnas.1010318107.

Bitoun, J. P.; Wen, Z. T. (2016): Transcription factor Rex in regulation of pathophysiology in oral pathogens. In *Mol. Oral Microbiol.* 31 (2), pp. 115–124. DOI: 10.1111/omi.12114.

Borrel, G.; Adam, P. S.; Gribaldo, S. (2016): Methanogenesis and the Wood-Ljungdahl pathway: an ancient, versatile, and fragile association. In *Genome Biol. Evol.* 8 (6), pp. 1706–1711. DOI: 10.1093/gbe/evw114.

Braun, K.; Gottschalk, G. (1981): Effect of molecular hydrogen and carbon dioxide on chemo-organotrophic growth of *Acetobacterium woodii* and *Clostridium aceticum*. In *Arch. Microbiol.* 128 (3), pp. 294–298. DOI: 10.1007/BF00422533.

Buckel, W.; Thauer, R. K. (2013): Energy conservation via electron bifurcating ferredoxin reduction and proton/Na^+ translocating ferredoxin oxidation. In *Biochim. Biophys. Acta* 1827 (2), pp. 94–113. DOI: 10.1016/j.bbabio.2012.07.002.

Burger, Y.; Schwarz, F. M.; Müller, V. (2022): Formate-driven H_2 production by whole cells of *Thermoanaerobacter kivui*. In *Biotechnol. biofuels bioprod.* 15 (1), p. 48. DOI: 10.1186/s13068-022-02147-5.

Cole, J. A.; Richardson, D. J. (2008): Respiration of nitrate and nitrite. In *EcoSal Plus* 3 (1). DOI: 10.1128/ecosal.3.2.5.

Collins, M. D.; Lawson, P. A.; Willems, A.; Cordoba, J. J.; Fernandez-Garayzabal, J.; Garcia, P. et al. (1994): The phylogeny of the genus *Clostridium*: proposal of five new genera and eleven new species combinations. In *Int. J. Syst. Bacteriol.* 44 (4), pp. 812–826. DOI: 10.1099/00207713-44-4-812.

Decker, K.; Jungermann, K.; Thauer, R. K. (1970): Energy production in anaerobic organisms. In *Angew. Chem. Int. Ed.* 9 (2), pp. 138–158. DOI: 10.1002/anie.197001381.

Demmer, J. K.; Huang, H.; Wang, S.; Demmer, U.; Thauer, R. K.; Ermler, U. (2015): Insights into flavin-based electron bifurcation via the NADH-dependent reduced ferredoxin:NADP oxidoreductase structure. In *J. Biol. Chem.* 290 (36), pp. 21985–21995. DOI: 10.1074/jbc.M115.656520.

Dietrich, H. M.; Müller, V. (2023): Ferredoxin as a physiological electron donor for carbon dioxide fixation to formate in a bacterial carbon dioxide reductase. In *ACS Catal.* 13 (18), pp. 12374–12382. DOI: 10.1021/acscatal.3c02753.

Dietrich, H. M.; Righetto, R. D.; Kumar, A.; Wietrzynski, W.; Trischler, R.; Schuller, S. K. et al. (2022): Membrane-anchored HDCR nanowires drive hydrogen-powered CO_2 fixation. In *Nature* 607 (7920), pp. 823–830. DOI: 10.1038/s41586-022-04971-z.

Dönig, J.; Müller, V. (2018): Alanine, a Novel Growth Substrate for the Acetogenic Bacterium *Acetobacterium woodii*. In *Appl. Environ. Microbiol.* 84 (23). DOI: 10.1128/AEM.02023-18.

Drake, H. L.; Gössner, A. S.; Daniel, S. L. (2008): Old acetogens, new light. In *Ann. N. Y. Acad. Sci.* 1125 (1), pp. 100–128. DOI: 10.1196/annals.1419.016.

Fontaine, F. E.; Peterson, W. H.; McCoy, E.; Johnson, M. J.; Ritter, G. J. (1942): A New Type of Glucose Fermentation by *Clostridium thermoaceticum*. In *J. Bacteriol.* 43 (6), pp. 701–715. DOI: 10.1128/jb.43.6.701-715.1942.

Fuchs, G. (2017): Allgemeine Mikrobiologie. 10., unveränderte Auflage. Stuttgart, New York: Georg Thieme Verlag.

Fuhrer, T.; Fischer, E.; Sauer, U. (2005): Experimental identification and quantification of glucose metabolism in seven bacterial species. In *J. Bacteriol.* 187 (5), pp. 1581–1590. DOI: 10.1128/JB.187.5.1581-1590.2005.

Furdui, C.; Ragsdale, S. W. (2000): The role of pyruvate ferredoxin oxidoreductase in pyruvate synthesis during autotrophic growth by the Wood-Ljungdahl pathway. In *J. Biol. Chem.* 275 (37), pp. 28494–28499. DOI: 10.1074/jbc.M003291200.

Furlan, C.; Chongdar, N.; Gupta, P.; Lubitz, W.; Ogata, H.; Blaza, J. N.; Birrell, J. A. (2022): Structural insight on the mechanism of an electron-bifurcating FeFe hydrogenase. In *eLife* 11. DOI: 10.7554/eLife.79361.

Gibson, M. I.; Chen, P. Y. T.; Drennan, C. L. (2016): A structural phylogeny for understanding 2-oxoacid oxidoreductase function. In *Curr. Opin. Struct. Biol.* 41, pp. 54–61. DOI: 10.1016/j.sbi.2016.05.011.

Gill, S.; Forterre, P. (2016): Origin of life: LUCA and extracellular membrane vesicles (EMVs). In *Int. J. Astrobiology* 15 (1), pp. 7–15. DOI: 10.1017/S1473550415000282.

Goldet, G.; Brandmayr, C.; Stripp, S. T.; Happe, T.; Cavazza, C.; Fontecilla-Camps, J. C.; Armstrong, F. A. (2009): Electrochemical kinetic investigations of the reactions of FeFe-hydrogenases with carbon monoxide and oxygen: comparing the importance of gas tunnels and active-site electronic/redox effects. In *J. Am. Chem. Soc.* 131 (41), pp. 14979–14989. DOI: 10.1021/ja905388j.

Hackmann, T. J.; Firkins, J. L. (2015): Electron transport phosphorylation in rumen butyrivibrios: unprecedented ATP yield for glucose fermentation to butyrate. In *Front. Microbiol.* 6, p. 622. DOI: 10.3389/fmicb.2015.00622.

Hanahan, D. (1983): Studies on transformation of *Escherichia coli* with plasmids. In *J. Mol. Biol.* 166 (4), pp. 557–580. DOI: 10.1016/s0022-2836(83)80284-8.

Heise, R.; Müller, V.; Gottschalk, G. (1989): Sodium dependence of acetate formation by the acetogenic bacterium *Acetobacterium woodii*. In *J. Bacteriol.* 171 (10), pp. 5473–5478. DOI: 10.1128/jb.171.10.5473-5478.1989.

Hess, V.; Poehlein, A.; Weghoff, M. C.; Daniel, R.; Müller, V. (2014): A genome-guided analysis of energy conservation in the thermophilic, cytochrome-free acetogenic bacterium *Thermoanaerobacter kivui*. In *BMC Genomics* 15 (1), p. 1139. DOI: 10.1186/1471-2164-15-1139.

Huang, H.; Wang, S.; Moll, J.; Thauer, R. K. (2012): Electron bifurcation involved in the energy metabolism of the acetogenic bacterium *Moorella thermoacetica* growing on glucose or H_2 plus CO_2. In *J. Bacteriol.* 194 (14), pp. 3689–3699. DOI: 10.1128/JB.00385-12.

Hungate, R. E. (1969): Chapter IV A Roll Tube Method for Cultivation of Strict Anaerobes. In J. R. Norris, D. W. Ribbons (Eds.): Methods in Microbiology, vol. 3: Academic Press, pp. 117–132. Available online at https://www.sciencedirect.com/science/article/pii/S0580951708705038.

Imkamp, F.; Biegel, E.; Jayamani, E.; Buckel, W.; Müller, V. (2007): Dissection of the caffeate respiratory chain in the acetogen *Acetobacterium woodii*: identification of an Rnf-type NADH dehydrogenase as a potential coupling site. In *J. Bacteriol.* 189 (22), pp. 8145–8153. DOI: 10.1128/JB.01017-07.

Jain, S.; Dietrich, H. M.; Müller, V.; Basen, M. (2020): Formate is required for growth of the thermophilic acetogenic bacterium *Thermoanaerobacter kivui* lacking hydrogen-dependent carbon dioxide reductase (HDCR). In *Front. Microbiol.* 11, p. 59. DOI: 10.3389/fmicb.2020.00059.

Jain, S.; Katsyv, A.; Basen, M.; Müller, V. (2021): The monofunctional CO dehydrogenase CooS is essential for growth of *Thermoanaerobacter kivui* on carbon monoxide. In *Extremophiles* 26 (1), p. 4. DOI: 10.1007/s00792-021-01251-y.

Jund, R.; Lacroute, F. (1970): Genetic and physiological aspects of resistance to 5-fluoropyrimidines in *Saccharomyces cerevisiae*. In *J. Bacteriol.* 102 (3), pp. 607–615. DOI: 10.1128/jb.102.3.607-615.1970.

Katsyv, A.; Essig, M.; Bedendi, G.; Sahin, S.; Milton, R. D.; Müller, V. (2023a): Characterization of ferredoxins from the thermophilic, acetogenic bacterium *Thermoanaerobacter kivui*. In *FEBS J.* DOI: 10.1111/febs.16801.

Katsyv, A.; Jain, S.; Basen, M.; Müller, V. (2021a): Electron carriers involved in autotrophic and heterotrophic acetogenesis in the thermophilic bacterium *Thermoanaerobacter kivui*. In *Extremophiles* 25 (5-6), pp. 513–526. DOI: 10.1007/s00792-021-01247-8.

Katsyv, A.; Kumar, A.; Saura, P.; Pöverlein, M. C.; Freibert, S. A.; Stripp, S. T. et al. (2023b): Molecular basis of the electron bifurcation mechanism in the [FeFe]-hydrogenase complex HydABC. In *J. Am. Chem. Soc.* 145 (10), pp. 5696–5709. DOI: 10.1021/jacs.2c11683.

Katsyv, A.; Müller, V. (2022): A purified energy-converting hydrogenase from *Thermoanaerobacter kivui* demonstrates coupled H^+-translocation and reduction in vitro. In *J. Biol. Chem.* 298 (8), p. 102216. DOI: 10.1016/j.jbc.2022.102216.

Katsyv, A.; Schoelmerich, M. C.; Basen, M.; Müller, V. (2021b): The pyruvate:ferredoxin oxidoreductase of the thermophilic acetogen, *Thermoanaerobacter kivui*. In *FEBS Open Bio* 11 (5), pp. 1332–1342. DOI: 10.1002/2211-5463.13136.

Keller, K. L.; Wall, J. D. (2011): Genetics and molecular biology of the electron flow for sulfate respiration in *Desulfovibrio*. In *Front. Microbiol.* 2, p. 135. DOI: 10.3389/fmicb.2011.00135.

Kelley, D. S.; Karson, J. A.; Früh-Green, G. L.; Yoerger, D. R.; Shank, T. M.; Butterfield, D. A. et al. (2005): A serpentinite-hosted ecosystem: the Lost City hydrothermal field. In *Science* 307 (5714), pp. 1428–1434. DOI: 10.1126/science.1102556.

Keulen, G.; Girbal, L.; Bergh, E. R.; Dijkhuizen, L.; Meijer, W. G. (1998): The LysR-type transcriptional regulator CbbR controlling autotrophic CO_2 fixation by *Xanthobacter flavus* is an NADPH sensor. In *J. Bacteriol.* 180 (6), pp. 1411–1417. DOI: 10.1128/JB.180.6.1411-1417.1998.

Kolesnik, M. V.; Fedorova, I.; Karneyeva, K. A.; Artamonova, D. N.; Severinov, K. V. (2021): Type III CRISPR-Cas systems: Deciphering the most complex prokaryotic immune system. In *Biochemistry* 86 (10), pp. 1301–1314. DOI: 10.1134/S0006297921100114.

Köpke, M.; Held, C.; Hujer, S.; Liesegang, H.; Wiezer, A.; Wollherr, A. et al. (2010): *Clostridium ljungdahlii* represents a microbial production platform based on syngas. In *Proc. Natl. Acad. Sci. USA* 107 (29), pp. 13087–13092. DOI: 10.1073/pnas.1004716107.

Kpebe, A.; Guendon, C.; Payne, N.; Ros, J.; Berbar, M. K.; Lebrun, R. et al. (2023): An essential role of the reversible electron-bifurcating hydrogenase Hnd for ethanol oxidation in *Solidesulfovibrio fructosivorans*. In *Front. Microbiol.* 14, p. 1139276. DOI: 10.3389/fmicb.2023.1139276.

Kröger, A.; Biel, S.; Simon, J.; Gross, R.; Unden, G.; Lancaster, C. R. D. (2002): Fumarate respiration of *Wolinella succinogenes*: enzymology, energetics and coupling mechanism. In *Biochim. Biophys. Acta* 1553 (1-2), pp. 23–38. DOI: 10.1016/S0005-2728(01)00234-1.

Krooth, R. S.; Hsiao, W. L.; Potvin, B. W. (1979): Resistance to 5-fluoroorotic acid and pyrimidine auxotrophy: a new bidirectional selective system for mammalian cells. In *Somatic Cell Genet.* 5 (5), pp. 551–569. DOI: 10.1007/BF01542694.

Kuhns, M.; Schuchmann, V.; Schmidt, S.; Friedrich, T.; Wiechmann, A.; Müller, V. (2020): The Rnf complex from the acetogenic bacterium *Acetobacterium woodii*: Purification and characterization of RnfC and RnfB. In *Biochim. Biophys. Acta Bioenerg.* 1861 (11), p. 148263. DOI: 10.1016/j.bbabio.2020.148263.

Kulkarni, G.; Mand, T. D.; Metcalf, W. W. (2018): Energy conservation via hydrogen cycling in the methanogenic archaeon *Methanosarcina barkeri*. In *Mbio* 9 (4). DOI: 10.1128/mBio.01256-18.

Künkel, A.; Vorholt, J. A.; Thauer, R. K.; Hedderich, R. (1998): An *Escherichia coli* hydrogenase-3-type hydrogenase in methanogenic archaea. In *Eur. J. Biochem.* 252 (3), pp. 467–476. DOI: 10.1046/j.1432-1327.1998.2520467.x.

Lane, N.; Allen, J. F.; Martin, W. (2010): How did LUCA make a living? Chemiosmosis in the origin of life. In *Bioessays* 32 (4), pp. 271–280. DOI: 10.1002/bies.200900131.

Leavitt, W. D.; Murphy, S J. L.; Lynd, L. R.; Bradley, A. S. (2017): Hydrogen isotope composition of *Thermoanaerobacterium saccharolyticum* lipids: Comparing wild type with a nfn- transhydrogenase mutant. In *Org. Geochem.* 113, pp. 239–241. DOI: 10.1016/j.orggeochem.2017.06.020.

Lehmann, M.; Prohaska, C.; Zeldes, B. M.; Poehlein, A.; Daniel, R.; Basen, M. (2023): Adaptive laboratory evolution of a thermophile toward a reduced growth temperature optimum. In *Front. Microbiol.* 14, p. 1265216. DOI: 10.3389/fmicb.2023.1265216.

Leigh, J. A.; Mayer, F.; Wolfe, R. S. (1981): *Acetogenium kivui*, a new thermophilic hydrogen-oxidizing acetogenic bacterium. In *Arch. Microbiol.* 129 (4), pp. 275–280. DOI: 10.1007/BF00414697.

Lemaire, O. N.; Jespersen, M.; Wagner, T. (2020): CO_2-fixation strategies in energy extremophiles: What can we learn from acetogens? In *Front. Microbiol.* 11, p. 486. DOI: 10.3389/fmicb.2020.00486.

Lenz, O.; Bernhard, M.; Buhrke, W.; Schwartz, E.; Friedrich, B. (2002): The hydrogen-sensing apparatus in *Ralstonia eutropha*. In *J. Mol. Microbiol. Biotechnol.* 4 (3), pp. 255–262.

Lenz, O.; Friedrich, B. (1998): A novel multicomponent regulatory system mediates H_2 sensing in *Alcaligenes eutrophus*. In *Proc. Natl. Acad. Sci. USA* 95 (21), pp. 12474–12479. DOI: 10.1073/pnas.95.21.12474.

Li, Q.; Li, L.; Rejtar, T.; Lessner, D. J.; Karger, B. L.; Ferry, J. G. (2006): Electron transport in the pathway of acetate conversion to methane in the marine archaeon *Methanosarcina acetivorans*. In *J. Bacteriol.* 188 (2), pp. 702–710. DOI: 10.1128/JB.188.2.702-710.2006.

Li, Y.; Hu, J.; Qu, C.; Chen, L.; Guo, X.; Fu, H.; Wang, J. (2019): Engineered *Thermoanaerobacterium aotearoense* with nfnAB knockout for improved hydrogen production from lignocellulose hydrolysates. In *Biotechnol. Biofuels* 12 (1), p. 214. DOI: 10.1186/s13068-019-1559-8.

Lindahl, P. A.; Chang, B. (2001): The evolution of acetyl-CoA synthase. In *Orig. Life Evol. Biosph.* 31 (4-5), pp. 403–434. DOI: 10.1023/a:1011809430237.

Lipscomb, G. L.; Conway, J. M.; Blumer-Schuette, S. E.; Kelly, R. M.; Adams, M. W. (2016): A highly thermostable kanamycin resistance marker expands the tool kit for genetic manipulation of *Caldicellulosiruptor bescii*. In *Appl. Environ. Microbiol.* 82 (14), pp. 4421–4428. DOI: 10.1128/AEM.00570-16.

Ljungdahl, L. G. (1986): The autotrophic pathway of acetate synthesis in acetogenic bacteria. In *Annu. Rev. Microbiol.* 40, pp. 415–450. DOI: 10.1146/annurev.mi.40.100186.002215.

Lo, J.; Zheng, T.; Olson, D. G.; Ruppertsberger, N.; Tripathi, S. A.; Tian, L. et al. (2015): Deletion of *nfnAB* in *Thermoanaerobacterium saccharolyticum* and its effect on metabolism. In *J. Bacteriol.* 197 (18), pp. 2920–2929. DOI: 10.1128/JB.00347-15.

Lunine, J. I. (2006): Physical conditions on the early Earth. In *Philos. Trans. R. Soc. Lond., B, Biol. Sci.* 361 (1474), pp. 1721–1731. DOI: 10.1098/rstb.2006.1900.

Malki, S.; Luca, G.; Fardeau, M. L.; Rousset, M.; Belaich, J. P.; Dermoun, Z. (1997): Physiological characteristics and growth behavior of single and double hydrogenase mutants of *Desulfovibrio fructosovorans*. In *Arch. Microbiol.* 167 (1), pp. 38–45. DOI: 10.1007/s002030050414.

Manhes, G.; Allègre, C. J.; Dupré, B.; Hamelin, B. (1980): Lead isotope study of basic-ultrabasic layered complexes: Speculations about the age of the earth and primitive mantle characteristics. In *Earth Planet. Sci. Lett.* 47 (3), pp. 370–382. DOI: 10.1016/0012-821X(80)90024-2.

Martin, W.; Russell, M. J. (2007): On the origin of biochemistry at an alkaline hydrothermal vent. In *Philos. Trans. R. Soc. Lond., B, Biol. Sci.* 362 (1486), pp. 1887–1925. DOI: 10.1098/rstb.2006.1881.

Martin, W. F. (2020): Older than genes: The acetyl CoA pathway and origins. In *Front. Microbiol.* 11, p. 817. DOI: 10.3389/fmicb.2020.00817.

Maru, B. T.; Munasinghe, P. C.; Gilary, H.; Jones, S. W.; Tracy, B. P. (2018): Fixation of CO_2 and CO on a diverse range of carbohydrates using anaerobic, non-photosynthetic mixotrophy. In *FEMS Microbiol. Lett.* 365 (8). DOI: 10.1093/femsle/fny039.

Matsumoto, T.; Kabe, R.; Nonaka, K.; Ando, T.; Yoon, K. S.; Nakai, H.; Ogo, S. (2011): Model study of CO inhibition of (NiFe) hydrogenase. In *Inorg. Chem.* 50 (18), pp. 8902–8906. DOI: 10.1021/ic200965t.

Meuer, J.; Bartoschek, S.; Koch, J.; Künkel, A.; Hedderich, R. (1999): Purification and catalytic properties of Ech hydrogenase from *Methanosarcina barkeri*. In *Eur. J. Biochem.* 265 (1), pp. 325–335. DOI: 10.1046/j.1432-1327.1999.00738.x.

Meuer, J.; Kuettner, H. C.; Zhang, J. K.; Hedderich, R.; Metcalf, W. W. (2002): Genetic analysis of the archaeon *Methanosarcina barkeri* Fusaro reveals a central role for Ech hydrogenase and ferredoxin in methanogenesis and carbon fixation. In *Proc. Natl. Acad. Sci. USA* 99 (8), pp. 5632–5637. DOI: 10.1073/pnas.072615499.

Mojzsis, S. J.; Arrhenius, G.; McKeegan, K. D.; Harrison, T. M.; Nutman, A. P.; Friend, C. R. L. (1996): Evidence for life on Earth before 3,800 million years ago. In *Nature* 384 (6604), pp. 55–59. DOI: 10.1038/384055a0.

Moon, J.; Henke, L.; Merz, N.; Basen, M. (2019): A thermostable mannitol-1-phosphate dehydrogenase is required in mannitol metabolism of the thermophilic acetogenic bacterium *Thermoanaerobacter kivui*. In *Environ. Microbiol.* 21 (10), pp. 3728–3736. DOI: 10.1111/1462-2920.14720.

Moon, J.; Jain, S.; Müller, V.; Basen, M. (2020): Homoacetogenic conversion of mannitol by the thermophilic acetogenic bacterium *Thermoanaerobacter kivui* requires external CO_2. In *Front. Microbiol.* 11, p. 571736. DOI: 10.3389/fmicb.2020.571736.

Moon, J.; Poehlein, A.; Daniel, R.; Müller, V. (2024): Redirecting electron flow in *Acetobacterium woodii* enables growth on CO and improves growth on formate. In *Nat. Commun.* 15 (1), p. 5424. DOI: 10.1038/s41467-024-49680-5.

Müller, V.; Imkamp, F.; Biegel, E.; Schmidt, S.; Dilling, S. (2008): Discovery of a ferredoxin:NAD+-oxidoreductase (Rnf) in *Acetobacterium woodii*: a novel potential coupling site in acetogens. In *Ann. N. Y. Acad. Sci.* 1125, pp. 137–146. DOI: 10.1196/annals.1419.011.

Nguyen, D. M. N.; Schut, G. J.; Zadvornyy, O. A.; Tokmina-Lukaszewska, M.; Poudel, S.; Lipscomb, G. L. et al. (2017): Two functionally distinct $NADP^+$-dependent ferredoxin oxidoreductases maintain the primary redox balance of *Pyrococcus furiosus*. In *J. Biol. Chem.* 292 (35), pp. 14603–14616. DOI: 10.1074/jbc.M117.794172.

Nies, S. C.; Dinger, R.; Chen, Y.; Wordofa, G. G.; Kristensen, M.; Schneider, K. et al. (2020): Systems analysis of NADH dehydrogenase mutants reveals flexibility and limits of *Pseudomonas taiwanensis* VLB120's metabolism. In *Appl. Environ. Microbiol.* 86 (11). DOI: 10.1128/AEM.03038-19.

Öppinger, C.; Kremp, F.; Müller, V. (2022): Is reduced ferredoxin the physiological electron donor for MetVF-type methylenetetrahydrofolate reductases in acetogenesis? A hypothesis. In *Int. Microbiol.* 25 (1), pp. 75–88. DOI: 10.1007/s10123-021-00190-0.

Peters, J. W.; Miller, A. F.; Jones, A. K.; King, P. W.; Adams, M. W. (2016): Electron bifurcation. In *Curr. Opin. Chem. Biol.* 31, pp. 146–152. DOI: 10.1016/j.cbpa.2016.03.007.

Peters, V. (1998): Efficiency of hydrogen utilization during unitrophic and mixotrophic growth of *Acetobacterium woodii* on hydrogen and lactate in the chemostat. In *FEMS Microbiol. Ecol.* 26 (4), pp. 317–324. DOI: 10.1016/S0168-6496(98)00047-6.

Petersen, H. A.; Miller, E. N.; Pham, P. H.; Katsirubas, K. J. L.; Koltunski, H. J.; Luca, O. R. (2023): On the temperature sensitivity of electrochemical reaction thermodynamics. In *ACS Phys. Chem. Au* 3 (3), pp. 241–251. DOI: 10.1021/acsphyschemau.2c00063.

Pierce, E.; Xie, G.; Barabote, R. D.; Saunders, E.; Han, C. S.; Detter, J. C. et al. (2008): The complete genome sequence of *Moorella thermoacetica* (f. *Clostridium thermoaceticum*). In *Environ. Microbiol.* 10 (10), pp. 2550–2573. DOI: 10.1111/j.1462-2920.2008.01679.x.

Pinske, C.; Sawers, R. G. (2016): Anaerobic formate and hydrogen metabolism. In *EcoSal Plus* 7 (1). DOI: 10.1128/ecosalplus.ESP-0011-2016.

Preiss, J. (2014): Glycogen: Biosynthesis and regulation. In *EcoSal Plus* 6 (1). DOI: 10.1128/ecosalplus.ESP-0015-2014.

Pueyo, J. J.; Gomez-Moreno, C.; Mayhew, S. G. (1991): Oxidation-reduction potentials of ferredoxin-$NADP^+$ reductase and flavodoxin from *Anabaena* PCC 7119 and their electrostatic and covalent complexes. In *Eur. J. Biochem.* 202 (3), pp. 1065–1071. DOI: 10.1111/j.1432-1033.1991.tb16471.x.

Ragsdale, S. W.; Kumar, M. (1996): Nickel-containing carbon monoxide dehydrogenase/acetyl-CoA synthase. In *Chem. Rev.* 96 (7), pp. 2515–2540. DOI: 10.1021/cr950058.

Ragsdale, S. W.; Ljungdahl, L. G. (1984): Purification and properties of NAD-dependent 5,10-methylenetetrahydrofolate dehydrogenase from *Acetobacterium woodii*. In *J. Biol. Chem.* 259 (6), pp. 3499–3503. Available online at https://pubmed.ncbi.nlm.nih.gov/6608524/.

Ragsdale, S. W.; Pierce, E. (2008): Acetogenesis and the Wood-Ljungdahl pathway of CO_2 fixation. In *Biochim. Biophys. Acta* 1784 (12), pp. 1873–1898. DOI: 10.1016/j.bbapap.2008.08.012.

Rainey, F. A.; Ward, N. L.; Morgan, H. W.; Toalster, R.; Stackebrandt, E. (1993): Phylogenetic analysis of anaerobic thermophilic bacteria: aid for their reclassification. In *J. Bacteriol.* 175 (15), pp. 4772–4779. DOI: 10.1128/jb.175.15.4772-4779.1993.

Rosenbaum, F. P.; Müller, V. (2021): Energy conservation under extreme energy limitation: the role of cytochromes and quinones in acetogenic bacteria. In *Extremophiles* 25 (5-6), pp. 413–424. DOI: 10.1007/s00792-021-01241-0.

Rosenbaum, F. P.; Poehlein, A.; Egelkamp, R.; Daniel, R.; Harder, S.; Schlüter, H.; Schoelmerich, M. C. (2021): Lactate metabolism in strictly anaerobic microorganisms with a soluble NAD^+-dependent $_L$-lactate dehydrogenase. In *Environ. Microbiol.* 23 (8), pp. 4661–4672. DOI: 10.1111/1462-2920.15657.

Russell, M. J.; Hall, A. J. (2009): A hydrothermal source of energy and materials at the origin of life. Available online at https://www.researchgate.net/profile/michael-russell-25/publication/313627545_a_hydrothermal_source_of_energy_and_materials_at_the_origin_of_life.

Sato, T.; Fukui, T.; Atomi, H.; Imanaka, T. (2003): Targeted gene disruption by homologous recombination in the hyperthermophilic archaeon *Thermococcus kodakaraensis* KOD1. In *J. Bacteriol.* 185 (1), pp. 210–220. DOI: 10.1128/JB.185.1.210-220.2003.

Sawers, R. G.; Clark, D. P. (2004): Fermentative pyruvate and acetyl-coenzyme a metabolism. In *EcoSal Plus* 1 (1). DOI: 10.1128/ecosalplus.3.5.3.

Schlegel, K.; Leone, V.; Faraldo-Gómez, J. D.; Müller, V. (2012a): Promiscuous archaeal ATP synthase concurrently coupled to Na^+ and H^+ translocation. In *Proc. Natl. Acad. Sci. USA* 109 (3), pp. 947–952. DOI: 10.1073/pnas.1115796109.

Schlegel, K.; Welte, C.; Deppenmeier, U.; Müller, V. (2012b): Electron transport during aceticlastic methanogenesis by *Methanosarcina acetivorans* involves a sodium-translocating Rnf complex. In *FEBS J.* 279 (24), pp. 4444–4452. DOI: 10.1111/febs.12031.

Schmehl, M.; Jahn, A.; Vilsendorf, A. M.; Hennecke, S.; Masepohl, B.; Schuppler, M. et al. (1993): Identification of a new class of nitrogen fixation genes in *Rhodobacter capsulatus*: a putative membrane complex involved in electron transport to nitrogenase. In *Mol. Gen. Genet.* 241 (5-6), pp. 602–615. DOI: 10.1007/BF00279903.

Schmidt, K.; Jensen, S. L.; Schlegel, H. G. (1963): Die Carotinoide der Thiorhodaceae. In *Arch. Microbiol.* 46 (2), pp. 117–126. DOI: 10.1007/BF00408204.

Schmittgen, T. D.; Livak, K. J. (2008): Analyzing real-time PCR data by the comparative C_T method. In *Nat. Protoc.* 3 (6), pp. 1101–1108. DOI: 10.1038/nprot.2008.73.

Schoelmerich, M. C.; Müller, V. (2019): Energy conservation by a hydrogenase-dependent chemiosmotic mechanism in an ancient metabolic pathway. In *Proc. Natl. Acad. Sci. USA* 116 (13), pp. 6329–6334. DOI: 10.1073/pnas.1818580116.

Schoelmerich, M. C.; Müller, V. (2020): Energy-converting hydrogenases: the link between H_2 metabolism and energy conservation. In *Cell. Mol. Life Sci.* 77 (8), pp. 1461–1481. DOI: 10.1007/s00018-019-03329-5.

Schuchmann, K.; Müller, V. (2012): A bacterial electron-bifurcating hydrogenase. In *J. Biol. Chem.* 287 (37), pp. 31165–31171. DOI: 10.1074/jbc.M112.395038.

Schuchmann, K.; Müller, V. (2013): Direct and reversible hydrogenation of CO_2 to formate by a bacterial carbon dioxide reductase. In *Science* 342 (6164), pp. 1382–1385. DOI: 10.1126/science.1244758.

Schuchmann, K.; Müller, V. (2014): Autotrophy at the thermodynamic limit of life: a model for energy conservation in acetogenic bacteria. In *Nat. Rev. Microbiol.* 12 (12), pp. 809–821. DOI: 10.1038/nrmicro3365.

Schuchmann, K.; Müller, V. (2016): Energetics and application of heterotrophy in acetogenic bacteria. In *Appl. Environ. Microbiol.* 82 (14), pp. 4056–4069. DOI: 10.1128/AEM.00882-16.

Schut, G. J.; Adams, M. W. (2009): The iron-hydrogenase of *Thermotoga maritima* utilizes ferredoxin and NADH synergistically: a new perspective on anaerobic hydrogen production. In *J. Bacteriol.* 191 (13), pp. 4451–4457. DOI: 10.1128/JB.01582-08.

Schwartz, E.; Fritsch, J.; Friedrich, B. (2013): H_2-Metabolizing Prokaryotes. In E. F. DeLong, E. Rosenberg (Eds.): The Prokaryotes. 4 ed. Berlin: Springer Reference, pp. 119–199. Available online at https://link.springer.com/referenceworkentry/10.1007/978-3-642-30141-4_65.

Schwarz, F. M.; Ciurus, S.; Jain, S.; Baum, C.; Wiechmann, A.; Basen, M.; Müller, V. (2020): Revealing formate production from carbon monoxide in wild type and mutants of Rnf- and Ech-containing acetogens, *Acetobacterium woodii* and *Thermoanaerobacter kivui*. In *Microb. Biotechnol.* 13 (6), pp. 2044–2056. DOI: 10.1111/1751-7915.13663.

Schwarz, F. M.; Müller, V. (2020): Whole-cell biocatalysis for hydrogen storage and syngas conversion to formate using a thermophilic acetogen. In *Biotechnol. Biofuels* 13, p. 32. DOI: 10.1186/s13068-020-1670-x.

Schwarz, F. M.; Schuchmann, K.; Müller, V. (2018): Hydrogenation of CO_2 at ambient pressure catalyzed by a highly active thermostable biocatalyst. In *Biotechnol. Biofuels* 11 (1), p. 237. DOI: 10.1186/s13068-018-1236-3.

Shaw, A. J.; Hogsett, D. A.; Lynd, L. R. (2010): Natural competence in *Thermoanaerobacter* and *Thermoanaerobacterium species*. In *Appl. Environ. Microbiol.* 76 (14), pp. 4713–4719. DOI: 10.1128/AEM.00402-10.

Siguier, P.; Gourbeyre, E.; Chandler, M. (2014): Bacterial insertion sequences: their genomic impact and diversity. In *FEMS Microbiol. Rev.* 38 (5), pp. 865–891. DOI: 10.1111/1574-6976.12067.

Tanner, R. S.; Miller, L. M.; Yang, D. (1993): *Clostridium ljungdahlii* sp. nov., an acetogenic species in clostridial rRNA homology group I. In *Int. J. Syst. Bacteriol.* 43 (2), pp. 232–236. DOI: 10.1099/00207713-43-2-232.

Thauer, R. K.; Jungermann, K.; Decker, K. (1977): Energy conservation in chemotrophic anaerobic bacteria. In *Bacteriol. Rev.* 41 (1), pp. 100–180. DOI: 10.1128/br.41.1.100-180.1977.

Tremblay, P. L.; Zhang, T.; Dar, S. A.; Leang, C.; Lovley, D. R. (2012): The Rnf complex of *Clostridium ljungdahlii* is a proton-translocating ferredoxin:NAD^+ oxidoreductase essential for autotrophic growth. In *Mbio* 4 (1), e00406-12. DOI: 10.1128/mBio.00406-12.

Turnbough, C. L.; Switzer, R. L. (2008): Regulation of pyrimidine biosynthetic gene expression in bacteria: repression without repressors. In *Microbiol. Mol. Biol. Rev.* 72 (2), 266-300, table of contents. DOI: 10.1128/MMBR.00001-08.

Vignais, P. M.; Billoud, B. (2007): Occurrence, classification, and biological function of hydrogenases: an overview. In *Chem. Rev.* 107 (10), pp. 4206–4272. DOI: 10.1021/cr050196r.

Ville, K. R. I.; Wikström, M. (2021): Architecture of bacterial respiratory chains. In *Nat. Rev. Microbiol.* 19 (5), pp. 319–330. DOI: 10.1038/s41579-020-00486-4.

Wächtershäuser, G. (2006): From volcanic origins of chemoautotrophic life to Bacteria, Archaea and Eukarya. In *Philos. Trans. R. Soc. Lond., B, Biol. Sci.* 361 (1474), 1787-806; discussion 1806-8. DOI: 10.1098/rstb.2006.1904.

Wang, S.; Huang, H.; Moll, J.; Thauer, R. K. (2010): $NADP^+$ reduction with reduced ferredoxin and $NADP^+$ reduction with NADH are coupled via an electron-bifurcating enzyme complex in *Clostridium kluyveri*. In *J. Bacteriol.* 192 (19), pp. 5115–5123. DOI: 10.1128/JB.00612-10.

Weghoff, M. C.; Müller, V. (2016): CO metabolism in the thermophilic acetogen *Thermoanaerobacter kivui*. In *Appl. Environ. Microbiol.* 82 (8), pp. 2312–2319. DOI: 10.1128/AEM.00122-16.

Weiss, M. C.; Sousa, F. L.; Mrnjavac, N.; Neukirchen, S.; Roettger, M.; Nelson-Sathi, S.; Martin, W. F. (2016): The physiology and habitat of the last universal common ancestor. In *Nat Microbiol* 1 (9), p. 16116. DOI: 10.1038/nmicrobiol.2016.116.

Welte, C.; Kallnik, V.; Grapp, M.; Bender, G.; Ragsdale, S.; Deppenmeier, U. (2010a): Function of Ech hydrogenase in ferredoxin-dependent, membrane-bound electron transport in *Methanosarcina mazei*. In *J. Bacteriol.* 192 (3), pp. 674–678. DOI: 10.1128/JB.01307-09.

Welte, C.; Krätzer, C.; Deppenmeier, U. (2010b): Involvement of Ech hydrogenase in energy conservation of *Methanosarcina mazei*. In *FEBS J.* 277 (16), pp. 3396–3403. DOI: 10.1111/j.1742-4658.2010.07744.x.

Westphal, L.; Wiechmann, A.; Baker, J.; Minton, N. P.; Müller, V. (2018): The Rnf complex is an energy-coupled transhydrogenase essential to reversibly link cellular NADH and ferredoxin pools in the acetogen *Acetobacterium woodii*. In *J. Bacteriol.* 200 (21). DOI: 10.1128/JB.00357-18.

Wiechmann, A.; Ciurus, S.; Oswald, F.; Seiler, V. N.; Müller, V. (2020): It does not always take two to tango: "Syntrophy" via hydrogen cycling in one bacterial cell. In *ISME J.* 14 (6), pp. 1561–1570. DOI: 10.1038/s41396-020-0627-1.

Wietzke, M.; Bahl, H. (2012): The redox-sensing protein Rex, a transcriptional regulator of solventogenesis in *Clostridium acetobutylicum*. In *Appl. Microbiol. Biotechnol.* 96 (3), pp. 749–761. DOI: 10.1007/s00253-012-4112-2.

Wohlfarth, G.; Diekert, G. (1991): Thermodynamics of methylenetetrahydrofolate reduction to methyltetrahydrofolate and its implications for the energy metabolism of homoacetogenic bacteria. In *Arch. Microbiol.* 155 (4), pp. 378–381. DOI: 10.1007/BF00243458.

Zeldes, B.; Mittelstedt, S.; Baum, C.; Shakirova, A.; Poehlein, A.; Daniel, R. et al. (2024): Knock-down of genes essential for homoacetogenic growth using sugar inducible promoters in the thermophile *Thermoanaerobacter kivui*. In *bioRxiv*, 2024.06.18.598388. DOI: 10.1101/2024.06.18.598388.

Zeldes, B. M.; Keller, M. W.; Loder, A. J.; Straub, C. T.; Adams, M. W.; Kelly, R. M. (2015): Extremely thermophilic microorganisms as metabolic engineering platforms for production of fuels and industrial chemicals. In *Front. Microbiol.* 6, p. 1209. DOI: 10.3389/fmicb.2015.01209.

Zeldes, B. M.; Poehlein, A.; Jain, S.; Baum, C.; Daniel, R.; Müller, V.; Basen, M. (2023): DNA uptake from a laboratory environment drives unexpected adaptation of a thermophile to a minor medium component. In *ISME commun.* 3 (1). DOI: 10.1038/s43705-022-00211-7.

Appendix

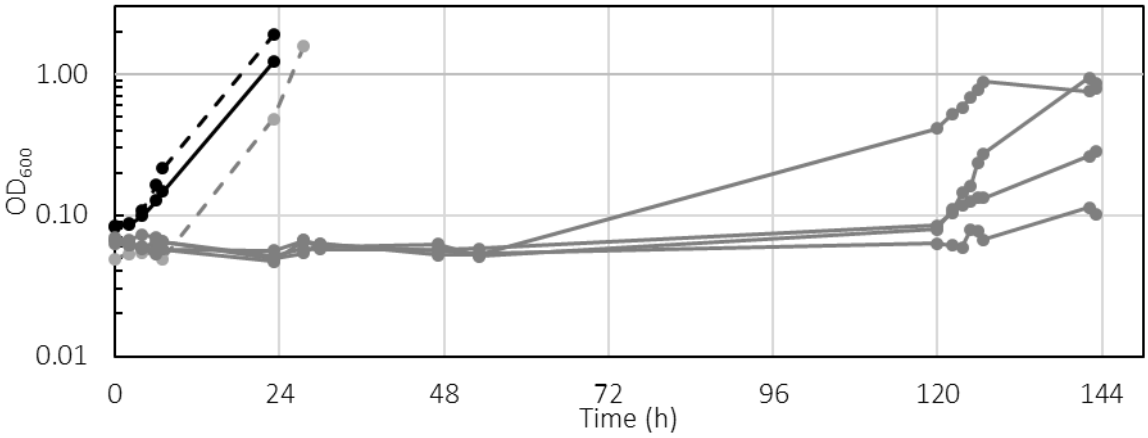

Figure A-1 Growth of Δ*ech2* strain on pyruvate.
Representative growth curves of the first transfer of Δ*ech2* strain (gray) and the wild type (black) grown on glucose transferred to medium containing 50 mM pyruvate (line) or 25 mM glucose (dashed line). The experiment was performed in Hungate tubes with 5 ml complex medium at 65 °C (n = 4). Several growth curves on pyruvate of Δ*ech2* strain are shown.

Table A-1 Overview of the attempts to delete the ech1 operon with the plasmid pEch1TK02K and the T. kivui strain TKV002 (ΔpyrE).
The number of colonies per plate (n = 2-3) and the deletion of the precultures used for plating are shown. The fields marked with x indicate that the transferred colonies in the transfer-hungate tubes did not grow between the first and second selection steps.

		Colonies				
Attempt	Substrate	First selection (dilution)		Second selection (dilution)		Result
1	Glucose	0-5 (10^{-0})		0-61 (10^{-3})	0-5 (10^{-5})	no mutant
2	Glucose	15-16 (10^{-5})	5-6 (10^{-6})	x	x	
3	Glucose	0 (10^{-5})	0 (10^{-6})	x	x	
4	Pyruvate	0 (10^{-5})	0 (10^{-6})	x	x	
5	Glucose	7-158(10^{-5})	0-10 (10^{-6})	x	x	
6	Glucose	≥10 (10^{-0})		≥10 (10^{-0})		no mutant
7	Glucose	162-208 (10^{-6})		x	x	
8	Glucose	0 (10^{-0})		x	x	

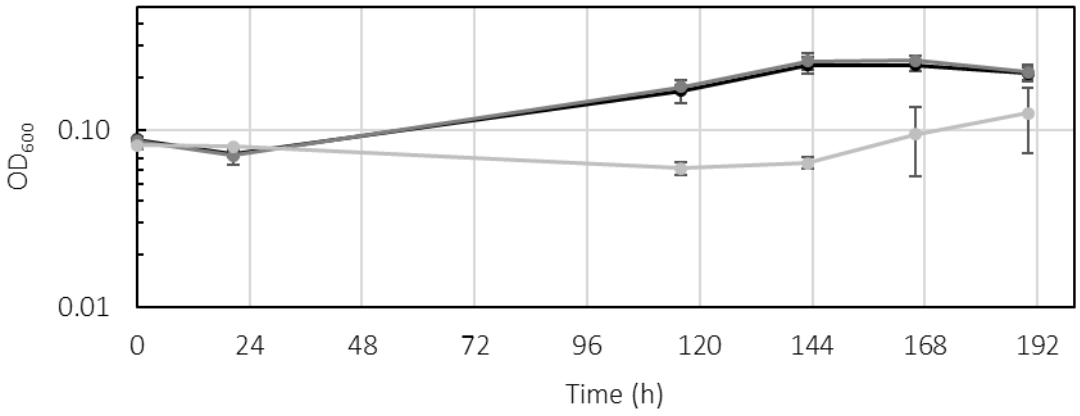

Figure A-2 First transfer of *T. kivui* strains from glucose to H_2/CO_2.
Growth of the *T. kivui* wild type (black), P_{frc}*ech1* (dark gray) and P_{frc}*ech1*Δ*ech2* (light gray) strains in the presence of $2x10^5$ Pa H_2/CO_2 The experiment was performed in defined medium at 65°C (n = 3).

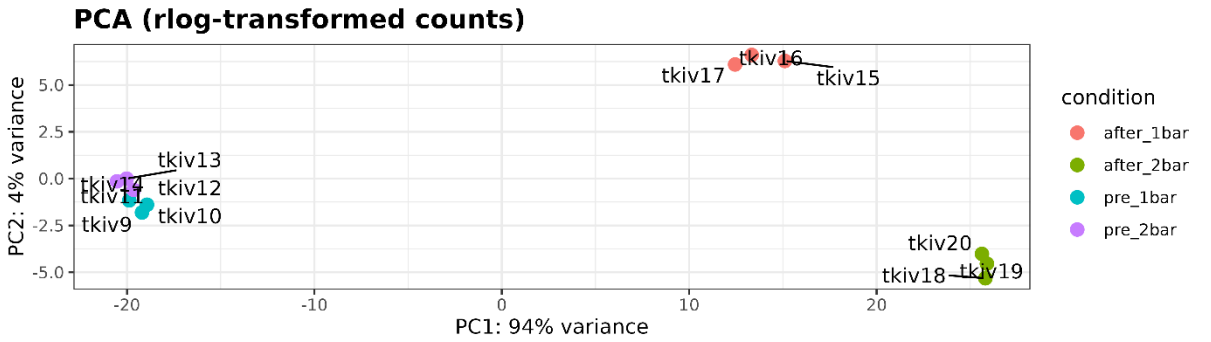

Figure A-3 Principle components analysis of mRNA sequencing samples of *T. kivui* (Figure 29). Shown are three glucose samples pre shock 1 bar H_2/CO_2 (tkiv 9-11), three glucose samples pre shock 2 bar H_2/CO_2 (tkiv12-14), three glucose samples after shock 1 bar H_2/CO_2 (tkiv15-17) and three glucose samples after shock 2 bar H_2/CO_2 (tkiv18-20).

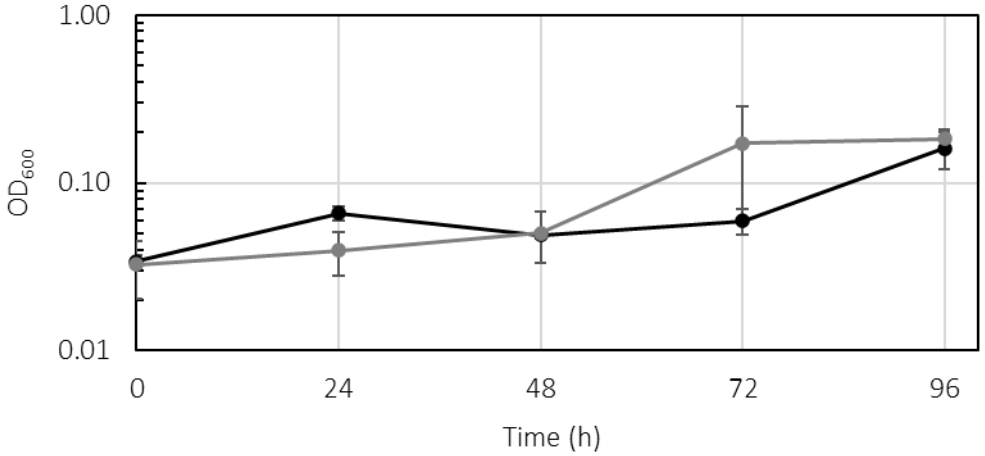

Figure A-4 First transfer of *T. kivui* strains from glucose to H_2/CO_2. Growth of the *T. kivui* wild type (black) and the *nfnB* mutant (dark gray) strains in the presence of $1x10^5$ Pa H_2/CO_2 The experiment was performed in defined medium at 65°C (n = 3).

Table A-2 Transcriptome analysis of *T. kivui* shocked with H_2/CO_2.
$log_2(x)$ values of the transcriptome analysis of *T. kivui* (DSM 2030) grown on defined medium containing glucose before (b. H_2) and after (a. H_2) the addition of H_2/CO_2 (Figure 29). Shown are the 27 upregulated genes after the addition of H_2/CO_2 to the atmosphere with different overpressures of H_2/CO_2 $1x10^5$ Pa (1) and $2x10^5$ Pa (2). The ratio of mRNA reads was calculated and the log_2(ratio [test/calibrator]) was determined. Hypothetical protein with log2(x) value below 2.5 were removed. Threshold for up (blue) regulation is 2.

		Test	Glucose a. H_2 (1)	Glucose a. H_2 (2)
		Calibrator	Glucose b. H_2	
Locus tag / Annotation	TKV_c17550	hypothetical protein	2.57	4.82
	TKV_c00720	glycosyltransferase	3.15	4.18
	TKV_c00710	glycosyltransferase	2.95	4.04
	TKV_c08210	transposase	2.17	3.89
	TKV_c22450	transposase family protein	3.53	3.81
	TKV_c11030	C4-alpha-glucan branching enzyme GlgB	2.68	3.64
	TKV_c11040	glucose-1-phosphate adenylyltransferase GlgC	2.44	3.40
	TKV_c11050	glycogen biosynthesis protein GlgD	2.16	3.17
	TKV_c00270	serine--tRNA ligase SerS	2.13	3.14
	TKV_c00700	putative mannose-1-phosphate guanyltransferase Mpg	2.25	3.12
	TKV_c21590	ABC-type multidrug transportsystem	2.04	3.06
	TKV_c01890	D-ribose-binding periplasmic protein RbsB	1.68	2.88
	TKV_c11080	ABC-2 type transporter	2.01	2.88
	TKV_c08010	lactococcin-G-processing and transport ATP-binding protein LagD	2.40	2.87
	TKV_c11060	glycogen synthase GlgA	1.91	2.79
	TKV_c18810	pyrophosphate-fructose 6-phosphate 1-phosphotransferase Pfp	1.97	2.78
	TKV_c21600	ABC-2 type transport system ATP-binding protein	1.85	2.73
	TKV_c21610	transcriptional regulator	1.82	2.72
	TKV_c10530	phosphoenolpyruvate synthase PpsA	1.75	2.66
	TKV_c01880	ribose transport system permease protein RbsC	1.49	2.65
	TKV_c17540	dinitrogenase iron-molybdenum cofactor biosynthesis protein	1.86	2.60
	TKV_c23560	CRISPR subtype III-B-associated RAMP protein Cmr2/Cas10	2.34	2.52
	TKV_c08020	putative bacteriocin ABC transporter	2.06	2.51
	TKV_c22460	hypothetical protein	1.73	2.49
	TKV_c08810	propeptide PepSY amd peptidase M4	1.55	2.48
	TKV_c07710	DNA polymerase beta-like protein	1.86	2.41
	TKV_c17530	cobyrinic acid ac-diamide synthase	1.76	2.36
	TKV_c17500	beta-lactamase domain-containing protein	1.63	2.27
	TKV_c22300	ABC-2 family transporter protein	1.56	2.26
	TKV_c23540	CRISPR subtype III-B-associated RAMP protein Cmr1	2.26	2.25
	TKV_c01910	polyferredoxin NapH	1.43	2.20
	TKV_c07910	hypothetical protein (CAAX protease family protein)	1.72	2.17
	TKV_c23110	small heat shock protein C4	0.99	2.15

Table A-3 Transcriptome analysis of *T. kivui* shocked with H_2/CO_2.
$log_2(x)$ values of the transcriptome analysis of *T. kivui* (DSM 2030) grown on defined medium containing glucose before (b. H_2) and after (a. H_2) the addition of H_2/CO_2 (Figure 29). Shown are the 40 downregulated genes after the addition of H_2/CO_2 to the atmosphere with different overpressures of H_2/CO_2 $1x10^5$ Pa (1) and $2x10^5$ Pa (2). The ratio of mRNA reads was calculated and the log_2(ratio [test/calibrator]) was determined. Threshold for down (red) regulation is –2.

		Test	Glucose a. H_2 (1)	Glucose a. H_2 (2)
		Calibrator	Glucose b. H_2	
Locus tag / Annotation	TKV_c14430	aspartate carbamoyltransferase PyrB	-8.50	-9.10
	TKV_c05060	hypothetical protein (niacin transporter)	-8.59	-8.80
	TKV_c14420	dihydroorotase PyrC	-7.83	-8.08
	TKV_c14400	dihydroorotate dehydrogenase B	-5.72	-6.63
	TKV_c14410	orotidine 5'-phosphate decarboxylase PyrF	-6.14	-6.26
	TKV_c14390	dihydroorotate dehydrogenase B	-5.40	-5.98
	TKV_c14380	orotate phosphoribosyltransferase PyrE	-4.82	-5.20
	TKV_c16530	ABC-type Fe_3^+-hydroxamate transport system	-2.80	-4.33
	TKV_c16510	putative transporter protein	-2.83	-4.30
	TKV_c10330	glutathione-binding protein GsiB	-3.22	-4.29
	TKV_c04990	amino acid ABC transporter membrane protein	-3.66	-4.24
	TKV_c10340	glutathione-binding protein GsiB	-3.35	-4.13
	TKV_c16480	putative ABC transporter ATP-binding protein	-2.84	-4.05
	TKV_c22200	carbamoyl-phosphate synthase small chain	-2.91	-3.78
	TKV_c16540	radical SAM domain-containing protein	-2.14	-3.76
	TKV_c22210	acetylornithine aminotransferase ArgD	-2.89	-3.70
	TKV_c17450	ABC-type Fe_3^+-hydroxamate transport system	-2.50	-3.69
	TKV_c22220	acetylglutamate kinase ArgB	-2.70	-3.63
	TKV_c22190	carbamoyl-phosphate synthase large chain	-2.84	-3.62
	TKV_c05000	amino acid ABC transporter ATP-binding protein	-3.17	-3.59
	TKV_c05150	hypothetical protein	-2.51	-3.58
	TKV_c04980	amino acid ABC transporter substrate-binding protein	-3.11	-3.54
	TKV_c16550	ABC-type polysaccharide/polyol phosphate export system	-2.15	-3.54
	TKV_c22170	argininosuccinate lyase ArgH	-2.65	-3.54
	TKV_c21470	uracil permease PyrP	-3.50	-3.52
	TKV_c00520	putative fluoride ion transporter CrcB	-2.03	-3.48
	TKV_c22180	argininosuccinate synthase ArgG	-2.73	-3.46
	TKV_c22240	N-acetyl-gamma-glutamyl-phosphate reductase ArgC	-2.77	-3.41
	TKV_c22230	arginine biosynthesis bifunctional protein ArgJ	-2.73	-3.39
	TKV_c16560	daunorubicin resistance ABC transporter ATPase subunit	-1.91	-3.34
	TKV_c21380	hypothetical protein	-1.82	-3.34
	TKV_c17410	formylmethanofuran dehydrogenase subunit E region	-2.28	-3.28
	TKV_c20660	50S ribosomal protein L7/L12	-1.97	-3.23
	TKV_c20520	50S ribosomal protein L22	-1.72	-3.10
	TKV_c05510	ferredoxin-dependent glutamate synthase	-1.91	-3.10
	TKV_c01470	hypothetical protein	-2.14	-3.09
	TKV_c17430	ABC-type cobalamin/Fe3+-siderophore transport system	-2.22	-3.06
	TKV_c23100	abortive infection protein	-1.86	-3.05
	TKV_c24210	adenylosuccinate synthetase PurA	-2.29	-3.03
	TKV_c20460	50S ribosomal protein L24	-1.68	-3.02

Table A-4 Transcriptome analysis of *T. kivui* shocked with H_2/CO_2.

$log_2(x)$ values of the transcriptome analysis of *T. kivui* (DSM 2030) grown on defined medium containing glucose before (b. H_2) and after (a. H_2) the addition of H_2/CO_2 (Figure 29). Shown are the mRNA reads and the change in expression of genes investigated in qPCR analysis after the addition of H_2/CO_2 to the atmosphere with an overpressure of $2x10^5$ Pa (2). The ratio of mRNA reads was calculated and the log_2(ratio [test/calibrator]) was determined. Threshold for up (blue) or down (red) regulation is 2 or –2.

Gene Locus tag	Gene cluster	Annotation	mRNA reads		$log_2(x)$ value
			Calibrator Glucose b. H_2	Test Glucose a. H_2 (2)	
TKV_c00090	*gyrAB*	DNA gyrase subunit B	2616	1602	-0.71
TKV_c00100		DNA gyrase subunit A	3184	1597	-1.00
TKV_c04340	*nifJ1* (PFOR1)	pyruvate-flavodoxin oxidoreductase NifJ1	128609	299763	1.22
TKV_c05420	*rex*	redox-sensing transcriptional repressor Rex	1048	1474	0.49
TKV_c09620	*fd2*	hypothetical protein (ferredoxin)	251	135	-0.90
TKV_c16340	*gap*	glyceraldehyde-3-phosphate dehydrogenase Gap	64179	66728	0.06
TKV_c16450	*fd1*	ferredoxin	526	230	-1.19
TKV_c19260	*2OxFOR*	pyruvate ferredoxin oxidoreductase subunit gamma	565	575	0.03
TKV_c19270		pyruvate ferredoxin oxidoreductase subunit beta	416	372	-0.16
TKV_c19280		pyruvate ferredoxin oxidoreductase subunit alpha	399	420	0.07
TKV_c19580	*hydABC*	electron bifurcating hydrogenase subunit HydA1	30456	10747	-1.50
TKV_c19590		electron bifurcating hydrogenase subunit HydB	35775	14308	-1.32
TKV_c19600		electron bifurcating hydrogenase subunit HydC	5831	2770	-1.07
TKV_c19930	*fhs*	formyl-tetrahydrofolate synthetase Fhs	124801	88988	-0.49
TKV_c19950	*fdhF*	hydrogen dependent carbon dioxide reductase subunit FdhD	5829	7743	0.41
TKV_c19960		hydrogen dependent carbon dioxide reductase subunit HydA2	11651	16834	0.53
TKV_c19970		hydrogen dependent carbon dioxide reductase subunit HycB4	5079	7177	0.50
TKV_c19980		hydrogen dependent carbon dioxide reductase subunit HycB3	1996	2901	0.54
TKV_c19990		hydrogen dependent carbon dioxide reductase subunit FdhF	38371	63388	0.72
TKV_c23150	*fruK*	1-phosphofructokinase	10	24	1.23
TKV_c21450	*nifJ2* (PFOR2)	pyruvate-flavodoxin oxidoreductase NifJ2	1152	1092	-0.08
TKV_c22270	*nfnAB*	transhydrogenase subunit A	17659	8524	-1.05
TKV_c22280		transhydrogenase subunit B	36559	15949	-1.20

Table A-5 Transcriptome analysis of *T. kivui* shocked with H_2/CO_2.

$log_2(x)$ values of the transcriptome analysis of *T. kivui* (DSM 2030) grown on defined medium containing glucose before (b. H_2) and after (a. H_2) the addition of H_2/CO_2 (Figure 29). Shown are the mRNA reads and the change in expression of genes of the *ech1* and *ech2* gene clusters after the addition of H_2/CO_2 to the atmosphere with an overpressure of $2x10^5$ Pa (2). The ratio of mRNA reads was calculated and the log_2(ratio [test/calibrator]) was determined. Threshold for up (blue) or down (red) regulation is 2 or –2.

Gene Locus tag	Gene cluster	Annotation	mRNA reads		$log_2(x)$ value
			Calibrator Glucose b. H_2	Test Glucose a. H_2 (2)	
TKV_c01230	*ech1*	Ech-type complex subunit Ech1A	39146	21170	-0.89
TKV_c01240		Ech-type complex subunit Ech1B	18579	10422	-0.83
TKV_c01250		Ech-type complex subunit Ech1C	9579	5337	-0.84
TKV_c01260		Ech-type complex subunit Ech1F	2335	1323	-0.82
TKV_c01270		Ech-type complex subunit HycB1	8465	3673	-1.20
TKV_c01280		hypothetical protein	3177	1395	-1.19
TKV_c01290		hypothetical protein	5183	2538	-1.03
TKV_c01300		Ech-type complex subunit Ech1D	1118	441	-1.34
TKV_c01310		Ech-type complex subunit Ech1E	21670	8257	-1.39
TKV_c19680	*ech2*	Ech-type complex subunit Ech2F	1017	373	-1.45
TKV_c19690		Ech-type complex subunit Ech2B	1600	571	-1.49
TKV_c19700		Ech-type complex subunit Ech2C	684	279	-1.30
TKV_c19710		Ech-type complex subunit Ech2A2	1229	369	-1.74
TKV_c19720		Ech-type complex subunit Ech2A1	3942	1128	-1.81
TKV_c19730		Ech-type complex subunit HycB2	1042	306	-1.77
TKV_c19740		Ech-type complex subunit Ech2E	2379	621	-1.94
TKV_c19750		Ech-type complex subunit Ech2D	439	153	-1.52

Table A-6 Transcriptome analysis of *T. kivui* shocked with H_2/CO_2.
$log_2(x)$ values of the transcriptome analysis of *T. kivui* (DSM 2030) grown on defined medium containing glucose before (b. H_2) and after (a. H_2) the addition of H_2/CO_2 (Figure 29). Shown are the mRNA reads and the change in expression of genes encoding ferredoxins (Katsyv et al. 2023a) after adding H_2/CO_2 to the atmosphere with an overpressure of $2x10^5$ Pa (2). The ratio of mRNA reads was calculated and the log_2(ratio [test/calibrator]) was determined. Threshold for up (blue) or down (red) regulation is 2 or –2.

Gene Locus tag	Annotation	mRNA reads		$log_2(x)$ value
		Calibrator Glucose b. H_2	Test Glucose a. H_2 (2)	
TKV_c16450	ferredoxin	526	230	-1.19
TKV_c09620	hypothetical protein	251	135	-0.90
TKV_c10420	4Fe-4S ferredoxin iron-sulfur binding domain-containing protein	8	7	-0.13
TKV_c19530	4Fe-4S ferredoxin	157	377	1.26

Table A-7 Transcriptome analysis of *T. kivui* shocked with H_2/CO_2.
$log_2(x)$ values of the transcriptome analysis of *T. kivui* (DSM 2030) grown on defined medium containing glucose before (b. H_2) and after (a. H_2) the addition of H_2/CO_2 (Figure 29). Genes related to NAD+, NADH, NADP+ and NADPH synthase and dependency are shown. The threshold for up (blue) or down (red) regulation is 2 or –2.

Gene Locus tag	Annotation	mRNA reads		$log_2(x)$ value
		Calibrator Glucose b. H_2	Test Glucose a. H_2 (2)	
TKV_c06500	glutamine-dependent NAD(+) synthetase NadE	2106	1800	-0.23
TKV_c06800	NAD-dependent epimerase/dehydratase	56	13	-2.09
TKV_c07660	glutamate synthase (NADPH/NADH) small chain	17648	11208	-0.66
TKV_c10390	NADH:flavin oxidoreductase%2C Old yellow enzyme family	42	67	0.67
TKV_c10400	NADH:flavin oxidoreductase%2C Old yellow enzyme family	157	263	0.74
TKV_c14390	dihydroorotate dehydrogenase B (NAD(+))	1705	27	-5.98
TKV_c14400	dihydroorotate dehydrogenase B (NAD(+))	2292	23	-6.63
TKV_c16070	NAD-dependent protein deacetylase 2	819	628	-0.38
TKV_c16790	putative NADH dehydrogenase/NAD(P)H nitroreductase	1589	734	-1.11
TKV_c18760	NADH oxidase	689	1047	0.60
TKV_c22260	NADP-dependent isopropanol dehydrogenase Adh	364672	479400	0.39
TKV_c12160	NAD kinase NadK	3837	5252	0.45
TKV_c15130	glycerol-3-phosphate dehydrogenase [NAD(P)+]	1300	463	-1.49

Table A-8 Transcriptome analysis of *T. kivui* shocked with H_2/CO_2.
$log_2(x)$ values of the transcriptome analysis of *T. kivui* (DSM 2030) grown on defined medium containing glucose before (b. H_2) and after (a. H_2) the addition of H_2/CO_2 (Figure 29). Shown are the mRNA reads and the change in expression of genes encoding enzymes of the Embden-Meyerhof-Parnas pathway after the addition of H_2/CO_2 to the atmosphere with an overpressure of $2x10^5$ Pa (2). The ratio of mRNA reads was calculated and the log_2(ratio [test/calibrator]) was determined. Threshold for up (blue) or down (red) regulation is 2 or –2.

Gene Locus tag	Annotation	mRNA reads		$log_2(x)$ value
		Calibrator Glucose b. H_2	Test Glucose a. H_2 (2)	
TKV_c00920	glucokinase GlcK	1552	2347	0.60
TKV_c17910	glucokinase GlcK	1415	1885	0.41
TKV_c16780	glucose-6-phosphate isomerase Pgi	1996	3320	0.73
TKV_c16900	6-phosphofructokinase PfkA	969	755	-0.36
TKV_c01430	fructose-bisphosphate aldolase Fba	13574	9714	-0.48
TKV_c04080	fructose-bisphosphate aldolase class 1	853	1014	0.25
TKV_c16320	triosephosphate isomerase TpiA	13995	16470	0.23
TKV_c16340	glyceraldehyde-3-phosphate dehydrogenase Gap	64179	66728	0.06
TKV_c16330	phosphoglycerate kinase Pgk	34090	38729	0.18
TKV_c16310	C3-bisphosphoglycerate-independent phosphoglycerate mutase GpmI	34209	44599	0.38
TKV_c16300	enolase Eno	35947	46131	0.36
TKV_c16890	pyruvate kinase Pyk	11244	9414	-0.26

Table A-9 Transcriptome analysis of *T. kivui* shocked with H_2/CO_2.
$log_2(x)$ values of the transcriptome analysis of *T. kivui* (DSM 2030) grown on defined medium containing glucose before (b. H_2) and after (a. H_2) the addition of H_2/CO_2 (Figure 29). Shown are the mRNA reads and the change in expression of genes encoding transcriptional regulators after the addition of H_2/CO_2 to the atmosphere with an overpressure of $2x10^5$ Pa (2). The ratio of mRNA reads was calculated and the log_2(ratio [test/calibrator]) was determined. Threshold for up (blue) or down (red) regulation is 2 or –2.

Gene Locus tag	Gene cluster	Annotation	mRNA reads		$log_2(x)$ value
			Calibrator Glucose b. H_2	Test Glucose a. H_2 (2)	
TKV_c05420	*rex*	redox-sensing transcriptional repressor Rex	1048	1474	0.49
TKV_c19570	*lysR*	transcriptional regulator LysR family	402	611	0.61

Curriculum Vitae

Name Christoph Ferdinand Baum
Date of birth 17.081989
Place of birth Kassel, Germany

Education

Since Jun 2019	PhD student, Microbiology (Basen lab) University of Rostock, Germany
Oct 2016 – Jan 2019	Master of Science, Microbiology Friedrich-Schiller-University Jena, Germany
Oct 2012 – Sep 2016	Bachelor of Science, Biology Friedrich-Schiller-University Jena, Germany

Research Experience

PhD, Department of Microbiology, University of Rostock, Germany

Supervisor: Prof. Dr. Mirko Basen

Thesis: Function of energy-converting hydrogenases and transhydrogenase in metabolism of the thermophilic acetogenic bacterium *Thermoanaerobacter kivui*

- Cultivation of a thermophilic anaerobic microorganism
- Autotrophic cultivation (H_2/CO_2, syngas and CO)
- Genetic techniques, cloning and plasmid construction in *E. coli*
- Generation of a variety of deletion mutants of metabolic genes in *T. kivui*
- Phenotype characterization of knockout strains with growing and resting cells
- Monitoring of substrates and products with HPLC and GC
- RNA extraction and transcriptional analysis (RT-qPCR)
- Carbon and reducing equivalent balance of *T. kivui* central metabolism

Master Thesis: Friedrich-Schiller-University Jena, Germany

Supervisor: Prof. Dr. Gabriele Diekert and Dr. Torsten Schubert

Thesis: Biological relevance of different B12 vitamins for B12-dependent bacteria and microalgae.

- Cultivation of B12 vitamin producing anaerobic microorganism (*Sulfurospirillum multivorans*)
- Cultivation of B12-auxotrophic microalgae (*Ostreococcus tauri* and *Chlamydomonas reinhardtii*)
- Cyanide extraction of different B12 vitamin derivates from *S. multivorans and C. reinhardtii*

Bachelor Thesis: Friedrich-Schiller-University Jena, Germany

Supervisor: Prof. Erika Kothe

Thesis: Investigation of labeled heavy metal resistant Streptomyces strains in microcosm experiments.

- Cultivation of aerobic Streptomyces *mirabilis* and *S. acidiscabies*
- Genetic techniques for transformation/conjugation of *S. mirabilis* and *S. acidiscabies* (GFP label)
- Fluorescents microscopy to visualize GFP label

Publications

Baum C, Zeldes B, Poehlein A, Daniel R, Müller V, Basen M. (2024) The energy-converting hydrogenase Ech2 is important for the growth of the thermophilic acetogen *Thermoanaerobacter kivui* on ferredoxin-dependent substrates. Microbiology spectrum; doi.org/10.1128/spectrum.03380-23

Zeldes B, Poehlein A, Jain S, Baum C, Daniel R, Müller V and Basen M. (2023) DNA uptake from a laboratory environment drives unexpected adaptation of a thermophile to a minor medium component. ISME Communications; doi.org/10.1038/s43705-022-00211-7

Schwarz FM, Ciurus S, Jain S, Baum C, Wiechmann A, Basen M, et al. (2020) Revealing formate production from carbon monoxide in wild type and mutants of Rnf- and Ech-containing acetogens, *Acetobacterium woodii* and *Thermoanaerobacter kivui*. Microb Biotechnol; 13:2044–56 doi.org/10.1111/1751-7915.13663

Baum C, Menezes RC, Svatoš A and Schubert T. (2020) Cobamide remodeling in the freshwater microalga *Chlamydomonas reinhardtii*. FEMS Microbiology Letters, Volume 367, Issue 20; doi.org/10.1093/femsle/fnaa171

Conference contributions

Baum C, Schwarz F, Müller V, Basen M. The energy conserving hydrogenases Ech2 in *Thermoanaerobacter kivui* is not essential for acetogenic growth on H_2 + CO_2 but essential in CO metabolism.
Poster presentation, Extremophiles; Sep. 2022; Loutraki, Greece

Baum C, Schwarz F, Müller V, Basen M. The function of the energy converting hydrogenase Ech2 in *Thermoanaerobacter kivui*.
Poster presentation, VAAM; Feb. 2022; Online

Baum C, Menezes RC, Svatoš A and Schubert T. A new mode of B12-remodeling in microalgae?
Poster presentation, VAAM; Mar. 2020; Leipzig, Germany
Award: Best poster presentation

Declaration

I hereby declare in lieu of an oath that I have written this thesis independently and without outside help. I have not used any aids or sources other than those specified by me and I have marked the passages taken from the works used in terms of content and wording as such.

I confirm that I have not been given the opportunity to write this doctoral thesis for commercial purposes. In particular, I have not engaged any organization that seeks supervisors for the preparation of dissertations for a fee or that performs all or part of the duties incumbent upon me with regard to examinations.

_____

(Date) (Location) (Signature Christoph Ferdinand Baum)

Eidesstattliche Erklärung

Ich versichere hiermit an Eides statt, dass ich die vorliegende Arbeit selbstständig angefertigt und ohne fremde Hilfe verfasst habe. Dazu habe ich keine außer den von mir angegebenen Hilfsmitteln und Quellen verwendet und die, den benutzten Werken inhaltlich und wörtlich entnommenen Stellen, habe ich als solche kenntlich gemacht.

Ich versichere, dass mir die Gelegenheit zum vorliegenden Promotionsvorhaben nicht kommerziell vermittelt worden ist. Insbesondere habe ich keine Organisation eingeschaltet, die gegen Entgelt Betreuerinnen/Betreuer für die Anfertigung von Dissertationen sucht oder die mir obliegenden Pflichten hinsichtlich der Prüfungsleistungen für mich ganz oder teilweise erledigt.

_____

(Datum) (Ort) (Unterschrift Christoph Ferdinand Baum)

Danksagung

Zu guter Letzt möchte ich mich bei allen Personen bedanken, die mich während dieser aufregenden Zeit begleitet haben.

Mein besonderer Dank gilt meinem Betreuer Prof. Dr. Mirko Basen, für das Vertrauen mir die Freiheit zu gegeben mich wissenschaftlich zu entfalten, das konstruktive Feedback diese wissenschaftliche Freiheit zu lenken und generell seine Betreuung und seine Unterstützung während der gesamten Promotionszeit!

Ich möchte mich ganz herzlich bei Dr. Ben Zeldes für seine Unterstützung und den bereichernden wissenschaftlichen Austausch bedanken! Seine Begeisterung für die Wissenschaft ist wahrlich inspirierend!

Ein großes Dankeschön geht an alle anderen Kolleginnen und Kollegen Dr. Maria Lehmann, Carolin Döring, Lisa Engelhardt, Sonja Kurrer, Christoph Prohaska, Katja Bär, Dr. Nancy Magnus, Monika Timm, Manja Henneberg und Anne Haberberger und Dr. Ralf Fischer. Ich bin euch allen sehr dankbar für all die sehr unterhaltsamen Gespräche im Labor und außerhalb, sowie für die positiven Arbeitsatmosphäre!

Meinen Eltern bin ich unendlich dankbar für ihre bedingungslose Geduld, Unterstützung und die Freiheiten, die sie mir gegeben haben – ohne euch wäre ich nicht dort, wo ich heute bin! Von Herzen danke ich meinen beiden Geschwistern Josephine und Philipp – ihr seid die besten Geschwister, die man sich nur wünschen kann!

Am Ende möchte ich mich bei Laura Nissen bedanken! Ich danke dir von Herzen für deine Unterstützung in den letzten Jahren in allen Belangen, für die Zeit, die wir gemeinsam verbracht haben, sowie für den Spaß und die gemeinsamen „Abenteuer“! Du warst eine große Stütze für mich, und ich schätze alles, was wir zusammen erlebt haben!